DISSERTATION

Simulation and experimental validation of adiabatic and non-adiabatic capillary tubes

Martin Heimel, Dipl.-Ing.

Graz University of Technology

Institute for Internal Combustion Engines and Thermodynamics

Head: Helmut Eichlseder, Univ.-Prof. Dipl.-Ing. Dr.techn.
Supervisor: Raimund Almbauer, Ao.Univ.-Prof. Dipl.-Ing. Dr.techn.
1st Reviewer: Raimund Almbauer, Ao.Univ.-Prof. Dipl.-Ing. Dr.techn.
2nd Reviewer: Stephan Kabelac, Prof. Dr.-Ing. habil.

Graz, 12.01.2015

STATUTORY DECLARATION

I declare that I have authored this thesis independently, that I have not used other than the declared sources/resources, and that I have explicitly indicated all material which has been quoted either literally or by content from the sources used. The text document uploaded to TUGRAZonline is identical to the present doctoral dissertation.

EIDESSTATTLICHE ERKLÄRUNG

Ich erkläre an Eides statt, dass ich die vorliegende Arbeit selbstständig verfasst, andere als die angegebenen Quellen/Hilfsmittel nicht benutzt, und die den benutzten Quellen wörtlich und inhaltlich entnommenen Stellen als solche kenntlich gemacht habe. Das in TUGRAZonline hochgeladene Textdokument ist mit der vorliegenden Dissertation identisch.

16.01.2015 ..... date

..... signature

ACKNOWLEDGEMENTS

I'd like to thank first of all my supervisor Prof. Raimund Almbauer who kindly supported me during my research and who gave me much freedom and confidence in doing so. Prof. Helmut Eichlseder, head of the institute, provided the framework which made it possible to carry on research in the field of thermodynamic and particularly refrigeration.

My former colleagues Wolfgang Lang and Dalibor Jajcevic also contributed to my work in terms of acting as support-hotline for simulation related problems. Thank you for sharing your experience in programming and for lending me your ear in times of numerical divergence. Furthermore, Wolfgang Lang laid the foundations of a new project by writing a successful proposal which will provide a field of application for this thesis.
On the experimental side I want to particularly mention Robert Presl who spared no effort in helping me out with Data acquisition, transducers of all kind, hardware, software and the idea of GUM, despite he worked for another faculty he made it possible to help out with equipment when it was urgently needed and initiated many ideas during discussions at the local Irish Pub. Thanks to the Irish, as well.
My dear fellows from the research group "thermodynamics" contributed also by helping hands and not to forget the pleasant and profitable atmosphere in the office and the lab.

The former company ACC Austria (now Secop Austria GmbH) provided not just financial support but also in terms of technical knowledge and hardware when it came to setting up the experimental part.

Away from work, special gratitude deserves my girlfriend, Katharina, who has the amazing ability to encourage me when motivation is low, my friends who constantly needled me about the progress of the thesis and not to forget my family. All of them provide me with the necessary energy to work in a focused and carefree way.

KURZFASSUNG

Um Kompressions-Kälteanlagen im Haushaltsbereich besser verstehen und optimieren zu können, dient ein Simulationsmodell, welches unter anderem den Energieverbrauch bei vorgegebener Konfiguration und Umgebungstemperatur feststellen soll. Ein Teil dieses Kreislaufes ist das Expansionsgerät, das bei den untersuchten Anwendungen als gezogenes Rohr mit Durchmesser im Sub-Millimeter Bereich, meist mit Wärmetauscher, ausgeführt ist. Dieses Kapillarrohr trennt gemeinsam mit dem Kompressor die Hoch- von der Niederdruckseite, der Druckabbau erfolgt durch Reibung des Kältemittels an der Rohrinnenwand und durch die Beschleunigung der Strömung bis zur Schallgeschwindigkeit. Die Expansion des Kältemittels wird in dieser Arbeit experimentell und rechnerisch untersucht, die Herleitung des Rechenalgorithmus von den grundlegenden Erhaltungsgleichungen sowie alle untersuchten Korrelationen für Reibung und Wärmeübergang sind beschrieben.

Ziel der Arbeit ist ein validiertes eindimensionales homogenes Modell, welches stationäre Massenflüsse für definierte Randbedingungen berechnen kann. Für den Fall, dass zusätzlich Wärme während der Expansion abgeführt wird, soll die thermische Leistung mitberechnet werden. Die Validierung erfolgt mittels veröffentlichter Daten zu Experimenten mit verschiedenen Kältemitteln sowie mit Ergebnissen eines im Zuge der Dissertation gebauten Prüfstandes. Zudem liefert ein ausführlicher Literaturbericht einen Überblick über Experimente und Rechenmodelle anderer zu diesem Thema.

Nach diesen Schritten ist ein weiteres Ziel die Anwendung einer Klasse von Modellen, welche sich durch ihre hohe Rechengeschwindigkeit auszeichnet und damit eher für die Implementierung in einer Simulation geeignet ist. Diese Modelle basieren auf halbempirischen dimensionslosen Gleichungen sowie Neuronalen Netzwerken. Beide Varianten werden mit den Daten des 1d Modells abgestimmt und anschließend in ihrer Fähigkeit zum Einsatz in der Kreislaufsimulation verglichen.

ABSTRACT

For means of better understanding and optimization capabilities in the field of domestic vapour-compression cooling devices a simulation model is used to compute energy consumption at a given configuration of the device and a given ambient temperature. A sub-model of this simulation tool is the expansion device which is usually designed as a drawn metal tube with inner diameters below 1 mm and an additional heat exchanger. This so called capillary tube separates together with the compressor the high-pressure and the low pressure side, the pressure drop of the refrigerant is due to wall friction and acceleration of the flow up to the speed of sound. The expansion of the refrigerant is investigated theoretically and experimentally, the deduction of the algorithm based on conservation-equations as well as the correlations for friction and heat transfer are presented.

Aim of this work is a validated one-dimensional homogeneous model which is able to compute steady state mass flow rates for given boundary conditions. In case of a cooled expansion the thermal power should be an output as well. The validation is achieved by using published data of several experiments which apply different fluids as well as data obtained by a specifically designed test-rig. Additionally, an extensive literature survey gives an overview about approaches concerning experiments and simulation.

After completion of these steps another goal is the application of a class of models which distinguish themselves by higher computational speed, hence they are better suited for application in a cycle simulation. These models are based on semi-empiric dimensionless equations or Neural Networks. Both variants are trained with data calculated by the 1d code and are then compared in terms of applicability in cycle simulation.

CONTENTS

LIST OF FIGURES

LIST OF TABLES

NOMENCLATURE

	Greek letters			***Superscripts***
α	void fraction		i	cell number
α	heat transfer coefficient	$W/m^2 K$	.	time derivative
α	cell parameter		-	average value
β	cell parameter		*	corrected quantity
β	volumetric thermal expansion coefficient	1/K		
$\dot{\gamma}$	shear rate	1/s		
ε	absolute surface roughness	m		***Subscripts***
ε	coefficient of performance			
λ	heat conduction coefficient	W/m K	*a*	annulus
λ	friction coefficient		*av*	average
μ	mean value		*c*	circle
μ	dynamic viscosity	Pa s	*CAP*	capillary tube
ν	kinematic viscosity	m^2/s	*cond*	condensation
ν	specific volume	m^3/kg	*conf*	conflated
π	constant		*crit*	critical
ρ	density	kg/m^3	*diff*	difference
σ	surface tension	N/m	*e*	external
σ	standard deviation		*el*	electrical
τ	shear stress	N/m^2	*equil*	equilibrium
φ	correction factor		*evap*	evaporation
φ	angle	°	f_W	due to wall friction
Δ	difference		*fr*	friction
Π	dimensionless group		*g*	vapour
Φ	two phase multiplier		*h*	hydraulic
			HTX	heat exchanger
			i	inner
	Roman letters		*in*	inlet
			irr	irreversible
a, ***a***	neural network output		*l*	liquid
A	area	m^2	*lm*	liquid metastable
A_c	area circle	m^2	*lo*	liquid only
A_e	area ellipse	m^2	*ls*	liquid superheated
A	term		*m*	average
A_p	parameter		*o*	outer
2a	minor axes		*out*	outlet
b, ***b***	neural network bias		*pool*	pool boiling
2b	major axes		*red*	reduced
B	term		*sat*	saturation
c_p	specific heat	J/kg K	*sonic*	at sonic speed
C	coefficient		*sub*	subcooled
C	interaction parameter		*sup*	superheated
d	total number of cells		*tot*	total
D	inner diameter	m	*tp*	two phase
D	duty cycle ratio		*tt*	turbulent-turbulent
d	diameter	m	*v*	vapour

d_c	coil diameter	m	*vo*	vapour only
D'	reference length	m	*w*	wall
e	specific energy	J/kg	*x*	in x-direction
e	Euler number		*y*	in y-direction
f	function		*z*	in z-direction
F	forced convective heat transfer enhancement factor			
fg_i	function	N/m^3		
Fr	Froude number			
f_w	wall friction per volume			
f_3	function			
g	gravitational acceleration	m/s^2		
G	mass flux	kg/m^2 s		
h	distance	m		
h	specific enthalpy	J/kg		
H	enthalpy	J		
$\boldsymbol{IW}$	weight matrix			
k	Boltzmann constant	J/K		
k	thermal transmittance	W/m^2 K		
k	coverage factor			
$L_{pre\ HTX}$	capillary tube length before heat exchanger	m		
$\boldsymbol{LW}$	weight matrix			
m	mass	kg		
M	molar mass	g/mol		
n, $\boldsymbol{n}$	neural network input			
N	number of neurons			
Nu	Nusselt number			
p	pressure	Pa		
p_v	pressure at inception of evaporation	Pa		
Δp_f	frictional pressure drop	Pa		
q	specific heat	J/kg		
Q	heat	J		
q_l	liquid phase heat flux	W/m^2		
q_*	dimensionless heat flux			
r	radius	m		
Ra	Rayleigh number			
Re	Reynolds number			
s	specific entropy	J/kg K		
S	entropy	J/K		
S	suppression factor			
S	slip ratio			
t	time	s		
T	Temperature	K, °C		
u	velocity	m/s		
u_c	combined standard uncertainty			
v	velocity	m/s		
V	volume	m^3		
w_t	specific technical work	J/kg		
We	Weber number			
x	vapour quality			
x	x-direction			
x	input parameter			

X	Lockhart-Martinelli parameter		
y	physical quantity		
y	y-direction		
z	z-direction		
z	cell length	m	

ABBREVATIONS

VSD	Variable Speed Drive
ANN	Artificial Neural Network
ASHRAE	American Society of Heating, Refrigeration and Air Conditioning Engineers
GUM	Guide to the Expression of Uncertainty in Measurement
GWP	Global Warming Potential
IEA	International Energy Agency
ln	natural logarithm
$\log_{10}$	decimal logarithm
NI	National Instruments
NIST	National Institute of Standards and Technology
NTU	Number of Transfer Units
ODP	Ozone Depletion Potential
RMS	Root Mean Square
RMSE	Root Mean Square Error
HC	Hydrocarbons
CFC	Chlorofluorocarbons
HCFC	Hydrochlorofluorocarbons
HFC	Hydrofluorocarbons

1. Introduction

Plenty of introductions in scientific work feature the term "energy efficiency" – a key phrase which comes up relatively fast and also here no exception is made. Energy efficient household cooling is the reason why this work has been carried out. The scale of cooling applications is sometimes divided into three categories which are domestic, commercial and industrial. The focus lies on domestic cooling applications such as freezers, coolers, combinations, wine-coolers, and so on. Using the less electric energy for the same cooling purpose is desirable in many ways, the customer benefits financially, the manufacturer gains a competitive advantage and our environment is subject to less pollution by means of energy saving – at least theoretically. The driving forces of this process, since no change just happens from alone, are plentiful. Among them certainly is the awareness of people who see that a resource-saving way of living becomes the more important the higher the density of individuals, living together on a pile of only partly regenerative natural resources. According to an IEA-report [191] the amount of electric energy in private households which is used for refrigeration is estimated to be 29 % in Mexico (2008), 25 % in Brazil (2005) or 13 % in India (2007) or 15 % in Europe (2004), which corresponds in the last case to nearly 850 TWh for the year 2004. Due to energy performance labelling (for instance 2003/66/EG, [192]) a process of improvement of refrigeration systems is enforced and therefore in-depth knowledge has to be available about the basic principles on such systems.

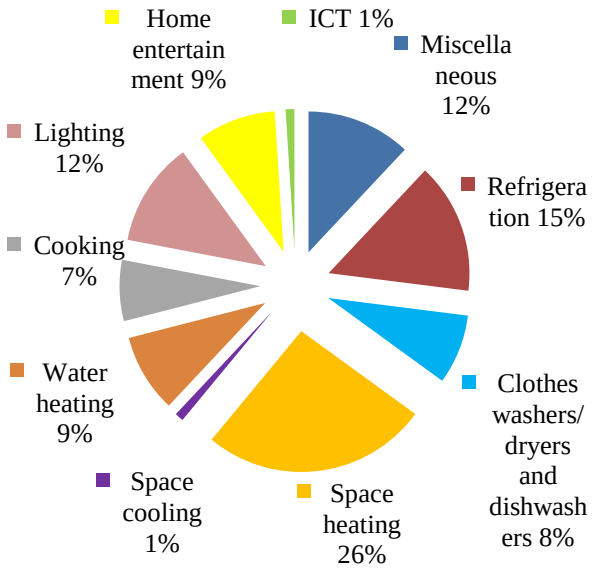

Fig. 1 Distribution of residential electricity by end-use, EU, 2004 [191].

1.1. Motivation

The illustration of potential (Fig. 1) shall be the driving force for this work, where a component of a refrigeration system is investigated. The approach to the question of energy reduction is chosen via simulation and this work serves as puzzle piece embedded in a framework of other models to achieve a tool which shall be able to precisely capture the extremely transient behaviour of a refrigeration cycle in general. Providing a tool which will predict temperatures, pressures, mass flow rates in a refrigerator or which will enable one to perform a detailed energetic evaluation, is a solid basis for understanding relationships and dependencies between main parameters. This simulation will consist of several sub-models where the expansion of the refrigerant is a main component and is treated in this work. Due to the lack of commercially available programs which can perform this task it was chosen to set up such a tool using a free integrated development environment (IDE). The availability of experimental data in literature and the possibility of performing in-house measurements gave

this work further impulse and not least the urge for understanding the links between the input- and output parameters.

1.2. Vapour compression cycles

The field of application which is covered by this work are vapour compression refrigeration cycles. Here, a short summary of its history and working principle is emphasized.

1.2.1. Historical review

Historically seen, the mass production of refrigeration systems has begun in the early 1920s [150] when technical capabilities became sufficient enough to build sealed systems. The use of capillary tubes as part of these systems was not right from the beginning since SO_2 was used as refrigerant. Its relatively high refrigerating capacity gave reason to comparably low mass flows and therefore the diameter of capillary tubes had to be decreased to a size where clogging became a realistic reason for using a different expansion device (cited by [42]). With the upcoming of halocarbons as refrigerants a couple of years later (early 1930s) this simple expansion device became more and more popular whereas the means of predicting the capillary's performance by simulation were developed, or rather applied, decades later when computers served to do the lion's share of mathematical operations (cited by [42]). Early papers presenting simulation strategies for small diameter tubes have been published at the beginning of the 1990s, laying groundwork for all different kinds of computational based investigations reaching from the appliance of simple friction drop correlations up to most complex two phase flow treatment including thermodynamic and fluiddynamic non-equilibrium. Nevertheless it has to be mentioned, that even nowadays models still use pressure drop, or viscosity correlations which were invented in the middle of the 20th century e.g. viscosity models after Davidson et al. (1943), Isbin et al. (1958), or friction models after Colebrook and White(1937 / 1938-1939), or Moody (1947) [132], [125].

1.2.2. Layout and thermodynamics

A refrigeration system consists in its most simple case of four components: *compressor, condenser, adiabatic expansion device* and *evaporator*. Fig. 2 shows such an idealized system with the simplifying assumptions of isentropic compression, no pressure drop in the heat exchangers and steady state behaviour. As refrigerant isobutane is chosen. Starting with the component which drives the cycle, the compressor (usually designed as hermetically sealed reciprocating compressor), the real compression curve leans somewhat to the left, that means the hot compressed vapour is cooled by colder tubing which leads the refrigerant out of the sealed shell. Next, the refrigerant condenses at high pressure, subcools and enters the capillary tube where expansion takes place. The expansion can be either without heat transfer (adiabatic) or non-adiabatic depending on the setup of the system. The end of the expansion device is located in the inside of the compartment which is ought to be kept at low temperature – from here on the benefit is measured, that is the ability to absorb heat energy by means of evaporation. The point where the benefit ends, depends – like everything – on the point of view. Refrigeration manufacturers, for instance, don't share their definition of "*benefit*" with compressor manufacturers and this results of course in at least two different

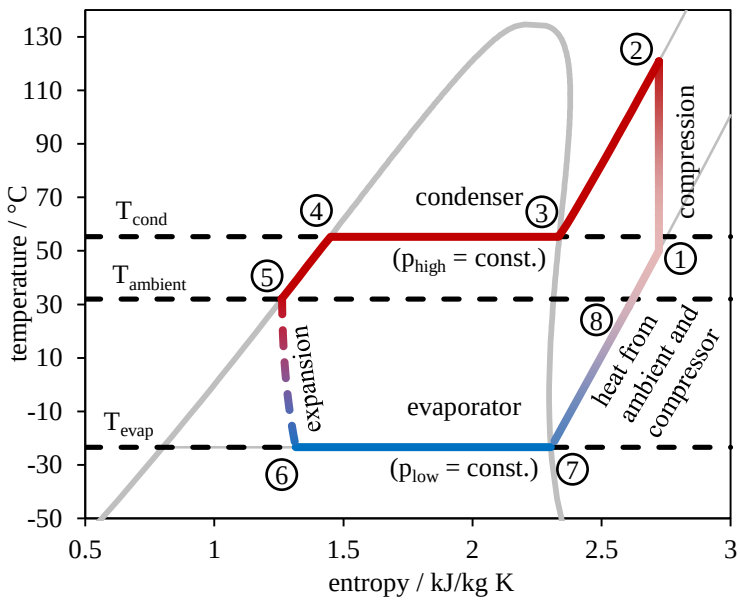

Fig. 2 Schematic drawing of a vapour compression cycle according to ASHRAE conditions [199][*].*

ways of defining "*efficiency*" within the scope of refrigeration. Generally speaking, efficiency in refrigeration is expressed as Coefficient of Performance (COP) and relates benefit to effort. Sticking close to Fig. 2, "*effort*" is the electric energy which is mainly used by the compressor (a small share remains for fans, light or user interface) whereas the amount of energy which can be used to remove heat from the compartment is the actual benefit, technically speaking, "*cooling capacity*", $\dot{Q}_0$ [W]. In terms of power, the Coefficient of Performance can be written like

$$\varepsilon = \frac{\dot{Q}_0}{P_{el}} \tag{1}$$

and reaches values well above unity. The cooling capacity, $\dot{Q}_0$, is determined under steady state conditions and can be expressed as mass flow rate times enthalpy difference between evaporator outlet and evaporator inlet.

$$\dot{Q}_0 = \dot{m} \cdot (h_7 - h_6) \tag{2}$$

Another perception of $\dot{Q}_0$ shown in eq. (3) where all temperatures below ambient temperature contribute to the cooling capacity.

$$\dot{Q}_0 = \dot{m} \cdot (h_8 - h_5) \tag{3}$$

The theoretical limit in terms of efficiency of such a cycle is defined by a reference cycle (Carnot-cycle), where the heat is transferred at constant temperature and the compression and expansion is isentropic. Eq. (4) expresses this limiting case

[*] Although the term "*ASHRAE conditions*" is common among compressor manufacturers (Embraco, Secop, Jiaxipera, Tecumseh, LG, …), the source of this term can not be traced back to its original definition. Usually, compressors are tested under certain reference conditions, commonly 90 °F (32.2°C) ambient, 130° F (54.4°C) condensing and -10 °F (-23.3°C) evaporation temperature. Subcooling and superheating reaches ambient temperature. As reference, the ANSI ASHRAE Standard 23-2005 is given, where at least the ambient condition is mentioned.

$$\varepsilon_{Carnot} = \frac{T_{evap}}{T_{cond} - T_{evap}} = \frac{1}{\eta_{Carnot}} \qquad (4)$$

from where it can be concluded that the smaller the gap between evaporation- and condensing temperature is, the higher the COP. Natural limits therefore pose the ambient temperature – the condensation process starts at temperatures above ambient and the desired temperature in the compartment defines the highest possible evaporation temperature.

A possibility to raise the performance of a refrigeration cycle when the temperature levels are given, is the implementation of an "internal heat exchanger". Why a heat exchanger? An answer to this question is not trivial at all, since the behaviour of a closed cycle is not easily predictable without closer thermodynamic considerations. First of all the overall efficiency of the refrigeration cycle can be increased when heat is transferred from the capillary tube to the suction line which leads back to the compressor, secondly it helps to avoid liquid refrigerant entering the compressor. This is illustrated in Fig. 3 where a refrigeration cycle covering the

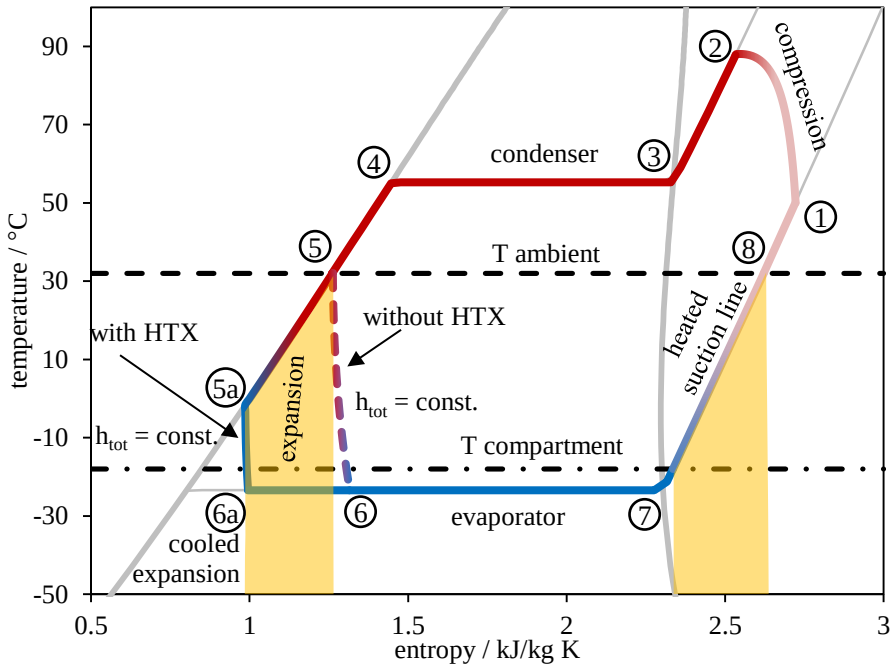

Fig. 3 Ts-diagram of isobutane showing an refrigeration cycle with and without capillary tube heat exchanger. The transferred heat is expressed by the yellow area.

two cases (with and without heat exchanger) is shown. The pressure drop in the heat exchangers (condenser, evaporator) is neglected, the compression process is simplified since the compressor is treated more or less as a "black box". In reality the compression process is more complicated since the refrigerant enters the cylinder at lower temperature than its surrounding walls (surface of piston, cylinder and valve plate). It is heated during the first phase of compression by these walls until its rise in temperature is high enough to reverse the direction of the heat flux. Then, the compressed gas usually cools even more since it has to pass through tubes and acoustic dampers which are still located inside the hermetic shell of the compressor. Also, for simplicity, the thermodynamic state of the working fluid at

beginning of the compression process is held constant. The two horizontal, dashed lines visualize the ambient temperature and the temperature in the compartment of the freezer. Accordingly, the part of the evaporator which is useful for keeping the compartment at low temperature has to have a lower temperature for sufficient heat transfer – in other words the interesting range of the evaporator is from the point on where the capillary discharges until the point where the temperatures of the compartment and the evaporator intersect. The capillary tube heat exchanger shifts the point of discharge to the left side in the Ts-diagram (5 to 5a), hence enlarging the amount of heat which can be removed from the compartment and which can be described as "benefit". The opposite side of the heat exchanger is the part of the evaporator which comes right after the compartment and which is often referred to as "suction line". At this point, the refrigerant will be heated by ambient air when the suction line leaves the insulation of the cooling appliance (7) and exactly this energy which is wasted can be used to cool the expansion process instead. One may argue that this capillary tube heat exchanger leads to a higher temperature in the shell and hence at the beginning of the compression process, a point which is certainly correct but the additional losses during compression are outweighed by the benefits of a cooled expansion. This advantage, together with the convenient and cheap production of the heat exchanger are the reason for its use in current domestic cooling applications.

Noteworthy, the above mentioned considerations are valid under steady state conditions – refrigerators like used in everybody's home never reach steady state conditions during their lifetime. The compressor is commonly connected with an On/Off-logic which regulates the target-temperature or in other cases is able to change its rotational speed (variable speed drive, VSD) in order to lower or raise the mass flow, hence the cooling power. Due to several requirements on the system like maximum cooling power for high freezing capacity or high efficiency under normal operation, the system spans a certain range of cooling power and is up to now operated intermittently. The relative duty cycle, *D*, is expressed as in eq. (5) and is around 30 % for common refrigeration devices. The duration of a single period can be minutes up to hours which makes the point clear that a steady state simulation hardly will reveal all the effects which occur in reality.

$$D = \frac{t_{on}}{t_{on} + t_{off}} \cdot 100 \quad [\%] \tag{5}$$

Fig. 4 shows results from a refrigeration cycle simulation where the inlet- and outlet conditions for capillary tube and compressor are shown. Likewise, it can be seen as boundary conditions for the heat exchangers, so the term "corner points" is more appropriate. The time interval between two neighbouring points is around 1 second. Anyway, the figure should

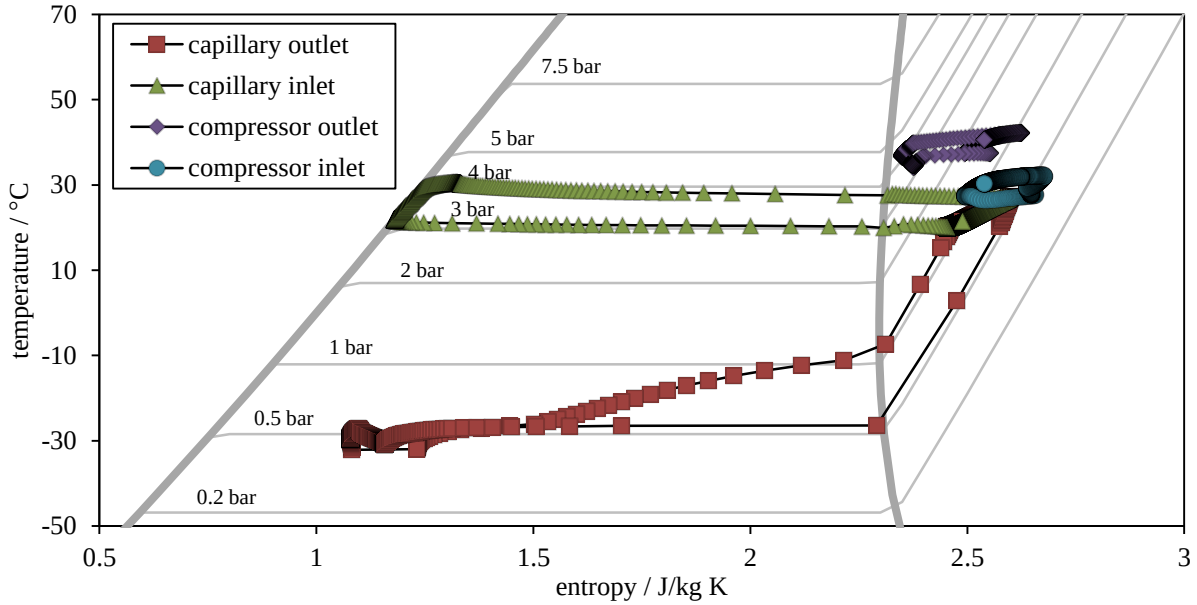

Fig. 4 Transient movement of corner points during an On/Off cycle.

demonstrate the transient nature of an On/Off controlled refrigeration cycle which certainly never reaches steady state conditions unless one switches it off. Aim of this work is to find answers on how a model may look like which primarily calculates mass flow rates for given boundary conditions (red rectangles and green triangles in Fig. 4).

1.3. Expansion devices

Before thinking of a virtual expansion device it's eventually paying off to take a short look at a physical one. The working principle of an expansion device is easy at first glance, fluid at high pressure is driven through a small bore tube where wall friction dominates. The high pressure drop leads to the effect that the actual pressure will sooner or later fall below saturation pressure and the fluid starts to evaporate. The increasing volume flow leads to a large acceleration up to the speed of sound hence to an additional pressure drop for the build-up of kinetic energy. This process comes to a halt when the low pressure level from the other end of the tube is reached. Thermodynamically speaking, after all the kinetic energy is dissipated, the fluid is at the same enthalpy as before expansion assuming that no heat had been exchanged with the wall. In general, heat transfer across the boundary has to be considered, so this case is also treated in the following discussion.

For a steady state flow the energy equation can be written like in equation (6), [169]. Index 1 indicates for this example high pressure and index 2 low pressure, q_e stands for external heat transferred to the system.

$$w_t = h_2 - h_1 + e_{e2} - e_{e1} - q_e \tag{6}$$

After some modifications, the dissipation energy, q_{fr} (heat energy due to friction) can be expressed. Therefore, the definition of reversible heat, equation (7), is used [169].

$$dq_{rev} = du + p \cdot dv = dh - v \cdot dp \tag{7}$$

Integration of the reversible heat between state 1 and state 2 of a system leads to equation (8).

$$q_{rev} = h_2 - h_1 - \int_1^2 v \cdot dp \tag{8}$$

If friction is involved, the process from state 1 to 2 is considered to be irreversible. To be able to treat this transition still as a reversible process, a reversible equivalent thermodynamic process is introduced. Here, the reversible heat (related to 1 kg) is split up in two parts, that are q_e – the heat transferred over the system boundaries and q_{fr} – the heat which originates from friction.

$$q_{rev} = q_e + q_{fr} \tag{9}$$

Putting equation (6), (8) and (9) together, the following expression can be obtained.

$$w_t = \int_1^2 v \cdot dp + e_{e2} - e_{e1} + q_{fr} \tag{10}$$

In a next step we can say, that no mechanical work is done on the system ($w_t = 0$) and the difference in external energies (potential or kinetic energy) shall be neglected ($e_{e2} \approx e_{e1}$). This results in equation (11).

$$q_{fr} = -\int_1^2 v \cdot dp \tag{11}$$

During expansion of a fluid, equation (11) balances the main energy terms and shows, that friction plays an important role. It is not specified yet how friction is introduced technically since there are several ways of doing so. For instance an orifice, a small diameter tube or any other device which leads to a similar pressure drop can be used (Fig. 5). Very popular for household applications, cheap and reliable are drawn copper or aluminium tubes, some meters in length with inner diameters below one millimeter. The name for these kinds of expansion devices "capillary-tubes" might be misleading, since the so called physical phenomenon "capillary-action" has nothing to do with its operating principle. Capillary tubes bear many advantages, they are not only cheap and easily fabricable. They also enable an equalization of system pressures in a refrigeration system during the Off-phase, which effectively reduces the starting torque for the compressor [97]. The reason why no small diameter orifice is taken is simply because of the fact, that the corresponding diameter would be so small, that the device would be prone to blocking because of impurities in the refrigerant [200]. For larger applications controlled expansion devices are in use where several designs exist. For instance electronically controlled expansion devices apply a motor to move a needle-valve in order to adjust the flow rate whereas thermally controlled expansion devices adjust the mass flow rate

according to the superheating of the evaporator-outlet. If a two-phase refrigerant leaves the evaporator because of low heat load in the compartment, this valve will close to avoid losses.

Fig. 5 Expansion Devices: Capillary tube (left), electronically controlled expansion device (middle), thermally controlled expansion device (right). Images with friendly permission of Danfoss Group Global.

1.4. Refrigerants – a short survey

The working media inside a cooling cycle is called refrigerant and has to meet certain criteria according to technical, environmental, safety and thermodynamic aspects. From these categories several knock-out criteria for using substance in a cooling application emerge and therefore make the choice a tedious endeavour.

- **Technical considerations:**

Due to the working principle of a conventional refrigeration cycle the refrigerant undergoes phase change, compression and expansion. Since during phase change pressure and temperature are dependent on each other, the low pressure is determined by the desired target temperature on the cold side which means the evaporation temperature has to be below target temperature. On the other hand side, during condensation, heat shall be transferred to ambient air and therefore the temperature has to lie above ambient temperature which fixes the high pressure in the system. To come finally to the point, if the condensing temperature is at let's say 45 °C and therefore the corresponding condensing pressure, simply the saturation pressure at this temperature, will be so high that leakage or safety risks emerge, the refrigerant obviously is not suited for this application. The critical point of carbon dioxide is at 30.1 °C and 73.8 bar which means that for its use in vapour compression cycles the vapour has to be compressed beyond the critical point – therefore CO_2 plays no role in the field of domestic cooling applications.

Firstly, the refrigerant properties should feature low pressure at condensing temperatures of the system due to mechanical considerations [196].

Secondly, the refrigerant is required to have a freezing point below the evaporation temperature which for instance knocks out pure water as refrigerant for domestic cooling appliances [196].

Thirdly, a non-corrosive media concerning copper, aluminium and steel is preferred since most of the refrigeration components consist of these materials [196].

- **Environmental considerations:**

Zero Ozone Depletion Potential (ODP) are the nowadays' requirements not just within Europe but in all states who signed the Montreal Protocol which took effect first in 1989. Five changes to the original protocol followed (1990, 1992, 1995, 1997, 1999) which all in all lead to a ban of CFCs and HCFCs. For the exact limits on dates for individual countries the reader is referred to [194]. As a matter, several "old" refrigerants had and still have to be replaced. Table 1 provides a survey over 13 refrigerants together with their chemical and thermodynamic data.

Low Global Warming Potential (GWP) becomes an increasingly important property since some refrigerants (like R11, R12, R125, ...) unfortunately feature CO_2 - equivalents (100 year) between 10^3 and 10^4. Regulations and restriction are influencing the scope of application of such refrigerants and will lead to a change to low- or zero-GWP working media [195].

- **Safety considerations:**

Concerning safety, "Non-toxic" and "inflammable" are the keywords here. Some refrigerants used in domestic refrigeration, though, are flammable (butane, pentane) but since the amounts stored in a refrigerator (around 30 g to maximum 150 g) are of minor concern if released in an average sized room the flammability matters less than toxicity. The regulations IEC 60335-2-24 and IEC 60335-2-89 of the International Electrotechnical Commission restrict the maximum charge of flammable refrigerants to 150 g per device, toxic refrigerants are not used in domestic refrigeration.

- **Thermodynamic considerations:**

The volumetric cooling capacity is the cooling capacity (section 1.2) related to the specific volume of the saturated vapour at evaporation temperature:

$$q_v = \frac{q_0}{v_{v,sat}} \tag{12}$$

Assuming two refrigerants in a cycle with different volumetric cooling capacities but with equal volume flow rates and cooling capacities, the mass flow rate for the parts facing vapour phase would be different. This means, a refrigerant with high volumetric capacity demands a smaller compressor to reach the same cooling capacity. If this is favourable or not can't be said as a general rule since in domestic refrigeration the compressors' size is already close to the technical limits of what's reasonable in terms of efficiency. For commercial cooling purposes a refrigerant with high volumetric capacity certainly can show its advantage.

Table 1 Properties of refrigerants. Source: NIST standards [201] and BITZER Kältemittelreport 16 [193].

refrigerant	elemental formula	p_{crit}	T_{crit}	M	Safety group	GWP (100a)	ODP
-	-	bar	°C	g/mol	-	CO_2=1.0	R11=1.0
R290	$CH_3CH_2CH_3$	42.51	96.74	44.10	A3	3	0
R600a	$CH(CH_3)_2CH_3$	36.29	134.66	58.12	A3	3	0
R11	CCl_3F	43.50*	197.96*	137.4*	A1†	4750†	1†
R12	CCl_2F_2	40.82*	111.97*	120.9*	A1†	10900†	1†
R22	CHC_lF_2	49.9	96.15	86.47	A1	1700	0.055
R123	$CHCl_2CF_3$	36.62	183.68	152.93	B1	90	0.02
R1234yf	CF_3CFCH_2	33.82	94.70	114.04	n.a.	4	0
R32	CH_2F_2	57.82	78.11	52.02	A2	650	0
R125	CHF_2CF_3	36.18	66.02	120.02	A1	3400	0
R134a	CH_2FCF_3	40.59	101.06	102.03	A1	1300	0
R717	NH_3	113.33	132.25	17.03	B2	0	0
R744	CO_2	73.77	30.98	44.01	A1	1	0
R410a	R32/R125	49.01	71.34	72.59	A1	1980	0
R407c	R32/R125/R134a	46.32	86.20	86.20	A1	1650	0

These refrigerants can be classified according to their chemical composition:

- **Pure Fluids**
  - **HC (Hydrocarbons)**
    - R290 (propane)
    - R600a (isobutane)
  - **CFC (Chlorofluorocarbons)**
    - R11 (Trichlorofluoromethane / Freon-11) – BANNED
    - R12 (Dichlorodifluoromethane / Freon-12) – BANNED
  - **HCFC (Hydrochlorofluorocarbons)**
    - R22 (chlorodifluoromethane) – BANNED
    - R123 (2,2-dichloro-1,1,1-trifluoroethane) – BANNED
  - **HFC (Hydrofluorocarbons)**
    - R32 (difluoromethane)
    - R125 (pentafluoroethane)
    - R134a (1,1,1,2,-tetrafluoroethane)
    - R1234a (2,3,3,3,-tetrafluoropropene)

* http://encyclopedia.airliquide.com/encyclopedia.asp (accessed 11.03.2014)
† http://www.carrier.de/dasat/images/6/100256-die-qual.pdf (accessed 11.03.2014)

Alternative refrigerants

R717 (ammonia)
R744 (carbon dioxide)

- **Blends**

  R410a (R32 / R125)
  R407c (R32 / R125 / R134a)

Coming back to the question *"what is a good refrigerant?"* it firstly has to be specified in terms of kind of refrigeration (domestic/commercial/industrial, air-conditioning/cooling, country, ...). Since this work is meant to support projects which deal with domestic refrigeration in Europe the answer concerning the choice of refrigerant is as follows. The media must be non-toxic, zero ODP and low GWP which reduces the possible scope to a few candidates. In Europe R600a is predominant and is chosen despite its flammability whereas R134a dominates in many other regions of the world.

A short look on two different temperature-entropy plots of R134a and R600a shows the different shapes of the saturation curve (Fig. 6). The most obvious difference is the shape of the saturation lines particularly the vapour saturation line. R600a even changes slope from negative to positive and is named a "dry" fluid therefore. This term comes from the fact that in an expansion process (e.g. turbine) this fluid is unlikely to expand from superheated vapour into the two phase regime which would lead to formation of droplets and damage ("wet" fluid). But, since a cooling cycle is of opposed direction in the Ts-plot and compression replaces expansion, not the "dry" but the "wet" refrigerant (R600a) may theoretically cause problems during compression. That is when nearly isentropic compression starts at low pressure and little superheating and would lead right into the two-phase region. Since in domestic cooling applications the superheating of compression start- and end-temperature is sufficiently high this issue is of low importance. Since temperature is coupled to pressure in the two phase region, the evaporating pressure of a refrigeration system

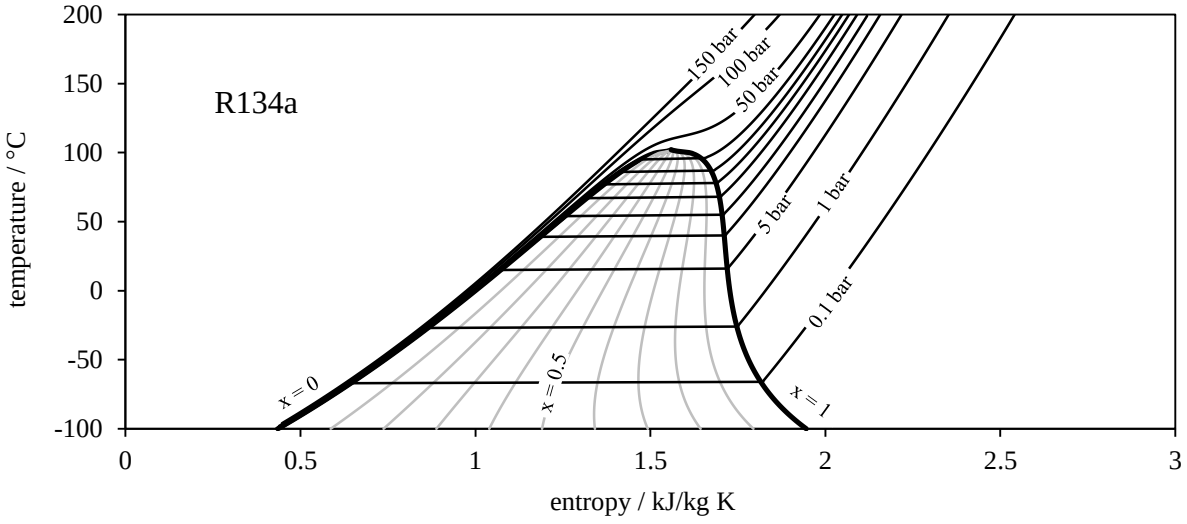

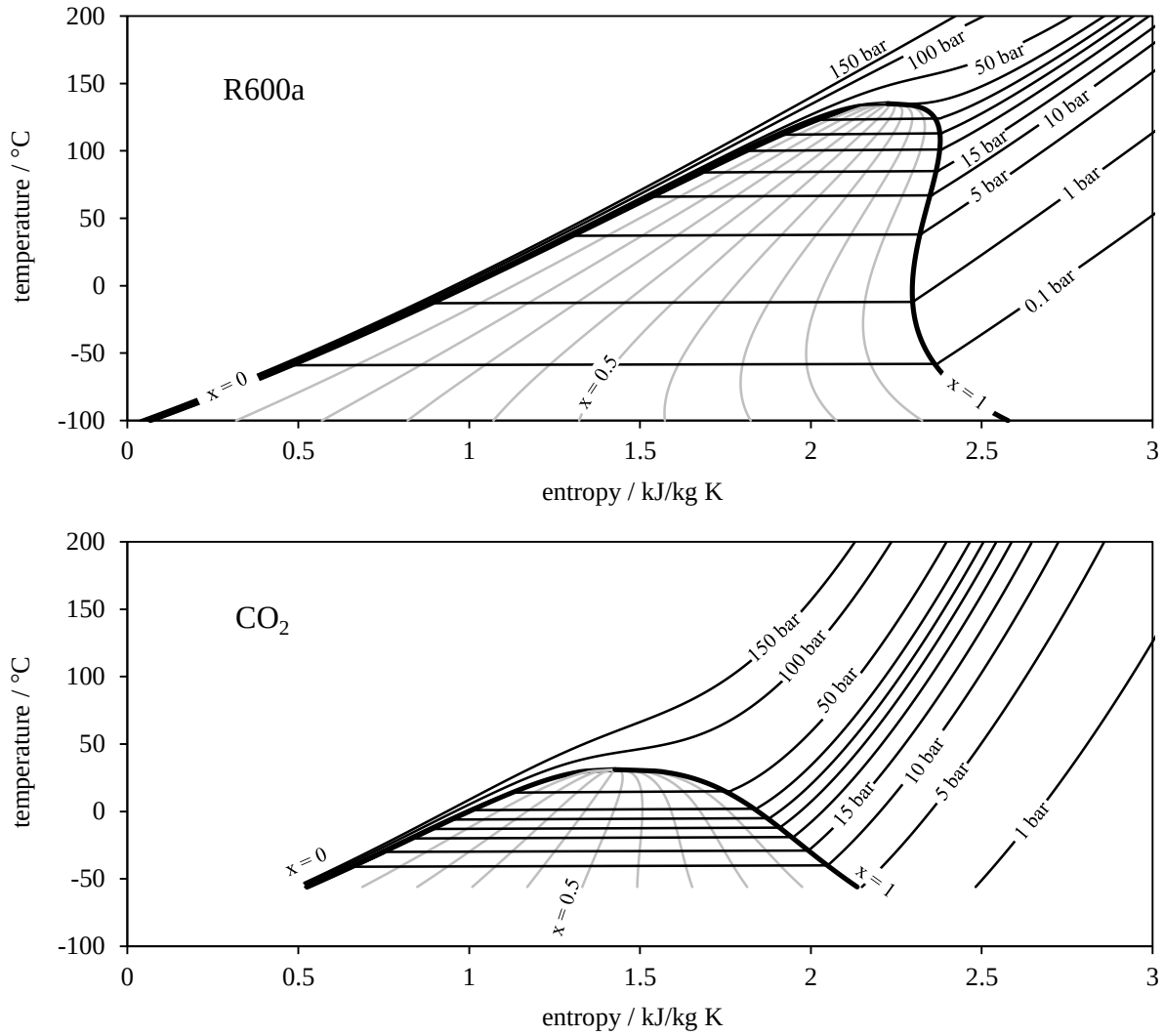

Fig. 6 Ts-diagrams of R134a (top), R600a (middle) and CO_2 (bottom). Source: NIST standards [201].

is determined by the desired compartment temperature minus the temperature difference of the heat exchanger. Since the cycle-efficiency grows with decreasing temperature difference between condensing and evaporating, the condensing pressure is limited – it must be higher than saturation pressure at ambient temperature. Since under standardized test-conditions the ambient temperature is raised up to 43°C the resulting condensing pressure peak must be resisted by the system. For CO_2 this would mean operation under supercritical conditions and a condensing pressure beyond 74 bar and certainly is more challenging in terms of manufacturing and safety.

2. Pipe flow – friction and viscosity

Among all phenomena which are of interest in pipe flow for engineering purpose, friction is most certainly topping the list. Heat transfer or oscillations may also be worthy candidates, but heat transfer gets its own chapter later on and oscillations are not subject of this thesis – so friction comes first. In fact, for capillary tubes friction *is* the most important effect where one can introduce significant errors by choosing correlations which are out of range for this application and in fact most of the friction correlations are set up originally for pipe flow in more "applied" solutions without phase change. On the other hand – friction correlations for heat exchangers may comprise phase change but are designed for low pressure drop and usually higher mass flow rates than 1 kg/s. So, first of all let's take a closer look at the characterization of the flow and try to find common ground for all capillary tubes in order to have some restrictions in choosing well suited empirical friction laws. Then, friction models are presented for single phase flow, a short investigation on viscosity follows and finally friction laws for two phase flow are explained with knowledge that the range of application is domestic refrigeration which determines more or less the size and flow parameters in advance. A closer selection follows when the capillary tube model is set up and ready to be validated (section 4.2.3).

2.1. Flow regimes

A word on the differentiation of flow regimes in pipe flow shall be given here. When it comes to phase change (evaporation, condensation) this phenomenon is not restricted to a single cross section but happens along a region, depending on flow parameters, the heat flux, the shape of the pipe, gravity and the thermophysical properties of the fluid. Since that amount of

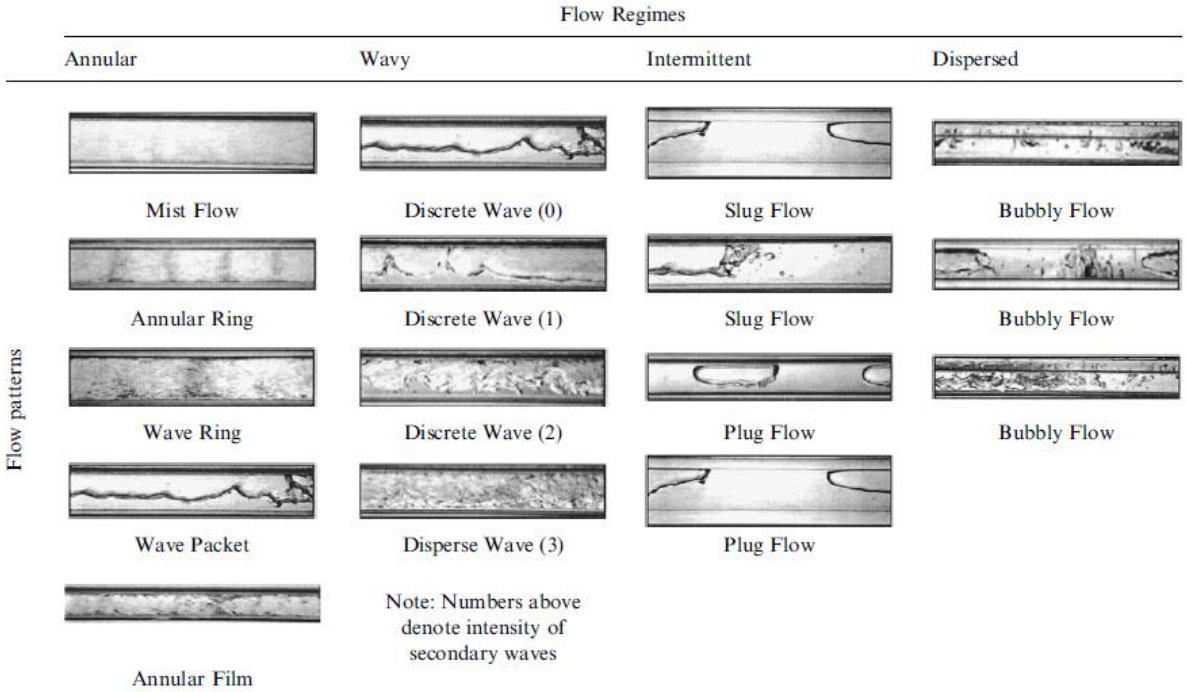

Fig. 7 Condensation flow regimes for R134a in pipe flow, reprinted from Coleman and Garimella [139] with permission of Elsevier.

dependencies general predictions can't be made but detailed investigations of each case are necessary. Fig. 7 shows exemplarily flow regimes for condensation of R134a where four flow regimes are examined and subdivided to patterns. Although the shown pipes are of larger diameter than capillaries some of these patterns may emerge also in latter ones. Many attempts have been made in order to describe the different flow regimes in terms of heat transfer and friction resulting in a vast amount of empirical formulae and flow pattern maps. A flow pattern is a chart where the transition lines between the regimes are plotted, commonly mass flux [kg/m^2 s] versus vapour quality [-], for a certain tube geometry (cross section, diameter, position), fluid, temperature and mass flux. In other words, flow maps have to be specifically designed for each application – for capillary tubes operated with R600a not much work has be done up to now. Existing flow maps for microchannels feature refrigerants other than R600a and maps for R600 flow are out of range regarding diameter. Keeping that in mind an attempt is made using the flow maps of El Hajal et al. [141] for a typical operating point of a capillary tube. Although their correlations were designed primarily for condensation they also come with an extension for evaporation. The only drawback is the diameter range of their charts which is given by 3.14 < d < 21.4 mm. Additionally, it is unlikely that critical flow and flash evaporation are treated in their investigations so the outcome has to be treated with care. Simply for curiosity, assuming a 0.7 mm adiabatic capillary with a nominal mass flow rate of 1 kg/h, R600a as working media, one can draw Fig. 8 and within this figure the solid red line shows the transition of regimes when it crosses the solid black lines. The blue region points out the range of a typical capillary tube, so one can see clearly that an intermittent flow type is predicted for most of the time which doesn't agree with observations. Intermittent flow or wavy flow is gravity clearly influenced whereas in our case gravity influences to a negligible amount the critical mass flow rate. Therefore the inadequacy of this flow pattern map is demonstrated and since no better ones are mentioned for this application the visual investigations of Motta et al. [68] justify the assumption of bubbly flow along the tube.

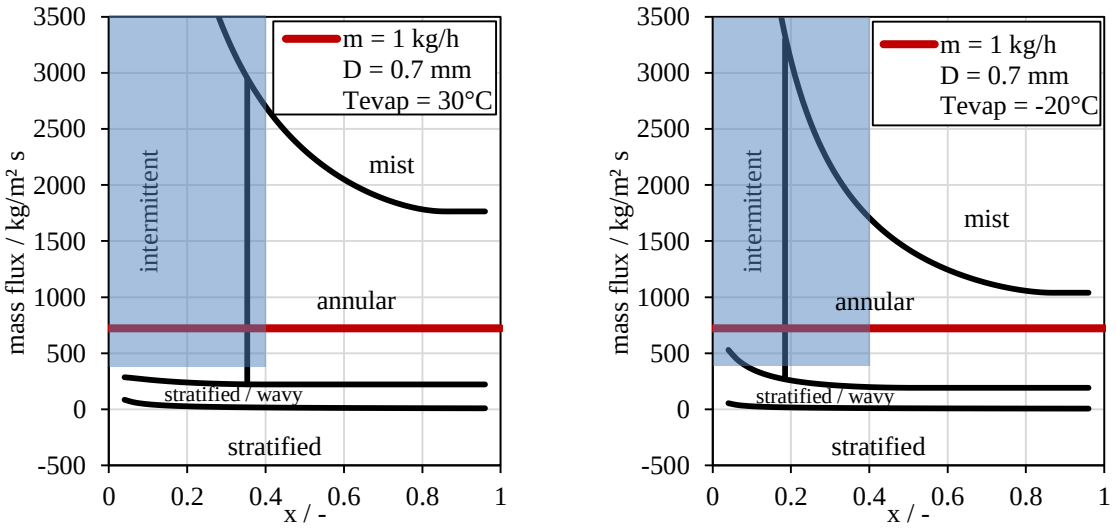

Fig. 8 Expected flow patterns for capillary tubes under operating conditions (blue area). Maps according to El Hajal et al. [141] for 30°C (left) and -20°C (right) evaporation temperature..

The differentiation of flow regimes may be necessary when friction and heat transfer are concerned since a change of flow pattern also can lead to a change in these parameters. Hence, one can expect that the knowledge of the correct flow pattern is important in heat exchanger design, where a single phase is transferred via condensation or evaporation fully to its counterpart and where the quality (and void fraction) spans a range covering every value between 0 and 1. In a capillary tube this is not the case since the refrigerant enters subcooled and leaves with a quality around 0.3 depending on the inlet enthalpy and the heat flux in the heat exchanger section which reduces the amount of possible flow patterns for this application from the start. Also the fact that the Reynolds number is fairly high in the two phase region in a capillary, mixing between the phases occurs therefore excluding regimes like wavy or stratified flow completely.

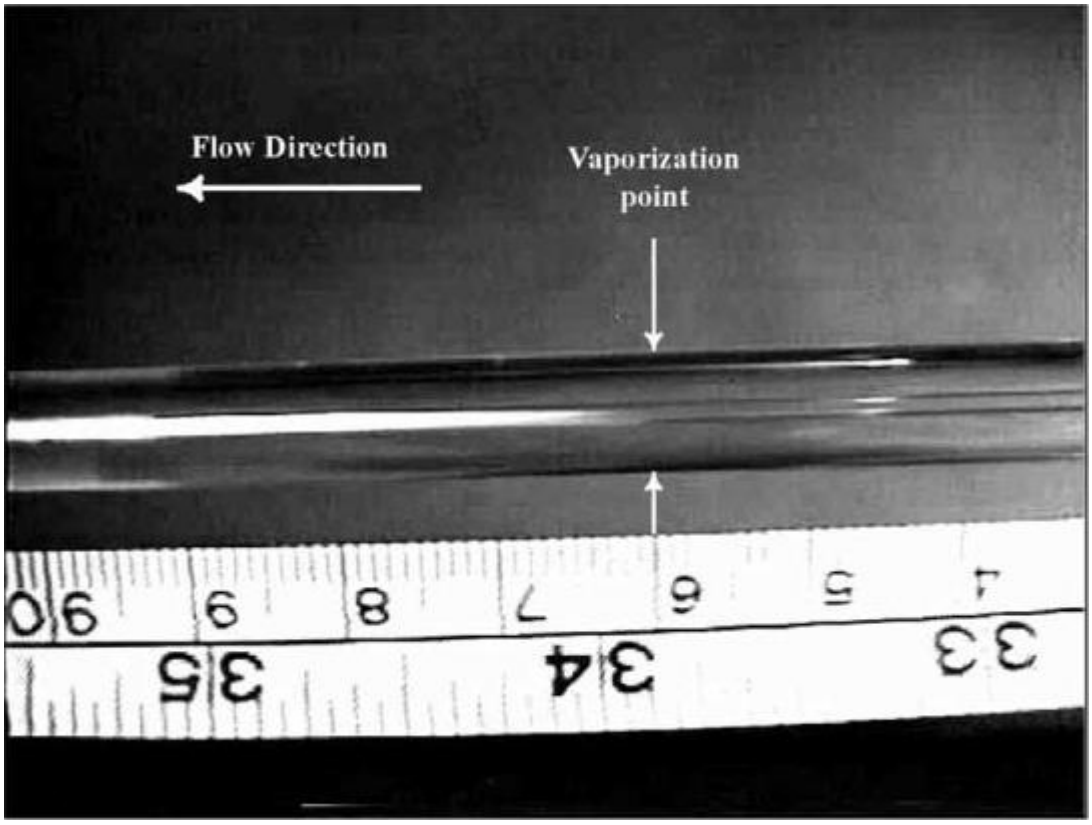

Fig. 9 Onset of vaporization of R404a/oil in a glass capillary tube, reprinted from [68]with permission of Elsevier.

Motta et al. [68] concluded from visual observations in a glass capillary tube operated with R404a that the main flow regime is bubbly-type (Fig. 9). They also mention a reference where a stroboscope was used to get a clear snapshot of the flow after onset of evaporation. The investigation fortifies the guess that small bubbles under turbulent conditions occur and prevail throughout the capillary. Therefore the assumption of a single flow regime is justified.

Seixlack and Barbazelli [83], however, differentiate for their two fluid model (working with R134a) between bubble, churn and annular flow and use fixed values for void fraction as transition criteria (0.3 for bubble/churn transition and 0.8 for churn/annular transition). They are aware of the fact that the transition doesn't occur at these fixed values but depends on the

geometry of the tube and flow parameters. Owing to the absence of an applicable flow pattern map this solution seemed to be the most promising one. The same flow regimes along with the same transition criteria are reported in [154], also a two fluid model.

For reasons concerning heat transfer calculations, Garcia Valladares [32], takes the annular and wavy regime for condensation into account where the Froude number serves as transition criterion and applies it also for evaporation. He uses it also for a separated flow model with capillary tube heat exchanger.

Concludingly, for this work a detailed flow regime differentiation does not make sense due to the lack of specific correlations for each regime as can be seen in the next chapters. Also the differentiation itself causes some problems since the high pressure drop in combination with the unfortunate geometry (small inner diameter vs. large length) doesn't seem to favor visual studies and efforts to characterize the flow therein. For the homogeneous model, friction and heat transfer are calculated using expressions depending only on main flow parameters (velocity, quality, density, ...) which feature a continuous behaviour irrespective of the flow regime but yield good predictability. This assumption dominates also in literature, the few exceptions (two fluid models) use the regime differentiation mainly for reasons of vapor-liquid interaction which has not to be treated in a homogeneous model.

2.2. Friction models

The dominant effect in microchannel flow is friction. Therefore a whole sub-chapter seems not too much for summarizing methods and equations which are all part of the capillary tube model (or at least seemed to promise good agreement at the beginning). Friction in general occurs where moving meets resting, where bodies with diverse speed interact – due to the irrelevance of who is moving relative motion may be named as cause for friction. The other one is the nature of two bodies to interact in such a way where the faster accelerates the slower, the slower brakes the faster, the motivated ones electrify the lazy, the even tempered calms the hothead. To speak from now on a little more in terms of fluid dynamics the requirements for friction are a gradient in velocity and viscosity. Exemplarily shown in Fig. 10, the most frequent example of friction in fluids is a flat rigid plate, pulled across a reservoir of fluid. The plate as well as the direction of movement is oriented parallel to the ground and the distance between plate and ground (y-direction) is denoted by h. Assuming infinite extension of the domain in directions other than y one experiences that the shear stress is proportional to $\dot{\gamma}$, the shear rate or the gradient of velocity u in respect to y. This relation was already known to Newton, who, according to Franco and Partal [186] wrote in the first English edition of *Philosophiae Naturalis Principia Mathematica*, translated by Andrew Motte in 1729:

"The resistance arising from the want of lubricity in the parts of a fluid, is others things being equal, proportional to the velocity with which the parts of the fluid are separated from one another."

Derived from Newton's statement and put into mathematical style like eq. (13) this formula is named "Newton's law of viscosity".

$$\tau(y) = \mu \frac{du}{dy} = \mu \dot{\gamma} \tag{13}$$

$$\mu = f(p,T) \quad [Pa\ s] \tag{14}$$

Often, the term "Newtonian fluid" is mentioned at this particular place and definitions like *"... the shear stress is proportional to the shear rate ..."* are meant to be in good hands. However, more precisely, Newtonian fluids are defined in such a way that its viscosity is a function of temperature, pressure and nothing else [186]. When "viscosity" is mentioned here, the dynamic viscosity (Greek "mu", μ) is meant with its unit "Pa s". This must not be confused with the kinematic viscosity (Greek "nu", ν) and units "m^2/s" which is the ratio of dynamic viscosity and density. The reason why they are mixed up so commonly may be the fact that they are always mentioned at the same time (as it is here). Within the scope of this work the dynamic viscosity is used throughout to prevent confusion. For one-dimensional pipe flow some steps still have to be explained in order to be able to calculate the pressure drop for a given flow. Therefore equation (15) is used which relates the coefficient of friction to a pressure difference. D is the diameter of the pipe element, l its length, $\bar{u}$ the average velocity and $\bar{\rho}$ the average density of the fluid.

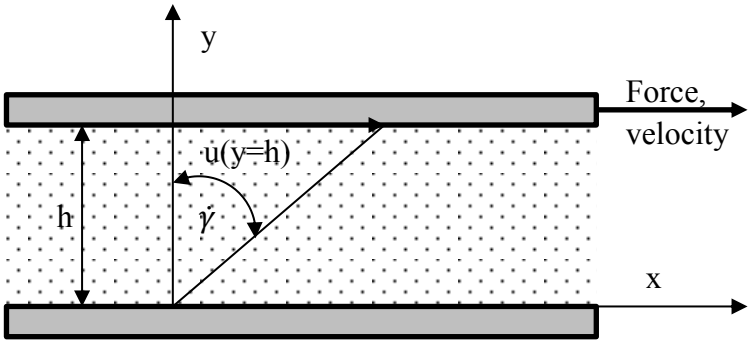

Fig. 10 Visualization of shear in fluids.

$$\Delta p = \lambda \frac{l}{D} \bar{\rho} \frac{\bar{u}^2}{2} \quad where \quad \lambda = \lambda\left(Re, \frac{\varepsilon}{D}\right) \tag{15}$$

In the following the friction coefficient λ has to be found – this is usually done experimentally, particularly when it comes to turbulent flow which is the case for capillary tube flow. A short collection of the most common equations in the scope of this work shall be given. All of these equation are primarily used in applications for single phase flow.

Churchill (cited by [16], [102], [125])

Range of validity: laminar, transition and turbulent

$$\lambda = 8\left(\left(\frac{8}{Re}\right)^{12} + \frac{1}{(A+B)^{1.5}}\right)^{\frac{1}{12}} \tag{16}$$

$$A = \left(2.457 \cdot \ln\left(\frac{1}{\left(\frac{7}{Re}\right)^{0.9} + 0.27\left(\frac{\varepsilon}{D}\right)} \right) \right)^{16} \tag{17}$$

$$B = \left(\frac{37530}{Re}\right)^{16} \tag{18}$$

Colebrook-White (cited by [26], [100], [134])

Range of validity: $4 \cdot 10^3 \leq Re \leq 10^8$
$0 \leq \varepsilon/D \leq 0.05$

$$\frac{1}{\sqrt{\lambda}} = -2 \cdot \log\left(\frac{\varepsilon/D}{3.7} + \frac{2.51}{Re \cdot \sqrt{\lambda}}\right) \tag{19}$$

Blasius (cited by [26], [125])

Range of validity: $2320 \leq Re \leq 10^5$
hydraulically smooth

$$\lambda = 0.3164 \cdot Re^{-0.25} \tag{20}$$

Haaland (cited by [11])

Range of validity: $4000 \leq Re \leq 10^8$
$10^{-6} \leq \varepsilon/D \leq 0.05$

$$\lambda = \left(-1.8 \cdot log\left(\left(\frac{\varepsilon}{3.7 \cdot D}\right)^{1.11} + \frac{6.9}{Re} \right) \right)^{-2} \tag{21}$$

Nikuradse (cited by [131])

Range of validity: $10^5 \leq Re \leq 10^8$
hydraulically smooth

$$\lambda = 0.0032 + 0.221 \cdot Re^{-0.237} \tag{22}$$

Laminar flow [128]

Range of validity: $Re < 2300$

$$\lambda = \frac{64}{Re} \tag{23}$$

To better understand the requirements of a friction model for capillary tubes one has to note that for average drawn copper tubes the surface roughness is around 1 micron [189] and the inner diameter around 1 mm. This leaves us with a roughness/diameter ratio of about 0.001. The influence of surface roughness is accounted for in Churchill's, Haaland's and Colebrook-White's correlation. The rest of the correlations assume hydraulically smooth tubes, which means that the surface roughness lies within the laminar sublayer of the flow. Due to further investigations about the influence of surface roughness on the mass-flow and the broad range of applicability, the correlations by Churchill and Colebrook-White are first choice for this work. Fig. 11 shows the friction factors for Reynolds-numbers from 10^3 to 10^7 for a roughness/diameter ratio of 0.001.

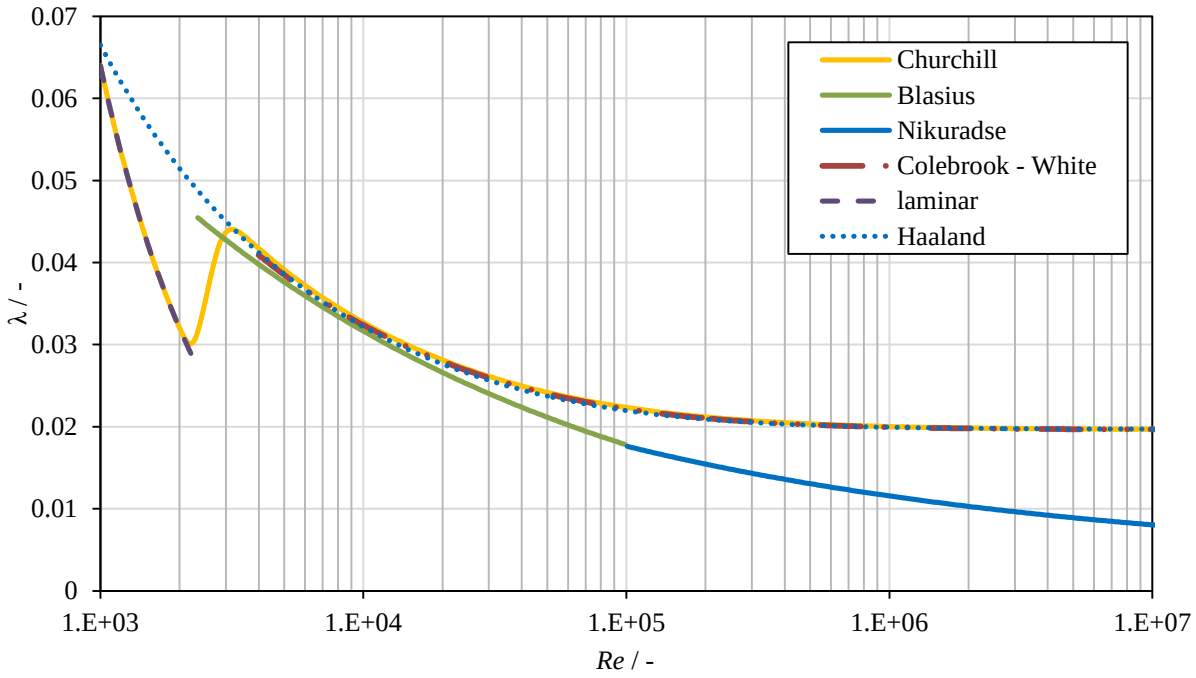

Fig. 11 Friction factor versus Reynolds number for different models.

2.3. Two phase viscosity models

When a homogeneous model is applied some thoughts have to be spent on the viscosity which is certainly well defined in the single phase region and computed according to latest NIST standards [201] but what happens in the two phase regime?

The basic idea is to assign a viscosity to each state within the two phase regime by means of averaging with the viscosities at saturation. Though the resulting viscosity is an artificial one it enables to predict pressure drops by using the same correlations as for single phase flow in chapter 2.2. If this method is not accurate enough, more sophisticated ones have to be chosen and this adjustment may also contain the computational scheme as a whole and suddenly one ends up with a set of 6 conservation equations and their coupling instead of 3. As a step between these two extrema the possibility still exists to identify in a homogeneous model different flow regimes and assign special empirical friction/viscosity laws to each of them. Since a capillary tube model can be accomplished by a homogeneous flow assumption quite well the essence of this model lies in the equations below. All of them have in common that the resulting average viscosity consists of parameters no other than liquid and vapour densities or viscosities, vapour quality and void fraction. The void fraction α is defined as ratio of the vapour cross section and the channel cross section, the quality *x* is related to the mass likewise (eq. (24)).

$$\alpha = \frac{A_v}{A} \quad and \quad x = \frac{m_v}{m} \tag{24}$$

The velocities of vapour and liquid can be expressed as

$$u_l = \frac{\dot{V}_l}{A_l} = \frac{\dot{m}_l}{\rho_l \cdot A_l} = \frac{\dot{m}}{\rho_l \cdot A} \cdot \frac{(1-x)}{(1-\alpha)} \tag{25}$$

$$u_v = \frac{\dot{V}_v}{A_v} = \frac{\dot{m}_v}{\rho_v \cdot A_v} = \frac{\dot{m}}{\rho_l \cdot A} \cdot \frac{x}{\alpha} \tag{26}$$

Combining eq. (25) and (26) the void fraction can be calculated and expressed as function of vapour quality, densities and slip ratio *S*, which is unity for homogeneous flow.

$$\alpha = \frac{1}{1 + \frac{1-x}{x} \cdot \frac{\rho_v}{\rho_l} \cdot S} \quad for \quad S = \frac{u_v}{u_l} \tag{27}$$

The following summary provides a survey over two phase viscosity models, the selection of appropriate viscosity and friction models is done in section 4.2.3:

Lin (cited by [124], [98], [125])

$$\mu_{tp} = \frac{\mu_l \cdot \mu_v}{\mu_v + x^{1.4} \cdot (\mu_l - \mu_v)} \tag{28}$$

Cicchitti (cited by [124], [98], [125])

$$\mu_{tp} = (1-x) \cdot \mu_l + x \cdot \mu_v \tag{29}$$

Isbin (cited by [124])
This equation is sometimes also referred to "**Mc Adams**" but it is not traceable to its original reference. For the sake of completeness this shall be mentioned here. Compared to Cicchitti's mixing equation (29) this would correspond to a parallel connection weighted by the mass fractions.

$$\frac{1}{\mu_{tp}} = \frac{x}{\mu_v} + \frac{1-x}{\mu_l} \tag{30}$$

Bittle and Weis (cited by [125])

$$\frac{1}{\mu_{tp}} = \frac{\alpha}{\mu_v} + \frac{1-\alpha}{\mu_l} \tag{31}$$

Dukler (cited by [124], [98], [125])

$$\mu_{tp} = \frac{(1-x)\cdot\mu_l/\rho_l + x\cdot\mu_v/\rho_v}{(1-x)/\rho_l + x/\rho_v} \tag{32}$$

Akers (cited by [124])

$$\frac{1}{\mu_{tp}} = \frac{1}{\mu_l}\cdot\left[(1-x) + x\sqrt{\frac{\rho_l}{\rho_v}}\right] \tag{33}$$

Beattie and Whalley (cited by [124], [98], [125])

$$\mu_{tp} = \mu_v\cdot\alpha + \mu_l\cdot(1-\alpha)\cdot(1+2.5\cdot\alpha) \tag{34}$$

Owen (cited by [98])

$$\mu_{tp} = \mu_l \tag{35}$$

Davidson (cited by [124])

$$\mu_{tp} = \mu_l\cdot\left[1 + x\frac{1/\rho_l - 1/\rho_v}{1/\rho_v}\right] \tag{36}$$

In Fig. 12 (a) variation of the quality shows the behaviour of the different models where some special features become obvious. Firstly: The model of Beattie and Whalley has the unfortunate property of mixture viscosities higher than liquid viscosity for small void fraction values. Secondly, the models of Owen, Davidson and Akers don't meet the vapour viscosity when the quality becomes unity – therefore a discontinuity has to be expected when one returns from the two phase regime to the single phase calculation of viscosities.

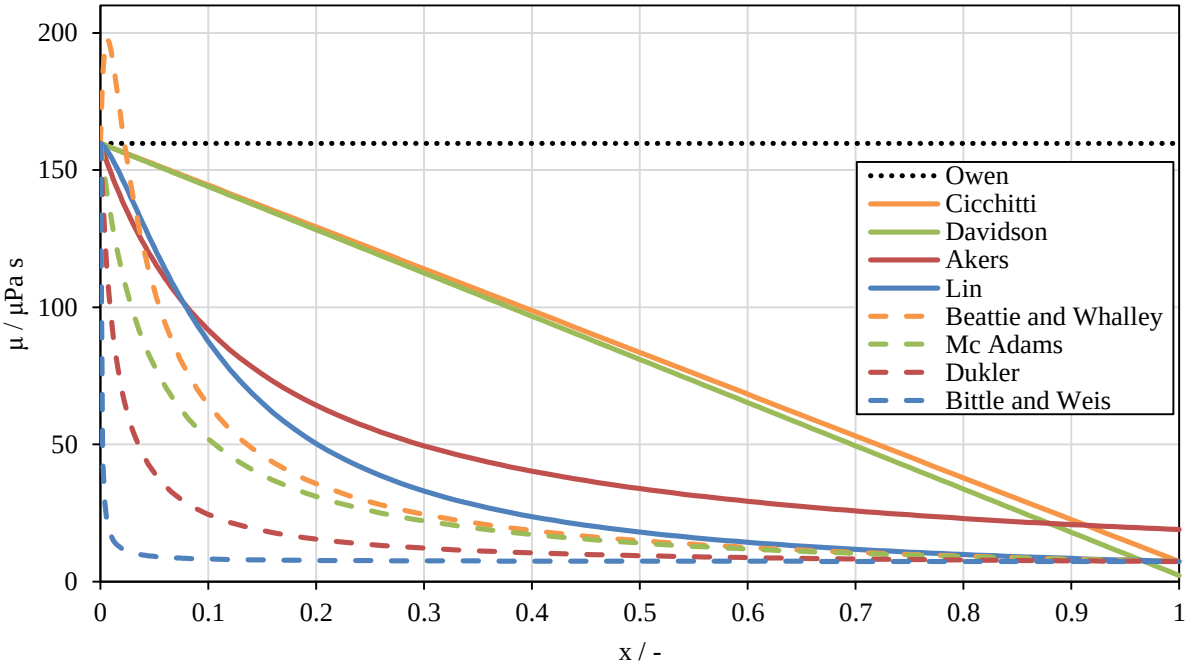

Fig. 12 Two phase viscosity versus quality at constant pressure (3 bar) for different models.

2.4. Two phase multipliers

The friction factors described in section 2.2 are applicable for flows of pure liquid or gas but not for a mixture of both. In order to achieve this, several approaches – all based on a more or less pinch of empiricism – exist. This section deals now with the friction factors for two phase flow where the flow is not treated as a homogeneous phase like it is the case in 2.3 where mean viscosities are utilized. Since a vast amount of correlations for frictions in any possible geometry exist the field is narrowed down in advance to the domain of capillary tube flow which is turbulent and which features bubbly flow with very small vapour bubbles compared to the diameter of the tube and low differential velocity between the two phases.

One way of treatment – implemented in the current capillary tube model and frequently cited in literature – is to extend the friction factor for single phase by a certain factor which depends on flow parameters. These kinds of factors are called two phase multipliers. A closer description of these factors according to Friedel, Lin, Lockhart-Martinelli and Chisholm follows now along with a step by step description of implementation. Before, a short explanation of the notation – "l" and "v" as subscripts mean "liquid" and "vapour" and refer to the liquid or vapour part of the flow whereas "lo" and "vo" mean "liquid only" and "vapour only". The latter means that the whole flow through the channel is assumed to be either liquid only or vapour only. This can be used for instance in the following way where the Reynolds number is evaluated under the assumption that the flow were liquid only: $Re_{lo} = (\dot{m}_{tot} \cdot d)/(\mu_l \cdot A)$ which means that the two phase fluid is replaced by a single fluid with the same mass flow rate.

Before setting up his own correlation for two phase pressure drop in 1980 Friedel [126] gave a survey of 14 common formulae for frictional pressure drop – he didn't leave the chance to

mention the innumerable amount of them – comparing them in terms of involved system parameters as well as accuracy. Concerning frictional pressure drop his opinion is that due to the complex fluid vapour interaction a purely theoretical approach is hindered and measurements are indispensable. A high error margin of 30 to 100 % has to be expected when correlations for frictional pressure drop are applied without prior knowledge and healthy caution.

Field and Hrnjak [125] provide an excellent overview of pressure drop correlations for single flow, homogeneous models (viscosity correlations) and separated flow models (two phase multipliers) and are therefore cited as main reference.

Friedel two phase multiplier ([127], [126] and cited by [125])

$$\Phi_{lo}{}^2 = C_1 + \frac{3.24 C_2}{Fr_{av}{}^{0.045} \cdot We_{av}{}^{0.035}} \tag{37}$$

$$C_1 = (1-x)^2 + x^2 \cdot \frac{\rho_l}{\rho_v} \cdot \frac{\lambda_{vo}}{\lambda_{lo}} \tag{38}$$

$$C_2 = x^{0.78} \cdot (1-x)^{0.24} \cdot \left(\frac{\rho_l}{\rho_v}\right)^{0.91} \cdot \left(\frac{\mu_v}{\mu_l}\right)^{0.19} \cdot \left(1 - \frac{\mu_v}{\mu_l}\right)^{0.7} \tag{39}$$

$$G = \frac{\dot{m}}{A} \tag{40}$$

$$Fr_{av} = \frac{G^2}{g \cdot d_h \cdot \rho_{av}{}^2} \tag{41}$$

$$\frac{1}{\rho_{av}} = \frac{x}{\rho_v} + \frac{1-x}{\rho_l} \tag{42}$$

$$We_{av} = \frac{G^2 \cdot d_h}{\sigma \cdot \rho_{av}{}^2} \tag{43}$$

The two phase multiplier is applied in the following way to get the friction coefficient:

$$\lambda_{tp} = \lambda_{lo} \cdot \Phi_{lo}{}^2 \tag{44}$$

As stated by Field and Hrnjak [125] the correlation doesn't lead to correct predictions when the viscosity ratio of the fluid μ_l/μ_v exceeds 1000. G is the mass flux, λ_{lo} and λ_{vo} are computed with any valid friction correlations for the single phase regime under the assumption the whole fluid were liquid or vapour. The average friction is evaluated according to eq. (42).

Lin two phase multiplier (cited by [101])

$$A_{lo} = \left(2.457 \cdot \ln\left(\frac{1}{(7/Re_{lo})^{0.9} + 0.27\,\varepsilon/d}\right)\right)^{\frac{1}{16}} \quad and \quad B_{lo} = \left(\frac{37530}{Re_{lo}}\right)^{\frac{1}{16}} \tag{45}$$

$$A_{tp} = \left(2.457 \cdot \ln\left(\frac{1}{(7/Re_{tp})^{0.9} + 0.27\,\varepsilon/d}\right)\right)^{\frac{1}{16}} \quad and \quad B_{tp} = \left(\frac{37530}{Re_{tp}}\right)^{\frac{1}{16}} \tag{46}$$

$$Re_{lo} = (\dot{m}_{tot} \cdot d)/(\mu_l \cdot A) \quad and \quad Re_{tp} = (\dot{m}_{tot} \cdot d)/(\mu_{tp} \cdot A) \tag{47}$$

With a two phase viscosity like in eq. (30) the multiplier looks like

$$\Phi_{lo}{}^2 = \left(\frac{A_{lo} + B_{lo}}{A_{tp} + B_{tp}}\right)^{\frac{1}{8}} \cdot \left(1 + x \cdot \left(\frac{\nu_g}{\nu_l} - 1\right)\right) \tag{48}$$

To get the friction coefficient this multiplier has to be used like in equation (44) in combination with the liquid only friction coefficient.

Lockhart – **Martinelli** – **Chisholm** – **Mishima & Hibiki** (cited by [125], [140] and [185])

Assuming known mass flow rates of liquid and vapour one can compute the pressure drops for each phase separately. The ration of these pressure drops is known as the Lockhart-Martinelli parameter X, defined like:

$$X^2 = \frac{\left(\frac{\Delta p}{\Delta l}\right)_l}{\left(\frac{\Delta p}{\Delta l}\right)_v} \tag{49}$$

1967 Chisholm recommended the following connection between the Lockhart-Martinelli parameter and the two phase pressure drop, where $\Phi_l{}^2$ is the factor to be multiplied with the liquid pressure drop:

$$\Phi_l{}^2 = 1 + \frac{C}{X} + \frac{1}{X^2} \tag{50}$$

and together with

$$\left(\frac{\Delta p}{\Delta l}\right)_{tp} = \Phi_l{}^2 \cdot \left(\frac{\Delta p}{\Delta l}\right)_l \tag{51}$$

one can expand to eq. (52) where C can be seen as interaction parameter between liquid and vapour phases.

$$\left(\frac{\Delta p}{\Delta l}\right)_{tp} = \left(\frac{\Delta p}{\Delta l}\right)_{l} + C\sqrt{\left(\frac{\Delta p}{\Delta l}\right)_{l} \cdot \left(\frac{\Delta p}{\Delta l}\right)_{v}} + \left(\frac{\Delta p}{\Delta l}\right)_{v} \tag{52}$$

Table 2 C- values given by Chisholm (cited by Thome [185] and Field and Hrnjak [125]).

liquid	vapour	*C*
turbulent	*turbulent*	20
viscous	*turbulent*	12
turbulent	*viscous*	10
viscous	*viscous*	5

For small diameter tubes (1.05 to 3.90 mm) Mishima & Hibiki found the following correlation (cited by Thome [185], chapter 20) when using air-water flow:

$$C = 21 \cdot (1 - e^{-0.319 d_h}) \tag{53}$$

which takes the dependency of the hydraulic diameter into account. Many variations for different channel geometries exist for the C-value, for this work eq. (53) is used.

For the turbulent regime Thome [185] uses the turbulent Lockhart Martinelli parameter X_{tt} to compute pressure drops. The subscript *tt* denotes that turbulence is assumed for both phases:

$${X_{tt}}^2 = \left(\frac{1-x}{x}\right)^{0.9} \cdot \left(\frac{\rho_v}{\rho_l}\right)^{0.5} \cdot \left(\frac{\mu_l}{\mu_v}\right)^{0.1} \tag{54}$$

A differentiation is made concerning the liquid Reynolds number where one time the liquid pressure drop and another time the vapour pressure drop serves as reference for the multiplier.

$${\Phi_{vtt}}^2 = 1 + C \cdot X_{tt} + {X_{tt}}^2 \quad for\ Re_l < 4000 \tag{55}$$

$$\left(\frac{\Delta p}{\Delta l}\right)_{tp} = {\Phi_{vtt}}^2 \left(\frac{\Delta p}{\Delta l}\right)_{v} \tag{56}$$

$${\Phi_{ltt}}^2 = 1 + \frac{C}{X_{tt}} + \frac{1}{{X_{tt}}^2} \quad for\ Re_l > 4000 \tag{57}$$

$$\left(\frac{\Delta p}{\Delta l}\right)_{tp} = {\Phi_{ltt}}^2 \cdot \left(\frac{\Delta p}{\Delta l}\right)_{l} \tag{58}$$

2.5. Coiling effects

Usually, due to simple restrictions in space – try to put a 2 m long stick inside a volume of 50x30x30 cm without breaking it! – the capillary tube is bended, coiled, warped and curved partly in order to make it fit. The expression "make it fit" may be a matter of seconds to a skilled worker at the production line but causes headache at other places. What is more and makes it even worse is that there are apparently no scruples to wrap parts of the tube *around* other objects like the filter/drier or parts of the suction line. The point is, that any flection from a straight horizontal line will bring in an additional effect which has to be treated separately in a model. Bending away from horizontal brings gravity into play and on the other hand side a deviation from friction laws which seemed to work well up to now. The influence of gravity can be neglected as shown in the parameter studies but the latter can't. The cause for that is a secondary flow pattern which emerges from centrifugal forces acting on the flow and that effect is more apparent the smaller the coil-diameter is. In experimental section 6.1 and 6.2 a statement on coils has been given, here some theoretical aspects will be highlighted.
The common method of taking the additional friction into account is to adept friction laws derived from physical models, try to plug a dimensionless factor in – usually the ration of inner diameter to coil diameter – together with exponents and constants determined by comparison to experimental datasets. The amount of models seems like an endless litany of ancient Greek and is summarized best in Chingulpitak [14] who compared more than twenty different friction models for coiled capillary tubes with the result that only four predicted the mass flow rate with an average error below 20 % (three models managed to predict with an error below 4 %) – These three models are listed in the following, for further information the reader is forwarded to [14]. Ali [121] also delivers a collection of 27 friction laws for coiled tubes and is mentioned here despite the fact that no small diameter tubes are treated in his work. Starting with 5 mm inner diameter, nevertheless some of the mentioned friction laws are still in use for capillary tube calculations.

Chingulpitak and Wongwises [15] show experimentally and numerically that a coiled capillary reduces the mass flow rate. The reduction is 6 to 7 % comparing a coil diameter of 300 mm with smaller ones. Park et al. [73] also conducted experiments and modelling to come to the conclusion that a reduction of 5 to 16 % in mass flow rate results from the use of a coiled capillary tube. A generalized correlation was developed which accounts for coiling based on dimensionless groups and nonlinear regression techniques. Other dimensionless correlations can be found in [67].

Mori and Nakayama (cited by [110], [111])

$$\lambda_{coiled} = \frac{C_1 \cdot (d/d_c)^{0.5}}{(Re \cdot (d/d_c)^{2.5})^{\frac{1}{6}}} \cdot \left(1 + \frac{C_2}{(Re \cdot (d/d_c)^{2.5})^{\frac{1}{6}}}\right) \quad with \quad C_1 = 0.192 \quad and \; C_2 = 0.068 \qquad (59)$$

For this general coiled friction factor equation the coefficients C_1 and C_2 are evaluated under consideration of the wall roughness by, unlike the original equation where they are constant

as in equation (151). The method of gaining the coefficients is described well in [110]. Here, for different surface roughness to diameter ratios, the coefficients are gained exemplarily.

Table 3 Dataset obtained by Zhou and Zhang [110].

d (mm)	ε/d	C_1	C_2
1.0	0.00025	0.207	0.0737
1.2	0.0004	0.216	0.0766
1.4	0.00122	0.248	0.0878
1.6	0.0014	0.253	0.0897
2.2	0.00116	0.245	0.0871

Garcia Valladares [31] applied a polynomial regression over abovementioned parameters in order to get continuous values for ε/d other than the given five base points. His formulae yields:

$$\begin{aligned} C_1 &= 1.88411177 \cdot 10^{-1} + 8.52472168 \cdot 10^{1} \cdot (\varepsilon/d) \\ &\text{-}4.63030629 \cdot 10^{4} \cdot (\varepsilon/d)^2 + 1.31570014 \cdot 10^{7} \cdot (\varepsilon/d)^3 \\ C_2 &= 6.79778633 \cdot 10^{-2} + 2.53880380 \cdot 10^{1} \cdot (\varepsilon/d) \\ &\text{-}1.06133140 \cdot 10^{4} \cdot (\varepsilon/d)^2 + 2.54555343 \cdot 10^{6} \cdot (\varepsilon/d)^3 \end{aligned} \tag{60}$$

Giri (cited by [110], [73])

$$\lambda_{coiled} = \frac{1.1258}{Re^{0.1938} \cdot (d_c/d)^{0.5391}} \tag{61}$$

Schmidt (cited by [14])

$$\begin{aligned} \frac{\lambda_{coiled}}{\lambda_{straight}} &= 1 + 0.14 Re^{x} \\ x &= \frac{1 - 0.0644/(d_C/d)^{0.312}}{(d_C/d)^{0.97}} \end{aligned} \tag{62}$$

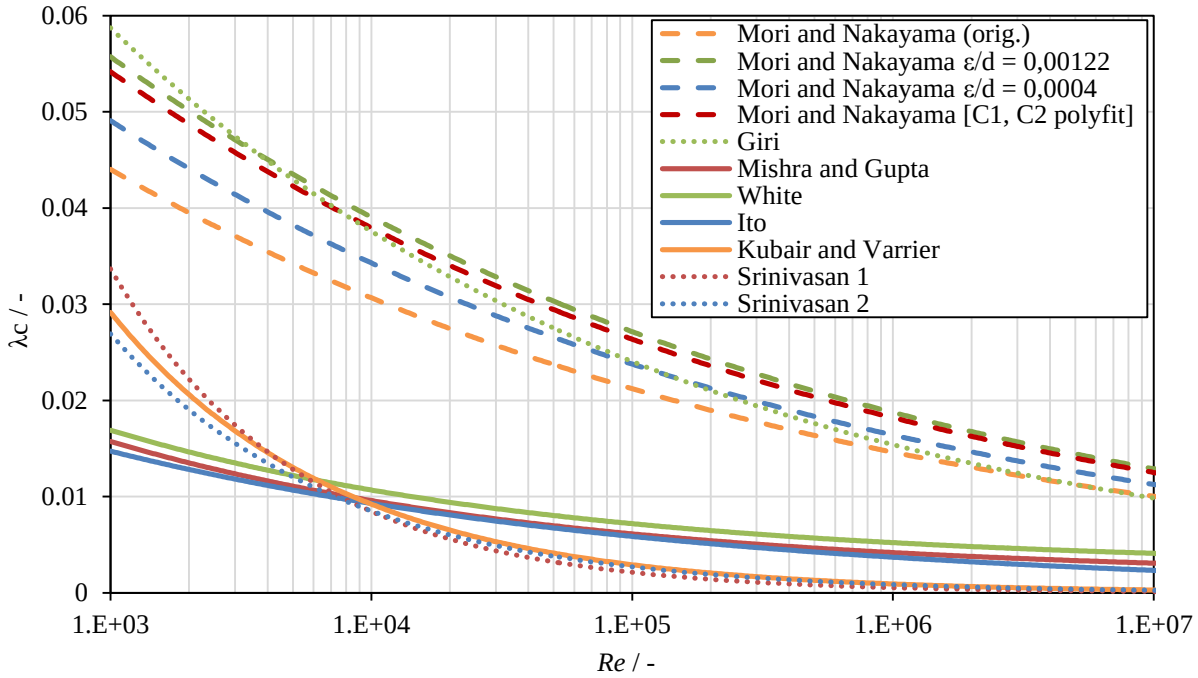

Fig. 13 Friction coefficient correlations for coiled tubes. ε/d = 0.001, d = 1 mm d_c = 20 mm. Correlations provided by [14].

The plot (Fig. 13) reveals a large spread between the single correlations for coiled friction coefficients, noteworthy, three groups of similar behaviour can be identified. This was also concluded by [14] when more than 26 correlations were tested amongst others against experimental data for R22 at a 1.5 mm diameter coiled capillary tube with coil diameters of 40, 120 and 200 mm. The span of relative error in mass flow is from -100 to 325 %. The equations of Mori and Nakayama, Schmidt as well as Giri are best suited in this investigation, the big deviation of other correlations may arise from a violation of the given applicable range or if the range were not violated it is obviously not applicable to the experimental cases in [14].

3. Heat transfer

Due to reasons of energy efficiency a capillary tube heat exchanger is meanwhile a standard component in domestic refrigeration. According to manufacturers the lion's share of all cooling devices uses this way of increasing the cycle efficiency. To better understand the numerical requirements when modelling such an element let's take a look at Fig. 14 where the main heat fluxes are depicted.

3.1. General Considerations

According to Fig. 14 the main part of heat exchange occurs between suction line and capillary tube, hence, in the next chapter correlations for the heat transfer coefficients are sought with respect to the pipe geometry (standard, concentric), the convection type (forced, natural), and the flow regime (laminar, turbulent). The heat exchange with ambient air can be neglected for some reason since usually the whole heat exchanger and the main part of the capillary tube are highly insulated and covered with foam; only a short part touches the air outside which is the part where subcooled liquid at nearly ambient temperatures or slightly above enters the capillary tube. Also, the piece of capillary which has left the heat exchanger and discharges into the evaporator is rather short in length. In some devices its length is in the range of some centimeters, hence the heat transfer to the cold air inside the compartment at this place is neglected, too. The main concern is the heat transfer between capillary tube and suction line

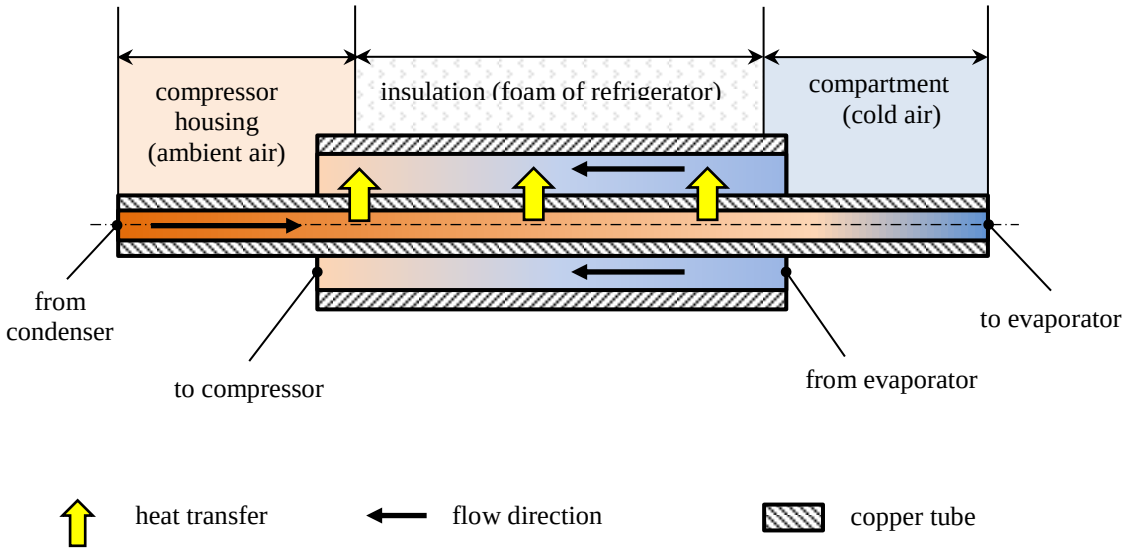

Fig. 14 Heat transfer between hot side and cold side.

(the suction line is sometimes referred to as "annulus"). Inside the capillary tube liquid phase and two phase evaporation heat transfer mechanisms are important, whereas in the suction line usually superheated vapour is present. In the following, correlations are listed which are used in this work and commonly referred to in literature, concludingly, some comments about the usefulness and applicability are given in chapter 3.3.

3.2. Correlations

General equations which occur frequently in this scope are mentioned here quasi in a header. These comprise characteristic numbers and basic equations of heat transfer. It is assumed that the flow is thermally and hydraulically fully developed.

The hydraulic diameter for an annulus with d_i as inner diameter and d_o as outer diameter is calculated by:

$$d_h = d_o - d_i \tag{63}$$

The reduced pressure of a fluid:

$$p_{red} = \frac{p}{p_{crit}} \tag{64}$$

The Prandtl number is the ratio of kinematic viscosity to thermal diffusivity:

$$Pr = \frac{\mu \cdot c_p}{\lambda} \tag{65}$$

The liquid only velocity together with the liquid only Reynolds number assume the whole mass flow is liquid:

$$v_{lo} = \frac{\dot{m}}{\rho_l \cdot A} \tag{66}$$

$$Re_{lo} = \frac{\rho_l \cdot d \cdot \mathrm{v}_{lo}}{\mu_l} \tag{67}$$

The Grashof number relates buoyancy to the viscous forces:

$$Gr = g \cdot \frac{d^3}{\nu^2} \cdot \beta \cdot \left(T_{fluid} - T_{wall}\right) \tag{68}$$

Rayleigh Number:

$$Ra = Pr \cdot Gr \tag{69}$$

The heat transfer coefficient with the inner diameter as characteristic length:

$$\alpha = \frac{Nu \cdot \lambda}{d} \tag{70}$$

Single phase heat transfer

This correlation is used to compute the heat transfer coefficient for single phase (liquid or vapour). A differentiation is made concerning flow regime (turbulent, laminar) and tube geometry (annulus, or standard tube) which leaves us with four cases. The main source is VDI Wärmeatlas, 2002, 9th edition, Gb2-Gb3. All Nusselt numbers are average values and are computed for each cell element of the code.

- annulus (concentric) – laminar flow

  Three cases are differentiated, namely heat transfer through the outer, the inner or both walls at the same time. Since the outer wall borders to ambient air, it is assumed that the lion's share concerns only the inner wall and accordingly the boundary conditions are chosen. The equations for the Nusselt number are similar to the Dittus-Boelter equation.

$$Nu_{1,i} = 3.66 + 1.2 \cdot \left(\frac{d_i}{d_o}\right)^{-0.8} \tag{71}$$

$$fg_i = 1.615 \cdot \left(1 + 0.14 \cdot \left(\frac{d_i}{d_o}\right)^{-0.5}\right) \tag{72}$$

$$Nu_2 = fg_i \cdot \left(\frac{Re \cdot Pr \cdot d_h}{l}\right)^{\frac{1}{3}} \tag{73}$$

  The average Nusselt number is calculated from (71) and (73):

$$Nu_m = \left({Nu_{1,i}}^3 + {Nu_2}^3\right)^{\frac{1}{3}} \tag{74}$$

- standard tube – laminar flow
  VDI Wärmeatlas, 2002, 9th edition, Ga1 recommends for laminar flow and constant wall temperature:

$$Nu_1 = 3.66 \tag{75}$$

$$Nu_2 = 1.615 \cdot \left(\frac{Re \cdot Pr \cdot d_h}{l}\right)^{\frac{1}{3}} \tag{76}$$

$$Nu_m = \left({Nu_1}^3 + 0.7^3 + (Nu_2 - 0.7)^3\right)^{\frac{1}{3}} \tag{77}$$

- annulus (concentric) – turbulent flow

The friction is according to Gnielinski [128] who proposes to use a "correction-factor", φ, which is 1 for a tube and 2/3 for a plain gap, along with the Konakov equation (80).

$$\varphi = \frac{\left(1 + \left(\frac{d_i}{d_o}\right)^2\right) \cdot ln\left(\frac{d_i}{d_o}\right) + \left(1 - \left(\frac{d_i}{d_o}\right)^2\right)}{\left(1 - \left(\frac{d_i}{d_o}\right)\right)^2 \cdot ln\left(\frac{d_i}{d_o}\right)} \tag{78}$$

$$Re^* = \varphi \cdot Re \tag{79}$$

$$\lambda = (1.8 \cdot \log(Re^*) - 1.5)^{-2} \tag{80}$$

The Nusselt correlation stems from work by Petukhov and Roizen (cited by VDI Wärmeatlas, 2002, 9th edition, Gb3) and features a correction for small diameter tubes – the power of the diameter ratio of the annulus as well as a correction factor for the influence of the tube length. The range of validity is given by $10^4 \leq Re \leq 10^6;\ 0.6 \leq Pr \leq 1000;\ 0 \leq d_h/l \leq 1$. The correction factor which takes the temperature-dependency of the thermodynamic properties into account and therefore often mentioned $(Pr/Pr_w)^{0.11}$ is neglected, since its influence on the heat transfer is very small (less than one percent) for both liquid and vapour phase and additionally the exact knowledge of wall temperatures is not given. The subscript "w" denotes the Prandtl-number of the fluid in wall-proximity.

$$Nu_m = \frac{\frac{\lambda}{8} \cdot Re \cdot Pr}{1 + 12.7 \cdot \left(\frac{\lambda}{8}\right)^{0.5} \cdot \left(Pr^{\frac{2}{3}} - 1\right)} \cdot \left(1 + \left(\frac{d_h}{l}\right)^{\frac{2}{3}}\right) \cdot 0.86 \cdot \left(\frac{d_i}{d_o}\right)^{-0.16} \tag{81}$$

- standard tube – turbulent flow

Friction is calculated according to Konakov (cited and recommended by [128]). The Nusselt correlation is similar to the one for annuli and nearly all references meet at the publication by Gnielinski [143]. In this work several possibilities are depicted in a more or less chronological order. The equation with a correction term (*Re* - 1000) for Reynolds numbers down to 2300 is taken for this model. Another option would be an equation including the correction factor for short tubes like in eq. (81), i.e. when the tube length has impact on the heat transfer but due to the fact that the inner diameter is several dimensions below the tube length this correction is neglected by good conscience. The range of validity is given by $2300 \leq Re \leq 10^6;\ 0.6 \leq Pr \leq 1000;\ 0 \leq d_h/l \leq 1$ although the sources differ in respect to the Prandtl number.

$$\lambda = (1.8 \cdot \log(Re) - 1.5)^{-2} \tag{82}$$

$$Nu_m = \frac{\frac{\lambda}{8} \cdot (Re - 1000) \cdot Pr}{1 + 12.7 \cdot \left(\frac{\lambda}{8}\right)^{0.5} \cdot \left(Pr^{\frac{2}{3}} - 1\right)} \tag{83}$$

Two phase boiling (known heat flux)

Stated many times in literature the two phase boiling heat transfer coefficients can be calculated according to Liu and Winterton [148] (cited by [5]). All properties are calculated at the saturation temperature. The heat transfer coefficient consists of two contributions: the forced convective part ($F \cdot \alpha_l$) and the pool boiling part ($S \cdot \alpha_{pool}$). Forced convective boiling arises from vapour generation in the boundary layer of the flow, that is close to the wall and its transport into colder regions of the flow whereas the pool boiling mechanism stem from boiling characteristics of a fluid which is not in motion. Among other researchers the method of combining these two contributions is applied by Liu and Winterton [148] who assume a quadratic connection between these two contributions:

$${\alpha_{tp}}^2 = (F \cdot \alpha_l)^2 + \left(S \cdot \alpha_{pool}\right)^2 \tag{84}$$

If the heat flux is known instead of the wall temperature, the following way can be used to obtain heat transfer coefficients. *F*, *S* and α_l can be calculated like given in equation (87), (88) and (90). The contributions of pool boiling and convective boiling are combined as given in eq. (84). This method is favoured and used for this work instead the version where the wall temperature is known.

$$\alpha_{pool} = 55 \cdot {p_{red}}^{0.12} \cdot q^{\frac{2}{3}} \cdot \left(-\log(p_{red})\right)^{-0.55} \cdot M^{-0.5} \tag{85}$$

with *M* as molecular weight, *q* as heat flux and p_{red} is the reduced pressure of the fluid.

The Froude number is defined as:

$$Fr = \frac{\mathrm{v}_l}{\mathrm{v}_{sonic}} \tag{86}$$

α_l is calculated from the Dittus-Boelter equation:

$$\alpha_l = 0.023 \cdot {Re_{lo}}^{0.8} \cdot {Pr_l}^{0.4} \cdot \frac{\lambda_l}{d} \tag{87}$$

$$F = \left(1 + x \cdot Pr_l \cdot \left(\frac{\rho_l}{\rho_v} - 1\right)\right)^{0.35} \tag{88}$$

A correction factor for the Froude number is suggested for horizontal tubes and low Froude numbers:

$$if \quad Fr < 0.05: \quad F = F \cdot Fr^{0.1-2 \cdot Fr} \tag{89}$$

$$S = \left(1 + 0.055 \cdot F^{0.1} \cdot {Re_{lo}}^{0.16}\right)^{-1} \tag{90}$$

Two phase boiling (known wall temperature)

$$A_p = 55 \cdot {p_{red}}^{0.12} \cdot \left(-log(p_{red})\right)^{-0.55} \cdot M^{-0.5} \tag{91}$$

$$q_l = F \cdot \alpha_l \cdot \left(T_{wall} - T_{fluid}\right) \tag{92}$$

$$C = \left(\frac{A_p \cdot S}{F \cdot \alpha_l}\right)^2 q_l^{\frac{4}{3}} \tag{93}$$

The cubic equation has to be solved for its single real root:

$${q_*}^3 - C \cdot {q_*}^2 - 1 = 0 \tag{94}$$

The final heat transfer coefficient is then calculated by

$$\alpha_{tp} = F \cdot \alpha_l \cdot q_*^{\frac{3}{2}} \tag{95}$$

Although the range of Liu and Winterton's experimental validation [148] starts with slightly bigger diameters (2.95 to 32.0 mm) than used here, no better correlation can be found up to now for boiling heat transfer in small diameter tubes. Due to the lower impact on the heat resistance the exact knowledge of the heat transfer coefficient inside the capillary tube is not an issue. Given a commonly used coaxial design of a capillary tube including a heat exchanger, the heat resistances can be estimated to be 97.5 % (convection single-phase), 0.1 % (heat conduction through capillary wall) and 2.4 % (convection two-phase). Compared to the higher resistance of the convective heat transfer between wall and superheated vapour, this law is perfectly suitable to be applied in capillary tube heat exchangers.

Two phase condensation

In rare cases, for instance if the evaporation in the capillary has set on before reaching the heat exchanger, which would then lead to recondensation, a model for condensation has to be at hand. In most of the cases the model of Shah [155] is used. Despite the fact of being out of the diameter range this correlation for condensation heat transfer calculation is recommended by Bansal and Yang [5]. Shah developed a dimensionless correlation to predict heat transfer coefficients for a broad range of refrigerants, geometry and thermodynamic conditions. A small drawback of this source is that isobutane is not among the tested refrigerants but due to

the fact that the reduced pressure is used here intentionally to take other fluids into account and due to the broad range of tested fluids (>10) it matters little. The second drawback is that the range of investigated tubes starts from 7 mm in diameter and goes as high as 40 mm which is above the capillary tube range.
In the course of the derivation, Shah uses the Dittus-Boelter correlation, assuming all the mass flow being liquid.

$$\alpha_{lo} = 0.023 \cdot {Re_{lo}}^{0.8} \cdot {Pr_l}^{0.4} \cdot \frac{\lambda}{d} \tag{96}$$

Then, to come to a heat transfer coefficient for the two-phase case, he suggests an extension which bases on his correlation for saturated boiling heat transfer and on empirical investigations, leading to

$$\alpha_{tp} = \alpha_{lo} \cdot \left((1-x)^{0.8} + \frac{3.8 \cdot x^{0.76} \cdot (1-x)^{0.04}}{{p_{red}}^{0.38}} \right) . \tag{97}$$

Shah describes his formula as a simple dimensionless correlation in contrast to many sophisticated treatments of condensation heat transfer at that time. The said strength of his work is the wide range of parameters, 474 datapoints from 21 independent studies have been analyzed and an absolute mean deviation of 15.4 % has been achieved.

3.3. Application to capillary tubes

To get a feeling about the flow which is to be expected a short anticipation is taken into account – a test run is made with the capillary tube model including a heat exchanger. Therefore a typical operating point was chosen – the capillary tube is choked, the evaporation is delayed in terms of spatial position and expectedly shifted towards the outlet. No evaporation occurs before the refrigerant enters the heat exchanger (from 0.6 m to 1.6 m in Fig. 15). The mass flow rate is around 2.5 kg/h, inlet pressure is at 5.7 bar and subcooling around 10 K. Slightly superheated vapour enters the suction line at a pressure of 0.7 bar. When using before-mentioned boundary conditions and correlations Fig. 15 arises where the range of some characteristic flow parameters can be experienced. The abbreviation "sat." is for saturation conditions, "sub." stands for subcooled and "sup." for superheated. "liquid only" refers to the assumption of all flow to be liquid even if it is not the case in reality – this assumption is necessary for some correlations mentioned earlier.

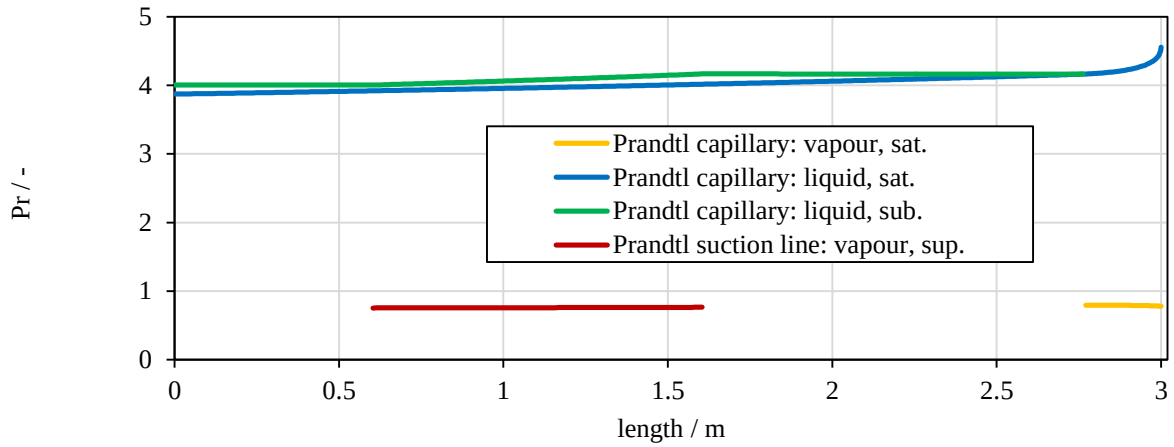
Pr / -
length / m
Prandtl capillary: vapour, sat.
Prandtl capillary: liquid, sat.
Prandtl capillary: liquid, sub.
Prandtl suction line: vapour, sup.

(a)

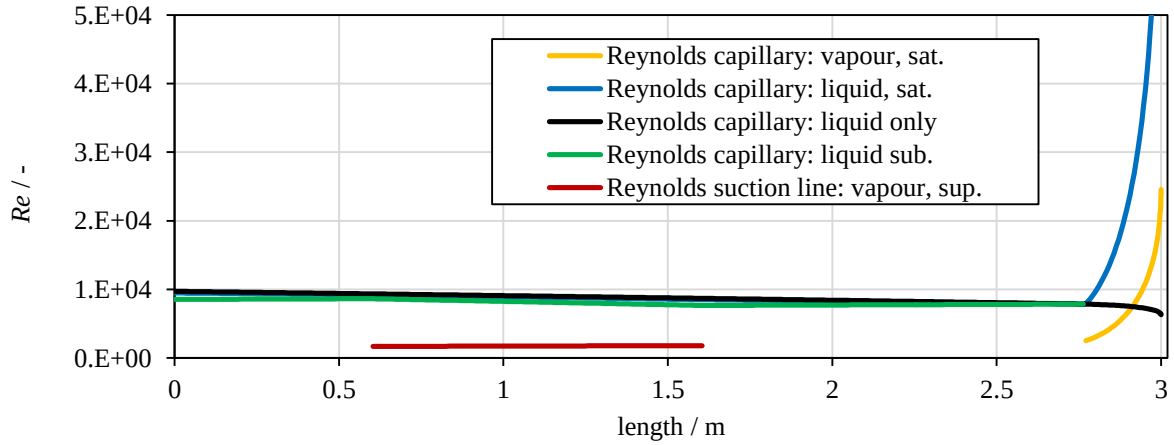
Re / -
length / m
Reynolds capillary: vapour, sat.
Reynolds capillary: liquid, sat.
Reynolds capillary: liquid only
Reynolds capillary: liquid sub.
Reynolds suction line: vapour, sup.

(b)

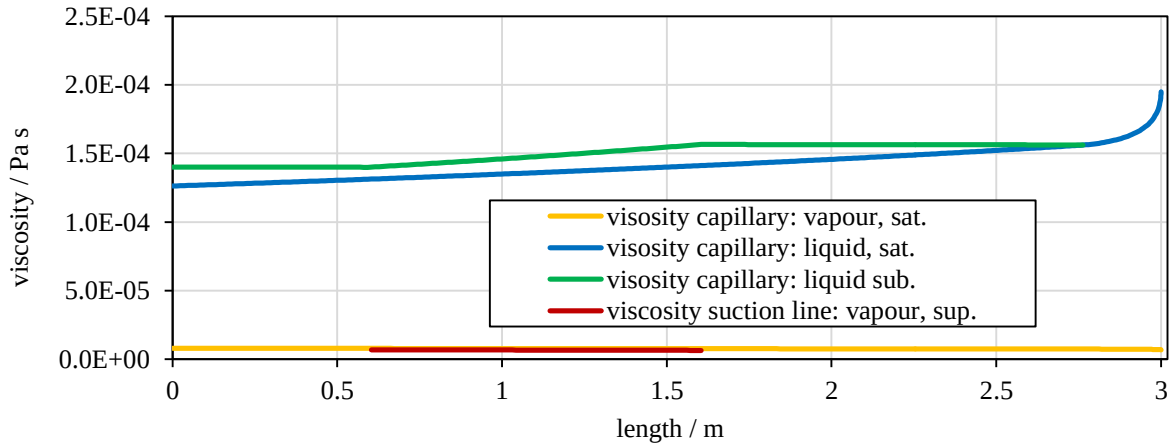
viscosity / Pa s
length / m
visosity capillary: vapour, sat.
visosity capillary: liquid, sat.
visosity capillary: liquid sub.
viscosity suction line: vapour, sup.

(c)

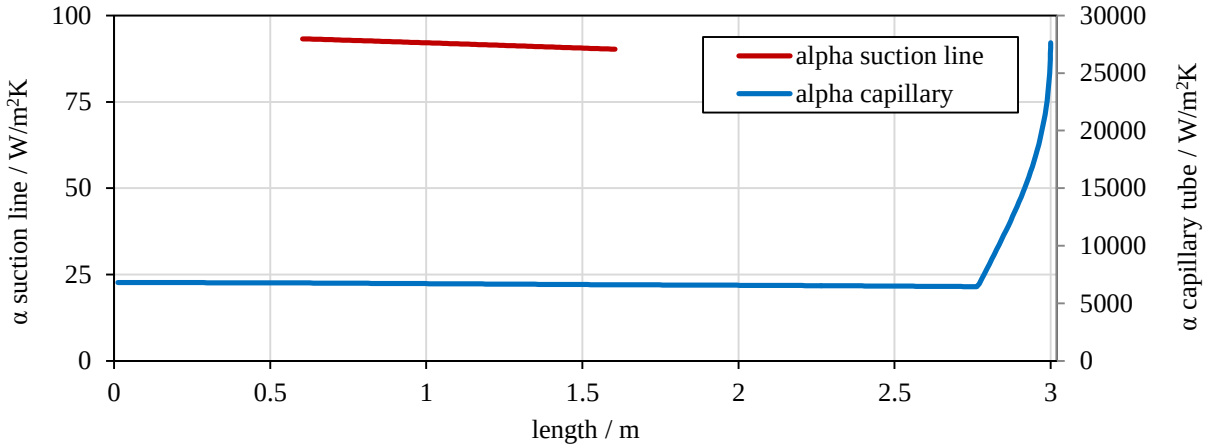

(d)

Fig. 15 Characteristic values for flow through a capillary and a suction line heat exchanger. Prandtl number (a), Reynolds number (b), viscosity (c) and heat transfer coefficients (d).

One sees, that the red line represents the suction line in the heat exchanger region which is solely superheated vapour, since the momentum equation is not solved only the heat transfer matters to this side. The regime is laminar as seen in Fig. 15 (b) and can maybe switch to turbulent for higher mass flow rates but since the assumed 2.5 kg/h are already rather high the flow can generally be expected to be laminar here. Nevertheless, to cover all cases in this region the laminar and turbulent heat transfer coefficients shall be computed for both standard tube and annulus. On the other side, the capillary tube features heat transfer coefficients 10 times higher than in the suction line (Fig. 15 (d)) which shows us that this side hardly will restrict the heat flux and some authors even report to have set the heat transfer coefficient to infinity obviously without introducing mentionable inaccuracies, [4]. Since the axial heat transfer is neglected (see chapter 4.2.1) and the two phase region is well behind the heat exchanger the heat transfer mechanism is of lower importance – the outer side can be treated as adiabatic. The models of computing the two phase condensation and evaporation heat transfer are nevertheless mentioned and implemented since the computer-routine should also be able to handle off-design situations where condensation and evaporation might occur in the heat exchanger region. In the case above the flow inside the capillary tube is turbulent (Re ~ 8000) and single phase liquid. The important thing for this part is correct friction in the liquid and two phase regime, secondly the heat transfer for liquid flow.

4. Capillary tube models

In the following chapter approaches are explained how the flow through small diameter pipes can be modelled, taking two phase flow (evaporation and condensation), critical outlet conditions (gas reaches sonic speed), heat transfer and wall friction into account. Existing publications are reviewed before formulae of a homogeneous model are deduced. More complex models than the homogeneous one exist but are not investigated within the scope of this work. The main focus lies on the implementation of a capillary tube model in a cooling-cycle simulation which demands stable and quick results. Therefore, homogeneous models provide a solid foundation. The following chapter also deals with speeding up the process of predicting mass flow rates by other methods than 1d calculations. The classification of capillary tube models in literature does not always follow a clear convention so here is the right point to make some comments about that matter. Fig. 17 is one way of classification and gives an overview of publications which can be assigned to each category. The classification is chosen similar to the one used in Wein [93] which, by the way, features comprehensive work on drift flux models comprising transient calculations or evaporation delay. In the following, categories and attributes which occur in the course of capillary tube modelling are explained briefly.

One way of categorization is to differentiate between **0d**, **1d** and **3d** models, which means a 0d model doesn't resolve the geometric features of a tube and needs average values for all parameters (in axial and radial direction), whereas a 1d model divides a tube in certain pieces (cells) and is able to deal with changes in flow behaviour which wouldn't be the case for 0d. These kinds of models are a common trade-off between speed and accuracy for geometries where there is a main flow direction and secondary flows can be neglected. This usually is the case for geometries where the diameter to length ratio is very low. For usual capillary tubes, this ratio is somewhere between 0.0001 and 0.0005. 1d models can account for changes in cross sectional area but still assume uniform fluid properties at every cross section since the radial component is not resolved. Empirical laws can help out in order to model the friction and heat transfer, nevertheless. Formally, three dimensional modelling is mentioned and may be used for more complex geometries than pipes and tubes. According to the knowledge of the author, they have not been used for capillary tube modelling yet.

Transient or **steady state** is another aspect which can be used to divide the plurality of models. Few publications exist where the transient terms are treated, the main reason against this treatment is again calculational speed to make a software attractive for commercial usage.

According to Brennen [165] the most general expression **multiphase flow** can be divided into two subcategories, **disperse flow** and **separated flow**. The first one describes problems when finite particles or drops are embedded in a carrier fluid which interacts with the particles whereas in separated flow two or more continuous streams interact with each other along distinct surfaces. Further, disperse models can be divided in **trajectory models** which resolve the trajectories of particles in the flow but naturally can't be applied in 1d and **two fluid models**. The class of two fluid models always assumes two continuous fluids, also when one phase consists of particles or droplets. In that case the properties of the discrete phase are

approximated on a continuous phase. Two fluid models solve the basic equations for two phases (e.g. vapour and liquid of refrigerant) which naturally may differ in velocity (**hydrodynamic non-equilibrium**) and temperature (**thermal non-equilibrium**) whereas **homogeneous flow models** work with a homogeneously mixed fluid with artificial properties (viscosity, friction, ...) but with the advantage of only half of the amount of constitutive equations to solve. Additionally a slip (i.e. ration between the velocities of the phases in the system due to relative motion) can be introduced in a homogeneous flow model to account for different velocities and therefore more accurate friction and heat transfer – the term **slip model** is commonly used for this case. In other words, in homogeneous models there is in any case thermal equilibrium and if a slip model is implemented therein hydrodynamic non-equilibrium can be achieved. The designation "**drift flux model**" also might occur sometimes and describes a class of models where the relative velocity between phases is explicitly expressed as a function of flow parameters and external forces [165], [93].

Adiabatic in the scope of this work means that there is no heat exchange between the fluid inside the capillary and its surrounding irrespective if outside is ambient air or another flow of refrigerant. Models where this doesn't apply are referred to as **non-adiabatic**.

In literature the term "**coiled**" or "**helical**" describes a capillary tube which is bended to coils of diameters, usually lower than 300 mm since coils of bigger diameter don't seem to affect the flow when compared to a **straight** type [73]. This coiling leads to additional friction due to centrifugal forces and secondary flow. This effect is accounted for in empirical correlations for frictional pressure drop and can be applied to any kind of 1d model.

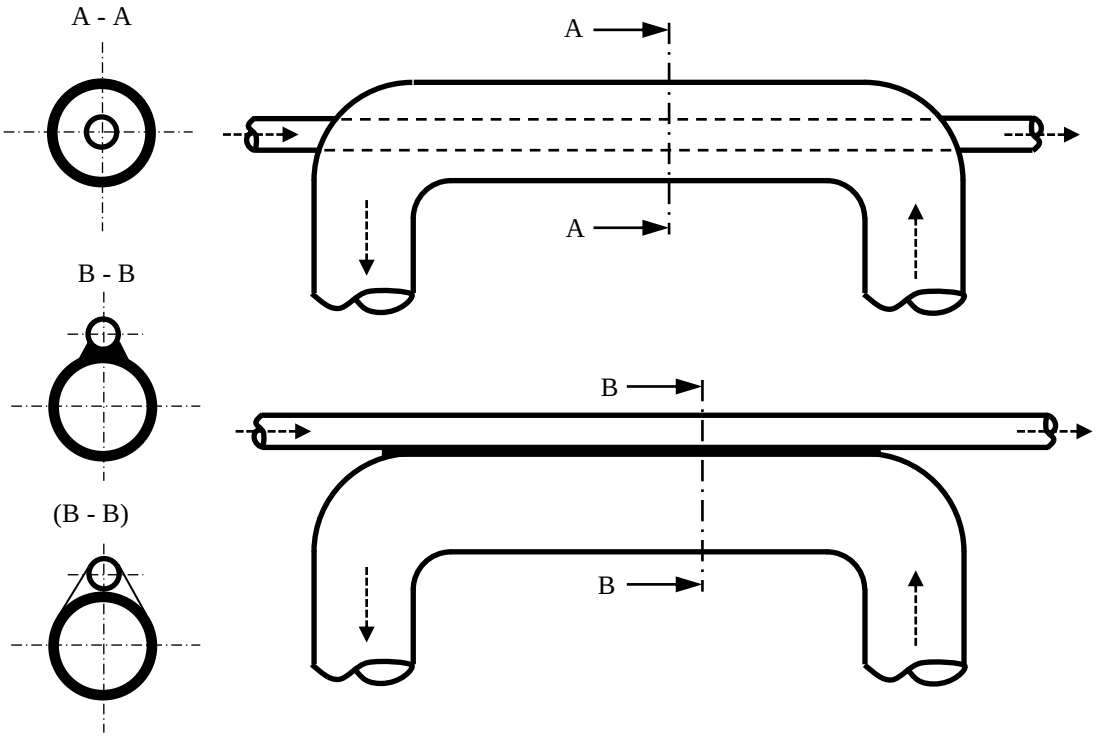

Fig. 16 A-A: non-adiabatic, coaxial, soldered, B-B: non-adiabatic, lateral, soldered, (B-B): non-adiabatic, lateral, fixed with foil.

Fig. 16 shows typical configurations of non-adiabatic capillary tubes. Nowadays, commonly a heat exchanger section is involved where the capillary tube can be inserted into the suction line (**coaxial**, **concentric** type) or soldered (sometimes just fixed with a shrink tube) onto the outside of the suction line (**lateral** type). In terms of heat transfer the coaxial design has better performance than the soldered one since the common area per unit length between capillary and suction line is larger than other designs and the wall thickness separating the two fluid streams is just the wall thickness of the capillary – therefore accounting for a higher heat transfer.

4.1. Review

This section considers capillary tube models which are based on solving the conservation equations. Empirical correlations and similar non-physical methods are described in chapter 5.

In the course of numerical mapping of capillary tubes different approaches depending on its later assignment have been realized. Comprehensive reviews about capillary tubes can be found in Ding [22], Fang [26], and Khan et al. [54]. All of the models are solved for the mass flow rate and, if non-adiabatic behaviour is assumed, also for the outlet temperature of the cold side.

A small number of **0d models** is presented in literature, among them Hermes et al. [43] who solve explicitly for the mass flow rate and compare their findings with other simplified analytical models in literature. The accuracy lies around ±15 % for more than 90 % of the data points which seems to be more appropriate for the calculated test cases than correlations by Zhang and Ding [107], Yilmaz and Ünal (cited in [43]) or Yang and Wang [105]. Used refrigerants for validation are refrigerants R134a and R600a. The solution is achieved by assuming isenthalpic flow and with the help of empirical correlations for the specific volume in the two phase region. Moreover the pressure drop due to acceleration is neglected and the mass flow rate is obtained by integration of the simplified governing equation. Hermes et al. [43] proposed a method which still requires iterative loops but solves explicitly for the mass flow rate. The model is described as an explicit semi-empirical algebraic equation by the authors and shows better results for the adiabatic case than the previous 0d models with R600a and R134a as refrigerants. The accuracy is said to be as high as 91.3 % within the ±10 % range and 99.1 % within the ±15 % range. The global RMS is denoted by 5.5 % in mass flow rate. Similar considerations can be found in Hermes et al. [44] which is valid for capillary suction line heat exchangers. 92 % of the data (mass flow rate) lies within the ±10 % error band and 98 % within the ±15 % error band. The temperatures on the suction line outlet can be computed within ±3 K compared to the measurements. The model scheme uses the ε-NTU (Number of Transfer Units) method for parallel temperature profiles which gives feedback on the heat exchanger effectiveness. Nevertheless, experimental data is necessary to fit several parameters, among them a *diabatic multiplier*, which expresses the impact of a heat exchanger on the adiabatic mass flow rate.

1d models on the other hand side solve a set of equations for every cell along the flow direction and a mass flow rate is found iteratively. Different numeric schemes exist, among them the homogeneous flow model which is by far the most popular one. Publications about this scheme can be looked up from Fig. 17. The numerical scheme is applied on a grid which usually consists of equally distributed cells. In some cases the grid is refined towards the end where the flow accelerates up to sonic speed, a formula for generating the cell distribution is given in Escanes et al. [25] and applied in Garcia-Valladares [31], [32], [36]. A similar method is used in this work where improvements to a uniform grid are shown. The equations solved for each cell comprise mass-, momentum- and energy equation which are integrated over each cell volume and discretized. Detailed instructions for homogeneous models can be taken from Bansal [6], Xu and Bansal [102], Chingulpitak [14], Sinpiboon and Wongwises [87], Gu et al. [38] or Vacek and Vins [91]. Four very well documented publications on the numerics of two fluid models applied to critical flow are from Seixlack and Barbazelli [83], Schwellnus and Shoukri [154], Richter [76] and Garcia-Valladares [31], [32], [36]. The detection of critical flow at the end of a capillary tube deserves attention too, since every model has to deal with this step. In order to stop the calculation at that point where the flow chokes, three different formulations can be found. One is to compare the average velocity of the flow at each cell with the local speed of sound and stop calculating when they become equal. This possibility is implemented in Bansal and Wang [3], Jung et al. [51] or Wong et al. [99], but since the calculation of sonic speed in two-phase regimes is rather difficult and more like an estimate than a reference, this method is often replaced by other criteria. Escanes et al. [25], Bansal and Rupasinghe [6], Fatouh [27] and Garcia-Valladares [34] use the second law of thermodynamics which can be interpreted in a way that entropy can not decrease in an isenthalpic process. It does so numerically after reaching critical flow conditions as explained in chapter 4.2.2 and that is the point where the calculation has to be terminated. Another way is the tracking of the pressure gradient dp/dz. it is reported in Wongwises et al. [100] that under choked conditions it reaches infinity and is treated as the identifying feature.

If heat transfer is not neglected thoughts have to be spent on the actual construction method of the heat exchanger. Like explained in section 4.3, mainly two main types exist (Garcia-Valladares [32], Sarker and Jeong [80]) that are concentric and lateral heat exchanger which are operated counter stream-wise. The copper walls are treated in most cases as heat resistance in radial direction, only Garcia-Valladares [32] accounts for axial heat transfer in his model. The diversity of heat transfer correlations is as abundant as the ones for friction and have to be chosen with care.

In some publications metastable models are implemented since it is well known that the mass flow rate is influenced by evaporation delay. Chen's correlation for metastable liquid region [13] which has been developed to predict the underpressure of vaporization (p_{sat} - p_{evap}) for the refrigerant R12, has been extended to R134a and R22 (cited by Zhou and Zhang [110] and Huerta [45]). The term "*underpressure of vaporization*" refers to the difference in saturation pressure and actual evaporation pressure and is a quantitative measure of boiling retardation (see chapter 4.4). For the metastable two phase region usually the correlation of Feburie et al. (Zhou and Zhang [110]) is used. It is mentioned by Melo et al. [61] that for R600a Chen's correlations leads to no improvement in terms of predictability, the predicted underpressure is

almost constant though the experiments indicate a more or less random behaviour of metastability. Ablanque et al. [1] mentions these three variants in his work.

Analysis on the impact of single parameters on the mass flow rate are crucial and follow a successful implementation of a model. For adiabatic models this is done by Fatouh [27], Bansal and Rupasinghe [6]. Outcome of these studies are that the inner diameter is most influential regarding the mass flow rate, followed by the length, inlet pressure and subcooling. For the diabatic case, the same considerations lead according to Sarker and Jeong [80] to the conclusion that the capillary's inner diameter, length and inlet pressure are the main players in terms of impact on mass flow rate. Melo et al. [66] concluded that the suction line outlet temperature is mainly influenced by the capillary's inner diameter and inlet pressure and also by the inner diameter and the length of the suction line. A more detailed inspection which focuses on two-factor interactions follows.

Concerning its accuracy it is difficult to state numeric values since many different descriptions of the quality of a model exist, and also the setup and the simulation parameters differ (adiabatic, non-adiabatic, helical geometry, choked, non-choked, …). Nevertheless a rough estimate can be given by ±5 % average deviation (Zhou and Zhang [110]), 5 % relative mean error (Seixlack and Barbazelli [83]) or an agreement between experimental data and calculated data within ±7 % (Bansal and Wang [3]). Other numeric schemes like two fluid models and drift flux models are the most sophisticated ones, taking the relative motion of vapour and liquid phase into account. The relative mean error for such well configured models drops down to 3.6 % (Seixlack and Barbazelli [83]).

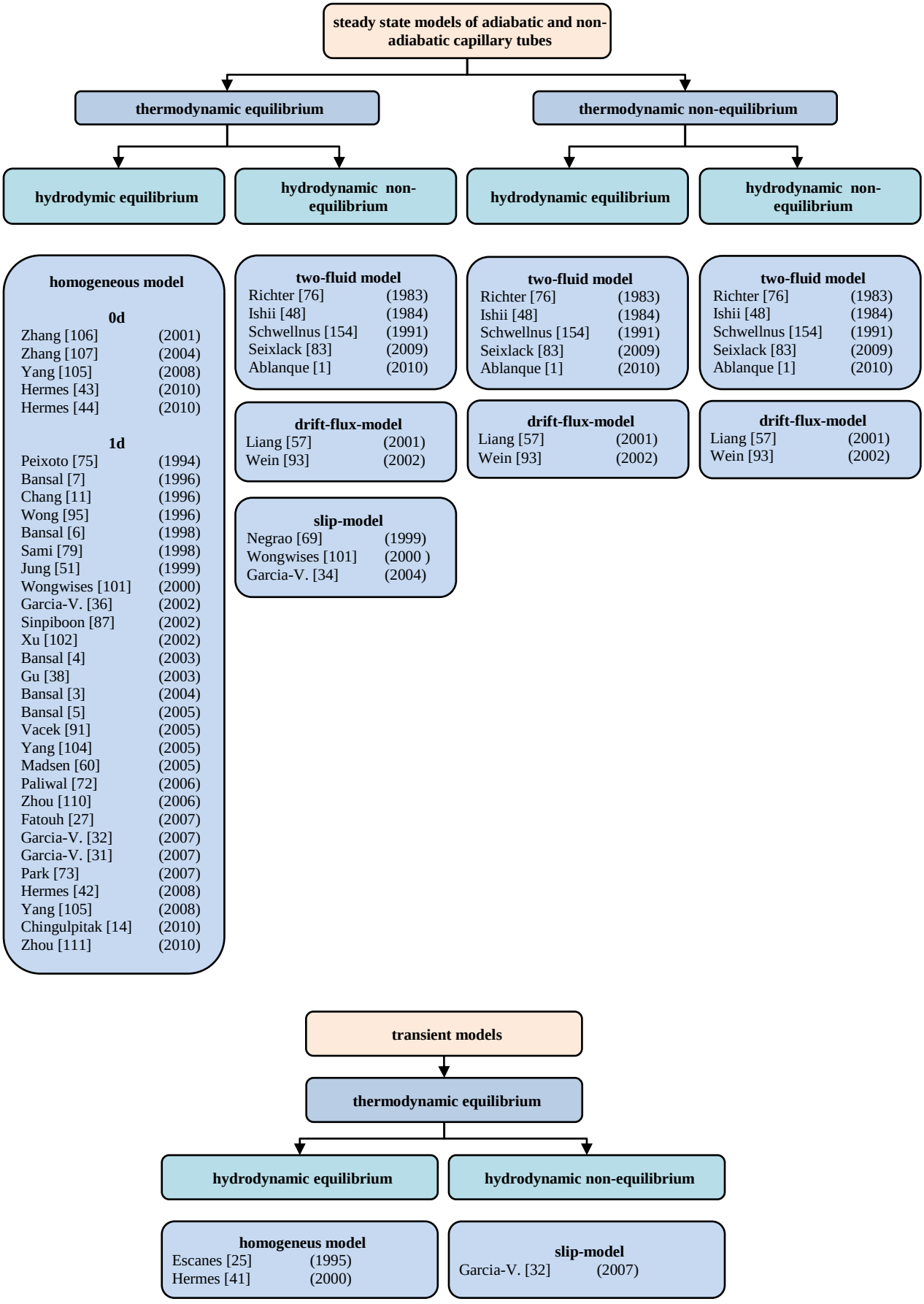

Fig. 17 Summary of literature dealing with capillary tube modelling.

4.2. Homogeneous adiabatic models

In this chapter the basics of a steady state homogeneous capillary tube model are derived. Under consideration of all simplifications a discretized set of equations, together with a schematic sketch of chronological commands how to solve them, is presented. Implemented empirical models are applied here but explained in-depth in chapter 2.

4.2.1. Theory

The homogeneous model described here is based on the conservative equations of mass, momentum and energy in one dimension (x-direction) for compressible fluids. The model assumes equal pressure, temperature and velocity for vapour and liquid phase for one position in x-direction. Although slip models can be applied to homogeneous models it is generally not used for capillary tube calculations. Seixlack et al. [83] report a maximum slip for choked capillary tubes of 3 %, whereas normal values range at 1 % slip. These calculations are carried out for real capillary tube geometries (L = 4 m, D = 0.61 to 0.83 mm). Older publications (Richter [76], Schwellnus et al. [154] claim a much higher slip ratio at the end of the choked tube when it comes to critical flow (slip ~ 2 to 10), but since the geometry for their test cases (L/D = 21.6) differs from standard capillary tubes for domestic refrigeration (L/D ~ 5000) a comparison cannot be done. Wein [93] compares his drift flux model with test cases calculated by Richter (1981) and comes to the conclusion that the slip ratio is much smaller (slip ~ 1.6 instead of 5.9). Also a capillary tube geometry is calculated (L = 1.829 m, D = 1.41 mm) with slip ratios below 10 %. Taking previous knowledge into account, it seems justifiable that slip correlations are put aside.

Other restrictions on behalf of the system must be stated before discretizing the equations. These are as follows:

- capillary is assumed to be straight.
- constant wall roughness, diameter and cross section over the length.
- refrigerant is pure and not contaminated with oil and other impurities.
- no delay of evaporation occurs.
- The axial heat transfer is neglected. This is concluded from an estimation of the transferred power in axial direction. Assuming standard geometry and a temperature drop from 30 °C to -25 °C the rate of axial heat flow would be around 0.02 W for the capillary tube. This equals a difference in outlet quality by 0.07 %.
- it behaves as a Newtonian fluid, i.e. its viscosity is not a function of shear velocity.
- the properties of refrigerant are constant over a cross section.
- no heat transfer between wall and refrigerant occurs and no heat sources (e.g. chemical reactions) are within the fluid ($q, \dot{q}_Q = 0$).
- transient behaviour is neglected ($\partial/\partial t = 0$). Based on Hermes et al. [41] the transient terms have minor influence on mass flow.
- the derivatives of the viscosity terms in eq. (105) stand for the power of the viscous forces and are not treated in the discretized equations.

- The derivatives of the shear stresses in eq. (107) are substituted due to the one-dimensional assumption by the term f_w which stands for the influence of wall friction. When f_w is to be modelled in eq. (110), its influence can be seen as a pressure loss or drop, hence the expression Δp_{avg} in eq. (113).

4.2.2. Deduction

The fundamental equations for fluid flow problems are the equations of mass-, momentum- and energy conservation, which means that for a one-dimensional domain three equations have to be solved in order to predict the flow. These conservation equations are written under the assumption of zero velocity in y- and z-direction, constant cross section, but taking transients and compressibility into account. Assuming the flow direction follows the x-axis, gravitational force and heat transfer play a role, the set of governing equations (eq. (98), (99) and (100)) reads like

$$\frac{\partial \rho}{\partial t} + \frac{\partial (\rho \cdot u)}{\partial x} = 0 \tag{98}$$

$$\frac{\partial (\rho \cdot u)}{\partial t} + \frac{\partial (\rho \cdot u \cdot u)}{\partial x} = -\frac{\partial p}{\partial x} + \frac{\partial \tau_{\mathrm{xx}}}{\partial x} + \frac{\partial \tau_{\mathrm{yx}}}{\partial x} + \frac{\partial \tau_{\mathrm{zx}}}{\partial x} + \rho \cdot g_{\mathrm{x}} \tag{99}$$

$$\begin{aligned} &\frac{\partial}{\partial t}\left[\rho \cdot \left(e + \frac{u \cdot u}{2}\right)\right] + \frac{\partial}{\partial x}\left[\rho \cdot u \cdot \left(e + \frac{u \cdot u}{2}\right)\right] = \\ &= -\frac{\partial}{\partial x}(p \cdot u) - \frac{\partial q}{\partial x} + \frac{\partial (u \cdot \tau_{\mathrm{xx}})}{\partial x} + \frac{\partial \left(u \cdot \tau_{\mathrm{yx}}\right)}{\partial y} + \frac{\partial (u \cdot \tau_{\mathrm{zx}})}{\partial z} + \rho \cdot u \cdot g_{\mathrm{x}} + \dot{q}_Q \end{aligned} \tag{100}$$

For steady state conditions all terms with $\partial/\partial t = 0$ vanish and so does q (heat transferred over the boundaries) and $\dot{q}_Q$ (heat source per unit volume) for an adiabatic case – the equations become

$$\frac{\partial (\rho \cdot u)}{\partial x} = 0 \tag{101}$$

$$\frac{\partial (\rho \cdot u \cdot u)}{\partial x} = -\frac{\partial p}{\partial x} + \frac{\partial \tau_{\mathrm{xx}}}{\partial x} + \frac{\partial \tau_{\mathrm{yx}}}{\partial x} + \frac{\partial \tau_{\mathrm{zx}}}{\partial x} + \rho \cdot g_{\mathrm{x}} \tag{102}$$

$$\frac{\partial}{\partial x}\left[\rho \cdot u \cdot \left(e + \frac{u \cdot u}{2}\right)\right] = -\frac{\partial}{\partial x}(p \cdot u) + \frac{\partial (u \cdot \tau_{\mathrm{xx}})}{\partial x} + \frac{\partial \left(u \cdot \tau_{\mathrm{yx}}\right)}{\partial y} + \frac{\partial (u \cdot \tau_{\mathrm{zx}})}{\partial z} + \rho \cdot u \cdot g_{\mathrm{x}} \tag{103}$$

Due to one dimensional flow domain, the gradients of shear stress can't be resolved. Therefore these terms are modelled by empirical functions which exist for a vast amount of different pipe geometries, fluids and flow patterns. In eq. (99) these terms are substituted later on in equation (110) by the term f_w which stands for the influence of wall friction. Using the connection between enthalpy and inner energy in eq. (104)

$$h = e + p/\rho \Leftrightarrow e = h - p/\rho \tag{104}$$

the energy equation can be rewritten as

$$\frac{\partial}{\partial x}\left[\rho \cdot u \cdot \left(h + \frac{u \cdot u}{2}\right)\right] = \frac{\partial(u \cdot \tau_{xx})}{\partial x} + \frac{\partial\left(u \cdot \tau_{yx}\right)}{\partial y} + \frac{\partial(u \cdot \tau_{zx})}{\partial z} + \rho \cdot u \cdot g_x \tag{105}$$

The work of the viscous terms in eq. (105) is neglected and finally we get

$$\frac{\partial(\rho \cdot u)}{\partial x} = 0 \tag{106}$$

$$\frac{\partial(\rho \cdot u \cdot u)}{\partial x} = -\frac{\partial p}{\partial x} + \frac{\partial \tau_{xx}}{\partial x} + \frac{\partial \tau_{yx}}{\partial x} + \frac{\partial \tau_{zx}}{\partial x} + \rho \cdot g_x \tag{107}$$

$$\frac{\partial}{\partial x}\left[\rho \cdot u \cdot \left(h + \frac{u \cdot u}{2}\right)\right] = \rho \cdot u \cdot g_x \tag{108}$$

In the momentum equation the gradients of the viscous terms are replaced by a force per unit volume (f_w) which is modelled by applying empirical formulae for friction later on. Next, integration along x-direction over a cell results in

$$\rho \cdot u \Big[{}^{i+1}_{i} = 0 \tag{109}$$

$$\rho \cdot u \cdot u \Big[{}^{i+1}_{i} = -\, p \Big[{}^{i+1}_{i} + \int_i^{i+1} f_w \cdot dx + \int_i^{i+1} \rho \cdot g_x \cdot dx \tag{110}$$

$$\rho \cdot u \cdot \left(h + \frac{u \cdot u}{2}\right) \Big[{}^{i+1}_{i} = \int_i^{i+1} \rho \cdot u \cdot g_x \cdot dx \tag{111}$$

Due to eq. (109) the product of $\rho \cdot u$ is constant and can be reduced in eq. (111). The integral over the term containing the gravitational acceleration g_x in the momentum equation is evaluated under the assumption of constant density since its influence is small compared to other terms. In the liquid regime constant density assumption is close to reality anyway and in the two phase regime the velocity rises quickly – the term $\rho \cdot u^2$ on the left hand side outweighs $\rho \cdot g_x$. The integral over the force per volume is substituted by the expression $\Delta\overline{p_{f_w}}$ which is evaluated by empirical friction laws using averaged cell properties.

Finally, we gain a set of discretized equations:

$$[\rho \cdot u]^{i+1} - [\rho \cdot u]^{i} = 0 \tag{112}$$

$$[\rho \cdot u \cdot u]^{i+1} - [\rho \cdot u \cdot u]^{i} = -([p]^{i+1} - [p]^{i}) + \Delta\overline{p_{f_w}} + \Delta x \cdot \bar{\rho} \cdot g \cdot \sin\varphi \tag{113}$$

$$\left[h+\frac{u\cdot u}{2}\right]^{\mathrm{i}+1}-\left[h+\frac{u\cdot u}{2}\right]^{\mathrm{i}}=\Delta x\cdot g\cdot\sin\varphi \tag{114}$$

where the angle φ is measured from a horizontal position and $\Delta x = x^{i+1} - x^{i}$.

$$\Delta\overline{p_{f_{\mathrm{w}}}}=\bar{\lambda}\cdot\frac{\Delta x}{D}\cdot\frac{\bar{\rho}\cdot\bar{u}^{2}}{2} \tag{115}$$

For the determination of critical flow conditions some authors use the entropy equation as aid to predict the point of critical flow ([25], [32], [91]). This equation is not a necessity for the code used in this work but is mentioned for the sake of completeness. The entropy equation can be written like in equation (116) where *S* stands for the entropy of a fluid within the control volume, S_Q is the entropy transported by heat transfer across the boundary, S_m is the entropy transported by inflow or outflow and S_{irr} is the irreversible entropy production [197]. The formulation describes the change of entropy in a system with heat and mass transferred over its boundaries during an infinitesimal small timestep, *dt*.

$$dS=dS_Q+dS_m+dS_{irr} \tag{116}$$

The assumption of steady state conditions, which will be used for the capillary tubes, forces the temporal change of entropy within a cell to become zero.

$$\frac{dS}{dt}=0\Rightarrow\dot{S}_{irr}=-\dot{S}_Q-\dot{S}_m \tag{117}$$

$\dot{S}_Q$ can be expressed as heat transfer rate $\dot{Q}$ related to the temperature T_Q. This temperature is determined at the point where $\dot{Q}$ enters the system (equation (118)).

$$\dot{S}_Q=\frac{\dot{Q}}{T_Q} \tag{118}$$

$\dot{S}_m$ is the sum of the entropy fluxes by transport of fluid across the boundaries.

$$\dot{S}_m=\dot{m}_{in}\cdot s_{in}-\dot{m}_{out}\cdot s_{out} \tag{119}$$

Positive mass flow rates are inflows and positive heat transfer rate means that heat is transferred into the system. For steady state problems $\dot{m}_{in} = \dot{m}_{out}$, secondly, the temporal change of the system's entropy must be zero. The specific entropy, [s] = J/kg K, is a thermodynamic state variable and determined by the fluid state.

$$0=\frac{\dot{Q}}{T_Q}+\dot{m}\cdot s_{in}-\dot{m}\cdot s_{out}+\dot{S}_{irr} \tag{120}$$

$$\dot{S}_{irr} = \dot{m} \cdot s_{out} - \dot{m} \cdot s_{in} - \frac{\dot{Q}}{T_Q} \geq 0 \tag{121}$$

The second law of thermodynamics states that $\dot{S}_{irr} \geq 0$. The result is an equation for the irreversible entropy generation. Due to the common case, that no heat is transferred from the capillary's outlet section due to insulation, the equation can be further simplified to a simple balance

$$\dot{S}_{irr} = \dot{m} \cdot (s_{out} - s_{in}) \geq 0 \tag{122}$$

This balance is checked for validity especially in the last cell and is also used by some authors ([25], [32] , [91]) to detect critical flow conditions at the outlet. If in the adiabatic last cell s_{in} gets bigger than s_{out} then the calculation has to be interrupted. In an enthalpy/entropy-diagram the adiabatic expansion follows a curve which is named "Fanno curve" [163]. Constant total enthalpy $h_0 = h + u^2/2$ is expressed as enthalpy h of the flow moving at velocity u. Assuming constant cross section A and mass flow rate $\dot{m}$, the relation can be expressed as

$$h_0 = h + \frac{v^2}{2} \cdot \left(\frac{\dot{m}}{A}\right)^2 \tag{123}$$

where v is the specific volume. Different velocities yield different thermodynamic states (h, v). The corresponding entropy can be calculated from enthalpy and specific volume. With growing velocity, the entropy also grows until it reaches a maximum. At this point the fluid is at maximum speed (sonic speed) and can't be accelerated further without appropriate cross-sectional profile.

4.2.3. Implementation and validation

The schematic of the procedure is shown in Fig. 18 where an initial guess of mass flow rate is used to determine an outlet pressure p_{out}. This pressure won't match with the desired outlet pressure, so the mass flow rate has to be iterated. The limits of this "outer" loop of iteration is the choked mass flow rate and zero mass flux (when p_{out} is equal to p_{in}). Due the nonlinear dependency of p_{out} and mass flow rate (Fig. 24 (b)) a Newton scheme can not be applied as stand-alone solver and has to stand behind a Regula-Falsi method. In every case, the choked mass flow rate is determined first, then, if the given outlet pressure is higher than the outlet pressure for choking the iteration continues. Otherwise the scheme stops and gives back the choked mass flow rate. The cell-wise iteration loop evaluates downstream values starting from a guess by a cubic polynomial from known upstream values. Then the iterative loop in Fig. 18 (b) is carried out until the changes in thermodynamic properties fall beyond a certain limit and the next cell is evaluated until the end of the capillary tube is reached.

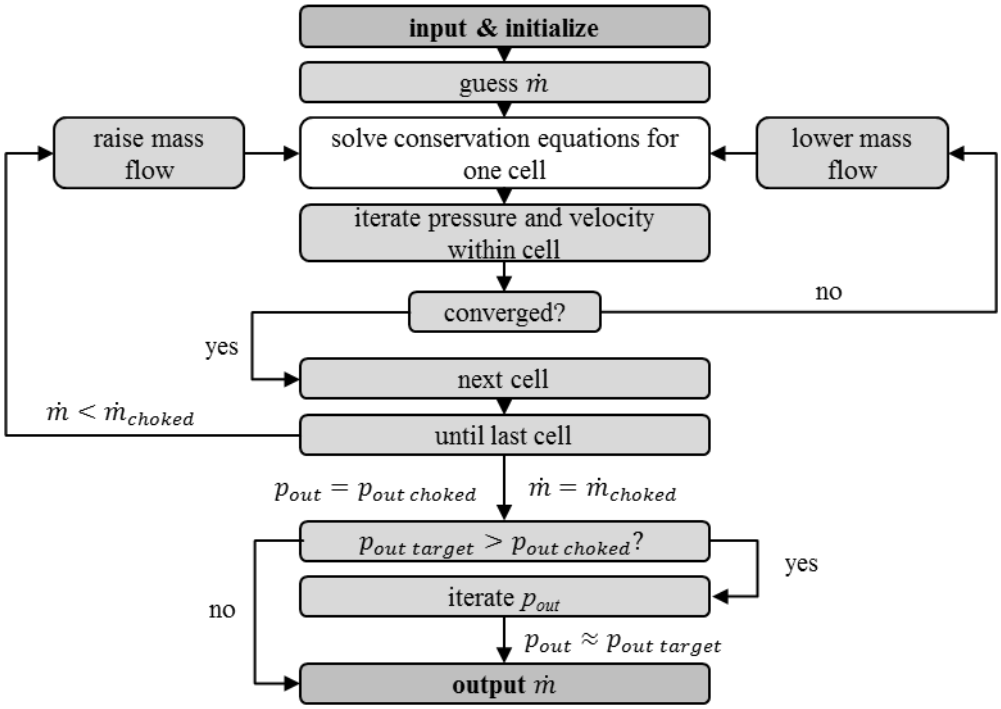

(a)

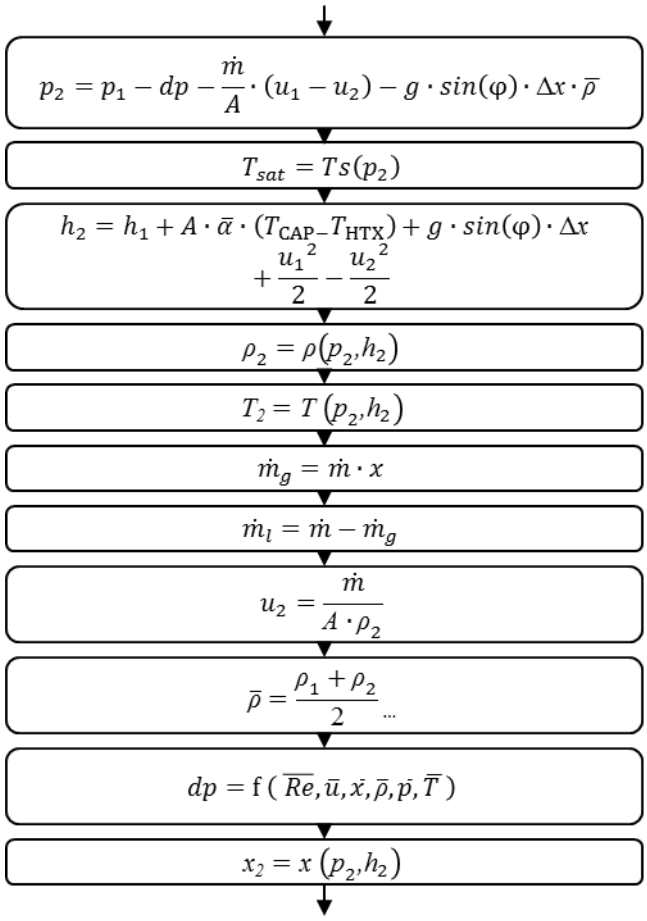

(b)

Fig. 18 Step by step procedure of the program (a). The inner loop (white) which is repeated for each cell is shown separately (b).

A mesh was set up which accounts for the spatial gradients in fluid properties. It is well known that after the onset of evaporation pressure and temperature start decreasing more and more rapidly. To account for such conditions a mesh was generated by using equation (124). This equation explicitly calculates the length of a cell, where *d* is the total amount of cells, *L* is a reference length of a cell element. Parameter α leads to a homogeneous cell size if its value is 1 and it decreases the cell size towards the outlet if it gets bigger than 1. Parameter β ranges between 0 and 100 and influences the rate of decrease. In Fig. 19 different configurations, varying α and β, are shown. For further computations $\alpha = 1.1$ and $\beta = 99$ are used which allow stable computations even on a 50 cell grid (adiabatic case) with the same accuracy than on a homogeneously distributed 100 cell grid. Similar methods can be found in (Escanes, 1995). The advantage of this formula lies in a better spatial resolution of the last cells, which turned out to be essential when it comes to choked flow.

$$\Delta z(i) = L \cdot \left[\alpha^{\tan\left(\frac{\beta}{100}\frac{\pi}{2}\frac{i}{d}\right)}\right]^{-1} \Big/ \sum_{i=1}^{i=d}\left[\alpha^{\tan\left(\frac{\beta}{100}\frac{\pi}{2}\frac{i}{d}\right)}\right]^{-1} \qquad (124)$$

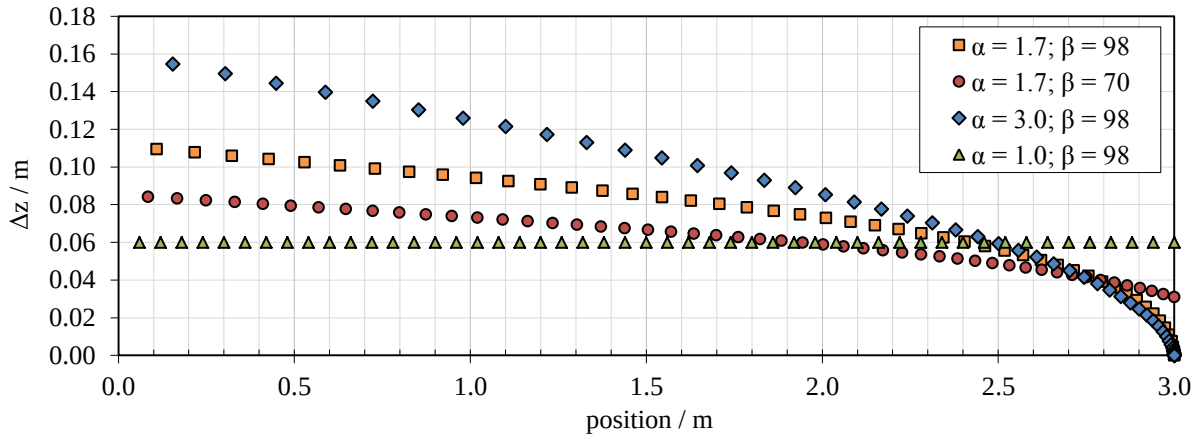

Fig. 19 Influence of α and β on the cell size distribution.

A comparison between a regular grid and a refined one is shown in Fig. 20 where the same boundary conditions which lead to choked flow are applied to different grids. Except the fact that the overall difference in mass flow rate is comparably small anyway (0.004 kg/h) it can be seen that the difference between a 50- and a 500-cell grid doubles when the advantages of a refined grid are abdicated – in other words a slight advantage is gained since using a homogeneous grid with 100 cells is as accurate as using a 50 cell refined grid – a saving of 50 % computational time. Apart from that another conclusion can be drawn: It doesn't make sense to use more than 500 cells since the error in spatial discretization seems to reach a limit according to this study. Concerning the computational scheme the following graphics illustrate the workflow for the adiabatic case. The initialization concerns not only a guess of mass flow rate – also the values downstream have to be guessed. Therefore the previous values can be used directly or extrapolated from the previous ones. Next, the conservation equations are solved according to the scheme. The order of function calls is given in Fig. 18,

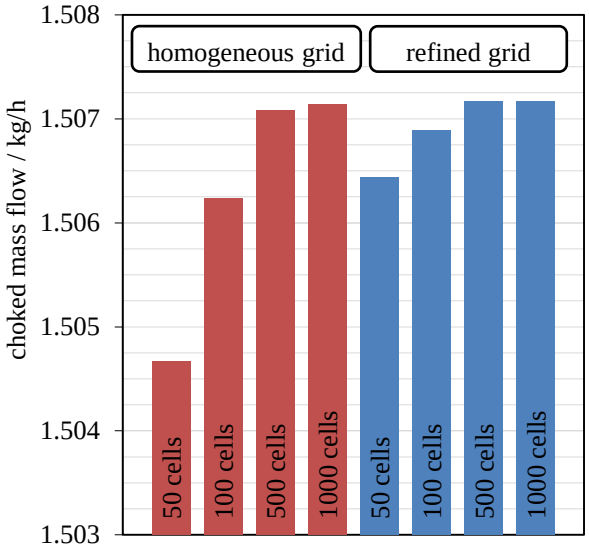

Fig. 20 Comparison of results on different grids.

averaged properties over the length of a cell are denoted with an overline. This loop is carried out until all properties have converged for a single cell, then the properties for the next cell can be extrapolated and this procedure is pursued until either the end of the capillary tube is reached or the scheme can't find a solution for a cell. In the first case it means that for a given mass flow rate a steady state solution has been found, for the latter one it means that the initial guess of the mass flow rate has been higher than the choked mass flow rate allows. To gain a predefined outlet pressure, another iterative loop over the whole capillary tube has to be carried out with varying mass flow rate. For this purpose a Newton scheme has been tried but with little success since the slope of the function $\dot{m}(p_{out})$ is very steep when it comes to choking. The better choice proved to be a simple Regula-Falsi method.

In a next step, the friction- and viscosity laws which were presented in chapter 2.2 – 2.4, are applied in a 1d-simulation. Different combinations of these correlations are possible and equally justifiable. The aim is, to find the best option for a given set of measured data. The dataset consists of 19 measurements under choked conditions for R600a by Melo et al. [63]. Since the 1d-model should be used for this refrigerant in future also the tuning is carried out with measurements where R600a is used. The deviation between calculated and measured results is shown in Fig. 21 in terms of mean relative error (red) and standard deviation (blue). On a first glance the viscosity model of Bittle and Weis shows unsatisfactorily high results irrespective of the friction correlation (Fig. 21 (a)). The model of Churchill as well as Haaland show a low mean relative error and are the preferred choice for future calculations. Vacek and Vins [91] for instance conclude that Colebrook works best for their copper capillary tubes – which means that there is obviously no valid universal combination of friction laws. Concerning two phase multipliers (Fig. 21 (b)) one sees that they perform not so well as the other models on this set of measurements, though Friedel's two phase multiplier is sometimes used for this kind of calculation. Fig. 22 (a, c) show exemplarily the ambiguity of this way of selecting friction laws since one set of measurements (c) has low average error whereas the second one (a) has definitely a underestimation of mass flow rates which could be lowered with other combinations of friction laws. Most of the cases in this work are calculated with the following setup: Churchill (friction liquid), Colebrook (friction vapour) and a two phase viscosity according to Lin. A closer description of these models can be looked up in chapter 2.

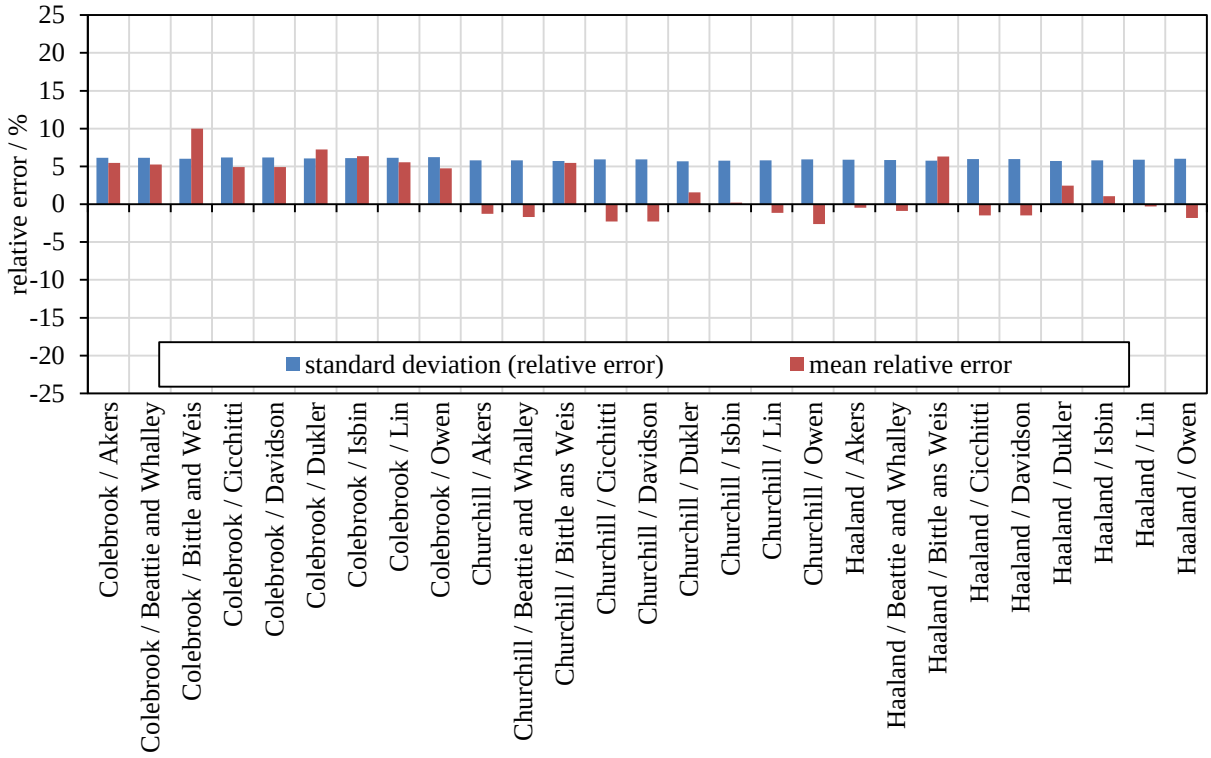

(a)

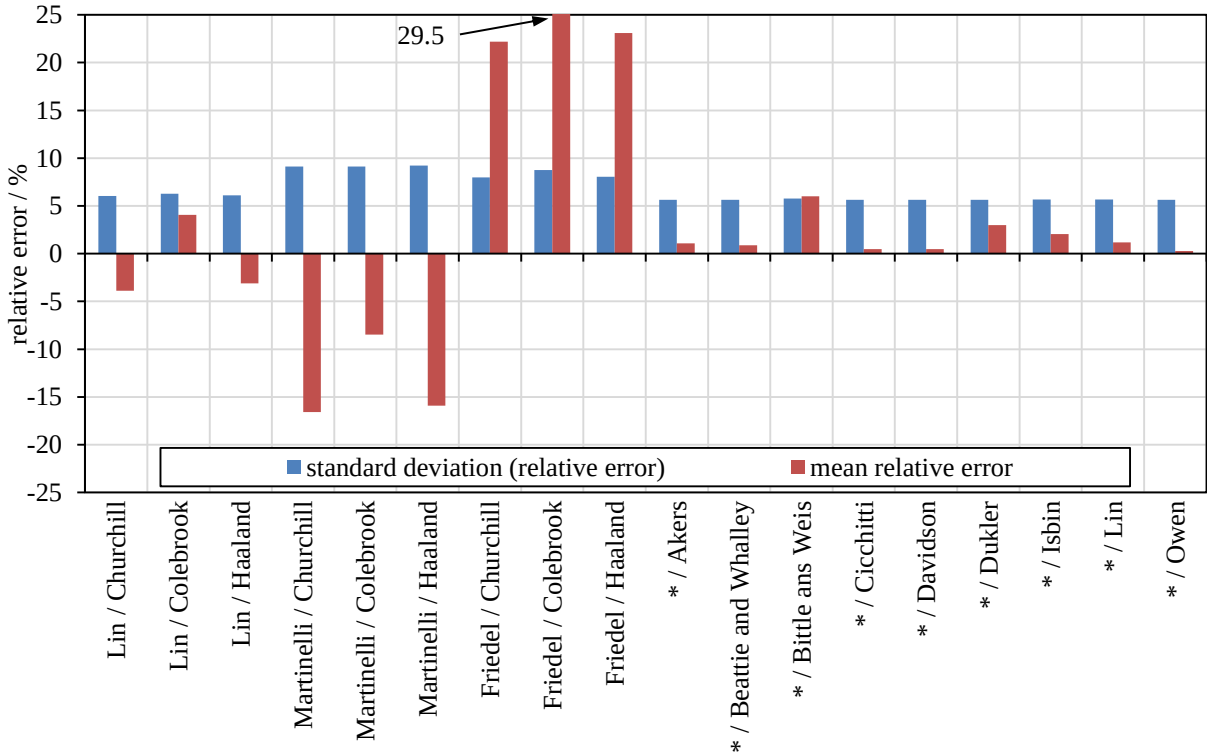

(b)

*Fig. 21 Comparison of correlations for friction and viscosity with experimental data by Melo et al. [63]. Two phase multipliers are compared in (b), * stands for Churchill's law in the liquid regime and Colebrook's law for vapour regime.*

For means of validation experimental sets of data have been collected in the course of this work for different refrigerants which are R600a, R134a, R152a, R12 and R22. The collection comprises measurements, designed and carried out by four independent groups of researchers including the author of this work. The range of input data is given in Table 4. Measurements by Schenk and Oellrich [82] cover the lowest range of mass flow rates, starting from 0.5 kg/h whereas some datasets exceed 100 kg/h. The model obviously covers the main parameters which have impact on the mass flow rate and it seems that the same level of accuracy applies to all sets. The standard deviation of the relative error (unit is percentage points) is 7.2 (a) / 4.7 (b) / 6.1 (c) / 2.2 (d) / 6.1 (e) / 5.1 (f) / 5.5 (g) / 4.5 (h). Mean deviation of the relative error is -6.0 (a) / -2.6 (b) / -0.4 (c) / -6.7 (d) / 3.5 (e) / 8.5 (f) / 1.2 (g) / -5.8 (h). The computations were carried out using an inhomogeneous 500 cell grid. The qualitative overall error for these 550 steady state points can be given by a final mean- and standard deviation of -0.45 kg/h and 1.33 kg/h. Excluding all sets with nominal mass flow rates higher than 10 kg/h (since they are simply not relevant for domestic refrigeration) the mean- and standard deviation drops down to -0.09 kg/h and 0.22 kg/h, respectively. Including all sets of measurements and speaking in terms of relative error the mean is -4.26 percentage points and standard deviation is 7.27 percentage points. One can also say that 96.9 % of the measurements are within ±10 % bounds and 88.9 % are within the ±5 % bounds.

$$\dot{m}_{err} = \dot{m}_{exp} - \dot{m}_{sim} \tag{125}$$

$$\mu_{\dot{m}} = \frac{1}{N} \cdot \sum_{i=1}^{N} \dot{m}_{err\,i} \tag{126}$$

$$\sigma_{\dot{m}} = \sqrt{\frac{1}{N-1} \cdot \sum_{i=1}^{N} \dot{m}_{err\,i}{}^{2}} \tag{127}$$

The error is defined like in equation (125), mean- standard deviation are calculated like in equation (126) and (127).

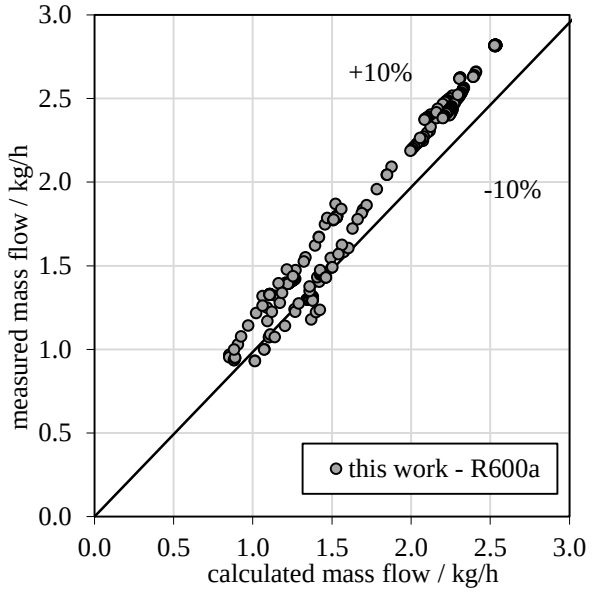
3.0
2.5
2.0
1.5
1.0
0.5
0.0
0.0 0.5 1.0 1.5 2.0 2.5 3.0
+10%
-10%
this work - R600a
measured mass flow / kg/h
calculated mass flow / kg/h

(a)

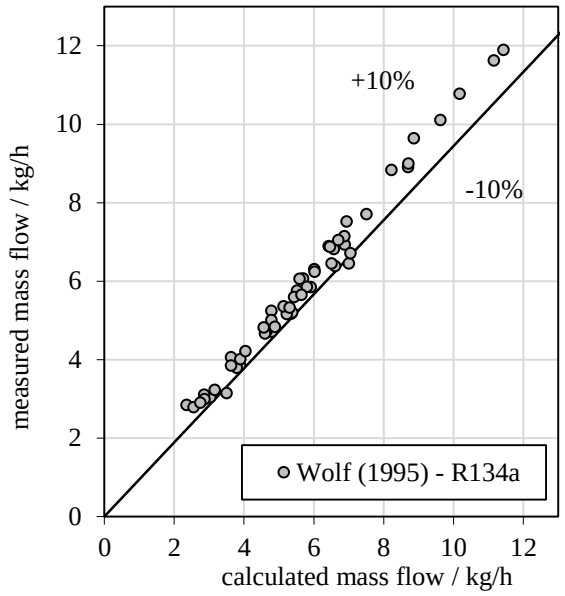
12
10
8
6
4
2
0
0 2 4 6 8 10 12
+10%
-10%
Wolf (1995) - R134a
measured mass flow / kg/h
calculated mass flow / kg/h

(b)

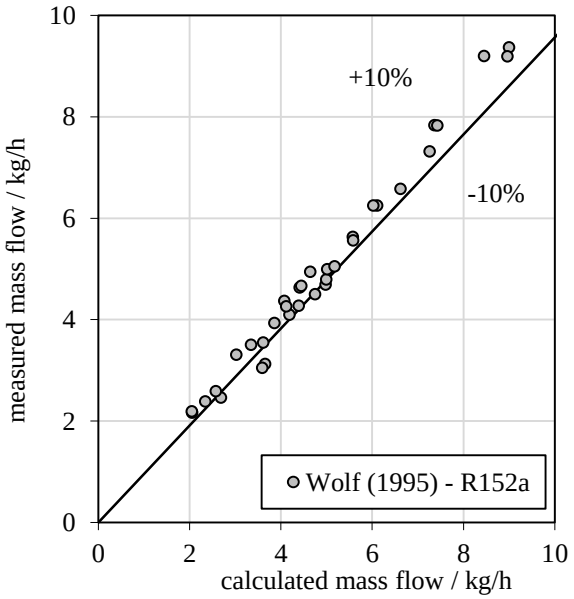
10
8
6
4
2
0
0 2 4 6 8 10
+10%
-10%
Wolf (1995) - R152a
measured mass flow / kg/h
calculated mass flow / kg/h

(c)

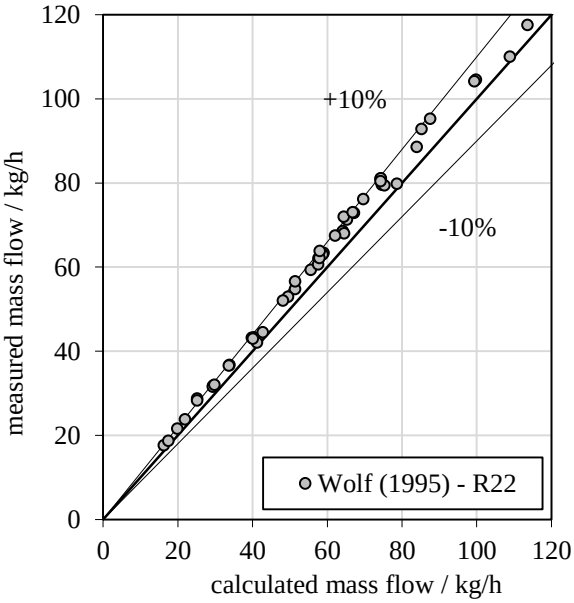
120
100
80
60
40
20
0
0 20 40 60 80 100 120
+10%
-10%
Wolf (1995) - R22
measured mass flow / kg/h
calculated mass flow / kg/h

(d)

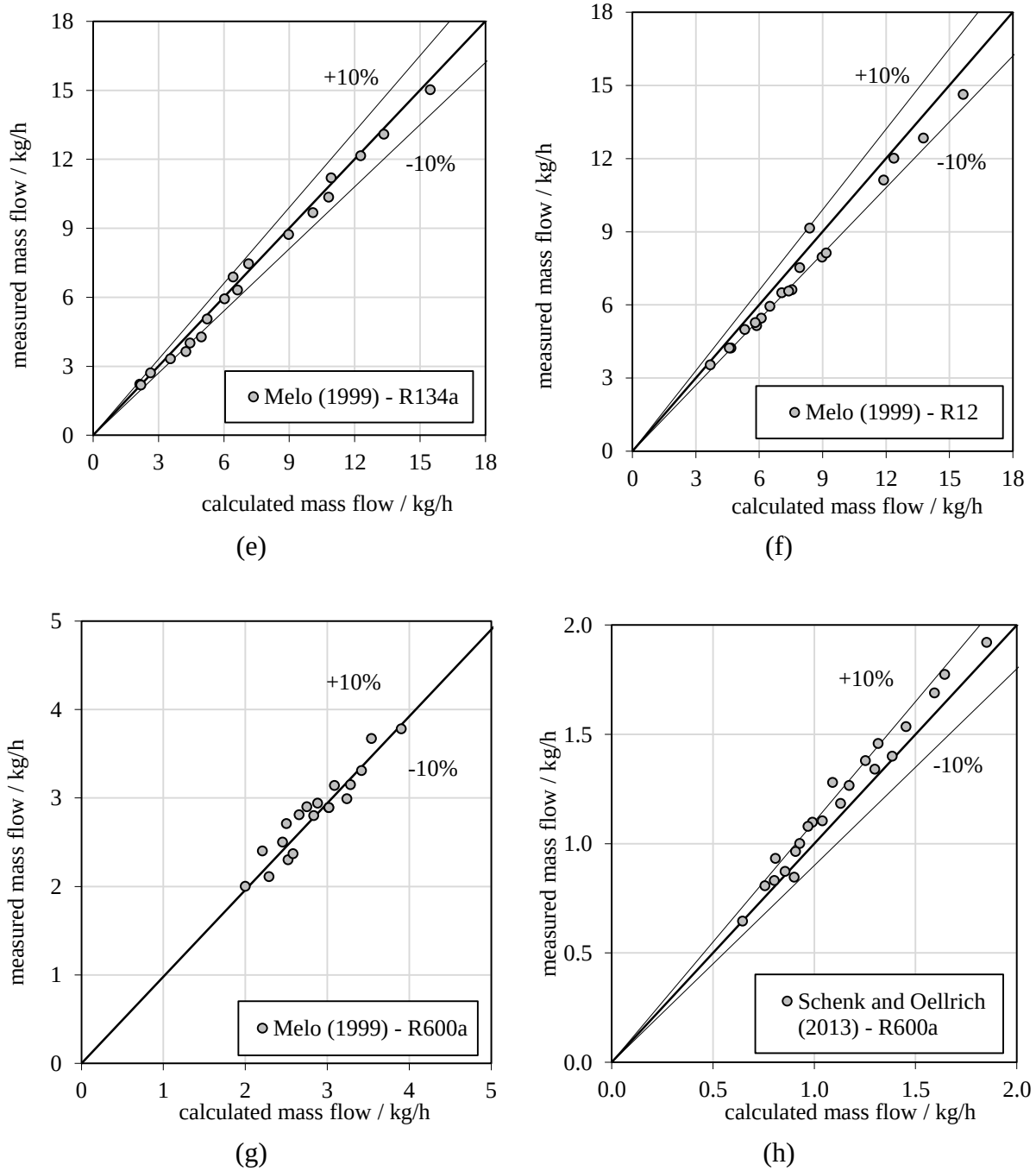

Fig. 22 Comparison of theory and practice. Measurements by the author (a), by Wolf et al. [96] (b-d), by Melo et al. [63] (e-g) and Schenk and Oellrich [82] recalculated with the given boundary conditions and refrigerants.

The reason for the remaining difference between experiment and prediction is estimated to stem from firstly delay in vaporization which is discussed in chapter 4.4, secondly from oil influence, thirdly uncertainty in measurement and last all other simplification mentioned in the chapter where the equations for the adiabatic model are derived.

Table 4 Range of experimental datasets for adiabatic case.

Fig. 22	**-**	**(a)**	**(b)**	**(c)**	**(d)**	**(e)**	**(f)**	**(g)**	**(h)**
fluid	**-**	**R600a**	**R134a**	**R152a**	**R22**	**R134a**	**R12**	**R600a**	**R600a**
min p_{out}	**bar**	0.6	1.4	1.7	3.2	1.0	0.9	1.0	0.5
max p_{out}	**bar**	1.8	2.1	3.1	6.9	1.7	1.9	1.1	1.0
min p_{in}	**bar**	4.9	6.9	5.3	12.5	9.0	9.2	7.1	4.0
max p_{in}	**bar**	9.3	13.8	11.0	20.7	15.1	18.2	11.3	6.0
min T_{sub}	**K**	2.5	1.7	2.7	1.0	3.4	2.9	3.3	2.6
max T_{sub}	**K**	12.5	17.4	16.9	16.8	13.3	13.4	15.7	13.0
min L	**m**	4.0	1.5	1.5	0.5	2.0	2.0	2.0	2.5
max L	**m**	7.0	5.1	5.1	2.5	3.0	3.0	2.9	4.0
min D	**mm**	0.71	0.66	0.66	1.07	0.61	0.77	0.77	0.61
max D	**mm**	0.98	1.07	3.05	2.29	1.05	1.05	0.77	0.69
min $\dot{m}$	**kg/h**	0.9	2.8	2.2	17.6	2.2	3.5	2.0	0.6
max $\dot{m}$	**kg/h**	3.0	11.9	93.4	163.7	15.0	14.6	3.8	1.9

4.2.4. Course of expansion

Plotting the thermodynamic properties over the length an easy judgment in respect to plausibility can be done. Here, an adiabatic capillary tube with 0.883 mm inner diameter, mass flow rate by 2.31 kg/h under choked conditions is used to demonstrate the functionality of the code. The subcooled liquid refrigerant is subject to friction, therefore the pressure drops until evaporation after 3 m in length sets on. The quality rises, more rapidly towards the end, until the flow exits the capillary tube with a quality of around 0.25, of course depending on the specific operating conditions. In Fig. 23 (c) the total specific enthalpy is compared to the specific enthalpy – the difference, simply $u^2/2$, becomes clearly visible at the outlet where up to 90 m/s are calculated for the exit velocity.

Given the fact that at the end of the capillary tube is commonly soldered directly into the beginning of the evaporator, this means an instant change in diameter by the factor of 5 to 10. Little pressure recovery can be assumed and for the case above it would mean that 2.5 W power are dissipated to heat. Also, noise stems from this rapid outlet and is still a spot of ongoing improvement from the refrigeration manufacturer's point of view.

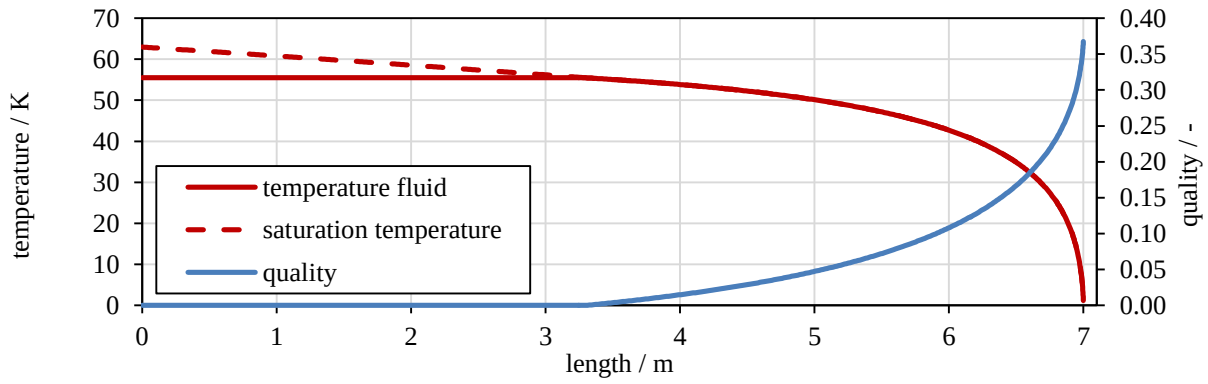

(a)

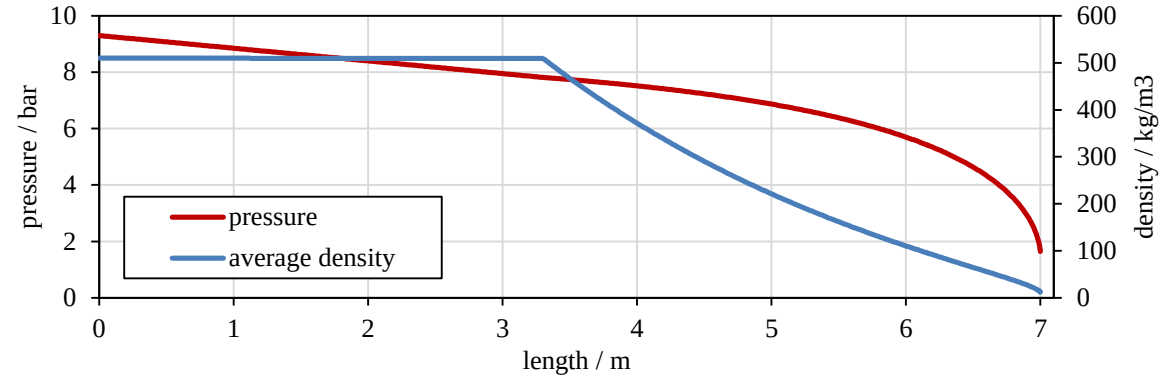

(b)

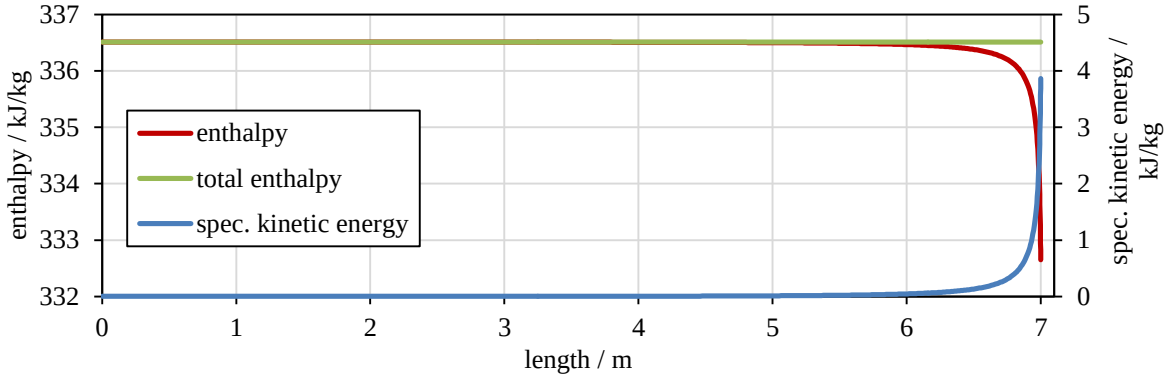

(c)

Fig. 23 Temperature and quality (a) pressure and average density (b) as well as enthalpy and specific kinetic energy.

4.2.5. Parameter studies

In this chapter parameter studies are carried out, i.e. varying a single parameter and observing the impact on others. This step gives important evidence on the priority of parameters when it has to be decided which influence can be neglected. Also the (non-) linearity of the functions can be visualized. Noteworthy, in Fig. 24 (b), the mass flow rate becomes independent of the outlet pressure at 2 bar, a sign of choking. Also length and inner diameter behave strongly non-linear where the latter one additionally has the highest impact on the flow. Originating from Fig. 24 and Fig. 25 it can be seen that inlet- and outlet pressure, subcooling, length and inner diameter are dominant and that the surface roughness is of minor importance. Modern copper drawing machines are capable of manufacturing capillary tubes with roughness below 1 micron [189] – a change in mass flow rate by 0.05 kg/h (3.7 kg/h nominal).

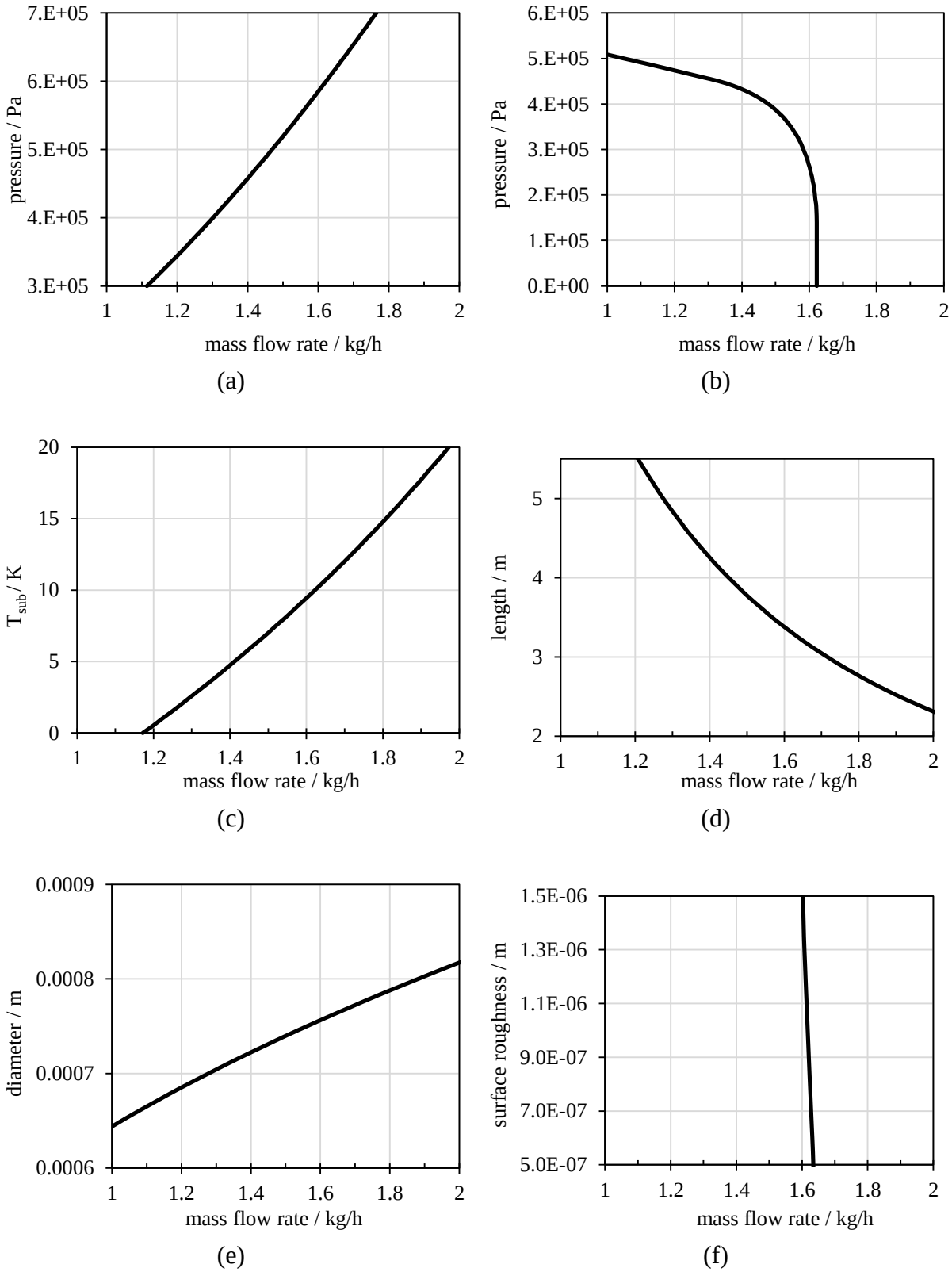

Fig. 24 Mass flow rates versus inlet pressure (a), outlet pressure (b), subcooling (c), length (d), diameter (e), and absolute surface roughness (f).

Fig. 25 features some additional information on how inclination of the tube matters and how important a well-adjusted friction law might be. A few words on the generation of this figure are given. A number of points (~250) which lie in the operating range of typical household

refrigerators is taken as a "reference"-field against which modified "test"-fields are compared. The modifications consist in a shift of + or –10 % of a certain input quantity. Since the temperature is measured as subcooling, no thoughts have to be spent on if the scale is in Celsius or Kelvin. The grey bar indicates the average deviation in mass flow rate (average of the relative deviations, to be exact). Since the outlet pressure for instance has no impact on mass flow under critical conditions and such conditions occur also in the scope of this study, its impact is not investigated further.

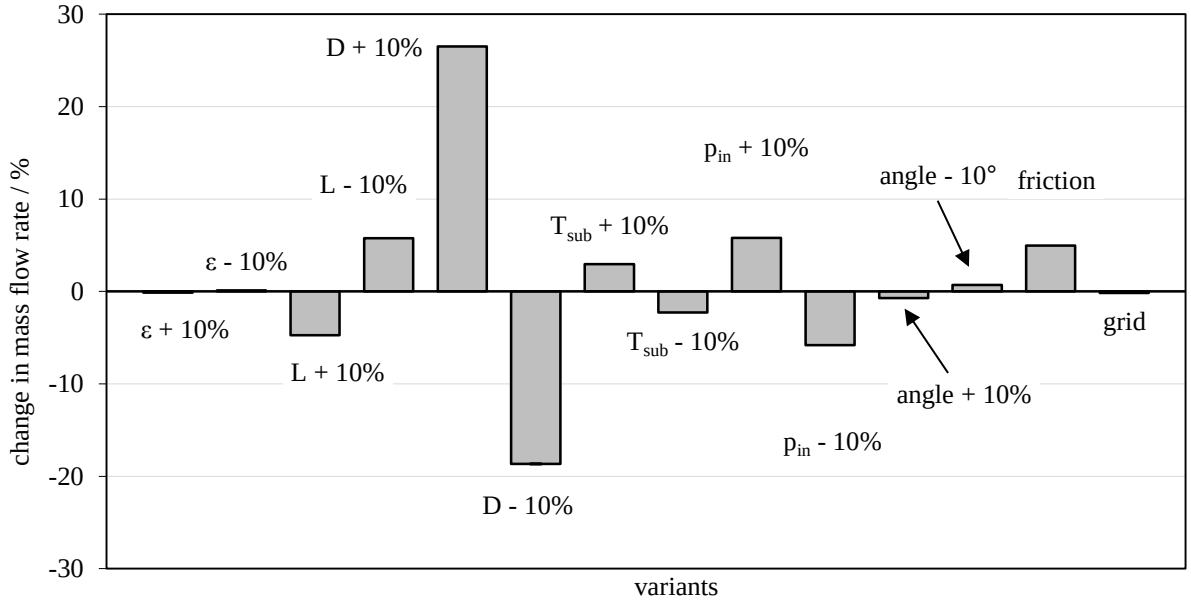

Fig. 25 Impact on mass flow rate.

A word about the absolute values of this study: The average mass flow rate is about 4 kg/h, subcooling at 7.5 K, diameter at 1 mm, length at 3 m, inlet pressure at 6.5 bar and surface roughness at 0.75 µm. The inclination, labeled "angle", shows that the difference between a horizontal and a vertical tube is negligibly small whereas the difference between certain friction correlations show 0.2 kg/h difference in mass flow rate at 4 kg/h nominal flow rate which is as much as 5 % – a good reason to pick proper friction laws. What can be neglected for further investigations is the influence of the grid and the surface roughness. A low variation in surface roughness for these kind of tubes can be expected, absolute values are around 1 µm [189]. All other parameters in particular the inner diameter should be taken care of in both simulation and measurement.

4.3. Homogeneous diabatic models

Similar investigations like above shall be applied to a setup including an internal heat exchanger. In chapter 1.2.2 the basics are already explained, here the governing equations, the simplifications and discretization as well as some computational results are presented.

4.3.1. Theory

Like for the adiabatic model, some simplifying assumptions have to be made before getting started with coding – For the coaxial type these are:

- perfectly parallel pipes – the gap between inner (capillary) and outer pipe (suction line) is constant.
- no heat transfer in axial direction. According to an estimation similar to the adiabatic case assuming standard geometry and operating conditions, the axially transferred rate of heat flow is less than 1 % for the suction line referred to the overall transferred heat.
- heat transfer is steady state – walls are treated as heat resistance only.
- heat transfer correlations are assumed between fluid and wall.

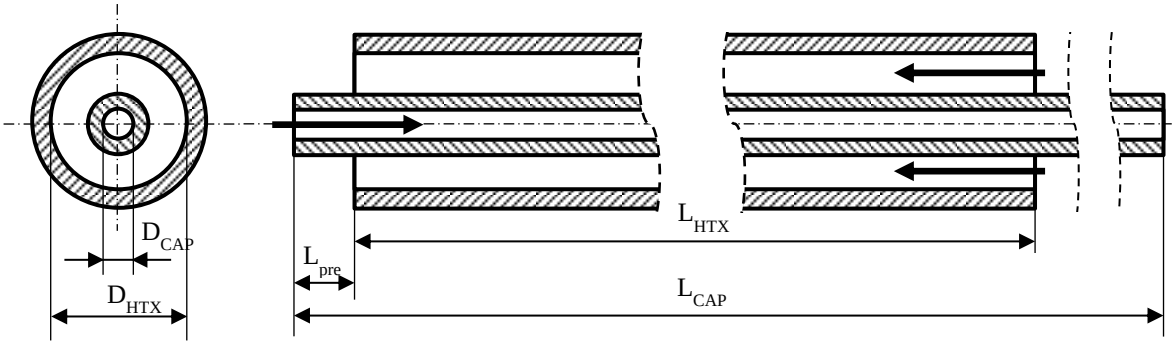

(a)

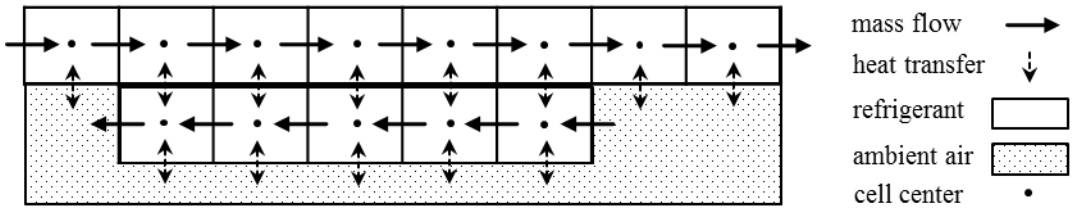

(b)

Fig. 26 Sketch of a coaxial counter-flow heat exchanger (a) and scheme of the computational domain (b).

A coaxial type was chosen for further studies, since no uncertainties concerning the structure and its shape exist like for other parallel heat exchangers where one pipe is soldered to the outside of the latter. In some cases it is not even soldered but fixed with a kind of heat shrink tube which makes analytical predictions concerning the heat transfer everything else but accurate. The main concern using a coaxial type is that in reality it can not be guaranteed that the inner pipe runs perfectly straight inside of the other. Because of bending in the heat exchanger for the ease of installation it might also be the case that the pipes get in contact with each other.

4.3.2. Deduction

The set of equations can be taken from chapter 4.2.2 where only the energy equation has to be adapted according to the heat transfer across the wall. For the flow in the capillary tube they can be written as

$$[\rho \cdot u]^{i+1} - [\rho \cdot u]^{i} = 0 \qquad (128)$$

$$[\rho \cdot u \cdot u]^{i+1} - [\rho \cdot u \cdot u]^{i} = -([p]^{i+1} - [p]^{i}) + \Delta\overline{p_{f_w}} + \Delta x \cdot \bar{\rho} \cdot g \cdot \sin\varphi \quad (129)$$

$$\dot{m} \cdot \left[h + \frac{u \cdot u}{2}\right]^{i+1} - \dot{m} \cdot \left[h + \frac{u \cdot u}{2}\right]^{i} = \dot{m} \cdot \Delta x \cdot g \cdot \sin\varphi + \dot{Q}_{wall} \quad (130)$$

where $\dot{m}$ is the capillary tube mass flow rate and

$$\dot{Q}_{wall} = A_o \cdot k_o \cdot (T_{Fluid\,1} - T_{Fluid\,2}) \quad (131)$$

$$k_a = \frac{1}{\frac{1}{\alpha_i} \cdot \frac{r_o}{r_i} + \frac{r_o}{\lambda} \cdot ln\left(\frac{r_o}{r_i}\right) + \frac{1}{\alpha_o}} \quad (132)$$

Index "o" stands for the outer and "i" for the inner surface of the pipe, "Fluid 1" and "Fluid 2" for the corresponding fluids inside or outside. This can be either refrigerant-refrigerant or refrigerant-air depending on the position along the tube. For the suction line the momentum equation can be neglected due to nearly constant fluid velocity and low friction. Hence, only the conservative equations of mass and energy play a significant role.

$$[\rho \cdot u]^{i+1} - [\rho \cdot u]^{i} = 0 \quad (133)$$

$$\dot{H}^{i+1} - \dot{H}^{i} = \dot{Q}_{wall} \quad (134)$$

4.3.3. Implementation and validation

The implementation is straightforward, a grid parallel to the adiabatic capillary tube as described in the previous chapter is set up where the flow parameters of the suction line are stored. Since the cell size of the capillary differs from cell to cell, the grid of the suction line is adapted to that shape. Heat transfer correlations are described in section 3.2 and used in this model accordingly. In the experiment the outer wall is insulated by putting the apparatus into a wooden box filled with glass wool – therefore it is assumed that the heat transfer to the surrounding air can be neglected and is set to zero during all runs. The heat exchange occurs solely between the suction line and the capillary tube. For validation a set of 30 steady state points at choked conditions are available (Melo et al. [66]). Care has to be taken at point number 9 from the regular dataset since the inlet temperature of the suction line is slightly below the evaporation temperature. Because of the difference (0.16 K) is within the range of uncertainty of the transducers this fact can be contributed to uncertainty of measurement. From Fig. 27 it can be seen that the mass flow rates are well predicted without changing the setup of the program. The outlet temperatures of the suction line are underpredicted by about 7 K but seem to give the right trend. The standard deviation of the error concerning mass flow rates can be given by 7.0 % (0.1 kg/h) and -0.3 % (-0.03 kg/h) mean value. For the temperatures the reader is referred to Fig. 27 (b). The reason for the offset in suction line outlet temperatures can be sought for different reasons – firstly the correlations for the alpha values in the suction line may underpredict the actual values since runs with a 1.5 times higher heat transfer coefficient lead to an average offset of nearly 0 K influencing just slightly

the mass flow rates. Secondly, the coaxial assumption may not be true, or better "half-true", since the position of the setup is horizontal and the heat exchanger length is over 2 m without support in between. Consequently, the formulae which are designed for coaxial assumption may not be have the ability to fully predict the heat transfer. A transition regime is not used and a Reynolds number of 2300 is used to differentiate between laminar and turbulent. In Fig. 27 (c, d) the same set of data is computed with a 1.5 times higher heat transfer coefficient for the annulus only. The impact on the mass flow rate is very small but this measure adjusts the temperatures to the measured ones. Concerning mass flow rates for the corrected case the mean deviation of relative error is 3.2 % (0.04 kg/h), standard deviation of 7.0 % (0.1 kg/h).

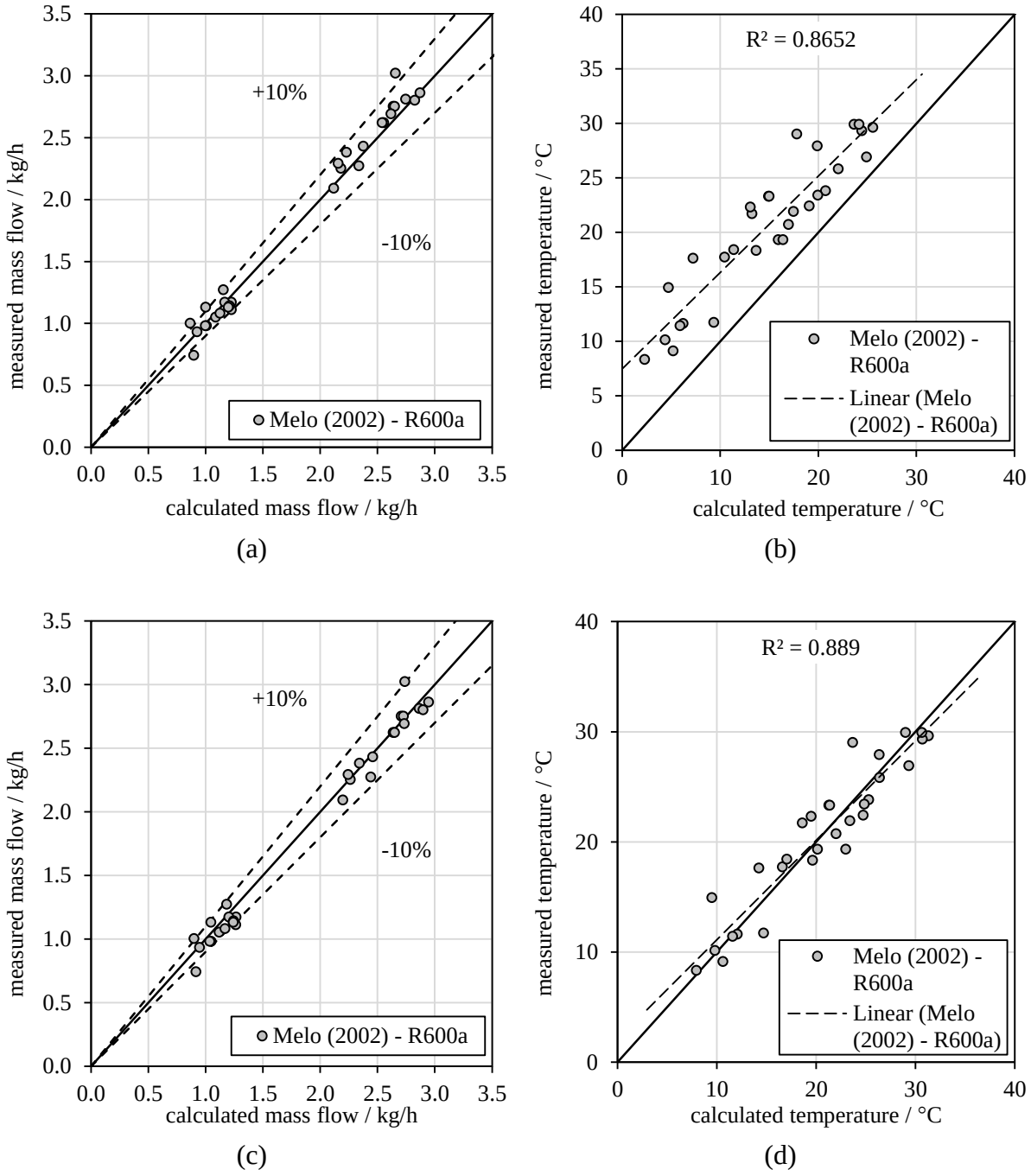

Fig. 27 Validation of the diabatic model against experiments conducted by Melo et al. [66]. Mass flow rate (left) and outlet temperature of the suction line (right).

The uncertainties concerning outlet temperature for the corrected case are -0.1 K mean and 2.3 K standard deviation and for the uncorrected case -5.6 K mean and 2.6 K standard deviation. All in all, considering the uncertainty of heat transfer coefficients in general, the model predicts also in this case the mass flow rates satisfactorily, which is the main purpose of the calculation program.

Another set of measurements was obtained by Wolf and Pate [97] in 2002. First of all, the drawback of this work is, that the test were conducted with a lateral instead of a coaxial configuration of the heat exchanger. The capillary is soldered onto the suction line. Unfortunately, neither the wall thicknesses nor the cross section of such a solder joint is reported, which makes this set only second choice for validation. Although the total heat transfer may not be evaluated well, the trends of the mass flow rate as well as the outlet temperature should be reproduced correctly.
Five refrigerants were investigated (R600a, R134a, R22, R152a and R410a) as possible "ozone-friendly" replacements for R12. During these experiments, the inlet conditions were varied from two phase inlet ($x < 0.1$) to subcooled inlet conditions (T_{sub} <16.7°C). Two phase inlet conditions could be accomplished by heating the subcooled refrigerant electrically. With the measured heating power together with known mass flow rate and fluid state the inlet conditions could be calculated. The range of geometrical variations is from 0.66 mm to 1.05 mm in inner diameter and 2032 mm to 4572 mm in length. The heat exchanger section is from 508 mm up to 2540 mm and the adiabatic length at the capillary tube inlet ranges between 152 mm to 610 mm. The diameter of the suction line is between 4.9 mm and 8.1 mm. The evaporation temperatures lie within -5 °C and -25 °C, the condensation temperatures between 15.6 °C and 48.9 °C. For information on the measurement uncertainty or the test bench setup, the reader is referred to the original report [97].

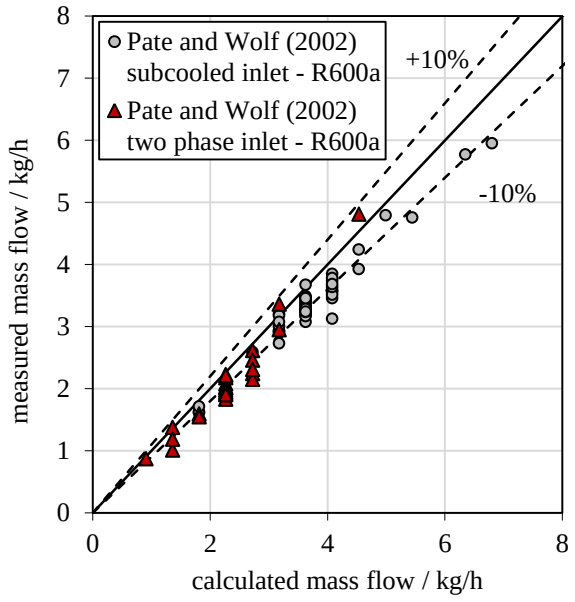

(a)

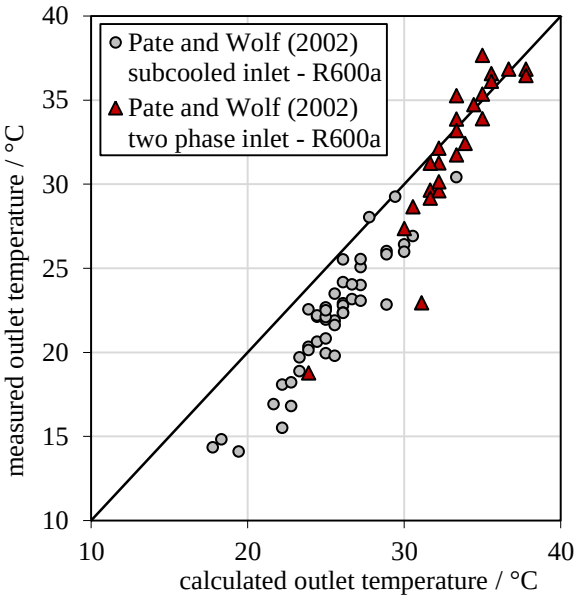

(b)

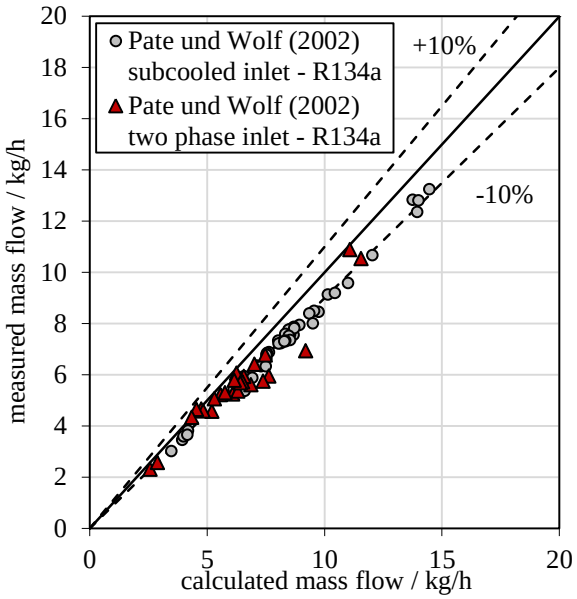
Pate und Wolf (2002)
subcooled inlet - R134a
Pate und Wolf (2002)
two phase inlet - R134a
+10%
-10%
measured mass flow / kg/h
calculated mass flow / kg/h
0
2
4
6
8
10
12
14
16
18
20
0
5
10
15
20

(c)

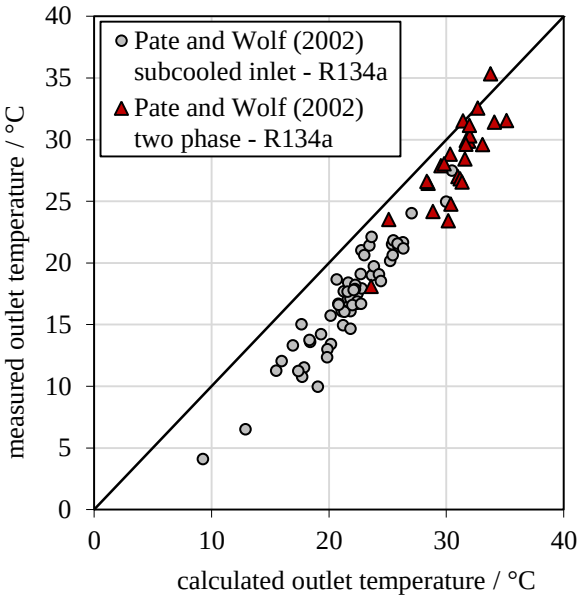
Pate and Wolf (2002)
subcooled inlet - R134a
Pate and Wolf (2002)
two phase - R134a
measured outlet temperature / °C
calculated outlet temperature / °C
0
5
10
15
20
25
30
35
40
0
10
20
30
40

(d)

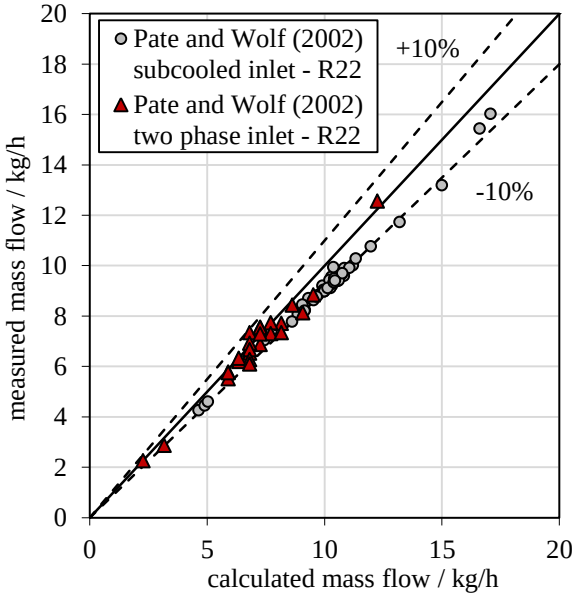
Pate and Wolf (2002)
subcooled inlet - R22
Pate and Wolf (2002)
two phase inlet - R22
+10%
-10%
measured mass flow / kg/h
calculated mass flow / kg/h
0
2
4
6
8
10
12
14
16
18
20
0
5
10
15
20

(e)

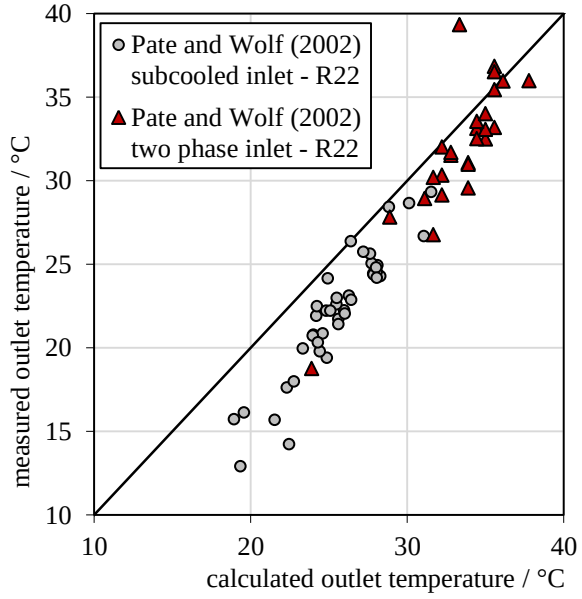
Pate and Wolf (2002)
subcooled inlet - R22
Pate and Wolf (2002)
two phase inlet - R22
measured outlet temperature / °C
calculated outlet temperature / °C
10
15
20
25
30
35
40
10
20
30
40

(f)

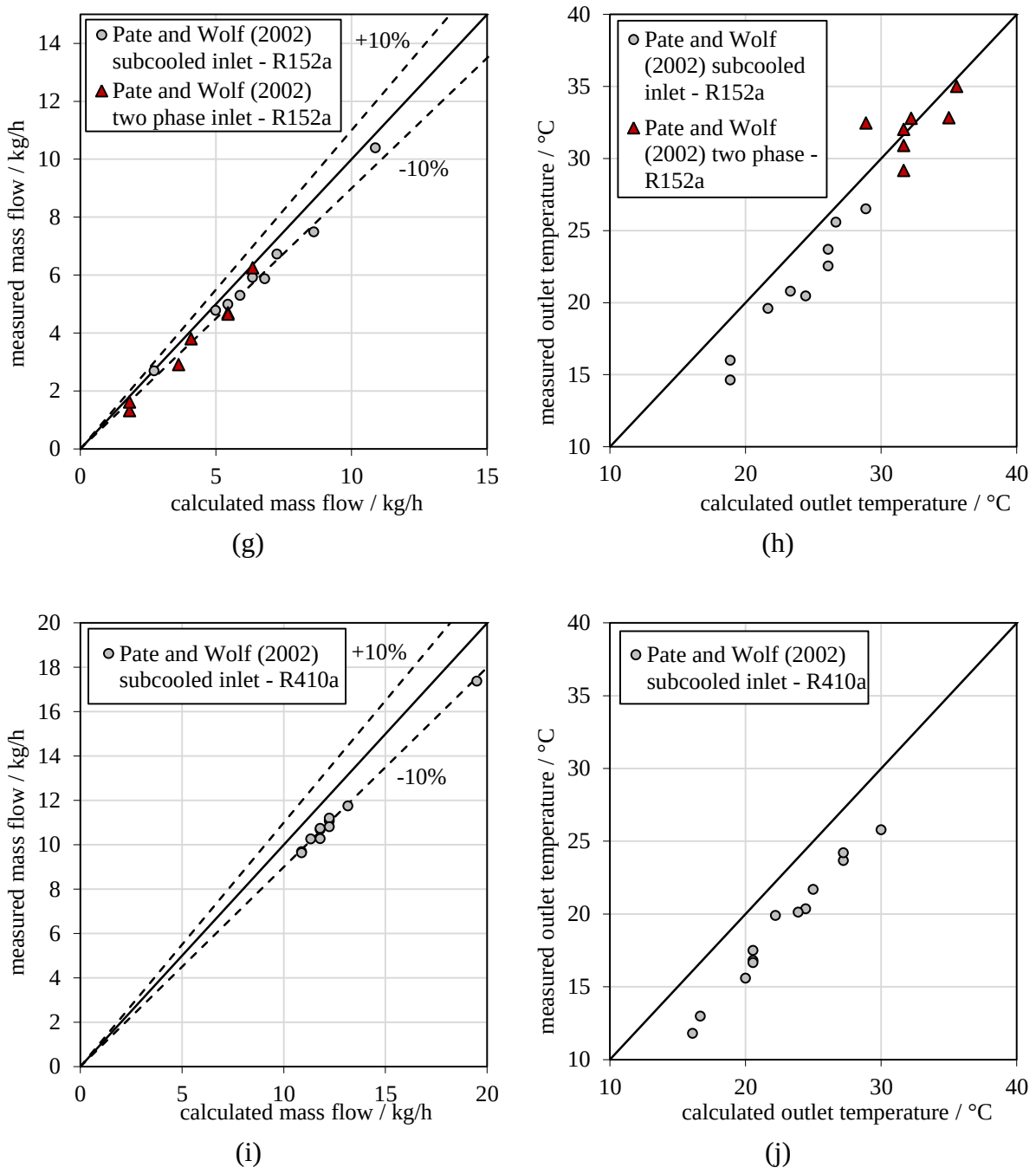

Fig. 28 Validation of the diabatic model against experiments conducted by Pate and Wolf [66]. Mass flow rate (left) and outlet temperature of the suction line (right).

As mentioned before, the use of a lateral heat exchanger design in these experiments instead of a coaxial design can not detract from the fact, that the trends in mass flow rate and outlet temperature can be predicted by a code tuned for coaxial capillaries. The mean deviation in mass flow rate for each refrigerant is between 6.7 and +10.9 % which means a constant overprediction. Also the outlet temperature is overpredicted throughout the sets between 1.7 and 4.1 K. This comparison in Fig. 28 should demonstrate that special adaption is needed if the lateral design should be treated by means of one-dimensional investigations. In particular the heat transfer within a cross section, which depends on the contact area between

suction line and capillary (soldered, heat conductivity past, tape) has to be known for more precise calculations.

4.3.4. Course of expansion

Like in 4.2.4 for adiabatic cases the thermodynamic properties of the fluid are plotted versus the axial position. in Fig. 29 (a) the temperatures from the capillary and from the suction line are shown. One can observe a delay in evaporation due to sufficient cooling – the pressure drop is not affected in any way. When the counterflow-heat exchanger section ends the liquid in the capillary is subcooled even more than it was at the inlet. Several centimeters before the exit the evaporation sets on and due to the boundary conditions (coaxial configuration, mass flow rate at 1.0 kg/h, low pressure at 0.6 bar) the flow accelerates within these last few centimeters at sonic speed at 45 m/s. The transferred heat is around 14 W which is enough to rise the suction line temperature by more than 30 K.

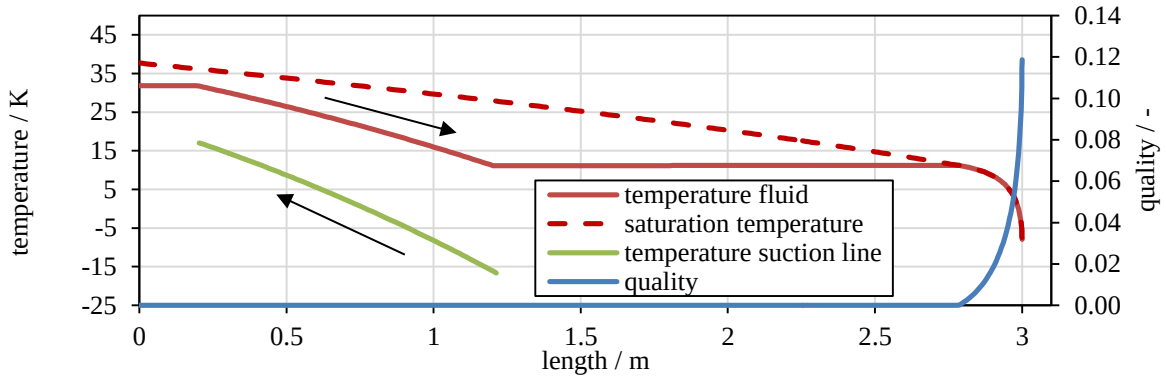

(a)

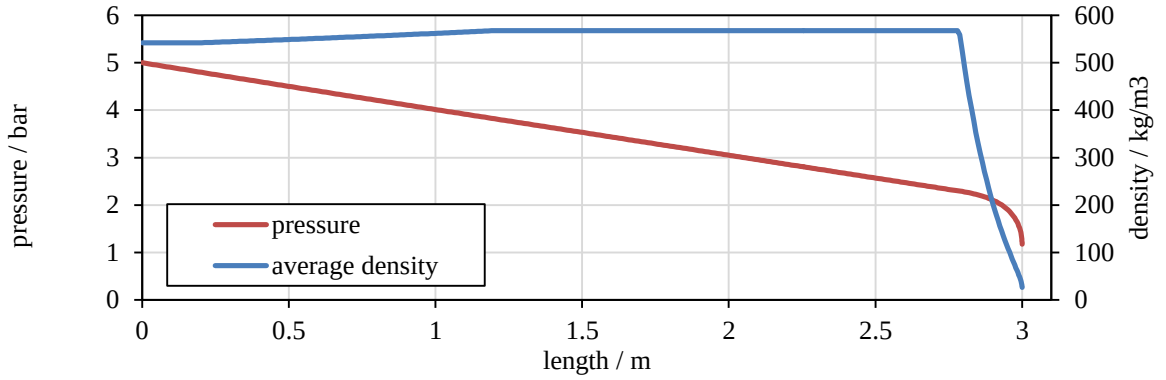

(b)

Fig. 29 Temperature and quality (a) as well as pressure and average density (b).

The rise of density in Fig. 29 (b) is explained by the cooling of the refrigerant. Simultaneously the pressure decreases but this has nearly no impact on the liquid density. From the pressure profile it can be seen that more than 90 % of the total length liquid refrigerant flows through the capillary and two phase flow is visible only in the last few centimeters.

4.3.5. Parameter studies

As in chapter 4.2.5 parametric studies are carried out concerning the main parameters of the heat exchanger assuming a concentric type under normal operating conditions. The impact on mass flow rate of the capillary as well as the transferred heat is investigated to be able to recognize the most influential parameters. Similar studies have been carried out by Melo et al. [66] or Sarker and Jeong [80]. A major difference compared to these studies is, that non-equilibrium between the capillary tube outlet conditions and the suction line inlet conditions are assumed. This means the mass flow rate or the pressure level are not necessarily the same because due to a relatively high pressure drop in the evaporator (depending on the geometry up to some tenth of a bar) and the fact that transient mass storage in the heat exchangers occurs this assumption seems not far-fetched. So, in the following investigation the capillary tube flow parameters and geometry are fixed but only the heat exchanger parameters are altered. It should be noted that suction line pressure and inlet temperature are not coupled here as it would be the case for superheating since superheating is always related to pressure. Here, the temperature (but not the superheating) at the inlet of the suction line heat exchanger is held constant when the pressure is changed, and the other way round.

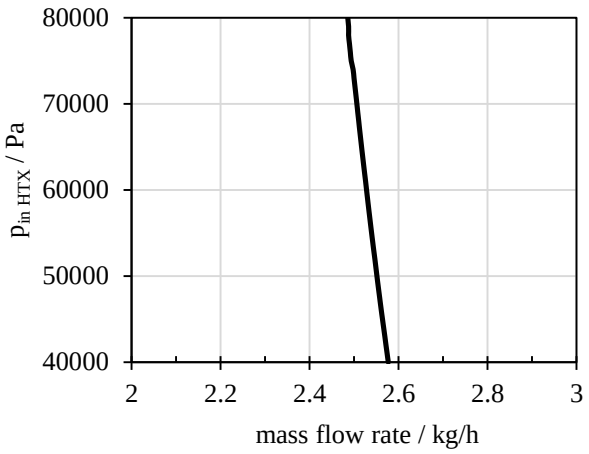

(a)

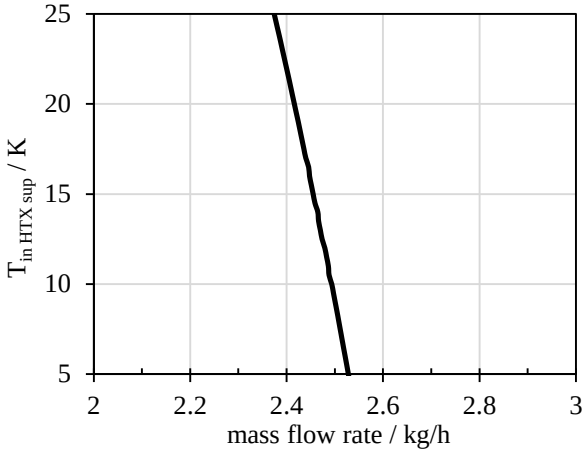

(b)

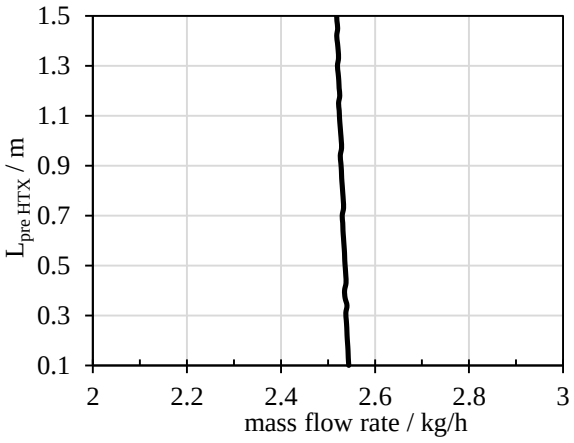

(c)

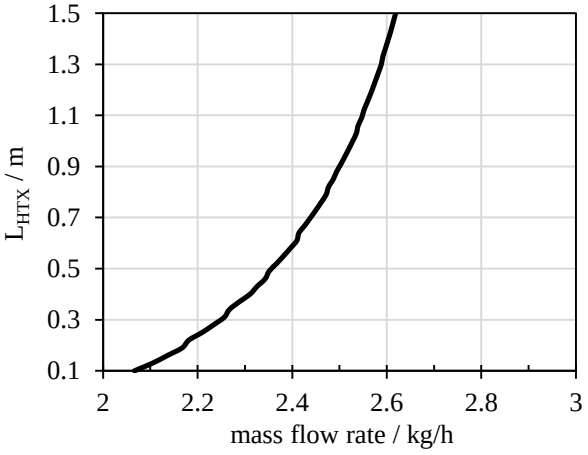

(d)

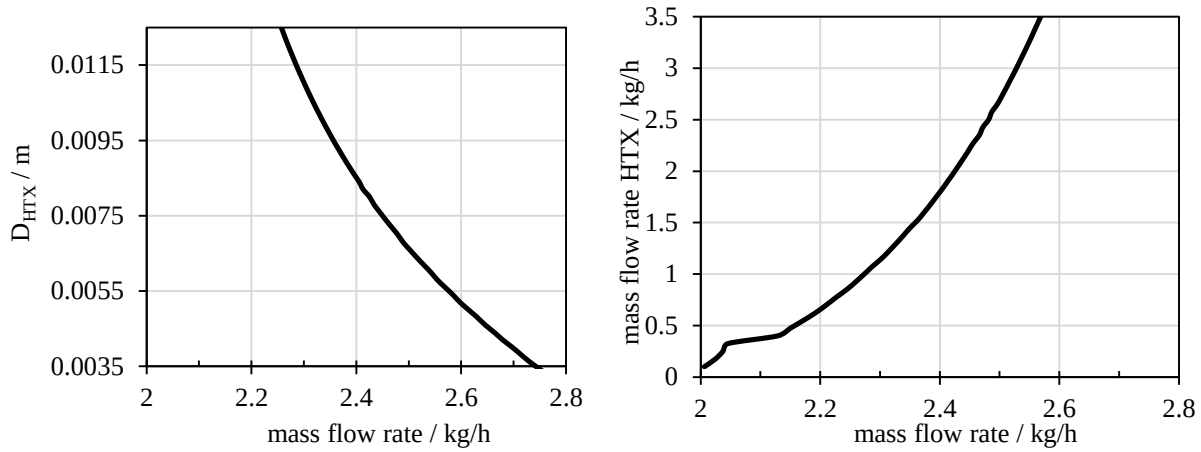

(e) (f)

Fig. 30 Variation of heat exchanger parameters and impact on capillary tube mass flow rate and transferred heat. (a) inlet pressure $p_{in\ HTX}$, (b) inlet temperature (degree of superheating) $T_{in\ HTX\ sup}$, position of heat exchanger $L_{pre\ HTX}$, heat exchanger length L_{HTX}, diameter D_{HTX} and mass flow rate $\dot{m}_{HTX}$.

Also, a sensitivity should be carried out to identify the main influencing factors. Fig. 31 is generated under similar conditions as Fig. 25 and features average relative changes in mass flow rate (a) and the transferred heat (b). The investigation reveals that the position of the heat exchanger region ($L_{pre\ HTX}$) has nearly no impact on both output parameters and is therefore neglected in other applications. Due to its usual construction method a short amount of capillary tube remains without heat exchanger when coming from the direction of the filter/dryer. This part is usually shorter than half a meter. On the other side the capillary tube enters on the cold side directly the evaporator – sometimes directly at this position the heat exchanger begins, too. Also, the pressure level doesn't seem to influence the transferred heat or the mass flow rate of the capillary tube, under the precondition that the inlet temperature is kept constant but not the degree of superheating – which would certainly lead to a much higher impact.

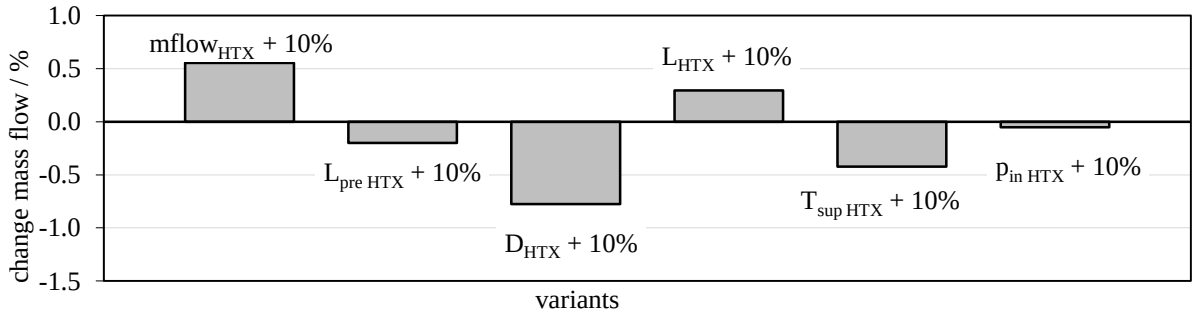

(a)

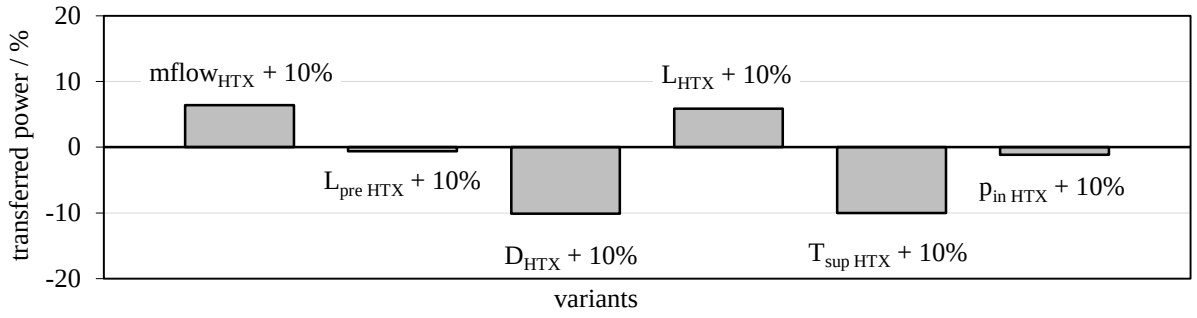

(b)

Fig. 31 Sensitivity study of capillary tube mass flow rate (a) and transferred heat (b).

Since the precedent sensitivity study has shown that the cases +10 % and -10 % mainly differ in sign but little in magnitude (apart the highly non-linear connection between capillary tube inner diameter and mass flow rate) only the impact of an increase by 10 % is studied. Again, the average absolute values for this study are 7 mm for suction line diameter, 1.3 m for heat exchanger length, 0.5 m for $L_{pre\ HTX}$, 1.6 bar for $p_{in\ HTX}$, 2.6 kg/h for the mass flow rate and 9 K superheating. Concluding recommendations for this chapter are that only general trends can be stated, but when it comes to quantification of the effects the exact boundary conditions have to be stated. For instance a 10 % higher inlet temperature not always leads to the same relative change in mass flow rate under different conditions. What can be said, though, is that the mass flow rate will decrease and so will the transferred heat.

4.4. Delay of vaporization and metastable states

Metastability in capillary tube measurements is an issue which may give both experimenters and simulation engineers a hard time. In experiments metastability occurs from the point on where the pressure meets the evaporation pressure – the place where one would assume that evaporation starts to occur. When it does not and liquid becomes superheated, evaporation delay takes place. For a certain distance downstream, the superheat is maintained until suddenly the liquid starts flashing, and after a while a stable state is reached again, the thermodynamic property charts can be applied again and no sign of metastability remains but a significant lower mass flow rate than expected. The zone where it all happens is depicted in Fig. 32 by II and III. Zone II contains superheated liquid and saturated liquid, zone III includes saturated vapour additional to the previously mentioned phases. Evaporation starts between zone II and III, after zone III thermodynamic equilibrium is reached again. The measure of "intensity" of metastability is for instance the difference in saturation pressure and evaporation pressure, called "underpressure of vaporization". In terms of temperature the amount of superheat can be used as characteristic quantity or in spatial terms the length between expected and real point of evaporation. Some authors use the expression "metastable length". Zone I is subcooled liquid and zone IV is two phase flow at saturation conditions.

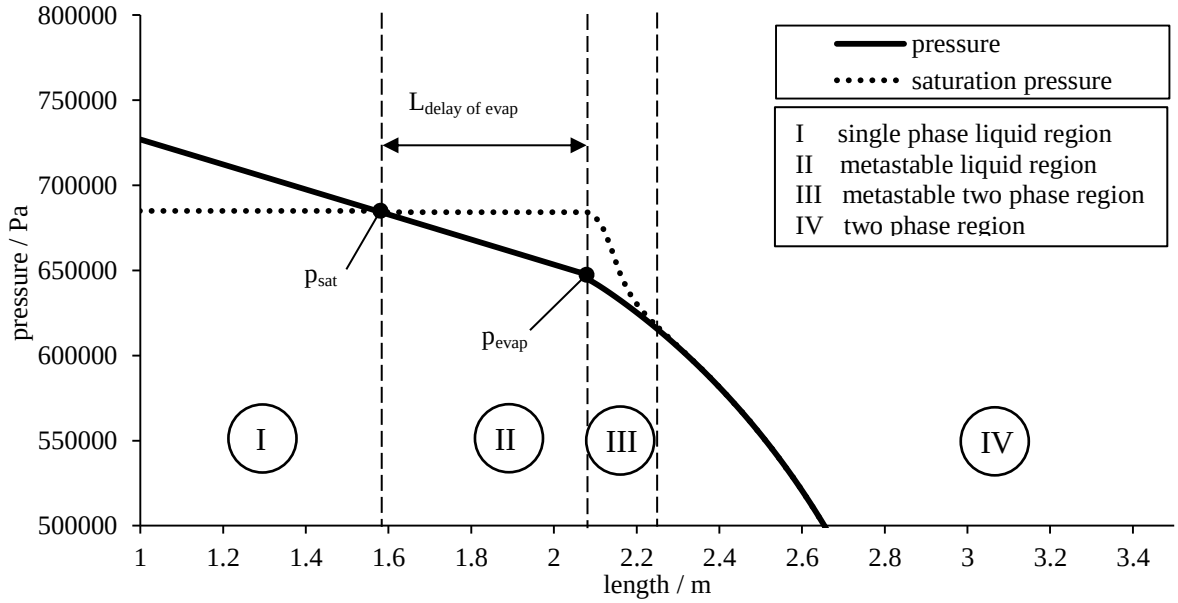

Fig. 32 Metastable regions during adiabatic expansion. p and $p_{sat}(T)$ over length.

Kuijpers and Janssen [56] tested capillary tubes using R12 and compared mass flow rates by a code with their measurements. Relative errors, in some cases higher than 10 % were contributed to metastable behaviour. After measuring the underpressure of vaporization for each test and including this quantity in the calculation as an input parameter, the error could be reduced to a maximum of about 6 %. Their conclusion was that higher mass flow rates reduce the underpressure. According to this observation the theory of a static and a turbulent part contributing to a common underpressure is stated. The higher the turbulence the lower the underpressure – a function which they described as quadratic dependency.

Huerta et al. [45] observed R600a flashing in a glass capillary tube and found a strong dependence between the flashing inception location and flow parameters which are degree of subcooling and mass flow rate. Furthermore, by experiments with R134a, it was shown that the underpressure of vaporization, which is a measure of the magnitude of metastability, is affected by subcooling, mass flow rate, condensing temperature and oil entrainment. Unfortunately also the mass flow rate depends on subcooling and so forth – that is why a clear distinction between the cause and effect is not visible in this work. What can be said for sure is: an increase in underpressure can be caused by either a decrease in mass flow rate or a decrease of subcooling. The length of the metastable region varies between 0.1 and 0.6 m for a capillary tube with 0.82 mm inner diameter and 2.03 m length.

Melo et al. [60] assumes that metastable flow is responsible for relative errors around ±15 % for R600a, R134a and R12 when they deduce correlations for mass flow rates from experiments. In another publication (Melo et al. [61]) evaporation delay was tried to be accounted for by the correlation from Chen et al. [13] but with little success. The evaporation delay seemed to have *"... random behaviour for the same operating conditions ..."* (0.1 to 1.3 bar) whereas the correlations which should predict underpressure generated almost a constant value (0.3 to 0.6 bar).

Prediction of underpressure has been achieved using heterogeneous nucleation theory including material properties, surface roughness and flow conditions influence the nucleation rate – unlike homogeneous nucleation theory which is governed by internal parameters such as surface tension, superheat or temperature [13]. Starting from a formula which describes the nucleation events per unit time, integration over the pressure domain and transformation has been applied. In a following step a dimensionless form has been derived where the exponents and a multiplier have to be found by a set of experiments and least square methods. It has to be mentioned that the final correlation predicts the underpressure of vaporization within a relative error of 26 %.

The dimensionless correlation of Chen et al. [13] for the metastable liquid region can be written as

$$\frac{(p_{sat} - p_v) \cdot \sqrt{k \cdot T_{sat}}}{\sigma^{1.5}} = 0.679 \cdot \left(\frac{\nu_v}{\nu_v - \nu_l}\right) \cdot Re^{0.914} \cdot \left(\frac{\Delta T_{sub}}{T_{crit}}\right)^{-0.208} \cdot \left(\frac{d}{D'}\right)^{-3.18} \qquad (135)$$

with D' as reference length, ν as specific volume, σ as surface tension and k as Boltzman constant. p_v is the underpressure of vaporization, the index "v" and "l" stand for "vapour" and "liquid", respectively.

$$D' = \frac{\sqrt{k \cdot T_{sat}}}{\sigma} \cdot 10^4 \qquad (136)$$

The coefficients for the dimensionless form are found using a set of 238 experiments. The range of validity for this equation is determined by the range of these experimental conditions and is given by Table 5.

Table 5 Range of validity for the metastable liquid region according to Chen et al. [13].

refrigerant: R12		
$0.464 \cdot 10^4 <$	Re	$< 3.76 \cdot 10^4$
0 °C <	ΔT_{sub}	< 17 °C
0.66 mm <	d	< 1.17 mm
($1.44 \cdot 10^3$ kg/s m^2 <	G	< $5.09 \cdot 10^3$ kg/s m^2)
(17 °C <	T_{in}	< 53 °C)
(6.3 bar <	p_{in}	< 13.2 bar)

In the work of Chen et al. [13] it says *"... It should be noted that during the experiment, there was a slight fluctuation in location of the inception of vaporization, despite the fact that all experimental parameters were fixed. ..."* a sincere hint admitting the erratic behaviour of the onset of evaporation.

For R134a and diabatic conditions the same equation (135) has been derived by Chen and Lin [12] using homogeneous nucleation theory in combination with experimental results. The

relative standard error is 28 % and according to the authors it stems partly from *"... the fluctuation and instability of the position of the inception of vaporization ..."*.

The correlation by Feburie et al. [28] for the metastable two-phase region reads:

$$y = \frac{(m_{ls} + m_v)}{(m_{lm} + m_{ls} + m_v)} \qquad x = \frac{m_v}{(m_{ls} + m_v)} \tag{137}$$

$$\frac{dy}{dl} = 0.02 \cdot \frac{U}{A} \cdot (1 - y) \left(\frac{p_{sat} - p}{p_{crit} - p_{sat}} \right)^{0.25} \tag{138}$$

Enthalpy and entropy of the mixture can be computed according to their mass fractions of saturated liquid, saturated gas or metastable liquid.

$$h_{av} = (1 - y) \cdot h_{lm} + (1 - x) \cdot y \cdot h_{ls} + x \cdot y \cdot h_v \tag{139}$$

$$s_{av} = (1 - y) \cdot s_{lm} + (1 - x) \cdot y \cdot s_{ls} + x \cdot y \cdot s_v \tag{140}$$

$$v_{av} = (1 - y) \cdot v_{lm} + (1 - x) \cdot y \cdot v_{ls} + x \cdot y \cdot v_v \tag{141}$$

The specific volume (eq. (141)) is suggested to be calculated by an equation of state, however Zhou and Zhang [35] use the same averaging technique as Feburie et al. for enthalpy or entropy. A brief remark is given to avoid mistakes. Zhou and Zhang as well as Garcia Valladares use a different definition of quality, that is $x = m_v/(m_{lm} + m_{ls} + m_v)$ which may lead to confusions when their formulae are compared to the one above. In their work the averaging equations look like

$$h_{av} = (1 - y) \cdot h_{lm} + (y - x) \cdot h_{ls} + x \cdot h_v \tag{142}$$

The implementation of these semi-empirical metastable models is done according to Garcia Valladares [31]. From equation (138) the mass ratio *y* of the saturated phase and from equation (139) the vapour mass fraction *x* can be computed. Then, an averaged temperature T_{av} has been defined which ranges between the superheated liquid (T_{lm}) and the saturation temperature (T_{sat}) like in eq. (143). The vapour mass fraction at assumed equilibrium x_{equil} is evaluated as $x_{equil} = (m_{lm} + m_v)/(m_{lm} + m_{ls} + m_v)$ and can be written like $x_{equil} = (1 - y + x)$ if one uses the notation of Zhou and Zhang or Garcia Valladares.

$$T_{av} = T_{sat} - \left(\frac{x - x_{equil}}{x_{equil}} \right) \cdot (T_{lm} - T_{sat}) \tag{143}$$

In Fig. 32 the two metastable regimes are shown during adiabatic expansion where the quantity $p_{sat} - p_{evap}$ is characteristic for the delay of vaporization and therefore appears on the left hand side of eq. (135). The physical length of this region can be measured if pressure transducers are installed along the length of the tube and simultaneously the temperature is

recorded, too. Assuming a length of several meters combined with the fact that the flashing point is likely to change its position several times, a high amount of junctions for the transducers will be necessary – according to the desired spatial resolution. However, since every junction imposes a little disturbance on the flow and the metastable region, combined with the fact that these regions are hardly predictable in position, good measurements are rare.

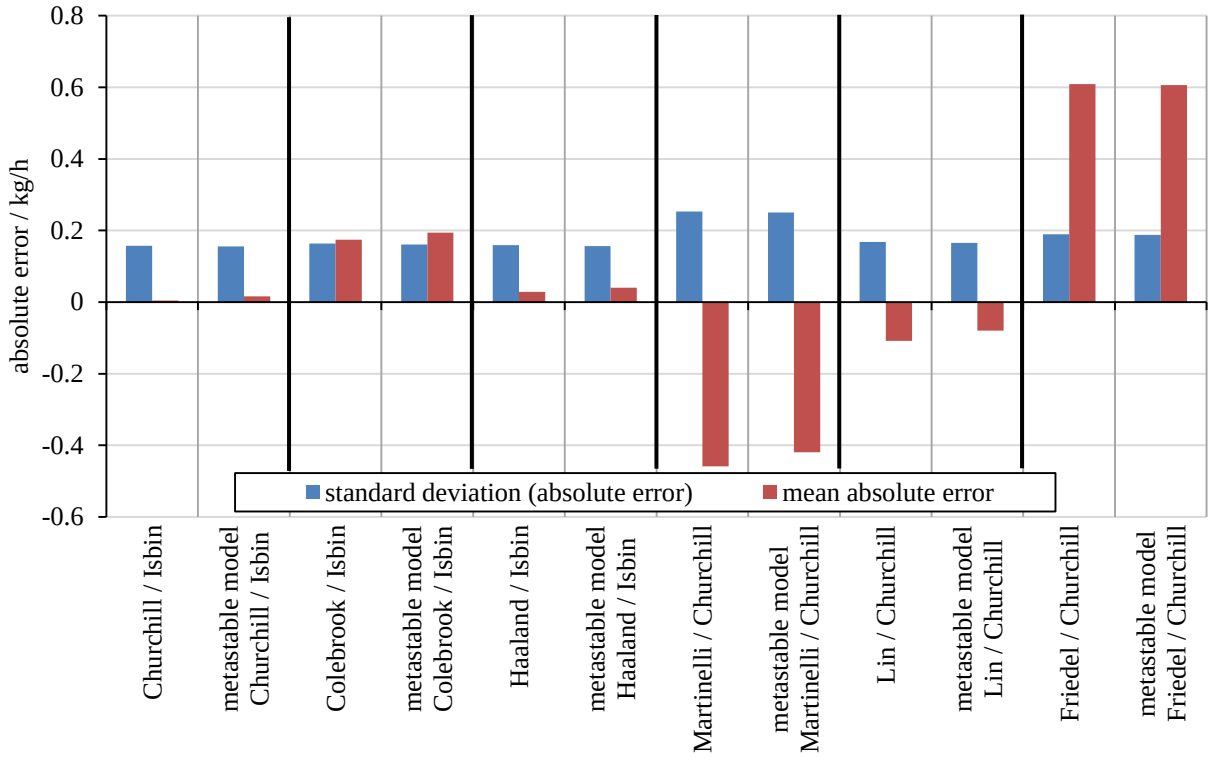

Fig. 33 Application and comparison of metastable models for various combinations of friction laws to an adiabatic expansion process. The data is provided by [63].

Fig. 33 tries to show the effect of using existing metastable models according to Chen et al. [13] and Feburie et al. [28]. A run without and with a corresponding model is compared and the used correlation for friction is stated beneath the x-axis. The basis for this test is again experimental data by Melo et al. [63] obtained from an adiabatic capillary tube under choked conditions. The refrigerant is isobutane (R600a). On the y-axis in Fig. 33 the absolute error in mass flow rate plus standard deviation compared to the measured dataset is given. The difference due to the metastable model is hardly evident, the change in mean mass flow rate is somewhere between 0.01 kg/h and 0.04 kg/h with nearly constant standard deviation. In other words, the implementation of models describing metastability lead to a vanishingly small rise in mass flow rates in this setup. Since the expected disturbances are much higher and in the order of up to 10 % of the nominal flow these models don't work for R600a and are therefore not used for further investigations in this work.

Concluding this section it can be said that one of the main uncertainties in mass flow predictions for capillary is evaporation delay. For certain cases the difference in mass flow might be up to 10 %, general trends are observed by [45] and [56] for the refrigerants R12 and R134a.

4.5. Influence of oil in the refrigeration system

In closed loop refrigeration systems driven by reciprocating compressors oil is used for lubrication of the compressor's moving parts and bearings and for enhanced heat transfer from the hot parts to the shell. The lion's share is stored in a sump and is distributed from there to other parts within the shell. The oil is absolutely necessary to guarantee flawless operation of the compressor [160]. If the amount of oil falls below a certain limit, the lubricating mechanism fails and shortly thereafter the compressor. The amount of oil differs according to the size and layout of the compressor, a lower range is around 80 g for small compressors driving a household refrigerator [198]. Along its way through the compressor the refrigerant gets in contact with oil not only under suction conditions inside the shell (low pressure, high temperature) but is also transported to the high pressure side where oil droplets are swept along with the refrigerant. Consequently, after a short period of time, one can assume that all surfaces inside the cycle are in touch with oil, the extent depends on the mass fraction of oil transported and its solubility according to the carrier fluid [160], [162]. Of course the chemical composition of oil and refrigerant play an important role too, and every mixture must be treated in a separate way as far as solubility and thermodynamic properties are concerned [162].

Basically, a differentiation between miscible and non-miscible oil-refrigerant mixtures can be made. As lubricants polyolester oil (POE) or mineral oil (MO) are in use where latter can be divided into two groups, that are paraffinic oil (PO) and naphtenic oil (NO). The compressor driving the refrigeration cycle for experimental validation in this work uses a paraffinic mineral oil (Fuchs RENISO WF5A). Besides its usefulness in the compressor the oil may cause some undesirable side effects like sickness after use of aspirin. Youbi-Idrissia and Bonjour [160] sum up the effects of oil in refrigeration – the main points of this review paper are presented shortly.

Impact on evaporator: It is said that this heat exchanger is influenced most by oil, particularly the superheated zone where the mixture of oil and refrigerant is continuously enriched with oil since the refrigerant evaporates. This leads to an increase in viscosity and hence pressure drop and a decrease in heat transfer.

Impact on capillary: Due to changed viscosity the pressure drop along the capillary changes and has an impact on the mass flow rate. Also, the length of the metastable region is affected by the presence of oil which also alters the performance of the device.

Impact on compressor: Foam, produced by the blade rotation of the compressor and/or dissolved refrigerant outgassing from the oil, can negatively influence the compressor performance when the level of foam becomes so high that it gets into touch with the rotor or even the annular clearance between rotor and stator. Last, the mixture enthalpy differs from the enthalpy of the pure refrigerant, a fact which may lead to a lower mass flow

Impact on condenser: The least sensitive component of the system in terms of lubricant oil is the condenser, hardly any investigations deal with this heat exchanger.

Impact on refrigeration systems: Depending on the combination of oil and refrigerant during longer Off-periods the refrigerant can be dissolved in the oil so that the equalization pressure of the system sinks significantly below the expected saturation pressure at ambient temperature. A decrease in COP has been observed by Lottin et al. [149] who state that below 0.5 % oil concentration no decrease is visible but for instance for 5 % the decrease in COP is as high as 13 %. The definition of the oil concentration in this context is $\dot{m}_{oil}/\dot{m}_{tot} \cdot 100$ and is measured by an ultrasonic oil concentration sensor.

From here on, only the impact on capillaries is described further. Huerta and Silvares [47] compare findings by applying a separated flow model which accounts for the mixture viscosity, density and vapour pressure with experimental data from other authors for R134a/POE. They find that the mass flow rate of the refrigerant is reduced by 3 % for oil concentrations of 5 %. The experimental mass flow rates between 2 and 8 kg/h can be reproduced by approximately 7 %.
In a following study Huerta et al. [46] observed mass flow rates experimentally on R134a/POE at varying oil concentrations, diameters and condensing temperatures. They used 10 pressure transducers and 20 thermocouples along a 2 m capillary tube in order to resolve metastable phenomena. A reduction in mass flow rate by 3 to 5 % for oil concentrations of 3 % is visible, an obvious trend which becomes even more evident at higher subcooling. Concerning evaporation delay they found a shorter liquid length (= earlier flashing) and also a shorter metastable region for oil entrained refrigerants and that is explained with changed thermophysical properties of the mixture.
Fukuta et al. [30] come to the same conclusions experimentally as far as the mass flow – oil dependency is concerned for both miscible and non-miscible oil/refrigerant combinations. For a miscible combination (R22/MO) the decrease in mass flow rate is as high as 8 % at 5 % oil concentration for subcooling by 3, 5 and 8 K. No influence by oil on the underpressure is observed although oil presence seems to stabilize the point of inception. During runs with an immiscible combinations (R134a/MO) where oil is not dissolved in the liquid refrigerant phase the same tendency in mass flow rate as with miscible combinations could be seen.
Another interesting study is the one of Motta et al. [124], a visual study of adiabatic R404a/POE flow with oil concentrations ranging from 5.6 to 6.9 %, subcooling from 6.2 to 21.5 °C and 18.25 bar condensing pressure. In the introductory section typical oil concentrations for refrigeration systems are assumed to be around 3 %, whereas 1.4 % – this percentage was used by other authors – seem to be a very low estimate. The main objective was to find whether there oil influences the onset of evaporation or not. The capillary was visually accessible so the point of flashing could be well observed. It could be seen that small bubbles form at the wall and quickly fill the whole cross section until a fog-like flow, homogeneous to the human eye, continues. This was for pure refrigerant. When it came to oil injection in every case the mass flow rate decreased and the liquid length was shorter than compared to the pure refrigerant. For instance the mass flow rate dropped from 17.23 kg/h to 16.25 kg/h and the liquid length from 0.945 m to 0.765 m when 5.7 % oil were added. Higher viscosity of the mixture was blamed for that behaviour since according to correlations the density as well as the saturation pressure seemed to be nearly unaffected when oil was added

(0.4 % lower density and 0.15 % lower saturation pressure), whereas the viscosity was predicted to be as high as 1.51 to 2 times the viscosity of the pure refrigerant.

Concludingly, oil in refrigeration systems can not be avoided and reaches every part of the cycle. Oil flow rates are hardly accessible and rarely mentioned in literature since it depends on many parameters, which can not be characterized by a single parameter. For instance the design of the compressor and its interoperability with the tubes connected to this device determine to a certain part the oil flow rate as well as the combination of oil and refrigerant as mentioned above. Under these circumstances no model for oil-influence is implemented in the capillary tube calculation procedure. Consequently, since no reports of oil treatment for these purposes exist, this oil-issue may well contribute to the uncertainty of several percent relative error when measured mass flow rates are compared to calculations which assume pure refrigerant.

5. Semi-empirical 0d methods

A working capillary tube model is a fine thing to have, but what is it good for? Well, some straightforward things to do are parameter studies which means one can find out how the output depends on certain input quantities. This helps to better understand the behaviour of the device in a setup where the boundary conditions change. Other, less academic but more applicable possibilities lie in solving the question "What's the optimum capillary tube length to achieve certain mass flow rates?". Therefore a computer program could be helpful, in many cases the exact length is still found by trial and error (i.e. cutting short pieces off repeatedly until the system behaviour seems okay). A third option is the implementation of this numeric scheme into a dynamic simulation where the mass flow is usually determined by the flow-driving element (compressor) and its counterpart the expansion device. Several publications exist (summary in Hermes and Melo [144]) which focus on such refrigeration cycle simulations.

This topic will also be the subject of matter of that chapter where two entirely different ways of implementation are presented. Both are dealing with the fact that the one-dimensional code, though working in C programming language, is too slow to meet the requirements of a simulation which should compute in real-time on a one-second basis. An approach is to use a common power-law function for computing mass flow rates. All the main input parameters are considered for the adiabatic tube and a comparison with experimental results is made. Secondly, a more sophisticated fit, an Artificial Neural Network (ANN) is introduced and compared with the power-law function.

From [144] it can be seen how many cycle simulations on refrigeration systems have been published up to the year 2008 and that all of them apply a model for simulating the expansion device. Ranging from a simple orifice formulation up to non-adiabatic models it seems that a broad variety of possibilities has been tried so far. Not only the kind of model in terms of mathematical description differs but also the kind of adjusting the model-parameters. Therefore, experiments are indispensable, but not the only way. In this work, for instance, a validated model is used to generate data which forms the basis of the final model to be used in the cycle simulation.

A word about the cycle simulation which can be seen as an accumulation of modules describing a single physical component. So, the condenser, evaporator, compressor, the shell which surrounds the compression unit, compartment and the capillary tube are modelled by making use of different approaches. For instance the heat exchangers are computed in a transient manner, whereas the capillary tube is formulated as steady state model. These models are called from a main-program and, one by one, passing on the output to the next model and so on. The role of the capillary model lies in being a counterpart to the compressor, both have the function of mass flow determination, additionally the suction line heat exchanger shifts heat from the left side of the Ts-plot to the right side in a more or less efficient manner (Fig. 3) depending on its design.

5.1. Dimensional analysis

Buckingham PI method – often referred to as "Dimensional Analysis", describes an approach of finding physical correlations between dimensionless groups of variables by applying collected data which was found either by measurement or by simulation. Some illustrative examples are given in Barenblatt [187] including the application of this method to different examples of use. The idea behind this method is described as simple – assuming a function has several input arguments which have to be physical quantities since the function itself also expresses a physical effect. In most cases a reduction of arguments thus can be achieved. As [187] argues, this reduction is deduced from the fact that "*physical laws do not depend on arbitrarily chosen basic units of measurement*". As a consequence quantities are sought which do not change when fundamental units of measurement are changed – such a quantity is named "Π-group". In the introductory example of [187] the oscillating frequency of a pendulum is investigated – the formula is well known by $f = 2\pi\sqrt{l/g}$ and can be derived without knowledge of the underlying differential formula. A Π-group can be found which is $f/\sqrt{l/g} = const.$ This factor is invariant to changes in fundamental units – the length can be switched to millimeters instead of meters without influencing the value of the Π-group. The value of the Π-group can be found by a single experiment and therefore the need for many experiments which may be necessary for finding the influence of length and gravity and the frequency are not necessary. Although this is a very simple and rather academic example, dimensional analysis can be used to reduce more complex problems.

5.1.1. Review

General usage of dimensional analysis is presented in Sonin [179]. This work, which I warmly recommend to anyone interested in this topic, demonstrates not just bare examples but also comes with historical background to this method and well-grounded explanations back to its physical origins.

Etymologically seen, the "Buckingham-Pi method" dates back to a publication by Edgar Buckingham [188] from 1914 who concludes that *"... any equation which describes completely a relation subsisting among a number of physical quantities of an equal or smaller number of different kinds is reducible to the form* $\psi(Q_1, Q_2, \dots, etc.) = 0$ *in which the Π's are all independent dimensionless products of the form* ${Q_1}^x, {Q_2}^y, \dots, etc.$ *that can be made by using the symbols of all the quantities* Q*."* Q stands for a physical quantity, *x* and *y* denote arbitrary exponents and ψ an unknown function.

For capillary tube modelling this method is not new, different kinds of dimensionless groups have been proposed (Choi et al. [18], [19], Melo et al. [63], [66], Vins and Vacek [92], Kim et al. [55]) in order to map effects as for instance the influence of geometry, refrigerant, subcooling, or pressure. The proceeding is the same in all cases Firstly, get a set of measurements, secondly, spend some thoughts about the choice of the Π-groups (chapter 5.1.2), thirdly fit the exponents for the Π-groups according to the experimental data and fourthly, hope for low mean and standard deviations. The advantage of this method theoretically allows a much smaller set of measurements to gain a predictive formula for mass flow rates than using lookup-tables based on measured values. Typical agreement between

theory and practice for adiabatic capillary tubes are exemplarily 0.2 % mean and 6.1 % standard deviation [18] for subcooled inlet conditions with relative errors ranging from -21 % to 18 %. Vins and Vacek [92] disclose a comprehensive table where mean and standard deviations in mass flow rate for adiabatic capillary tubes are presented for six different correlations plus the results from their Artificial Neural Network approach. They tested with seven different refrigerants and what immediately becomes obvious is that none of the correlations performs well on all the tests. All correlations show 15 % or more mean deviation for at least one refrigerant but may perform better for other sets, depending on the original purpose and training data. A model which has been trained using 300 measurements with R22, R12 and R134a is expected to give good results for these refrigerants but may show poorer performance on other working media, although the formulation theoretically would allow different refrigerants (i.e. use of reduced pressure and temperature).

For non-adiabatic cases no source can be found. The number of influencing parameters increases by the factor of two and not only a formulation for mass flow rate but also for outlet temperature of the suction line is needed. Melo et al. [66] states corresponding formulae which are explicitly designed for R600a and trained with 30 measurements. They don't apply the Buckingham-Pi method but compute mass flow rate and temperature by a sum of influencing factors. They are able to reproduce the 30 datapoints with maximum error in temperature at 2.4 K and mass flow rate at 0.15 kg/h. A comparison of the experiments with their 1d code "CAPHEAT" reveals an estimated 10 % offset in mass flow rate with maximum differences of 0.6 kg/h at 3 kg/h nominal flow. Unfortunately no statement concerning outlet temperature is made in their work.

5.1.2. Theory

As explained above, the special feature of this method is that, assuming a physical relationship exists between several variables, a formulation in the form of a power law function of dimensionless parameters can be found even if the knowledge of the exact kind of relationship is not known at the beginning. What has to be known, though, is which variables (Q_1, Q_2, …) have impact on a certain physical quantity Q_0. Since in capillary tube modelling the mass flow turns out to be the quantity which is looked for, variables have to be sought which could have influence. In a next step dimensional groups, so called Π-groups are derived from this set of variables. Basically, any of these Π-groups can be picked to be the left hand side term from equation (145) – in our case the group containing the mass flow rate is depicted as Q_0. The dependency of this group from the others is expressed by the unknown function *f*. The aim is now to find a solution which satisfies equation (145). Therefore a power law approach is used as in equation (146) where *c1*, *c2*, … are constants.

$$Q_0 = f(Q_1, Q_2, Q_3, \dots, Q_{\mathrm{n}}) \tag{144}$$

$$\Pi_0 = f(\Pi_1, \Pi_2, \Pi_3, \dots, \Pi_{\mathrm{n-k}}) \tag{145}$$

$$\Pi_0 = c_0 \cdot {\Pi_1}^{\mathrm{c1}} \cdot {\Pi_2}^{\mathrm{c2}} \cdot {\Pi_3}^{\mathrm{c3}} \cdot \dots \cdot {\Pi_{\mathrm{n-k}}}^{\mathrm{c_{n-k}}} \tag{146}$$

To keep the number of Π-groups (eq. (147)) low, in this work a division into four regimes according to the boundary conditions has been made. When choking occurs, the outlet pressure loses its impact on the mass flow – therefore, to avoid this sudden change in behaviour for mass flow computations it will be differentiated between choked and non-choked flow. Also there will be a differentiation between one phase inlet conditions and two phase inlet conditions, since in the two phase region the temperature is coupled with pressure so another parameter has to be used as boundary condition. Ultimately, this leads to a set of four equations for capillary mass flow modelling. Some of these groups can be found in literature in combination with other groups describing refrigerant properties, geometry ratios and more complex effects resulting from bubble growth or coiled geometry.

$$\Pi_0 = \frac{\dot{m}}{D \cdot \mu_\mathrm{l}} \quad \Pi_1 = \frac{L}{D} \quad \Pi_2 = \frac{p_\mathrm{in}}{p_\mathrm{out}} \quad \Pi_3 = \frac{D^2 \cdot \rho_l \cdot p_{in}}{{\mu_\mathrm{l}}^2} \quad \Pi_4 = x \quad \Pi_5 = \frac{D^2 \cdot {\rho_\mathrm{l}}^2 \cdot c_\mathrm{pl} \cdot T_\mathrm{sub}}{{\mu_\mathrm{l}}^2} \tag{147}$$

The exponents from eq. (146) are found by using either measurements or computed values of mass flow rates under different inlet and outlet conditions and geometry. Subject to the condition is that the characteristic map of the capillary covers a wide enough range of operation. The formulae (eq. (148)-(151)) are then obtained by means of least square method and Newton-iterations.

A disadvantage of this method is, though, that it leads to erroneous mass flow rates for conditions around saturation (subcooling or quality is close to zero) since the respective Π-groups become zero (Π_4 or Π_5 in eq. (147)). This issue is widely known but it seems that nevertheless these correlations are used since most of the operating time of a refrigerator the flow can be considered as choked with subcooled inlet conditions. However, if a simulation should cover *all* operating conditions, also Off-design has to be treated. After training with several thousand computed values from the previously validated simulation the following formulae are gained:

- one phase inlet, choked – training with 1335 points

$$\Pi_0 = \frac{0.03427}{3600} \cdot {\Pi_1}^{-0.4821} \cdot {\Pi_3}^{0.4789} \cdot {\Pi_5}^{0.1865} \tag{148}$$

- one phase inlet, non-choked – training with 2060 points

$$\Pi_0 = \frac{0.02495}{3600} \cdot {\Pi_1}^{-0.5182} \cdot {\Pi_2}^{0.09325} \cdot {\Pi_3}^{0.4893} \cdot {\Pi_5}^{0.1960} \tag{149}$$

- two phase inlet, choked – training with 438 points

$$\Pi_0 = \frac{0.001100}{3600} \cdot {\Pi_1}^{-0.4638} \cdot {\Pi_3}^{0.7647} \cdot {\Pi_4}^{-0.3053} \tag{150}$$

- two phase inlet, non-choked – training with 1422 points

$$\Pi_0 = \frac{0.0002735}{3600} \cdot {\Pi_1}^{-0.4922} \cdot {\Pi_2}^{0.1053} \cdot {\Pi_3}^{0.8228} \cdot {\Pi_4}^{-0.3297} \tag{151}$$

The training could also have been done with experimental results which would be more accurate for the single phase choked case. Since for the other options no measurements can be done reliably, the training data was generated via simulation. In some publications also the problem occurs that the variations of diameter are not carried out with a sufficient high number of different samples so the dependency on the diameter might not be reproduced correctly. The additional introduced uncertainty by applying the fit to simulated data is shown for all four cases in Fig. 34.

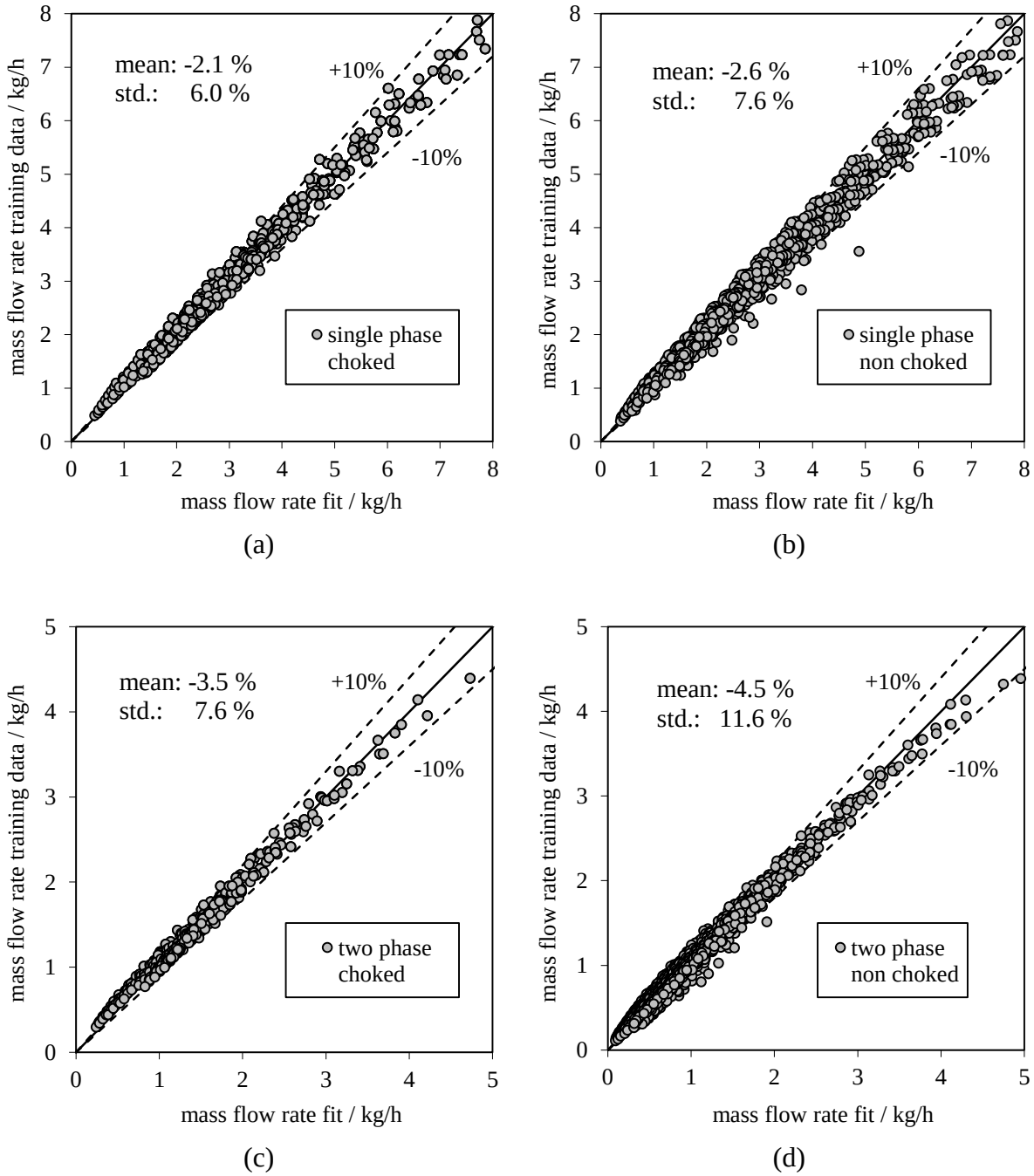

Fig. 34 Quality of fit by means of dimensional analysis.

The mean and standard deviation of the relative errors are as follows: -2.1 % and 6.0 % in Fig. 34 (a), -2.6 % and 7.6 % in Fig. 34 (b), -3.5 % and 7.6 % in Fig. 34 (c) and -4.5 % and 11.6 % in Fig. 34 (d). The range of parameters is given by Table 6.

Table 6 Range of parameters for dimensionless correlations.

	p_{out} bar	p_{in} bar	T_{sub} K	x -	L m	D mm	$\dot{m}$ kg/h
min	0.5	3.0	1	0.1	3	0.6	0.1
max	3.0	10.0	15	0.5	8	1.2	10.1

5.1.3. Application – adiabatic case

Applied to a set of measured data the dimensionless correlation performs not as well as the 1d code, expectedly, but still gives reasonable results. For comparison 19 choked points are used and evaluated by equation (148). The outcome can be seen in Fig. 35, where it seems that for these points the dimensionless correlation underpredicts the measurements most of the time, but still follows the trend in mass flow rate. The same can be concluded from Fig. 33, where a fictitious cycle of a refrigeration system is used as input for mass flow calculations. As a second test the formulae should be able to reproduce a start-up of a refrigeration cycle and handle the transient boundary conditions. The test covers non-choked and two phase inlet conditions and serves as a benchmark for the applicability of the models. The boundary conditions in Fig. 36 are not measured due to the lack of information on vapour quality and mass flow rate in the two phase regime. Therefore a hypothetical but realistic pressure and temperature trend is used to check the response of the mass flow formulae. As reference thereby serves the 1d code since measurements for the two phase inlet region are not available. Nevertheless the transition to single phase regime occurs usually two times per cycle and so this part should also be investigated.

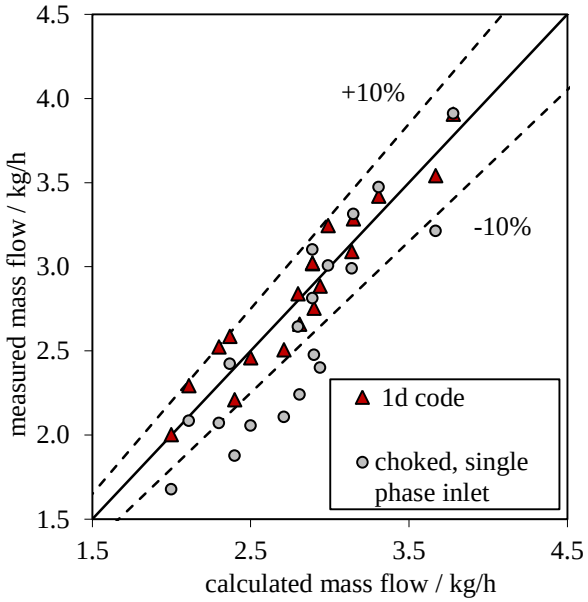

Fig. 35 Adiabatic steady state points reproduced (data by [63]).

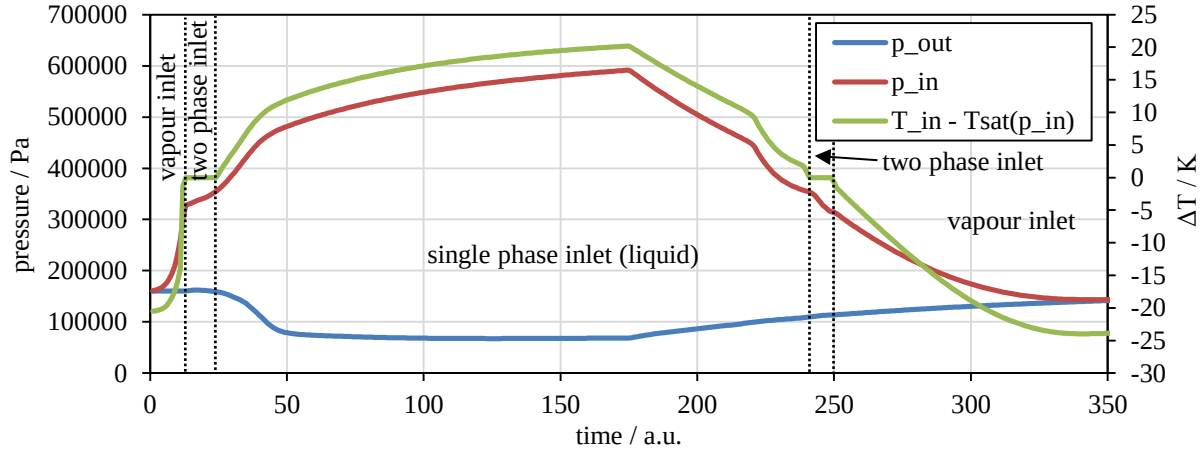

(a)

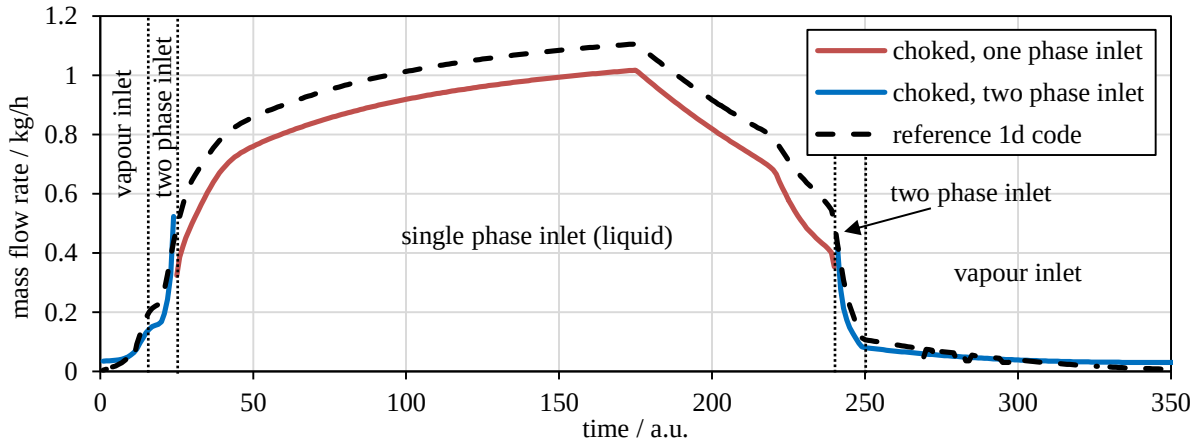

(b)

Fig. 36 Startup with dimensionless correlations (b) and corresponding boundary conditions (a).

In Fig. 36 (a) a closer look at the transition regions reveals a gap which is hardly tolerable in simulation tools and at the same time shows the limitations of this method. Due to before-mentioned problems, points around subcooling lead to erroneous mass flow rates. This approach is not seen as a proper tool for modelling capillary tubes satisfactorily in cycle simulations and especially not capillary tube heat exchangers. Although attempts exist where Π-groups are used and these cases don't assume a power law function but rather a sum of weighted groups. This case shall not be treated in the chapter "*dimensional analysis*" directly but is in section 5.3. Astonishingly the mass flow predictions in the two-phase inlet region as well as in the region where only vapour dominates (and which is out of range of the training data) seem to agree fine with the 1d code and common sense. This is contributed to the fact that these formulae are not solely empirical but *semi-empirical*.

5.2. Artificial Neural Networks (ANN)

This data prediction tool, getting more and more popular due to its flexibility, easy handling and application, had its first commercial utilization in 1984 which was stabilizing voice signals for long distance telephone systems (Demuth et al., [178]). Meanwhile its

implementation was successful in several fields of not only research but industry, entertainment, banking or defense.

5.2.1. Review

By the time Neural Networks have found their way to capillary tube and heat exchanger modeling. Islamoglu [49] compared results from ANN for capillary tube heat exchangers to empirical correlations from literature. The empirical correlations which use eight input parameters are used to compute the mass flow rate as well as the suction line outlet temperature. As a basis 50 test runs coming from two independent sets (also two different refrigerants – R600a and R152a, although nowhere a critical temperature, critical pressure or molar weight appears in the neural network formulation!) are taken. After applying the method using seven neurons and 10^6 learning cycles the absolute mean relative error for mass flow rates is 2.26 % and for temperature 1.94 %. Unfortunately it is not stated if Celsius or Kelvin is the basis of the scale, but since all temperatures are stated in Celsius and the experimental values are all positive it is believed that the percentage refers to Celsius. As suspected, ANN performs better than the two formulae which serve as reference.

Vins and Vacek [92] successfully applied this method to create a sum of dimensionless groups (as presented in eq. (147)) instead of the usual product from the Buckingham PI method to predict R218 mass flow rates for adiabatic capillary tubes. An excellent comparison of the neural network approach for adiabatic cases is featured here – 6 other correlations challenge their ANN. The fight ends in a tie since ANN performs well for R218 and R600a but is inferior when it comes to other refrigerants. One of the conclusions can be that there is no universal formula for predicting mass flow rates equally well for every refrigerant. To mention the quality of their ANN-fit, -0.12 % average and 3.45 % standard deviation for the first set (189 points) and -1.49 % average and 3.88 % standard deviation for the second set (34 points) of R218 data. For other refrigerants (e.g. R22) the average deviation is as high as 22 % and 9 % standard deviation.

Similarly, Zhang [108] approximated experimental results for seven different refrigerants at the same time with ANN, also comparing them with existing correlations on the basis of several experimental sets of data. With the help dimensional analysis and ANN (only one neuron in the hidden layer) he managed to get a standard deviation in mass flow rates of 6.6 % and an average deviation of 0.4 %.

Zhang and Zhao [109] created a predictive formula by ANN, trained with numeric data of a validated model and compared these results with experimental data from open literature for different refrigerants. This approach is close to the approach used in this work, due to the simplicity of data generation and the fact that big amounts of data are needed to represent all possible operating points.

5.2.2. Theory

ANN is a mathematical framework which basically connects a set of input data to a related set of output data. The connection between in- and output is achieved by matrix-operations,

simple addition and multiplication. The point of ANN is that these matrices which assign an output to every complete set of input have to be found, or better shaped from a random initialization by training with known values for in- and output. Unless no relation exists, ANN will reshape the matrices after every training run and increases its capability of prediction. The matrices often referred to as weight matrices, depend on the network structure the user has decided for in advance. This structure is described by the number of layers and the number of neurons in each layer where a neuron is the expression – influenced from the biological nervous system – for a data processing point embedded in the framework of ANN.

For this approach the "Neuronal Network Toolbox" developed by MathWorks implemented in MATLAB version 7.9.0.529 (R2009b) is used. To keep it short the mathematical details can be found in in the manual by Demuth et al. [178] and only the settings which are used for the computation and some considerations are pointed out. The structure of an ANN can be described by the number of input and output parameters, the number of layers, the kind of transfer functions used in each layer and the number of neurons in each layer. Fig. 37 serves as an example of how this can look like in an abstract way. "*Input*" stands for a set if input parameters where a single entry consists of let's say inlet-pressure, outlet-pressure, inlet-enthalpy, diameter, length. The number "5" in the figure stands for these five input parameters which shape the vector $\bar{\boldsymbol{n}}$. Bold abbreviations denote vectors or matrices and in this sense $\boldsymbol{IW}$ is a matrix of coefficients and its size corresponds to the number of neurons used in this layer and to the number of input arguments – in this case its size is of 20x5 – assuming 20 neurons. $\mathbf{b_1}$ is called "*bias*" and is added to the product of weight matrix and input vector. After that, the resulting vector of size 20x1 is evaluated via a transfer function (the model allows "*hard-limit*", "*linear*", "*Log-Sigmoid*" or "*Tan-Sigmoid*" functions). The preferred choice is a "*Tan-Sigmoid*" function which is used like in equation (152). The output of a layer can be a single parameter (a) or a set of variables ($\boldsymbol{a}$). The "*hidden layer*" is followed by an output layer which is a standard layer and features linear transfer functions and the number of neurons is equal to the number of output parameters. The method of operation of such a network like in Fig. 37 is that a sufficient high number of input data-sets with corresponding output data are available as training data and by iterative methods the matrices $\boldsymbol{IW}$, $\boldsymbol{b_1}$, $\boldsymbol{LW}$ and the scalar b_2 are determined by means of error minimization.

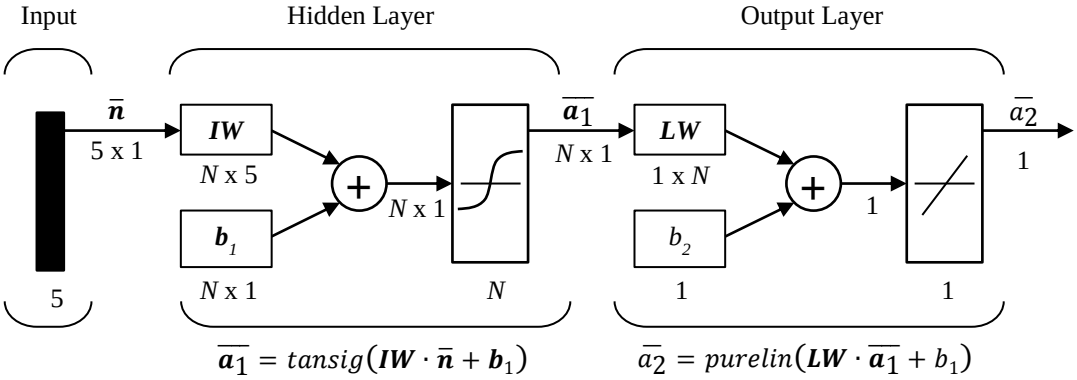

Fig. 37 Setup of a network with 5 inputs, a single output and a hidden layer with N neurons (figure originally by Demuth et al. [178] and modified in Heimel et al. [39], with permission of Elsevier).

Of course, more than a single hidden layer can be used – this would be accomplished by squeezing an additional layer between hidden- and output layer in the figure beneath gaining a third weight matrix and bias. Before starting working with a structure like in Fig. 37 all the input data is mapped to intervals between -1 and +1, see eq. (153). For re-usage of a trained network these scaling factors have to be known (*max*(***n***) and (*min*(***n***)) and have therefore to be stated as well as the scaling factors for the output to scale the artificial values back to physical quantities.

$$a = tansig(n) = \frac{2}{(1 + exp^{(-2 \cdot n)})} - 1 \tag{152}$$

$$\overline{\boldsymbol{n}} = 2 \cdot \frac{\boldsymbol{n} - min(\boldsymbol{n})}{max(\boldsymbol{n}) - min(\boldsymbol{n})} - 1 \tag{153}$$

$$\boldsymbol{n} = [p_{\text{in}}, p_{\text{diff}}, h_{\text{in}}, D, L, \dots] \tag{154}$$

$$\overline{\boldsymbol{a_1}} = tansig(\boldsymbol{IW} \cdot \overline{\boldsymbol{n}} + \boldsymbol{b_1}) \tag{155}$$

$$\overline{a_2} = \boldsymbol{LW} \cdot \overline{\boldsymbol{a_1}} + b_2 \tag{156}$$

After the network has been set up the crucial parameters for training are the kind of training method (backpropagation, conjugate gradient algorithms, quasi Newton methods, …), the number of datasets used for training, the target value of the Mean Squared Error (MSE), which should be reached as well as the maximum number of training cycles after which the learning process is stopped in case the target value is not reached.

To find out how many neurons would suffice to reproduce mass flow rates to a satisfactory degree different runs with various numbers of neurons were made in any case. The danger of having too many neurons – which certainly lead to a smaller MSE – is that between the fitted data oscillations might occur, so generally it is tried not to have a vast amount of neurons in any layer. The original dataset is divided randomly in three parts with a ratio of 60 %, 20 % and 20 %, respectively. In Fig. 38 it is shown how overfitting can be detected. Overfitting occurs if the number of neurons is large (corresponds to the degrees of freedom of the system), and the training data (corresponds to the constraints of a system) is low. If one is not careful enough something like in Fig. 38 occurs which is a typical sign of overfitting. The algorithm tries to shape the matrices according to the small set of reference data thereby neglecting to care about the intervals between the reference points. Now, it might be that the fit represents the given points well but leads to dangerous misinterpretations in between (Fig. 38 (right)). To detect this situation early in the ANN toolbox, the two remaining sets of data (40 % of the total input set) are used to see what is going on abroad the training set. The example below is calculated with 45 neurons, 5 input-, 1 output parameter and around 50 points (30 for training, 20 for test and validation). One can see easily that after some iterations the residuals start growing for the test- and validation-set whereas the residual for the training set still is decreasing. Knowing this, the three residuals are always studied after each fit, and

since the number of training points is kept high in this work (> 5000 random points with no more than 45 neurons) the danger of overfitting is minimized.

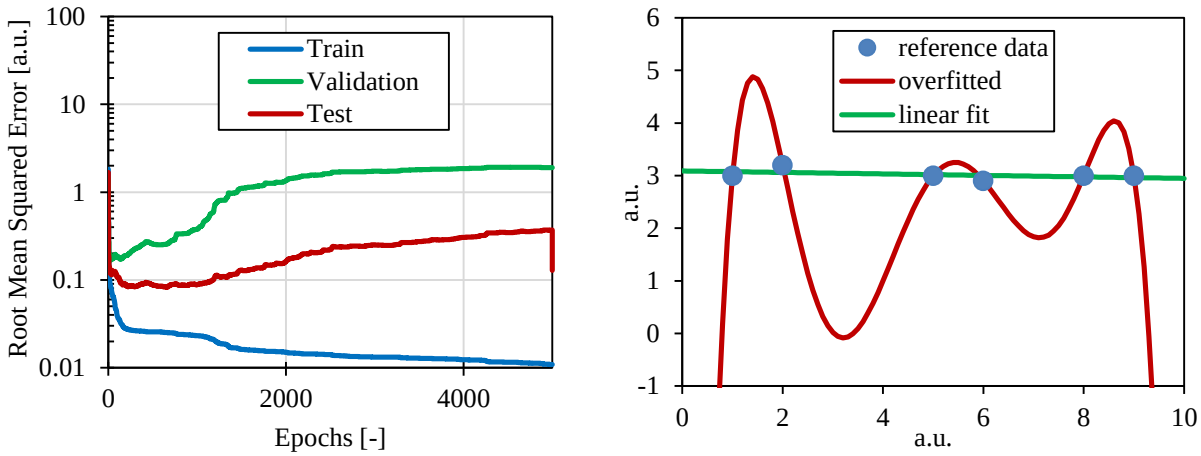

Fig. 38 Example of overfitting. Residuals for three independent sets of data (left) and exemplarily demonstration (right).

5.2.3. Application – adiabatic case

Concerning the structure of the ANN applied in this section (adiabatic case), inlet pressure, pressure difference, length, diameter and the inlet enthalpy are used (h_{in} instead of T_{sub} and x to avoid discontinuities at the saturation line). Zero point of enthalpy is for this case at T_0 = 298.15 K and p_0 = 1013.25 hPa. The mass flow rate is the output parameter. A static two layer network was chosen with varying number of neurons and a "*tan-sigmoid*" function, eq. (152), as transfer function for the first layer (hidden layer). It is recommended by Demuth et al. [178] to use either a log-sigmoid or a tan-sigmoid function for multilayer networks. The second layer (output layer) uses one neuron in combination with a linear transfer function. As training algorithm the "*Scaled Gradient Algorithm*" is used since it shows faster convergence compared to standard backpropagation algorithms [178]. Before processing the data and training the network all parameters have to be normalized by the "*mapminmax*" command which maps parameters to an interval between -1 and +1.

A good idea is to start with a variation of number of neurons (Fig. 39) to get an estimate on how the error (mean, min, max) will behave. Obviously, the error decreases by a non-linear relationship in respect to the number of neurons and concerning the good and bad sides of having too much or less neurons it can be concluded that a low number of neurons may lead to higher error in all respects and a higher number of neurons is prone to overfitting. To check if this is true the residuals are plotted for the 45-neuron case over the number of iterations and since none of the three sets of data show a rising slope, overfitting can be excluded.

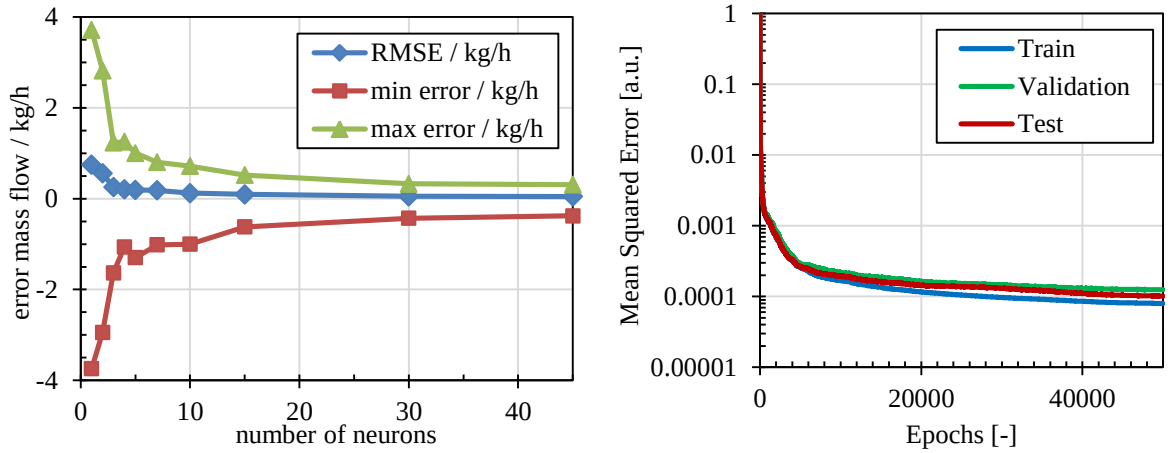

Fig. 39 Variation of number of neurons (left) and learning curve at 45 neurons (right).

Taking the ANN with 30x15 neurons, the training data can be reproduced to the degree like depicted in Fig. 40. The high relative error in the right figure results from nominal mass flow rates below 0.5 kg/h where the absolute error comes in the same order of magnitude as the nominal flow rate. This is not astonishing since the total range covers up to 10 kg/h with very low absolute and relative errors. To rise the predictability for small mass flow rates additional training points have been applied where the pressure difference is zero, hence the mass flow rate, too. When choking occurs, some extra training points can be easily gained by the fact that the pressure difference still can be raised but the mass flow rates stay the same. This means that a single point where choking occurs gives rise to a big number of training data without additional effort. It shall be noted, though, that this game should not be exaggerated and a good balance between choked, non-choked and zero-mass flux points should be aspired. Coming from left to right in the bottom of Fig. 40, the original points are first, followed by the points of zero mass flux, followed by additional choked points. The accuracy (1d code fitted by ANN) can be stated by 0.0004 kg/h mean error and 0.045 kg/h standard deviation which is a little better than a 45-neuron ANN.

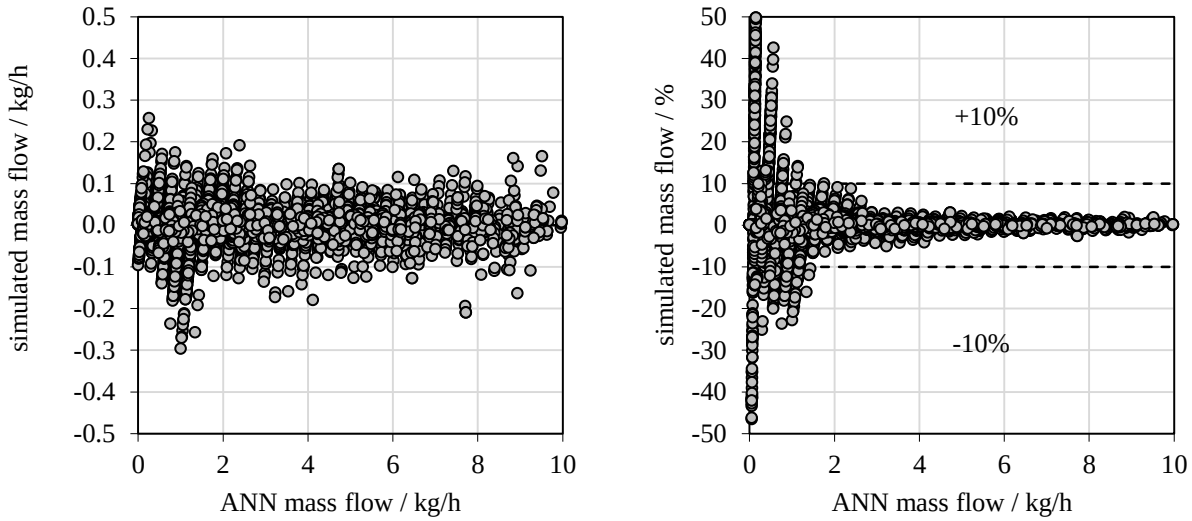

(a) *(b)*

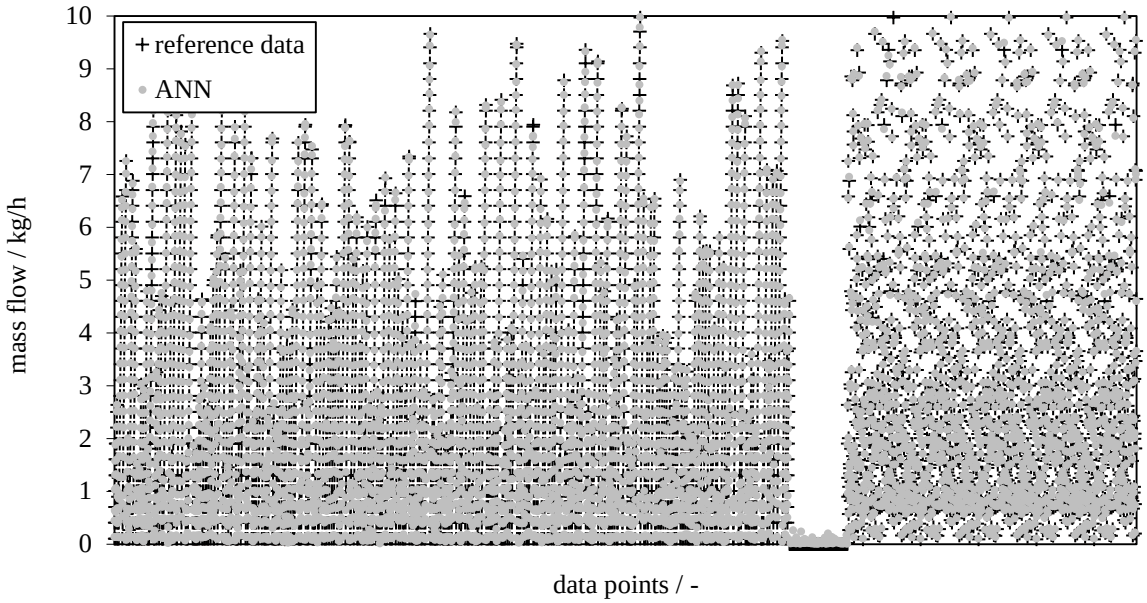

(c)

Fig. 40 Adiabatic training points reproduced (30x15 neurons, 6434 points). Absolute error (a), relative error (b) and datapoints (c).

Taking the configuration from Fig. 40 the same set of measurements like in section 5.1.3 is reproduced in Fig. 41. The fit follows perfectly the 1d code which forms also the training basis for ANN – it sticks more to the 1d code results than to the measurements. After an investigation on steady state behaviour an ON-cycle of a refrigeration device follows.

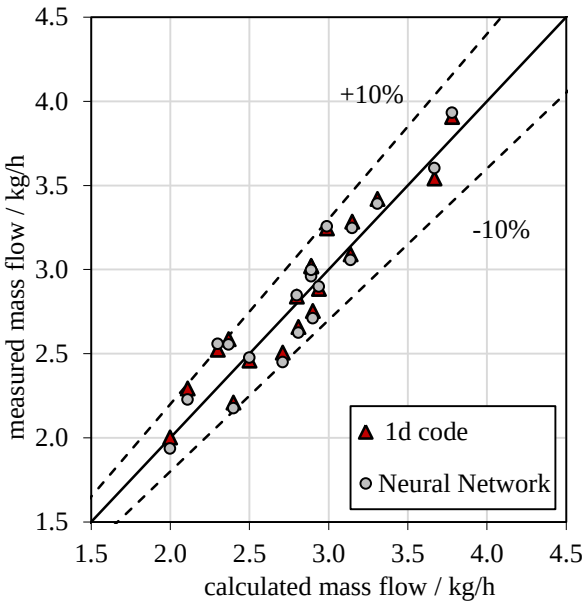

Fig. 41 Steady state points reproduced with a 30x15 Neural Network (data by [63]).

Therefore, the same boundary conditions as in Fig. 36 (b) are used to observe the mass flow rate when computed with a Neural Network. In the course of the work many configurations have been tried and more than one set of input data has been used since the sequence of processing data from the 1d code to applicable ANN matrices underlies constant improvement. This particular case has been tested with the 30x15 Neural Network described before. One can see that in Fig. 41 the measured mass flow rates are given back correctly by the ANN. The similarity between ANN and 1d result is obvious and proves the applicability of this method for the steady state case.

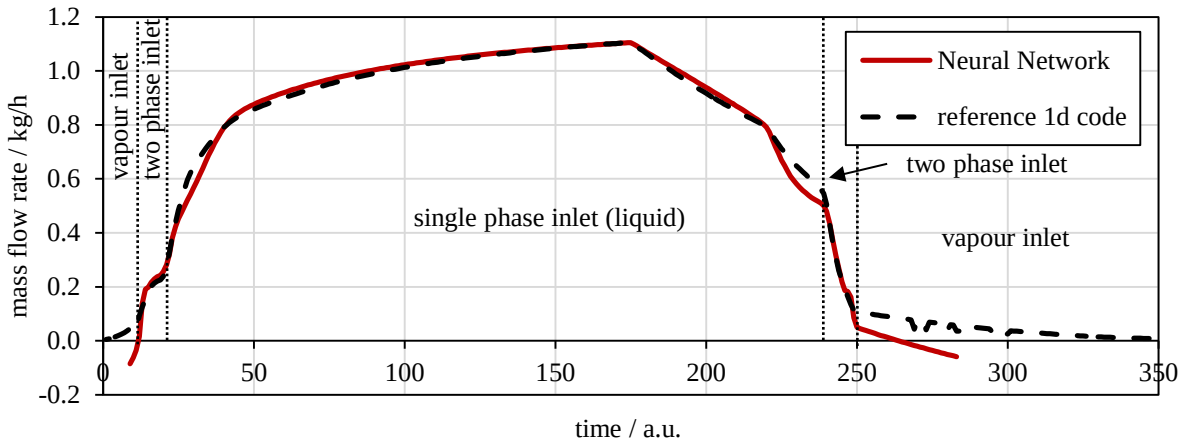

Fig. 42 Cycle with adiabatic capillary reproduced with a 30x15 Neural Network.

In the figure above it is shown how ANN computes mass flow rates – compared to the method in the previous chapter the advantage is a continuous transition between single- and two phase regimes at the inlet. But obviously ANN is not the answer to everything, drawbacks are also visible, that are a cut-off at the beginning (t = 10) and at the end of this run (t = 280) since the input-parameters are out of range for this case. Compared to the dimensional analysis example in Fig. 36 (b) it becomes visible that before implementation in a cycle simulation ANN has to be backed up at the places where it is expected to cross the border of the training data. Ignoring this advice, negative mass flow rates might for instance arise since ANNs lack any physical meaning. The fact that negative mass flows appear even within the training range in the figure above is explained by the standard uncertainty of this method which is in the order of 0.05 kg/h.

5.2.4. Application – non-adiabatic case

The same considerations as in the previous chapter can be accommodated here, where the complexity of the problem rises by addition of more input- and output parameters. The internal heat exchanger comes with a pressure level, a mass flow rate, inlet temperature, length and diameter. The position of the heat exchanger has according to previous investigations minor influence as well as surface roughness and inclination. The mass flow rate is deliberately not the same as the mass flow rate through the capillary tube since in reality an equilibrium is not always guaranteed. The same may be the case for the low-pressure levels, due to friction in the evaporator a pressure difference arises and results in two different pressures – one at the capillary tube outlet and one at the heat exchanger inlet. From in- house measurements it has been observed that the difference can be in the order of several tenth of a bar. Maybe this degree of freedom proofs to be unnecessary but in this attempt it is maintained.

Fig. 44 serves in detecting the influence of different ANN structures (one layer, two layers, different number of neurons) in respect to the error in output quantities. For this particular figure, more than 25000 points are used for training. Again, artificial data is added to the base-set of computed points. The more neurons, the lower the error maintaining no overfitting. Since the number of mathematical operations increases drastically with growing size of Neural Networks, also the computational time increases and therefore a 30x15 ANN

with ca. 30000 training points over 50000 iterations is the largest ANN in the scope of this work. Fig. 43, for instance, shows a set of training data, input and output of the 1d calculation. This set is used to train a Neural Network along with additional data such as geometry parameters or mass flow rate.

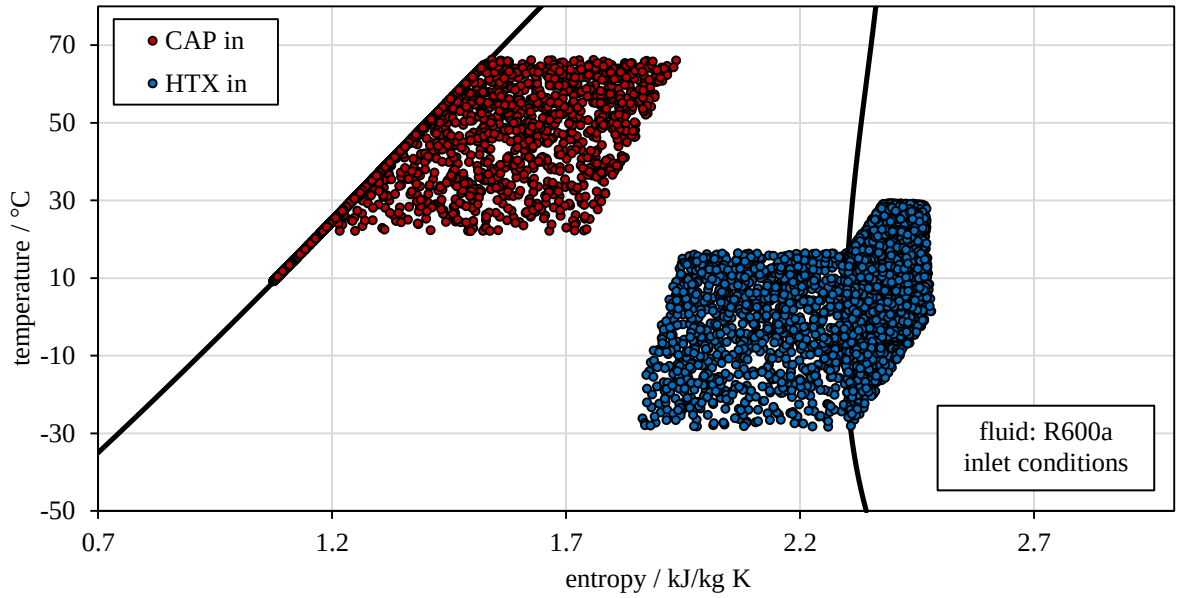

(a)

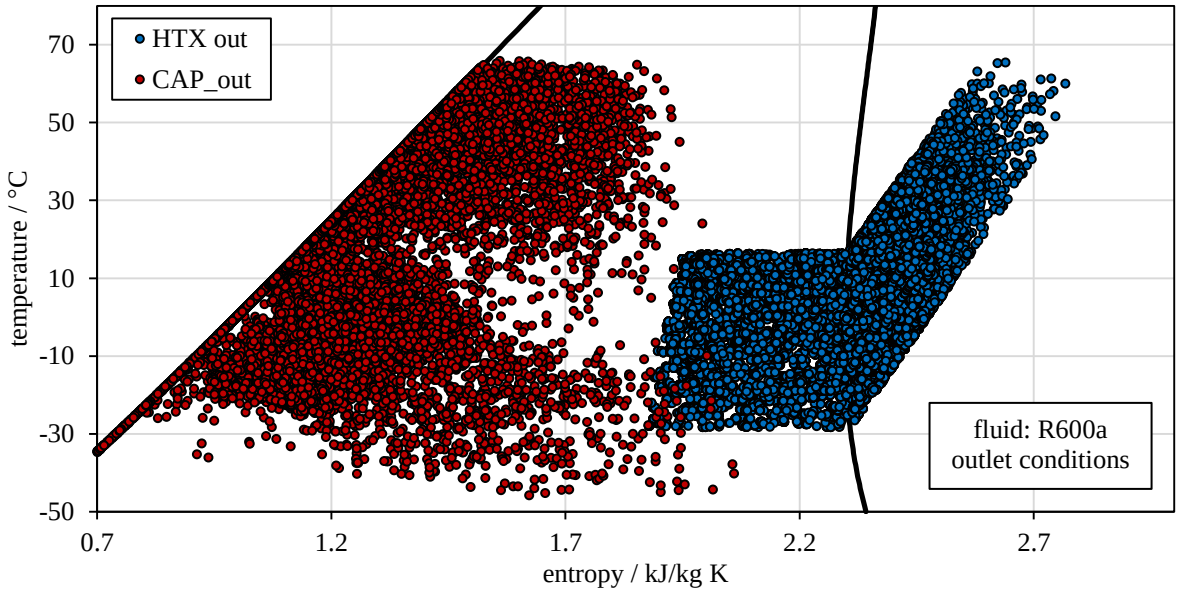

(b)

Fig. 43 Training data for capillary tube heat exchanger visualized in a Ts-diagram. Input parameters (a), output parameters (b).

A neuron variation has been carried out like for the adiabatic case to get a feeling about fitting quality. Firstly a single hidden layer is tried with up to 45 neurons and secondly, two hidden layers are used with 30 neurons in the first and a varying number of neurons in the second layer.

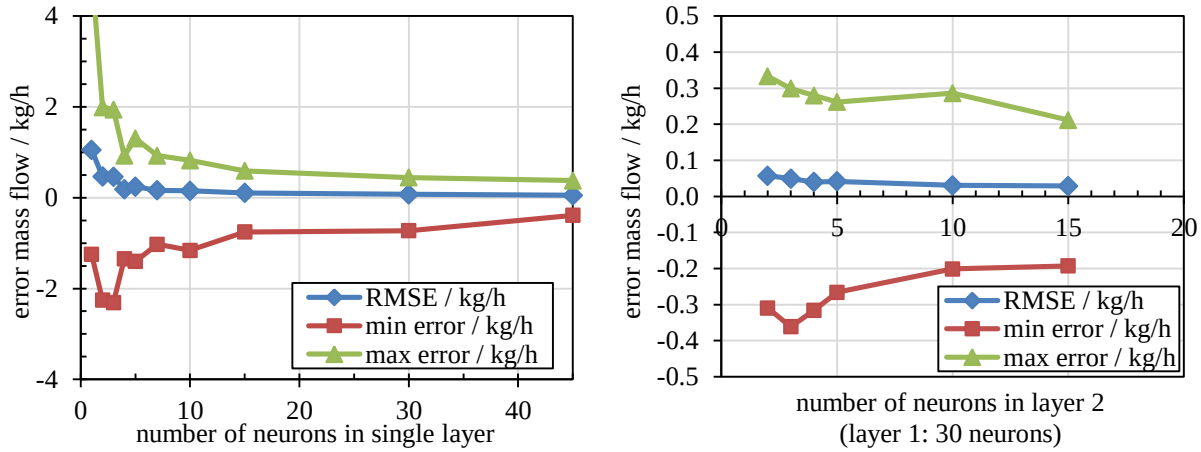

Fig. 44 Variation of number of neurons for diabatic capillary tube. As essential quantity the mass flow rate and not the transferred power is chosen.

Due to the low mean and standard deviation the 30x15 configuration is used from here on to reproduce the following validation and parameter studies (Fig. 45 and Fig. 46). As noticed earlier, the heat transfer is underestimated when compared to measurements and a correction has been introduced by enlarging the heat transfer coefficient at the wall of the suction line, Fig. 45 (c, d). The quality of the Neural Network fit in this example is for mass flow rate -0.0003 kg/h mean deviation and 0.042 kg/h standard deviation and for the transferred heat 0.01 W mean deviation and 2.25 W standard deviation. These stated values of accuracy refer to a comparison between 1d model and ANN. The absolute errors, compared to measurements, are shown in Fig. 45.

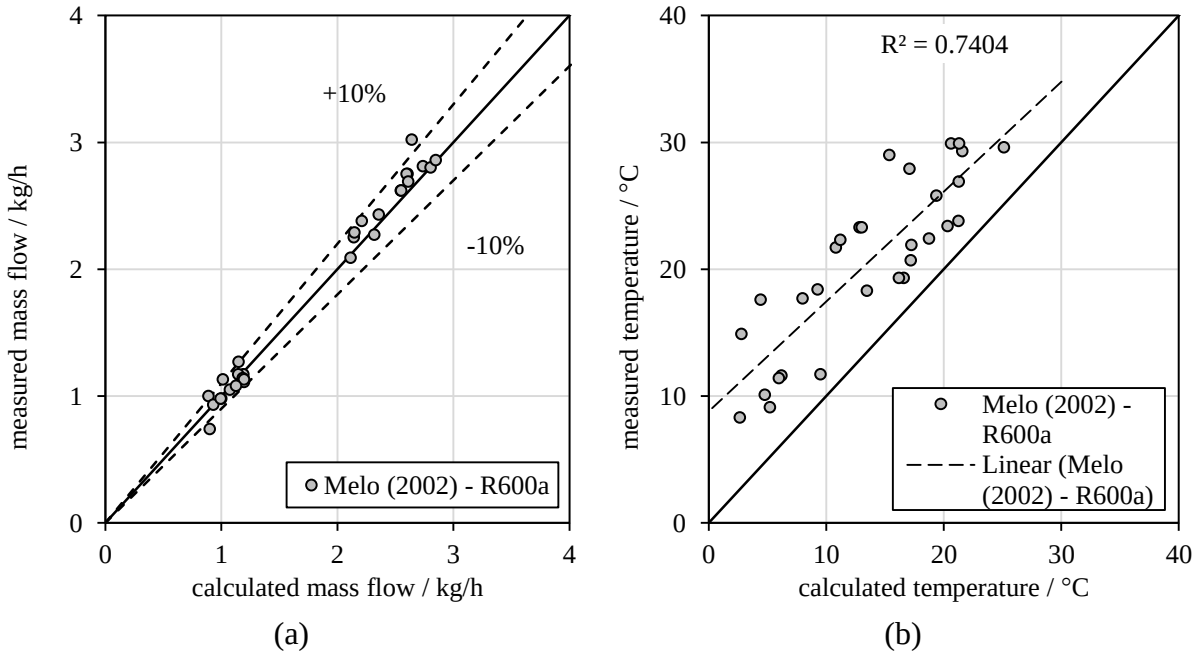

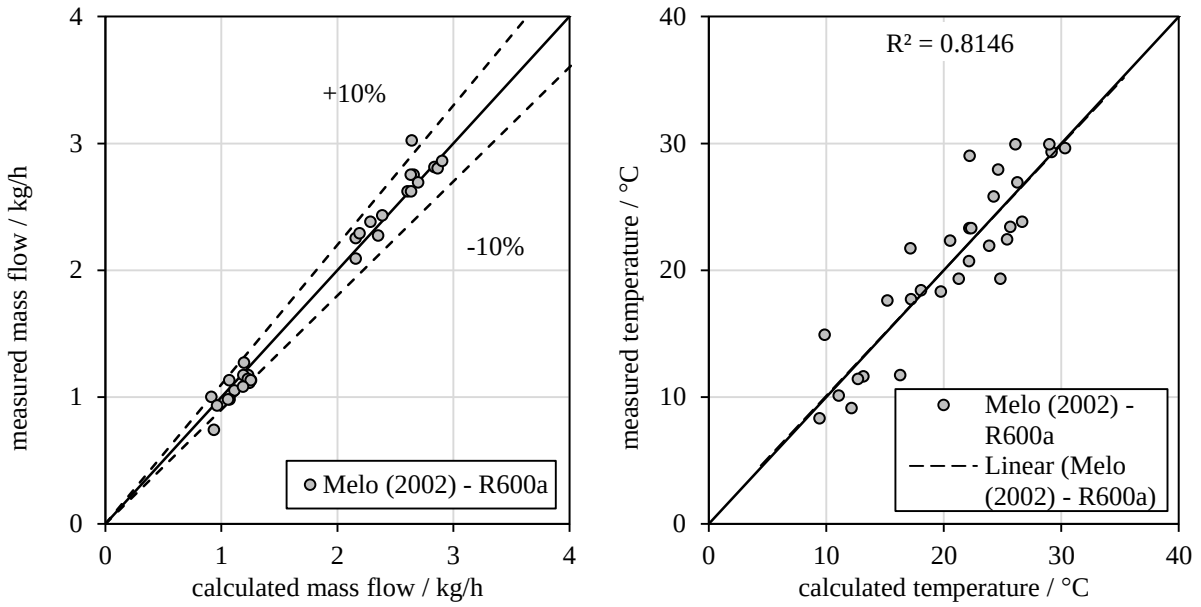

Fig. 45 Diabatic steady state points reproduced. The correction of the heat transfer according to measurements like in chapter 4.3.3 is done for (c) and (d).

A parameter variation using ANN follows to demonstrate the capability of this tool and to check for possible discontinuities. Fig. 46 reveals no such fears, even the variation of the capillary tube outlet pressure which visualizes the choking effect is reproduced credibly. The horizontal lines between 0.5 and 2.5 bar are slightly curved but lie within the range of standard uncertainty of this method.

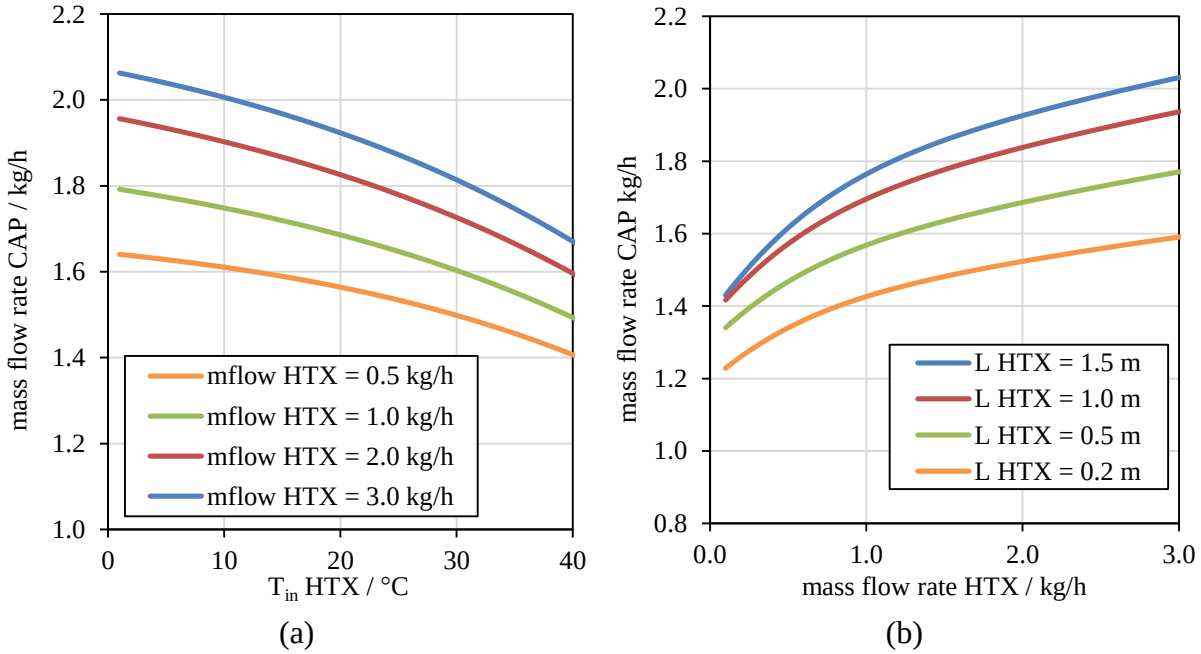

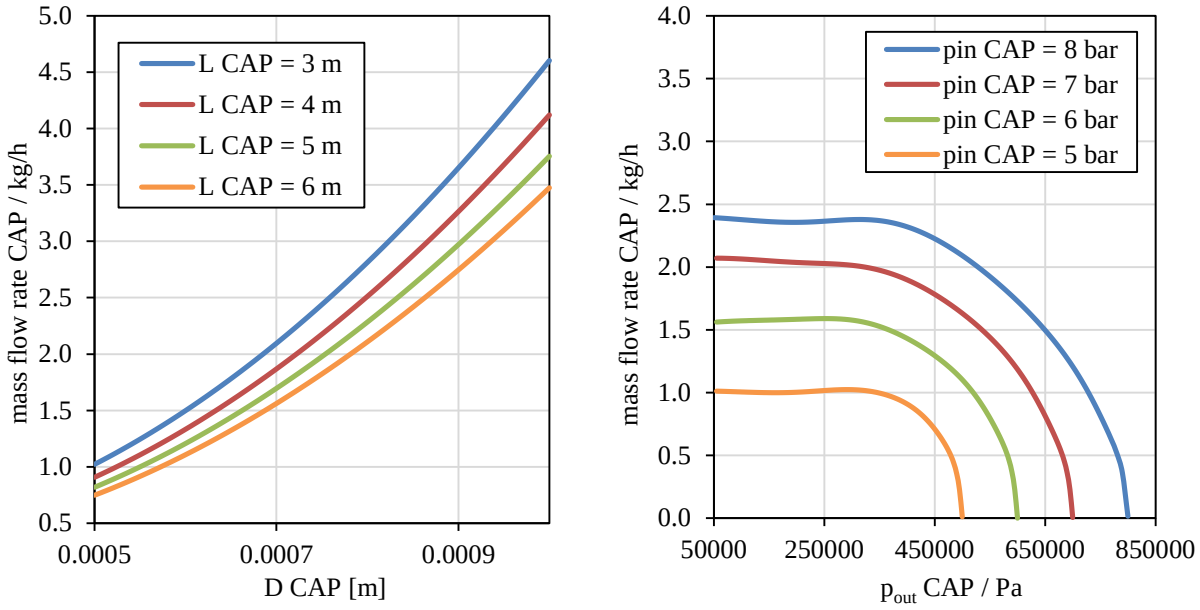

(c) (d)

Fig. 46 Parameter variations applying ANN. Neuron configuration (hidden layer): 30x15 using 34000 training points [39].

To conclude this chapter, the range of applicability of this particular configuration shall be given. However, the possibility of extending it in any desired direction is supposable and just limited by the 1d code or applicability in real devices. The advantage of limited training data is explained by a better reproducibility within this range paying the price of loss of generality.

Table 7 Range of parameters for diabatic ANN.

CAP	p_{out} bar	p_{in} bar	T_{sub} K	x -	L m	D mm	$\dot{m}$ kg/h
min	0.2	3.2	0	0.0	3.0	0.5	0.1
max	9.9	10.0	30	0.5	8.0	1.0	6.7

HTX		p bar	T_{sup} K	x -	L m	D mm	$\dot{m}$ kg/h
min		0.5	0	0.7	0.1	4.0	0.1
max		2.7	30	1.0	2.5	10.0	5.0

A quick note concerning Table 7 – the corresponding enthalpy is used instead of temperature and quality. For the sake of clarity the boundary conditions are not given in terms of enthalpy. Other parameters like the wall thickness, adiabatic length of the capillary before and after the heat exchanger section and so on are held constant. The suction line and the capillary tube don't necessarily have the same mass flow rate or pressure in common which is enabled also computationally in this case. Due to an automated routine which creates an ANN according to the predefined and customized range of parameters, this table is more a suggestion on the scale of possible variations and refers only to the example used to calculate Fig. 46.

5.3. Combined approach (adiabatic)

To account for the problems caused by zero subcooling or quality, in eq. (148) – (151) an approach suggested by Vins and Vacek [92] is applied. They used ANN to find a relation between Π-groups where the dimensionless groups could be summed up in order to compute the mass flow related dimensionless output parameter, Π_0. The procedure is as following: The 1d model calculates training points where the input and output data is saved. This set of data is used to compute the corresponding Π-groups for each point. Then, the Π-groups are fed to the training algorithm of ANN tries to find a relationship between input (Π_1... Π_5) and output (Π_0). The result of this computation-step, bias-vectors and weight matrices, are used to calculate the Π_0 -group which has to be converted back to a mass flow rate. With the same considerations as in 5.2 an ANN was set up varying in the network architecture from 2 to 10 neurons in the single hidden layer. As input parameters the Π-groups from eq. (147) are taken. It was found that more than 7 neurons don't seem to improve the predictability. Compared to measurements, Fig. 47 (a) reveals a slight over-prediction of the mass flow rates and a lower accuracy than the 1d code. All of these points are recorded by Melo et al. [63] under choked conditions with subcooled refrigerant at the inlet.

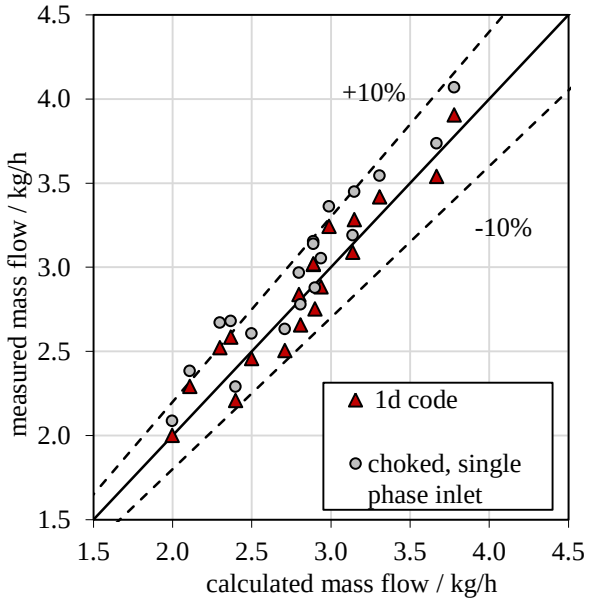

(a)

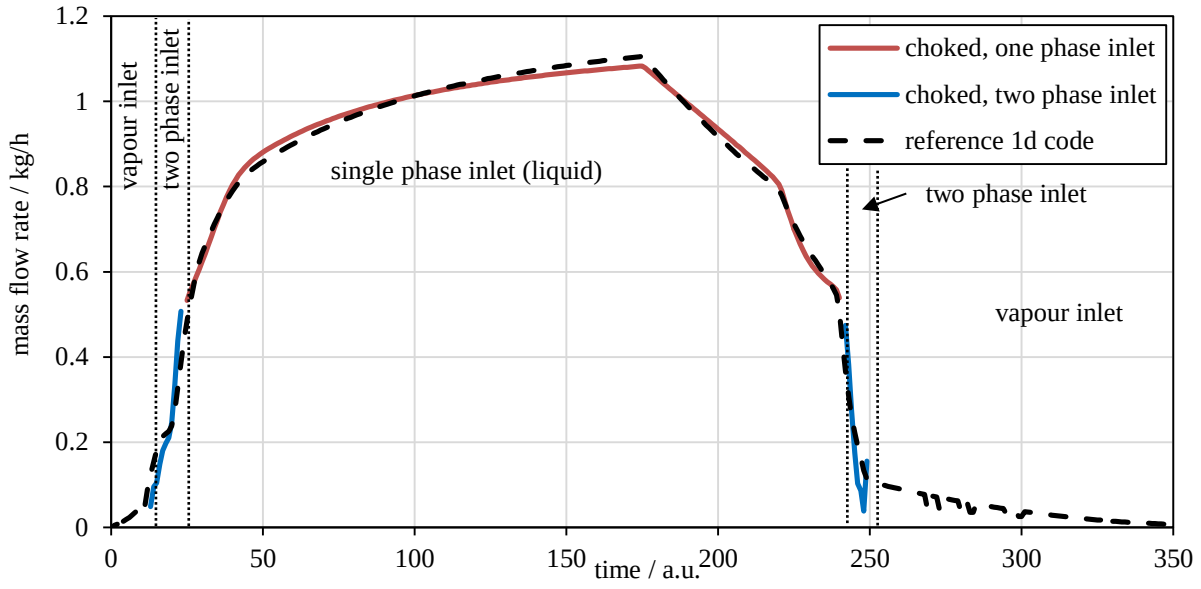

(b)

Fig. 47 Adiabatic steady state points (a) – data by [63] – and cyclic behaviour (b) reproduced.

The capability of computing cyclic behaviour is demonstrated in Fig. 47 (b), a comparably good fit in the choked single phase region and a tolerable behaviour aside this region is seen. Despite its quality in the both choked and subcooled region this method has drawbacks and is not to be considered a candidate for future cycle simulations. On one side, still a small gap at the transition between one-phase- and two-phase inlet conditions is there, and on the other hand the lack of training data in the region where only superheated vapour enters the capillary tube restricts this model even more. A third point has to be mentioned, even if the transition were smooth, with high accuracy and so on, the model would still need the information if the flow is choked or not. For practical reasons, the assumption that the flow is choked nearly all the time during operation holds but still poses a flaw.

5.4. Rating of methods

For means of comparison the methods described in chapter 5 are rated according to different categories with a view to its applicability in a cycle simulation. That means the preferred criteria is high speed, next stability and broad range of application and last high accuracy. The rating is done for the adiabatic and the non-adiabatic case, whereupon the non-adiabtic case is said to be more relevant due to its common application in real-world devices.

5.4.1. Adiabatic models

It has to be emphasized that the references according to accuracy are datapoints computed with the validated 1d homogeneous model. This could be circumvented if comprehensive and reliable experimental data for R600a were available to validate all other models against but due to the general difficulties in measuring two phase properties reliably the comparison is done in respect to the 1d code. In Table 8 the speed is calculated by averaging over the duration of each calculation from a set of 5255 points where only the duration of the core

code is evaluated and duration of in- and output is neglected. The overall RMSE is calculated by averaging the error over the 5255 data points. The dataset features all four cases (combinations of choked, non-choked, single phase inlet and two phase inlet). Concerning the choice of the configuration of the models it has to be noted that this comparison can be repeated endlessly with different training sets and a varying number of neurons. The RMSE would look different each time. To have at least something in common the test was carried out using the same set of data for each model both for training and validation.

Table 8 Rating of different adiabatic capillary tube models compared to the 1d code.

	Buckingham Π	**ANN (enthalpy inlet)**	**Combined approach**	**1d homogeneous**
time for computing mass flow rates (5255 points)	3 ms	15 ms	7 ms	$\sim 1 \cdot 10^7$ ms
Accuracy – RMSE	0.156 kg/h	0.094 kg/h	0.089 kg/h	reference

Calculation time: Obviously, the 1d code takes its time and falls six orders of magnitude behind all other models. The Neural Network takes longest among the 0d models due to the slightly higher number of mathematical operations.

Accuracy: The Buckingham Π method seems to have the highest uncertainty compared to the other models. This is hardly astonishing, since ANN can be tuned by taking a higher number of neurons. This can't be observed for the combined approach where a rising number doesn't lead to better predictibility.

The range of input parameters is limited in the 1d case to the thermodynamic property functions. This is not the case for the other models since they all together base on a set of existing datapoints, particularly on the 5255 points computed with the 1d model. Since ANNs lack any physical meaning and work basically as a data-fitting-tool, extrapolation beyond the underlying basis may lead to erroneous mass flow rates. Dimensionless analysis also bases on a set of points and should be used with care when it comes to extrapolation. Since the functions themselves, eq. (148) – (151), are of a simple kind the dependency of mass flow rates regarding to input parameters is predicted correctly, unlike in ANN where it might come to oscillations or even negative mass flow rates when input values far away from the training points are used. Therefore, as a suggestion for an adiabatic model in a cycle simulation either Neural Networks or dimensionless correlations can be taken. Both variants should nevertheless be implemented together with a "check-function" to avoid for instance negative mass flow rates.

5.4.2. Non-adiabatic models

This summary of the non-adiabatic models includes a comparison between numeric results of the validated 1d code, ANN and correlations from literature. The driving force behind this work was the need for a reliable capillary tube model to be used in cycle simulations, therefore a final test with realistic boundary conditions is made. For means of comparison, correlations for non-adiabatic capillary tubes according to Melo et al. [66], Sarker and Jeong

[80], Wolf and Pate [97] are used and applied. All of these correlations are said to work with R600a, also the geometry of the capillary tube and of the heat exchanger is within the applicable range. The thermodynamic boundary conditions, however, change rapidly from superheated to two-phase to subcooled and may not always lie within the stated range of applicability. Nevertheless, this comparison serves as a test to see how the models react and if the calculated values are in agreement with the 1d model. The boundary conditions therefore are taken from a cycle simulation which has been adapted for calculating an existing freezer. The dimensions of the used capillary tube are
0.75 mm inner diameter, 3.26 m in length and 1.6 m heat exchanger length. The measures of the suction line are 4.6 mm inner diameter. The design is assumed to be coaxial to be able to compare with other correlations. The mass flow in the suction line as well as the pressure are independent from the capillary tube exit pressure and mass flow and are given as input.

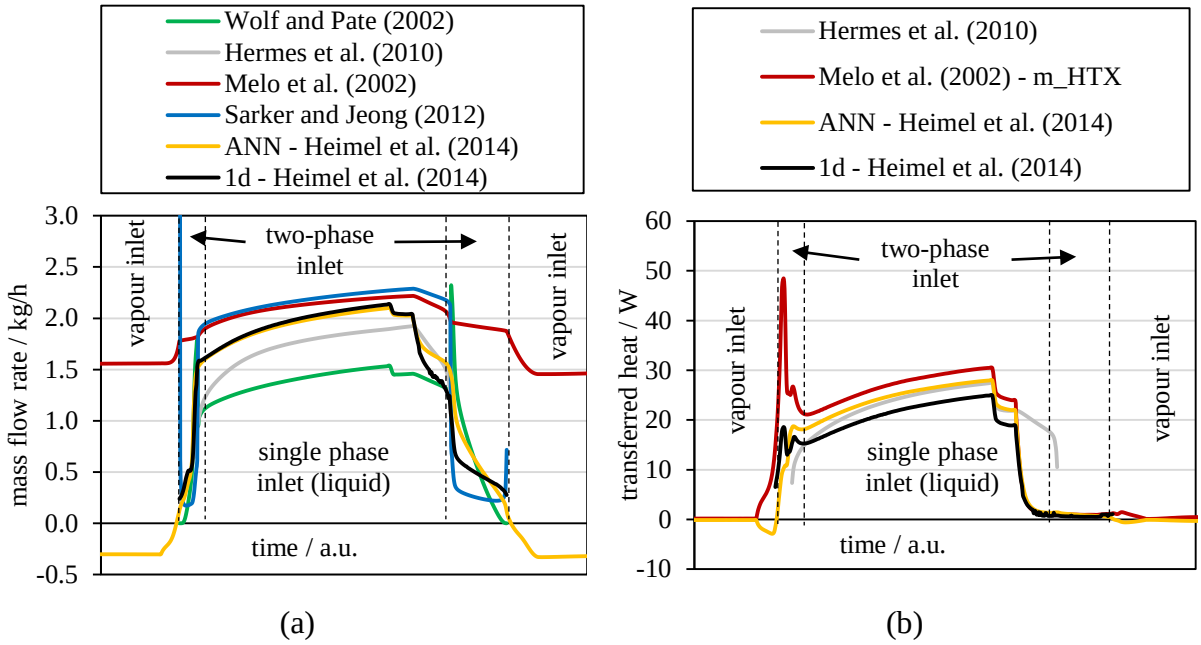

Fig. 48 Comparison of non-adiabatic models. Mass flow rates (a) and transferred heat (b). The designations for refer to the capillary tube inlet.

The comparison shows, that even during normal operation a discrepancy of nearly 100 % in mass flow rate and transferred heat between the models arises although the same boundary conditions are used. The neural network solution sticks as expected close to the 1d results, also during shutting On and Off of the system ANN maintains a similar trend compared to the 1d case. Noteworthy, assuming two phase inlet all over the On-period in other cases, the models of Hermes et al. [44] are not applicable and the mass flow model of Sarker and Jeong [80] as well as Melo et al. [66] show high offset and don't follow the trend of the 1d model. In Fig. 48 subcooled liquid is present during the On-period and makes the rest of the models applicable. Deviations and peaks can be seen at the beginning and the transition region of the quality in the models of Wolf and Pate [97] and Sarker and Jeong [80] which would be hard to cope with from the cycle simulation's point. Summing up, the only model from literature which is able to calculate mass flow rates and transferred heat under subcooled and two phase inlet conditions without breaking down is the one by Melo et al. [66]. Unfortunately, the error

in the two phase inlet region is too large to be applicable in a cycle simulation, so, the ANN – solution is considered to be the most robust one. When the inlet boundary conditions switch to superheated vapour, none of the models give back reasonable results, consequently a backup function for the mass flow must be used, anyway. Concerning calculational speed, the usage of any correlation mentioned above as well as the usage of ANN lies in the same order of magnitude. The exact timespan depends of course on the programming language, the implemented thermodynamic property tables and the programming skills. For methods other than the 1d-code, the duration of a single calculation is in the order of milliseconds whereas a 1d-code takes seconds up to several minutes due to iterative solution algorithms and countless calls of thermodynamic property-functions.

6. Experimental work

Experimental validation of calculations can not only be seen as a gruelling, disillusioning task but is an absolute necessity to check for plausibility of simulative results where different steps of abstraction, mathematical simplifications, approximations and interpretation are applied to come to a prediction about a certain physical property. Providing accurate measurements one might see that the mathematical procedure lacks accuracy or that major influences have been unaccounted for. True so far, but who calls the persuasive power of experiments into question? Least the people who should do it most – the ones who measure. Regarding this work, neither the simulation nor the measurements are perfect, both methods can be seen as attempts in order to focus on the same specific phenomenon from two very opposite points of view. Measurement and simulation (Or is it "*Simulation and measurement*" ?) don't compete against each other but rather complement one another, both flawed with uncertainties and doubts, to lead to a deeper understanding of a physical process. How far one can trust results, may be estimated or quantized by means of probability and is also an important step when different outcomes are compared.

In this work also both simulation and experiment are applied and cross-checked. Due to the relatively constricted usage of R600a as refrigerant on a global scale, correspondingly few published measurements exist. To avoid depending on a single published table for R600a mass flow rates, a test rig is set up whose requirements are defined in such a way that it should be able to operate at a steady state condition and measure input and output parameters of the adiabatic capillary tube model mentioned in chapter 4.2. The size of the system in terms of cooling capacity and corresponding mass flow rates is based on the dimensions of a commercially available refrigerator.

6.1. Review

Prior to the decision of setting up an own test rig (not only for capillary tube experiments but also for investigations on heat exchangers and the cooling system as a whole) a review of existing systems and published data was carried out. The summary is given in Fig. 49. Previous work can be classified into three categories. The most common investigation is to measure the mass flow rate at known inlet and outlet conditions (pressure, temperature), thus together with the geometry of the capillary tube all parameters for comparing the capability of a simulation tool are given. What happens between inlet and outlet stays unresolved and is partly matter of the second category of experiments, where also pressure and temperature is measured in between. By doing so, the point of evaporation can be found, hence evaporation delay can be quantized by measuring the length between the expected and the actual point of evaporation. Finally, visual studies have been conducted with small diameter glass capillaries – the motive is to get a clue about the occurrence of flow regimes and also to observe the onset of evaporation.

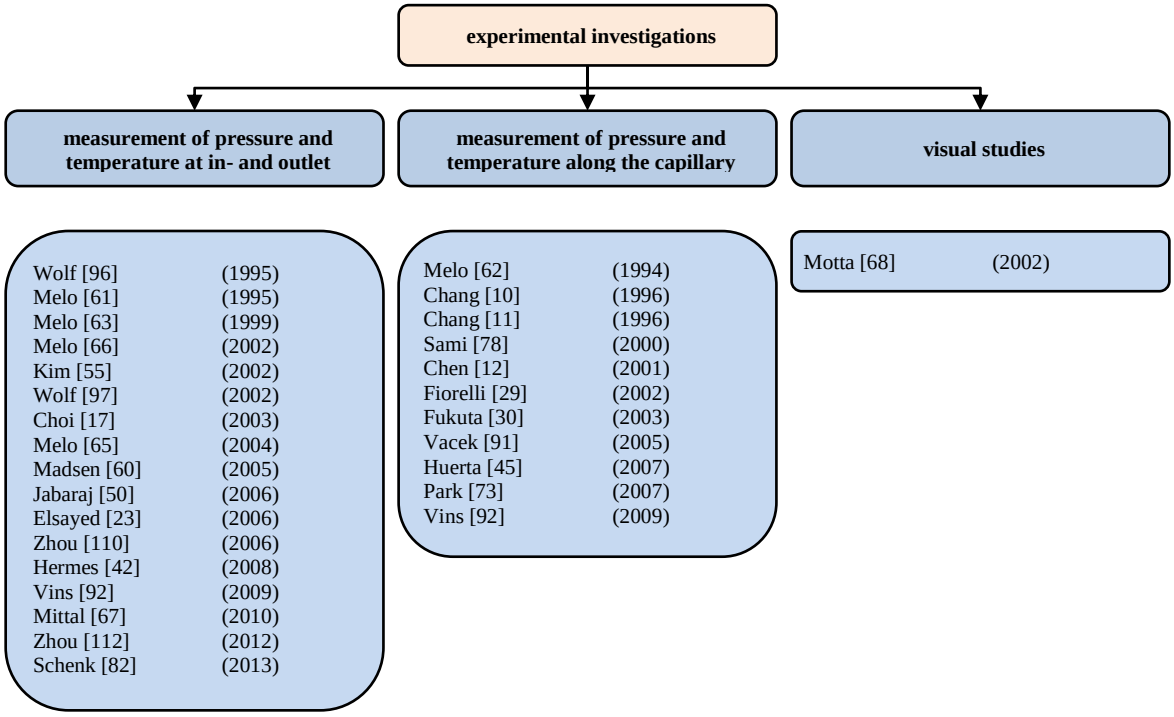

Fig. 49 Summary of literature dealing with experiments on capillary tubes.

Aiming for validation of a mathematical capillary tube model or the creation of a correlation from experimental data, a test rig needs to collect data at the tube's inlet and outlet. Additionally the mass flow rate and geometry must be known, but from the metrology's point of view, that's basically it. The rest of such a test rig is to achieve certain operating conditions and hold them for a defined period of time. The setup of such systems equals a refrigeration system with additional heaters and coolers. Mittal et al. [67] used for condensing a constant temperature bath after the compressor, followed by a subcooler and a preheater to condition the state of the refrigerant at the capillary tube inlet. An oil separator, filter/drier, mass flow meter and pressure- and temperature transducers were also installed in the system as well a sight glass at the tube's inlet. A manually controlled expansion valve bypasses the test section containing the capillary tube and finally a controlled heater (evaporator) leads back to the compressor. Similar functional schematics can be found in other publications (see Fig. 49, left column) with slight alterations concerning metrology and order of devices. Melo et al. [66] reports on a test rig for capillary tube heat exchangers and gives a detailed description on the construction of the concentric heat exchanger region. Here, the whole capillary tube section is placed into a long, wooden box filled with glass wool in order to prevent undesired heat transfer aside the heat exchanger region whereas Jabaraj et al. [50] uses several capillary tubes connected via a ball valve to a single reservoir where pressure and temperature is measured. Fiorelli et al. [29] uses a pressurized tank of refrigerant instead of a compressor to get around issues of controlling the input parameters of the test section which may occur when a closed loop system is used.

Since R600a is seldom used elsewhere than in Europe, only few experimental studies deal with this refrigerant. Amongst them are Melo et al. [61], [62], [63], [66], Schenk and Oellrich [82] and Huerta et al. [45]. Well documented measurements with other refrigerants where the measured mass flow rates are explicitly given can also be found in Fiorelli et al. [29] who

uses R410A and R407C. To mention is also the fact that in this work datasets for two-phase-inlet conditions are presented. Therefore, the quality is calculated from the electrical power consumption at the heater in front of the capillary tube. Extensive data (400 points) on R22 and M20 (a mixture of R600a R290 and R407C) is presented in Jabaraj et al. [50] for different geometry, pressure and subcooling. Data-points for R22, R407C and R410A are presented by Kim [55], however not in tabular format. Also Choi et al. [18] presents his data in diagrams, R22, R290 and R407C have been under the scope. Mass flow rates up to 160 kg/h with different refrigerants (R134a, R22, R152a, R410a) are published by Wolf et al. [96] and are commonly used in the field of capillary tube modelling as a source for validation as it is also done in this work.

Experiments on the effects of coiling were conducted by Mittal et al. [67], Kim et al. [55], Park et al. [73] and Zhou and Zhang [110]. The general opinion is that coiling reduces the mass flow rate compared to a straight capillary tube as additional friction leads to choking at lower mass flow rates. Moreover, non-dimensional correlations have been developed based on these experiments, accounting for this phenomenon.

Typical temperature sensors are T-type thermocouples (see section 6.3.2) with uncertainties reported between 0.2 K [66] and 0.5 K [55]. Jabaraj et al. [50] and Huerta et al. [45] use PT 100 resistance thermometers with uncertainties of 0.1 K for their measurements. The typical uncertainty of pressure transducers range between 0.02 bar [66] and 0.05 bar [67]. Mass flow meters are primarily Coriolis-type devices with reported uncertainties between 0.03 kg/h [66] and 0.1 kg/h [45]. Reported relative uncertainties are not given here since the reference (full scale, indicated value) is not always pointed out.

Concerning pressure and temperature measurements along the capillary tube, fewer studies have been conducted than for the latter branch. The difficulty is to apply the connectors for pressure to the tube without introducing a disturbance where the evaporation would start. Temperature is measured by attaching thermocouples at the outer wall of the tube since they would constitute a too big obstacle for a flow in a 0.7 mm tube. Usually, the reason of measuring pressure and temperature not only at the inlet and outlet is to get information on the point of evaporation. By comparing readings from pressure sensors with the saturation pressure as a function of the temperature measurements, the location of the evaporation can be detected and secondly evaporation delay (if occurring) can be quantized in terms of length. This can be done by subtracting the length of the ideally liquid region from the observed liquid region which is naturally a little longer due to the before mentioned delay of evaporation. Another common expression is explained in the section 4.4 where the term "underpressure of vaporization" stands for the pressure difference between the saturation pressure and the actual evaporating pressure. Studies pointing in this direction are carried out by Huerta et al. [45] who concluded a dependence of the evaporation delay on mass flow rate and degree of subcooling. The metastable length reached up to 0.4 m, the influence of oil leads to increased metastable regions. Chen and Lin [12] use diabatic capillary tubes and R134a for their studies and find that the underpressure of vaporization is related to the heat transfer between suction line and capillary tube. An increase in transferred heat leads to a

decrease in underpressure of vaporization. Chang and Ro [10], [11] and also Vacek and Vins [91] use temperature and pressure measurements along the tube in order to verify and adjust their models for pure refrigerants but also for mixtures [10]. Melo et al. [62] observed that in almost every case during his study underpressure of vaporization occurred. Since R600a was used here this work deserves special attention since metastability depends amongst others on the type of refrigerant. Melo reports random behaviour of metastability at the same operating conditions but observes a general trend towards higher underpressure when the subcooling at the inlet is increased.

Motta et al. [68] conducted experiments on a test rig where the influence of oil in refrigeration systems was in the focus of interest. Experiments were performed with R404a/oil in a glass capillary tube and the influence of oil affects the critical flow rate. It was concluded that the reason is the different viscosity of the refrigerant/oil-mixture compared to the pure refrigerant. Due to the transparent tube, the onset of evaporation could be tracked – it turned out that under the influence of oil the liquid length shortened. Another conclusion was that the flow regime is predominantly bubbly flow since after the point of evaporation a "blurry-like" flow regime spreads continuously until the whole cross section is filled homogeneously. According to Motta's references (Dudley JC. 1962, 'A photographic study of the two-phase flow of Freon in small bore tubes', MSc. Thesis, University of Wisconsin, USA.) high speed images reveal that the observed "blurry-like" flow consists of small vapour-bubbles.

6.2. Test rig

The setup can be seen in Fig. 50, where photographs and a schematic view of the refrigeration circuit are shown. A variable speed drive compressor HKK70 VSD (1) with a rated cooling capacity from 57 to 150 W according to the ASHRAE standard is used [199]. A chiller (2) with feed pump (3) cools the water bath (4) of the condenser and keeps it at constant temperature. Though the operating principle is a simple On/Off controlled one, the average water temperature can be held constant within ±0.5 K. The cooling capacity of the chiller is specified to be at 300 W which proves to be sufficiently high for any operating point of the system. Since the water-bath is insulated to its surrounding, no heat source is necessary to keep it at constant temperature since the transferred heat from the refrigerant is enough to let temperatures rise up to 60 °C. The pump for the secondary cooling circuit is always switched on to maintain the heat transfer in the condenser during a measurement independently of the chiller being switched on or off. After the refrigerant has been liquefied it enters at (5) a filter/drier which prevents small particles from plugging the capillary tube and hence the refrigeration circuit. The filter/drier also removes moisture and acids from the system by means of adsorption by molecular sieves [181]. Therefore these kinds of filters should be renewed in a regular pattern. After the filter/drier, the mass flow meter (6) is installed. The decision to place the flow meter at this position was motivated by the fact that its internal pressure drop for a gaseous phase would have been too high – in the order of several tenth of a bar – so measuring in the liquid region is preferred. Since a liquid state is desired at the capillary tube inlet, the flow meter has therefore been placed between the filter/drier and the

capillary tube inlet. To ensure subcooled refrigerant at the capillary tube inlet, a sight-glass (7) is installed additionally to support the reading of the temperature and pressure at the inlet.

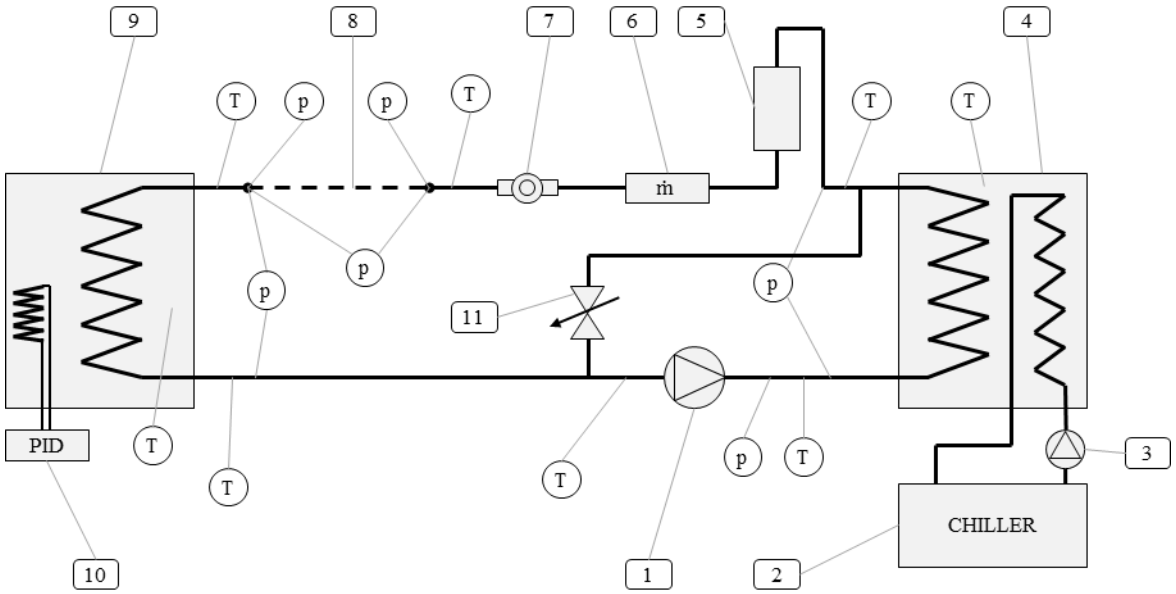

(a)

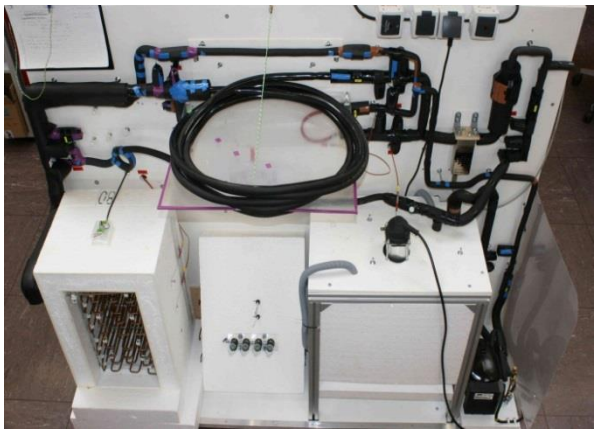

(b)

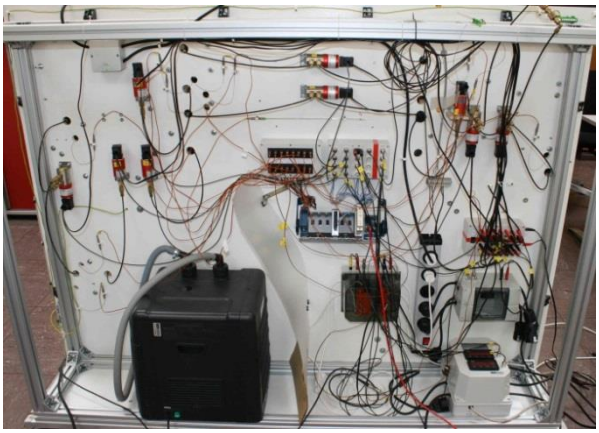

(c)

Fig. 50 Schematic drawing (a), front (b) and backside (c) of the test rig.

The capillary tube (8) itself is prepared in the following way. From a 30 m coil, the necessary length is cut by a special cutting tool which guarantees low deflection of the original cross section. A connecting thread is soldered to both ends and after insulation with foam material (wall thickness: 7 mm, thermal conductivity: 0.038 W/m K at 20 °C) the tube is rolled up to a coil of 700 mm in diameter due to restrictions in space. It is known that coiling in general reduces the mass flow rate due to increased friction as a consequence of secondary flows induced by centrifugal force. It is reported that a coiled diameter of 40 mm decreases the mass flow rate by up to 10 % whereas coiled diameters of more than 600 mm have negligible impact on the mass flow rate and therefore assumed to be straight [14], [31], [111].

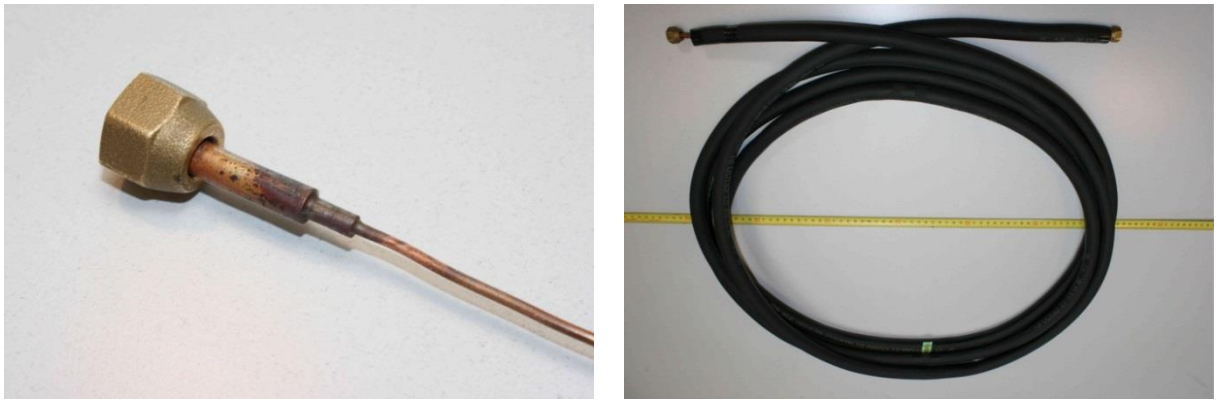

Fig. 51 Capillary tube end soldered to a connector (left) and insulated tube ready for installing (right).

To measure the pressure at the in- and outlet, flexible small diameter hoses are connected to T-fittings at the respective position. Temperature measurements are conducted inside the copper tubes. Therefore, the tip of each thermocouple has to be inserted to the middle of the cross section, fixed and hermetically sealed. This is achieved by T-fittings where a clamping collar is inserted – the thermocouple is lead through this construction up to the desired length and then fastened by the clamping collar (Fig. 52).

Fig. 52 Measuring points of pressure (right) and temperature (left) before being insulated.

The refrigerant can be heated in a controlled way by the evaporator which is placed in an insulated box with light bulbs and thermocouples (9). The light bulbs are variable in terms of electrical power consumption and are coupled via a PID controller (10) to one of the thermocouples inside. In other words, the air temperature can be held at constant value or the light bulbs can alternatively heat with constant power.

A bypass expansion device (11) is installed which connects the exit of the condenser to the inlet of the evaporator and omits therefore the filter/drier and all metrology for capillary tube measurements. The bypass consists of a 3 m capillary tube (0.7 mm ID) after a needle valve. The purpose is to be able to easily vary the mass flow rate through the main capillary tube during operation. Secondly, it is reported by [63] to be useful for changing the evaporating pressure a little for a short moment and monitor the impact on the mass flow rate. If it stays constant the flow is choked.

All measurement data is collected via a NI Data Acquisition System (NI cDAQ 9188 for ethernet) and recorded by a LABVIEW routine. Postprocessing and visualization is done in Excel and RefProp v9.0 (database 23) for calculation of saturation properties, density or enthalpy. The specialized modules for signal processing and conversion from analog to digital are connected to the DAQ. Since the sample rates of the modules differ, a 1 Hz temporal resolution is chosen for temperature readings and for all other signals. Since pressure and mass flow are recorded by a module featuring 250 kS/s per channel in contrast to the temperature recording module, an average of 1000 samples per recording easily can be achieved.

6.3. Metrology and uncertainty of measurements

Since no result of measurements whatsoever acts as a standalone-number and glorifies itself to be unique and hundred percent correct, a short reference to a well known and much cited convention shall be given. The "*Guide to the expression of uncertainty in measurement*" or simply GUM is used to evaluate the uncertainties for the following capillary tube measurements [172]. The expression "*uncertainty*" is used throughout this work whereas words like "*accuracy*" or "*precision*" are tried to be avoided. Uncertainty, literally speaking, reflects the doubts one may have after measuring a certain property. In its technical sense this meaning can be retained, as every measurement is an estimate of a "true" value and differs, ideally by zero, from the "true" value. Though it is tried to keep this difference low by means of calibration or simply carefully choosing appropriate measurement techniques, it is part of every single measurement and has therefore to be stated. This can be done for instance via a maximum / minimum error estimation where an upper and a lower limits encloses the "true" value and the measured one lies somewhere in between. Another way is defined in the GUM where the uncertainty (of measurement) is defined as follows [172]:

" *... parameter, associated with the result of a measurement, that characterizes the dispersion of the values that could reasonably be attributed to the measurand.*
NOTE 1 The parameter may be, for example, a standard deviation (or a given multiple of it), or the half-width of an interval having a stated level of confidence."

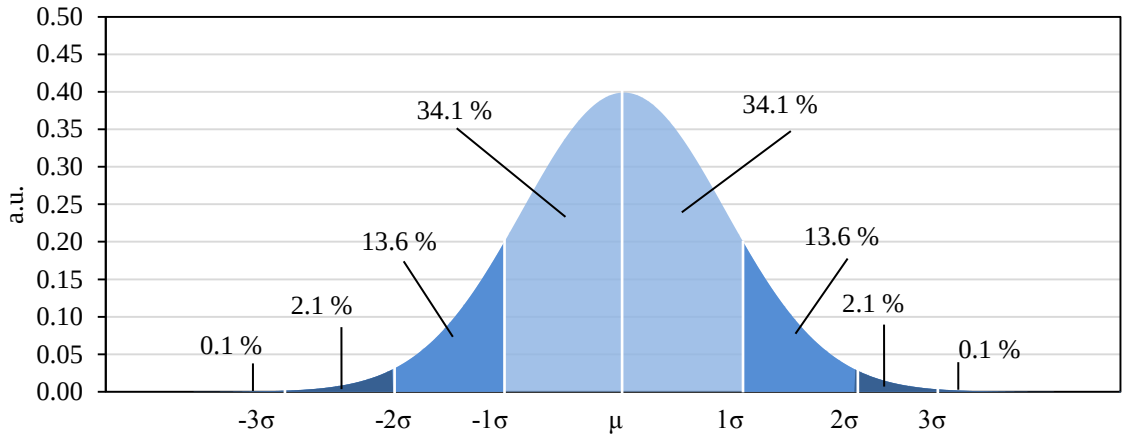

Fig. 53 Probability density function of a normal distribution with median μ and standard deviation σ.

In the sense of the definition above, stating p_{in} = 1.01 bar ±0.05 bar (k = 1) means that the true value lies within the interval of 0.96 and 1.06 bar with a probability of 68.3 %. k is the coverage factor and states how many multiples of the standard deviation are used to express the degree of uncertainty. A coverage factor of 2 would mean in the example above, that the true value lies within the before-mentioned interval with a probability of 95.5 %. In case the coverage factor is higher than 1, the term expanded uncertainty is commonly used [172]. All uncertainties of measurement in this work, unless explicitly stated, are valid for a coverage factor of k = 1.

In case more than one parameter has impact on a certain quantity $y(x_1, x_2, x_3, \dots, x_N)$, the combined standard uncertainty u_c for uncorrelated input data $(x_1, x_2, x_3, \dots, x_N)$ is determined as stated in [172],

$$u_c(y) = \sqrt{\sum_{i=1}^{N} \left(\frac{\partial y}{\partial x_i}\right)^2 u^2(x_i)} \qquad (157)$$

where y is a function of $x_1, x_2, x_3, \dots, x_N$ and $u(x_i)$ is the uncertainty of the single input parameter x_i. The partial derivative of y with respect to x_i is the sensitivity coefficient.

6.3.1. Pressure

For measuring pressures between 0.3 and 10 bar, absolute and differential pressure transducers, using thick-film technology, are applied. The principle of these transducers is a ceramic plate which acts as a membrane, dividing the chamber of unknown pressure and the reference pressure (High-vacuum for absolute type). The force acting on the ceramic plate bends it and changes the electrical resistance of the conducting paths which are stoved at the plate. The change of resistance can be measured indirectly providing constant voltage supply and be related to the pressure difference between the two chambers.

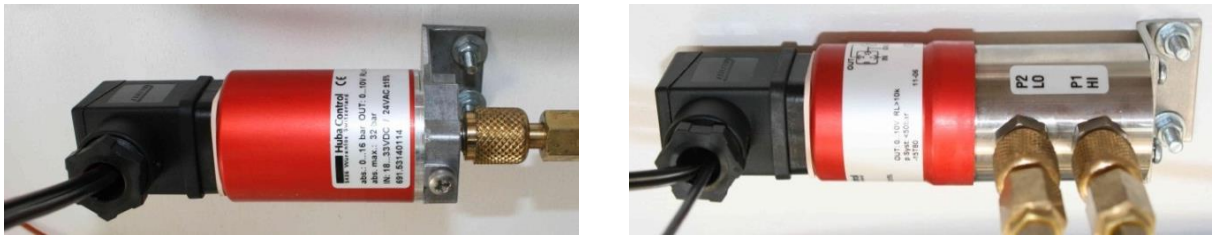

Fig. 54 Pressure transducer absolute (left) and differential (right).

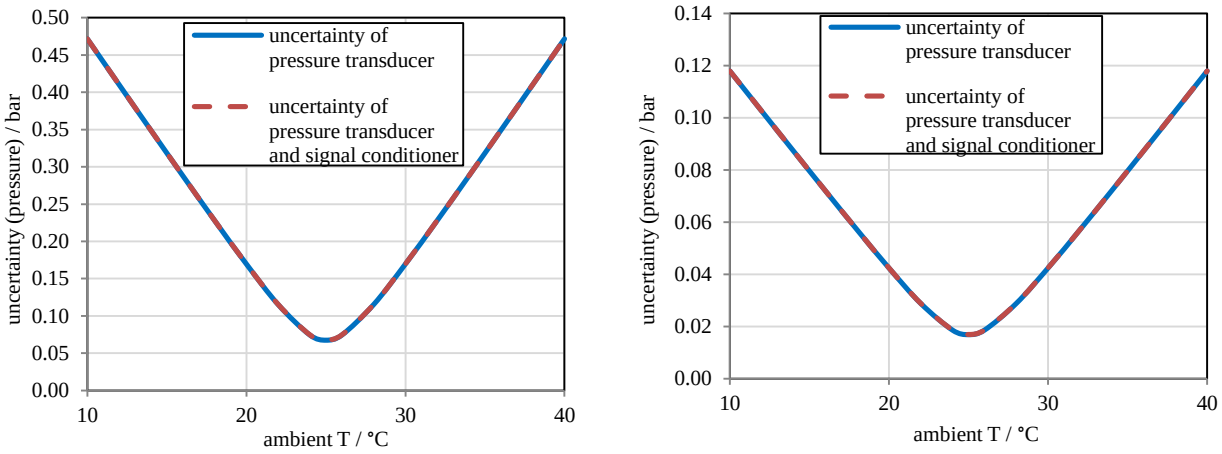

Fig. 55 Uncertainty of the pressure transducers against ambient temperature. Pressure range 0-16 bar absolute (left) and 0-4 bar absolute (right).

All pressure sensors in use (Huba Control 691 and 692) have been compared to readings of an absolute pressure meter Digitron 2025P and a relative digital pressure indicator DPI 705 IS. The lowest pressure recorded was achieved by plugging a refrigeration vacuum pump (Refco RL-4; 2 stages; p_{min} = 0.02 mbar) to a hose, connecting the sensor to be calibrated as well as to the pressure calibrator. A point at high pressure around 8 bar and one at ambient pressure were also used for calibration-purposes minimizing the systematic errors of signal processing. Due to the strong temperature dependence as shown in Fig. 55 the final uncertainty of the pressure transducers is taken from the data sheets of the manufacturer.

6.3.2. Temperature

T-type thermocouples are common in the field of refrigeration due to their applicability at low temperatures (down to -40 °C) and the low error around 0 °C compared to other thermocouples (±0.5 K max.) providing the highest accuracy class (class I) is chosen [190]. A spot-welded copper and constantan (copper/nickel) wire produces a thermally induced voltage (Seebeck-effect, [190]) which can be measured, assuming these small voltages which are approximately 0.04 mV / K at around 0 °C, can be measured properly. The characteristic of such a combination of two different metals has to be known from previous experiments and can then be used as a lookup table. Fig. 56 shows the thermoelectric voltage over temperature for a reference temperature at 0°C. These experimental results are fitted by polynomials – the coefficients are publicly available by the National Institute of Standards and Technology (NIST) and form the basis of temperature measurements using thermocouples. Though the

characteristic of a T-type thermocouple becomes nonlinear at low temperatures, the polynomial fit which is implemented in the signal conditioning device accounts for this.

Usually a second thermocouple is connected in series to the first one and held at a constant, known temperature – the so called "*cold junction*". The measured net voltage is the difference between the voltage generated by the thermocouple measuring the unknown temperature and the voltage from the second one, induced by the known temperature. In our case, the DAQ-module contains the reference temperature point.

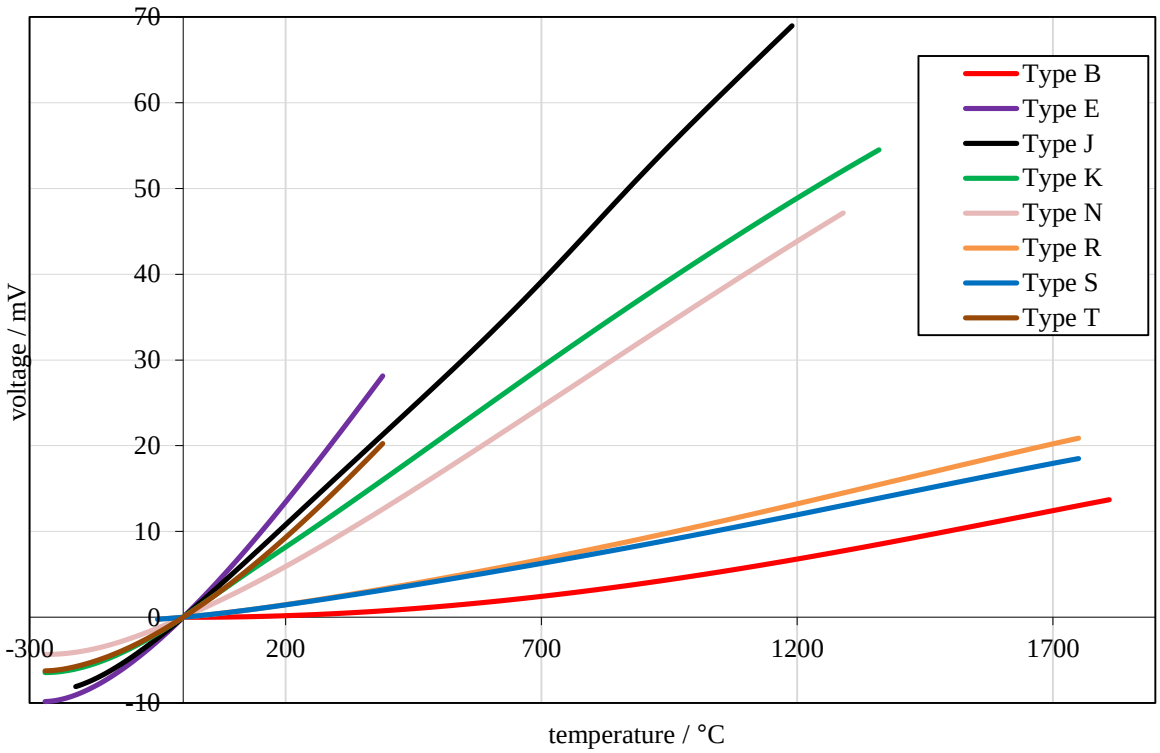

Fig. 56 Thermocouple voltage versus temperature [180].

The thermocouples used in this work (OMEGA type T, model HTMTSS-IM100E-300, accuracy class I) consist of the two wires which are embedded in a flexible, small diameter metal pipe and can be fastened by a clamping collar. The spot-welded ends are neither embedded nor covered with a protective layer and are inserted into the pipes of the cooling circuit in such a way that they measure the temperature of the refrigerant midstream.

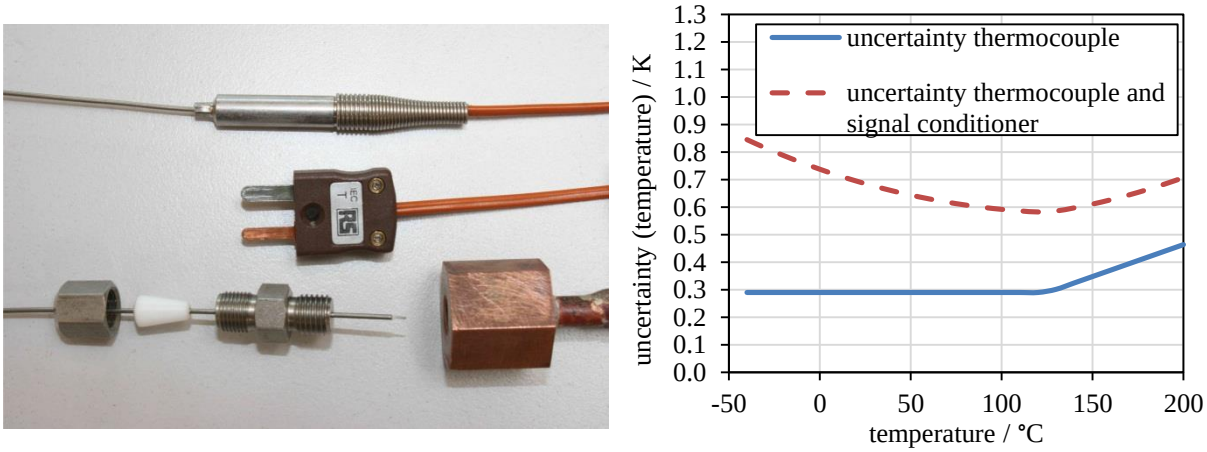

Fig. 57 Thermocouple with mounting block (left). Uncertainty in temperature over measured temperature before calibration for a T-type thermocouple (right).

The calibration of the thermocouples has been conducted according to the procedure proposed by National Instruments (NI). Therefore, all sensors were placed together with a Pt100 reference temperature sensor (HAREUS QUAT 100 with QUAT 200/290) into a constant temperature bath which was accomplished by a LAUDA Ecoline Staredition RE 210 filled with water for temperatures above 0 °C and a LAUDA Ecoline Staredition RE 310 with isopropyl alcohol for temperatures below 0 °C. Four different points (-20 °C, -15 °C, 20 °C, 80 °C) were recorded and processed by the software belonging to the temperature measuring module (NI 9214). After this procedure, the reading of all thermocouples differed by no more than ±0.1 K from each other. Fig. 57 shows the uncertainty of uncalibrated thermocouples and the signal conditioner (dotted red line) which is below 1 K in any case as claimed by the manufacturer. During calibration it could be observed, that no temperature reading of the uncalibrated device differed more than 0.4 K from the reference temperature. A plausibility check, where temperature and pressure readings in the two-phase-region at the exit of a capillary tube are compared, shows excellent agreement (Fig. 58). This check is performed at a capillary tube outlet with isobutane as the working media and the 0-4 bar absolute pressure transducer. The mean deviation between the signals (red and blue) is 0.075 K, the standard

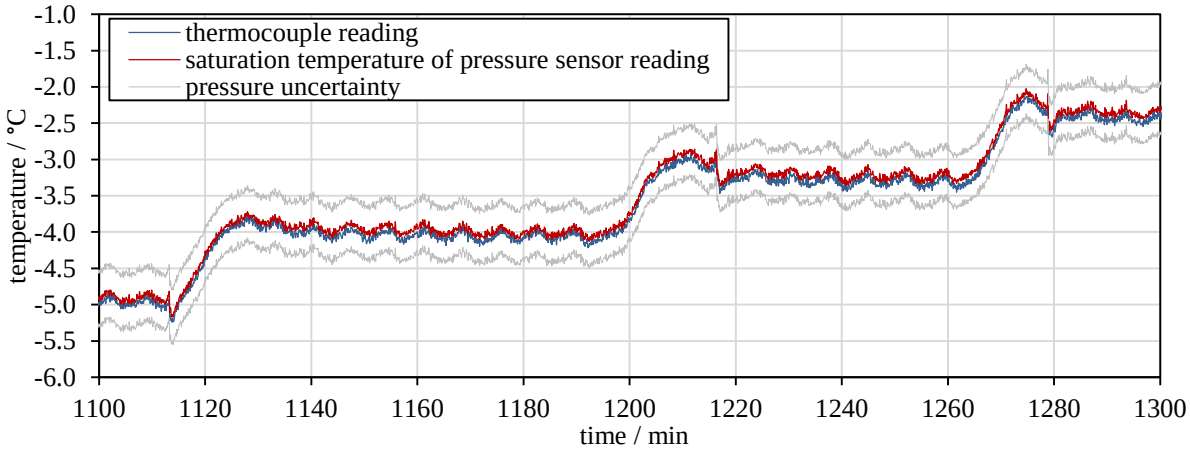

Fig. 58 Comparison of pressure and temperature in the two phase region.

deviation is 0.028 K. The grey line indicates the standard deviation of the pressure transducer (red) in terms of saturation temperature. To conclude from the findings above, it can be assumed that the maximum error is below 0.5 K for the observed temperature range, both the comparison with the saturation temperature and the reference temperature don't contradict and therefore the uncertainty is believed to be 0.29 K for the temperature range of the capillary tube experiments.

6.3.3. Mass flow rate

Precise knowledge of mass flow rates is crucial for capillary tube experiments, since this quantity usually is the one which is sought for in various computer models. So, desirably a direct measurement is taken instead of recalculating the mass flow rate by solving energy or momentum balances for any tube in the system since measurement errors sum up when for instance the inlet- and outlet temperature as well as the transferred heat over the boundary is measured. The device used in this work is a Coriolis type mass flow meter (BRONKHORST mini CORI-FLOW M14, serial no.: B11200585A, 10 kg/h Isobutane, 8 bar, 40 °C). Its special adequacy due to its principle of measurement is because of its independency of the fluid's heat capacity (unlike in thermal mass flow meters) as well as the ability to measure very low mass flow rates down to 0.03 kg/h [182]. The operating principle is explained by the manufacturer – the fluid flows through a bended, U-shaped tube which is excited to vibrate. Due to the Coriolis-effect caused by the moving fluid, the natural frequency, amplitude or phase shift of the tube is varied. This variation can be measured and is directly related to the mass flow rate. The uncertainties are low, Fig. 60 shows that after calibration by the manufacturer for a mass flow rate of 1 kg/h the uncertainty is around 0.007 kg/h.

Fig. 59 Mass flow meter.

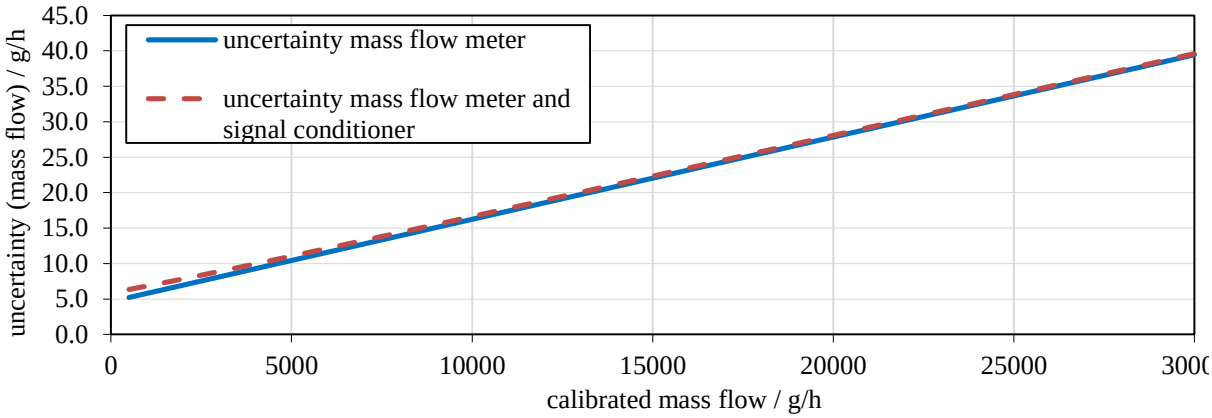

Fig. 60 Uncertainty of mass flow meter.

6.3.4. Inner diameter measurements

Since the nominal inner diameter is said to vary within ±25 µm and no additional information is provided from the manufacturer, the decision for measuring this crucial parameter stands to reason. Two methods are applied, a direct measurement under the microscope and a flow experiment with water. Firstly, the outcome of the microscopy is presented and compared afterwards with the results from the flow experiments. It has to be emphasized that the aim of these measurements is an equivalent inner diameter where the ideal shape is assumed to be circular no matter if the real cross section is elliptical or irregularly shaped. For means of microscopy the specimen have to be prepared in such a way that one avoids additional bending or creating edges since the final examination happens optically. Therefore, a straightened piece is filled with liquid tin to prevent the formation of a copper edge during the cutting and grinding process. The heating and cooling of tin as infill material leads to no measurable influence or deformation on the capillary tube itself since both the coefficient of expansion for tin (~$2.5 \cdot 10^{-5}$ / K) and the temperature difference (300 K) is small and theoretically leads to changes in diameter of no more than 1 µm. Then, short specimen are cut and mounted orthogonally at a specimen holder (Fig. 61). Finally, grinding and polishing leads to Fig. 62.

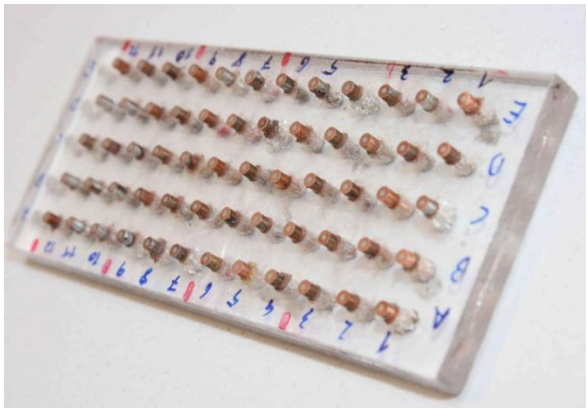

Fig. 61 Specimen of 4x15 pieces of capillary tubes prepared for microscopy.

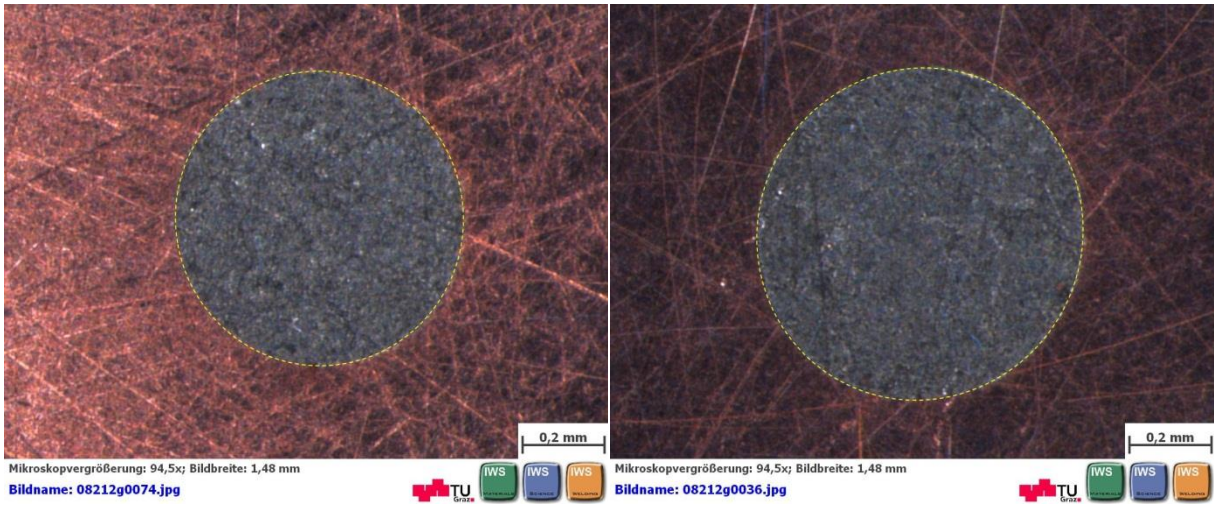

(a) (b)

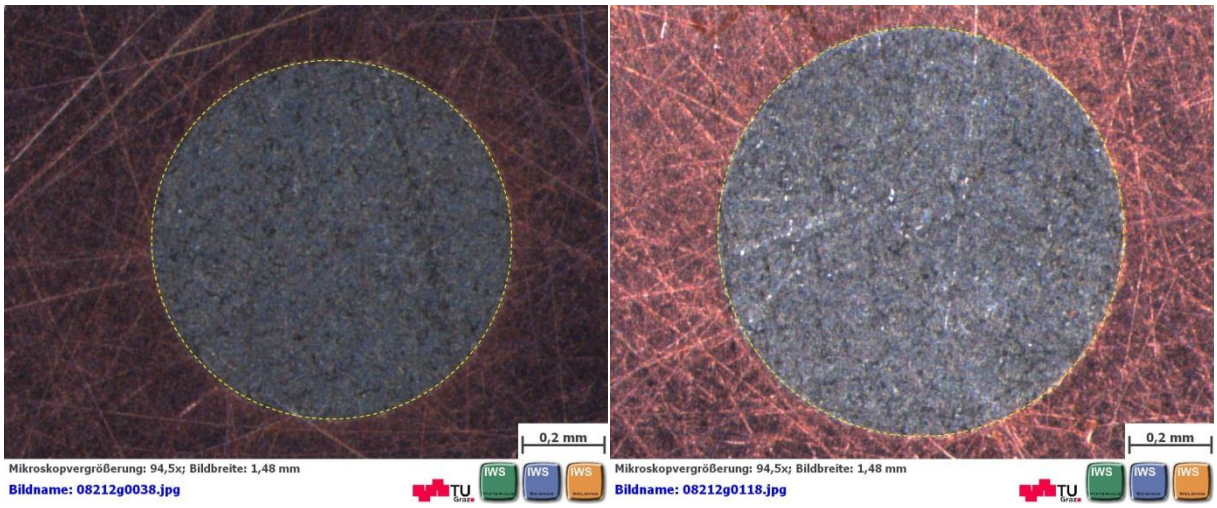

(c) (d)

Fig. 62 Capillary cross sections with nominal diameter of 0.7 mm (a), 0.8 mm (b), 0.9 mm (c) and 1.0 mm (d). The green dashed line visualizes the boundary of copper and infill material.

The images were taken by a stereomicroscope and recorded by a digital camera with a resolution of 1292x1064 pixels. The magnification was kept constant for each series of measurements. Since the long copper wire is rolled to a bundle and therefore bended, it can be assumed that the deformed perimeter, if at all, can be best approximated by an ellipse. The images of the microscope show in general an elliptic boundary which is measured for each image and then processed to a diameter of a circle, sharing the same cross sectional area with the real ellipse.

Table 9 Sample of the conversion from the image-file of an elliptical cross section to the final diameter of an equivalent circle. "c" stands for "circle", "2a" and "2b" are the length of the major and minor axes, "A" stands for cross sectional area and "D_c" for inner diameter.

image nr.	magnification	D_c nom.	image 2a	image 2b	2a	2b	$A_e = A_c$	D_c
-	-	mm	cm	cm	mm	mm	mm^2	mm
08212g0002	94.4	7	10.55	10.49	0.714	0.709	0.40	0.711
08212g0004	94.4	7	10.70	10.51	0.724	0.711	0.40	0.717
08212g0006	94.4	7	10.73	10.54	0.726	0.713	0.41	0.719
...	...	...	...	...	...	...	...	...

For the estimation of the uncertainty the individual uncertainties for the magnification of the microscope, the uncertainty of the reference length and the transcription error from pixel-to-length-conversion were taken into account.

Table 10 Results of the microscopy of 15 specimen of each diameter.

Type	**-**	$D_{0.7mm}$	$D_{0.8mm}$	$D_{0.9mm}$	D_{1mm}
average diameter	**mm**	0.715	0.799	0.885	0.992
standard deviation	**mm**	0.006	0.009	0.006	0.006
overall uncertainty	**mm**	0.0065	0.0095	0.0064	0.0069

A second method of measuring the inner diameter was found to be both easy going and accurate. The setup is shown in Fig. 63, where a short piece of capillary tube is fixed at a water tank. The water from the upper basin flows through the capillary into the lower basin which is placed atop of a weight. Given a small inner diameter and low velocity of fluid the flow will be laminar hence the friction coefficient close to the analytical relation [128]

$$\lambda = \frac{Re}{64} \quad with \quad \Delta p = \lambda \cdot \frac{\Delta l}{D} \cdot \rho \cdot \frac{\mathrm{v}^2}{2} \tag{158}$$

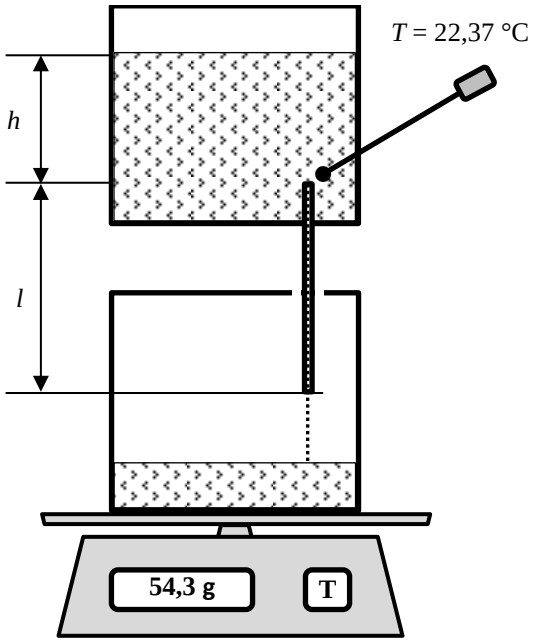

Fig. 63 Setup for diameter measurements via flow rate measurements with water.

A T-type thermocouple is placed upstream of the tube and all runs are conducted at constant room temperature. The viscosity of water is a function of temperature, the correction factors for the orifice at inflow and outlet were taken as 0.5. The weight is measuring the amount of water which flows through the tube and the time is taken by a stopwatch. When measured over a long enough time the uncertainties of the stopwatch and the weight become small compared to the absolute values of time and mass of water. The water in the basins is shielded from evaporation and the water level in the upper basin is held constant by continuously refilling from another water-source. The main measurement uncertainties result from estimating the density and viscosity of the water due to uncertainties of measuring the water temperature, from measuring the length of the tube, the distance *h* to the top water. After error propagation of these input-uncertainties an astonishingly small overall uncertainty of 0.003 mm of inner diameter is gained. The final result is presented in Table 11.

Table 11 Results of the laminar flow rate measurements.

nominal diameter	**mm**	0.7	0.8	0.9	1.0
average diameter	**mm**	0.711	0.789	0.882	0.981
uncertainty	**mm**	0.003	0.003	0.003	0.003

Together with the previous knowledge by microscopy, the inner diameters which are finally used in the computational part are gained by conflation of the two experiments by weighting the diameters according to their uncertainty. Fig. 64 graphically displays the procedure, green is the weighted inner diameter of each capillary tube and red is the nominal diameter with the given uncertainty of the manufacturer. The idea behind this conflation is explained in [183] where two sets of data (different mean value and standard deviation) from two independent experiments are merged to a single result. The formulae used are

$$\sigma_{conf}{}^{-2} = \sigma_1{}^{-2} + \sigma_2{}^{-2} \tag{159}$$

$$\mu_{conf} = \sigma_{conf}{}^{2}(\mu_1 \cdot \sigma_1{}^{-2} + \mu_2 \cdot \sigma_2{}^{-2}) \tag{160}$$

where μ is the mean value and σ the standard deviation of the respective experiment. This method may be questioned in terms of comparability of the two data-sets and also from the mathematical derivations' point of view but is chosen since for further computations a single value for the inner diameter is needed and the question arises which experiment is to trust more? Therefore the "true" diameter is likely to lie between the two results and to pay deference to the experiment with lower uncertainty the mean values are weighted according to the uncertainty of the corresponding experiment.

Table 12 conflated results for inner diameter.

nominal diameter	**mm**	0.7	0.8	0.9	1.0
average diameter	**mm**	0.712	0.790	0.883	0.980

Concerning uncertainty of the final diameters, the reader is referred to the individual experiments (Table 10 and Table 11) – no conflated value will be presented at this place due to the lack of accredited scientific methods of doing so.

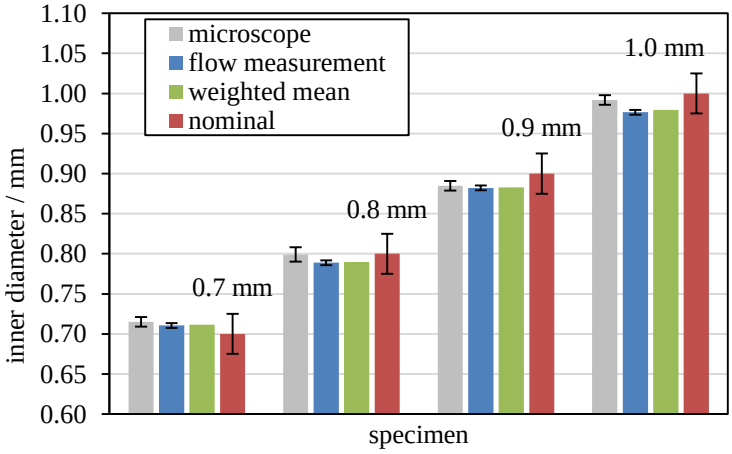

Fig. 64 Comparison and conflation of the diameters.

6.3.5. Length measurements

The length of all capillary tubes in use is determined by a measuring tape with accuracy class I – the maximum error for 10 m nominal length is 1.1 mm (for 1 m it is 0.1 mm). The influence of temperature differences on the tape can be neglected as long as the actual temperature differs no more than 8 K from the reference temperature which is 20 °C. Though, the temperature influences the actual capillary tube which is elongated by 0.17 mm (max., 10 m nominal) when the temperature changes by 1 K. When the length is measured, the tube has to be perfectly straight. To achieve that, a force is applied to stretch any bends. The elongation due to this force coming from the elasticity of the copper tube is estimated to be around 1.5 mm (max., 10 m nominal) but this influence might be compensated for by removing any bends and these 1.5 mm can be treated as worst case value. Taking into account that all these values are maximum errors, on can sum them up and express an uncertainty for a temperature band of 10 K for every capillary tube. The difference in uncertainty due to different diameters can be neglected, so merely the nominal length matters on the uncertainty in length. Since the longest measured tube exceeds 7 m, its uncertainty of 1.4 mm is also taken for the shorter ones. Anyway, due to the relatively weak link between length and mass flow rate, it is not worth arguing if the uncertainty in length is 1.4 or 1.5 mm since 1 mm corresponds to only 0.02 % of a capillary tube of 5 m in length.

6.3.6. Summary

To visualize the entanglement of all previously mentioned uncertainties, their impact on the mass flow rate is shown in Fig. 65 where an adiabatic capillary tube is simulated. The input parameters are chosen randomly from a normal distribution defined by an absolute value and the previously determined standard deviation. The calculated mass flow rate is therefore also normally distributed and from a high number of calculations, the standard deviation regarding the mass flow rate can be computed. This procedure is called Monte Carlo method. The first four bars show the influence of single measurement uncertainties (p_{in}, T_{sub}, D, L), whereas the fifth bar shows the combined uncertainty in mass flow rate. It is assumed, that the capillary tube is operated under choked conditions and that the inlet conditions is subcooled liquid (as it is normally the case). The uncertainty of the pressure transducer is taken at 25°C. The mean values for the input are: p_{in} = 7 bar, T_{sub} = 5 K, D = 0.7 mm, and L = 7 m. The calculated mass flow rate is 1.009 kg/h. The last bar (light blue) shows the uncertainty of the mass flow meter under these conditions.

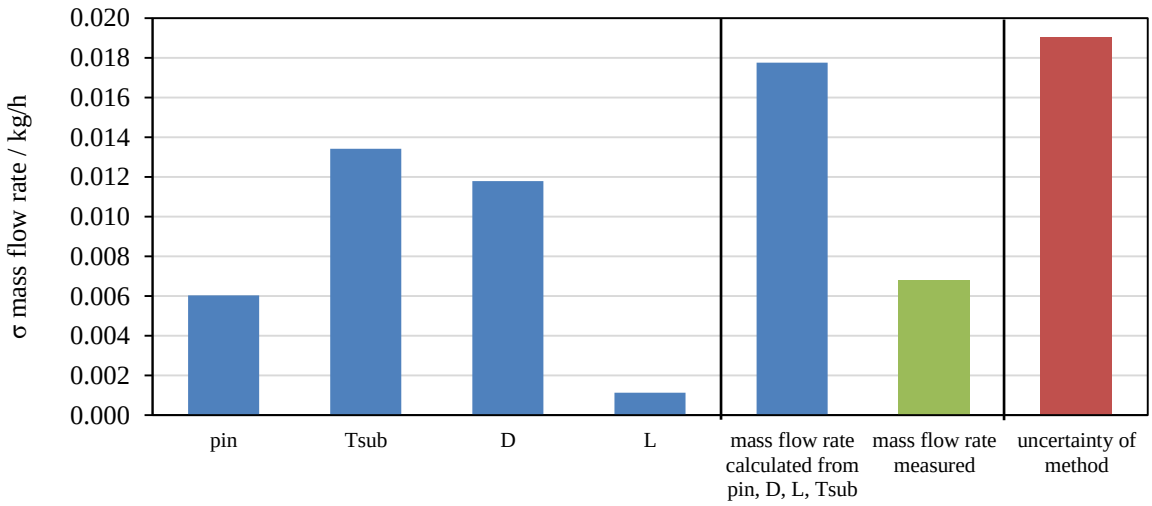

Fig. 65 Uncertainty of measurement of input parameters (p_{in}, T_{sub}, D, L,) in terms of mass flow rate. Blue is the overall uncertainty caused by the uncertainty of the input parameters and green is the uncertainty of measurement of the mass flow rate.

It can be seen that the major players in terms of uncertainty are the temperature and the diameter with an impact of 0.014 kg/h which is 1.4 % of the absolute mass flow rate. Taking the expectations of capillary tube models into account when compared to measurements, an accuracy of less than 5 % is hardly reported so the adequacy of the used metrology is shown. Finally, one can make the point that the total uncertainty has to contain also the uncertainty of the mass flow meter since firstly one measures p_{in}, T_{sub}, ... etc., the calculation provides a mass flow rate afflicted with the uncertainty shown by the blue bar and compare this one to the measured mass flow rate with its own uncertainty (green bar). Therefore, the correct uncertainty would be the root of the sum of each squares (red bar) and result in 0.019 kg/h or 1.9 %.

$$\sigma_{total}{}^2 = \sigma_1{}^2 + \sigma_2{}^2 + \cdots + \sigma_n{}^2 \qquad (161)$$

6.4. Results

The purpose of the experimental part is to gather data on isobutane flow through capillary tubes. Data should be recorded under steady state conditions where no transient disturbances lower the quality of the experiment. The recordings are taken for each point for a period of 30 minutes. Within this time, both the standard deviation and the drift of the recorded signals were restricted to the uncertainty of the respective sensor. In case of stepping over this limit within these 30 minutes, the measurement was rejected. By changing the capillary tubes as well as the boundary conditions, different mass flow rates could be achieved. In terms of time, after starting up the system the first stable point usually could be reached after approximately 1 hour, the following frequency of the recordings is around 1 recording per hour. Fig. 66 shows exemplarily raw data of pressure, temperature and mass flow rate after a start-up where the grey fields show the range for a steady state point. Though the compressor outlet temperature is still rising a little it obviously doesn't affect the capillary parameters, so this point is taken as steady state in terms of capillary recordings. The distortions in the mass flow

rate signal at 32 and 87 minutes arise from closing a valve for a short time after the mass flow meter.

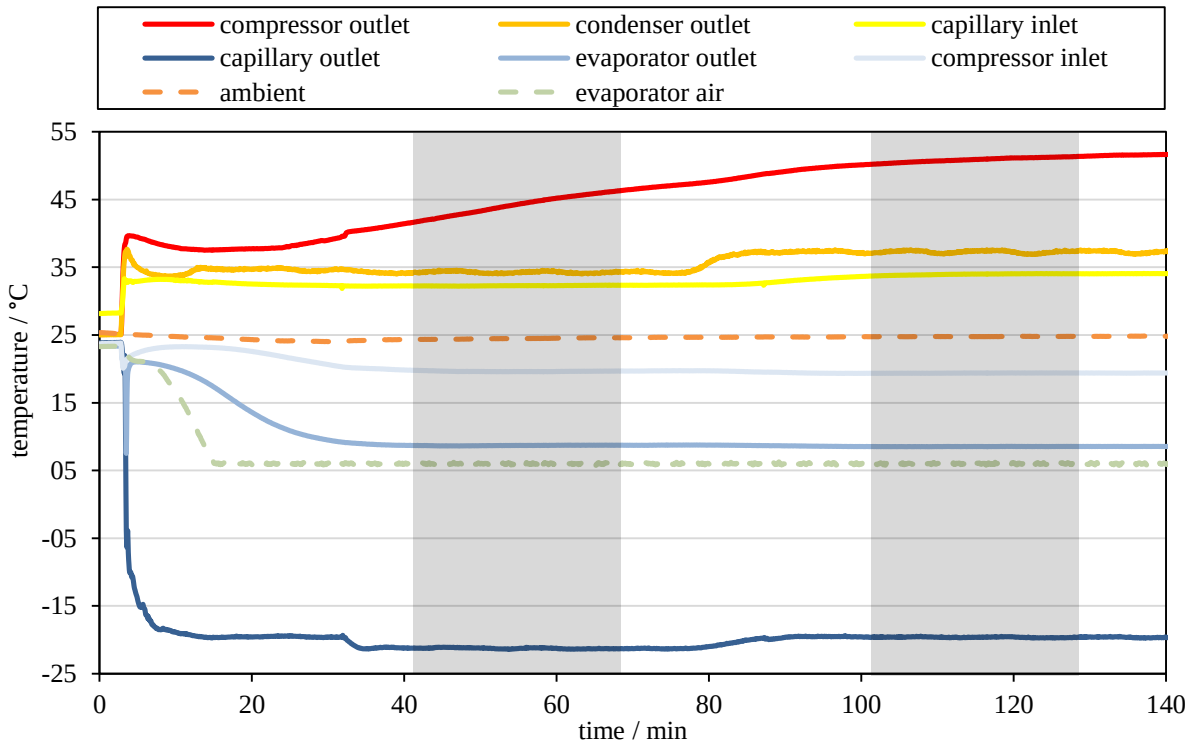

(a)

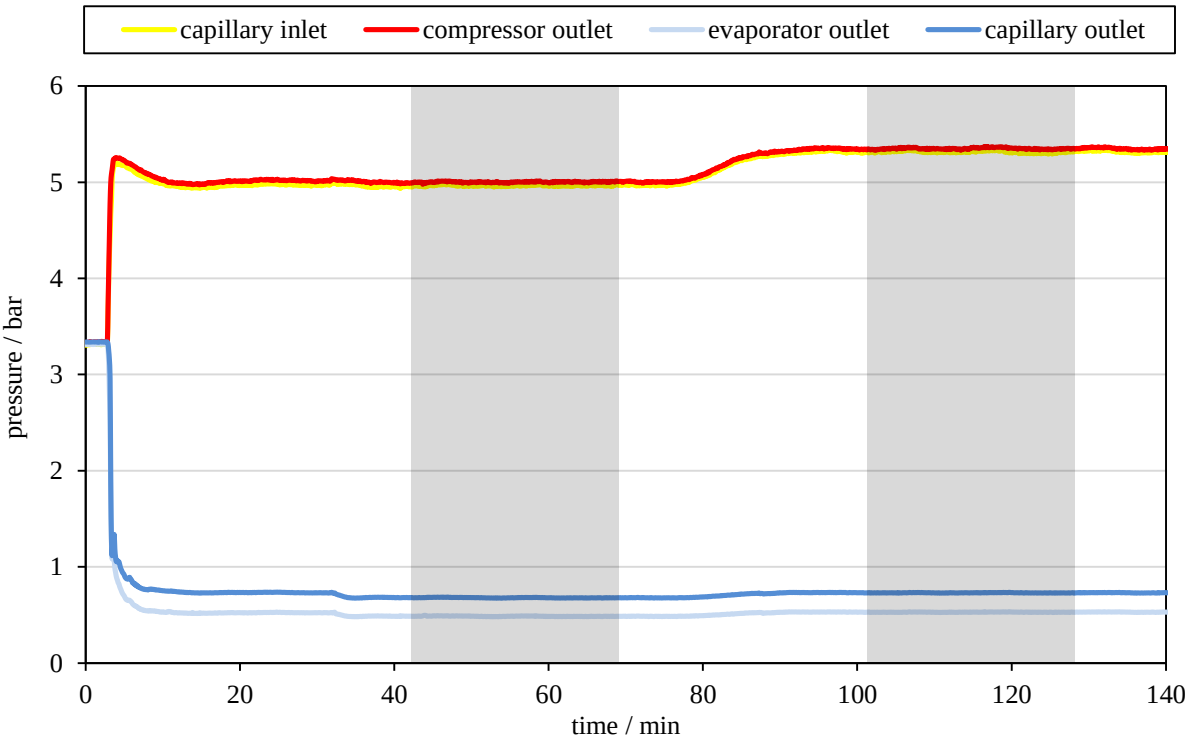

(b)

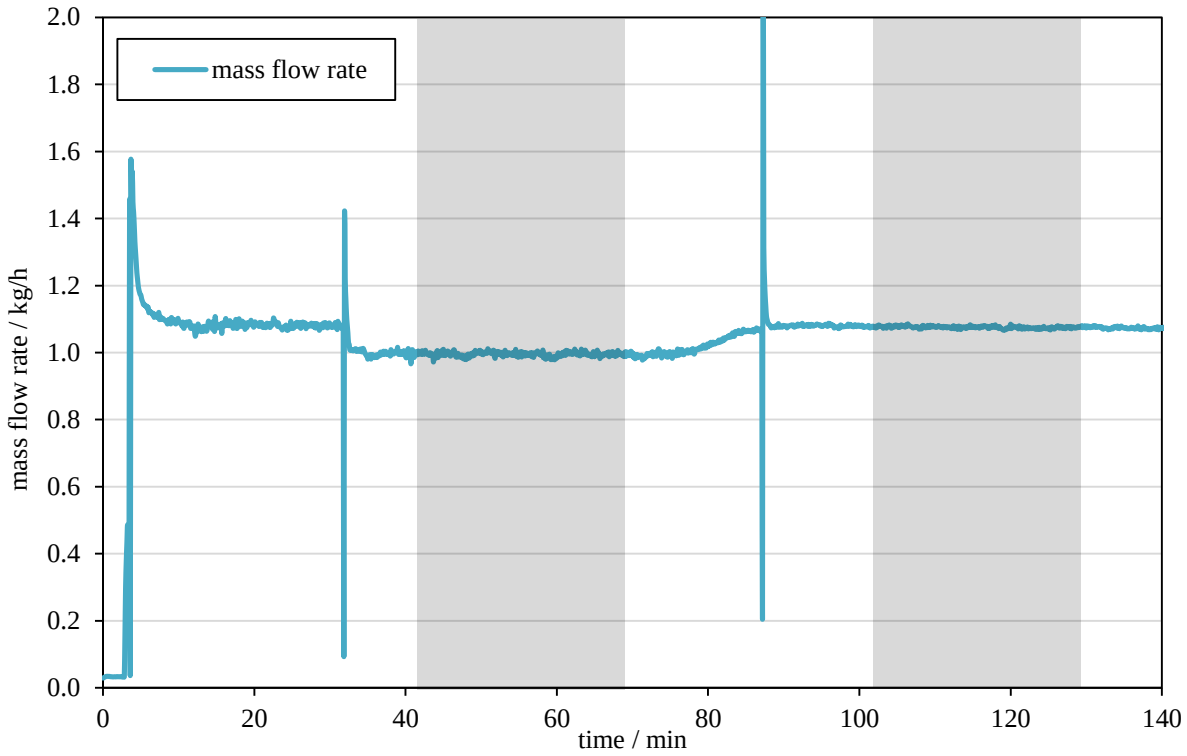

(c)

Fig. 66 Startup and steady state condtions: Temperature (a), pressure (b) and mass flow rate (c).

These kind of measurements were repeated with different operating conditions and different types of capillaries in terms of inner diameter and length. The collected dataset is given in table Table A 1.

7. Conclusion

At this point, time has come to summarize a few things. The core findings of this work shall be briefly mentioned and explained.

1) A 1d code has been set up according to the principles of mass-, momentum- and energy conservation which is able to treat flash evaporation and critical flow. The main principle behind the two-phase capability is the homogeneous assumption – a two-phase viscosity and other two-phase properties are taken to describe the flow as a homogeneous fluid. The code computes the mass flow rate for given thermodynamic boundary conditions which are pressure and enthalpy. The model also accounts for heat transfer via a counter-flow heat exchanger if desired and computes the outlet conditions of both tubes (capillary and suction line).

2) A formula (19) which generates an unequally spaced grid is used to account for the high gradients toward the end of the capillary tube and excels an equally distributed grid in terms of convergence and computational cost (or accuracy).

3) The validation was done in several steps and with different fluids, among them R600a, R12, R134a, R22 and R152a. 550 steady state operating conditions were reproduced with a final mean- and standard deviation of -0.45 kg/h and 1.33 kg/h. Considering that datasets with very high mass flows are included and that the absolute error of such sets is naturally higher than of sets with low nominal mass flow, the comparison can be embellished by saying that for sets with nominal mass flows smaller than 10 kg/h the mean- and standard deviation is -0.09 kg/h and 0.22 kg/h, respectively. In terms of relative error the mean is -4.26 percentage points and standard deviation is 7.27 percentage points if all sets of measurements are included. Another statement concerning error can be made, that is 96.9 % of the measurements are within ±10 % bounds and 88.9 % are within the ±5 % bounds. For the non-adiabatic case certainly more validation can be done in the future but for the investigated coaxial case the mean deviation is -0.03 kg/h and the standard deviation is 0.10 kg/h for mass flow rate or 28 of the 30 points lie within the ±10 % bounds. Concerning outlet temperature of the suction line the mean deviation is –5.75 K and the standard deviation is 2.55 K. Considering the uncertainty of the experimental configuration in combination with the correlations for the heat transfer coefficients the assumption is allowed that the experimental heat transfer is underestimated. A correction of the suction line heat transfer coefficient by the factor of 1.5 leads to a suction line temperature mean deviation of -0.1 K and a standard deviation of 2.3 K. The resulting mass flow rates are characterized by a mean deviation of 0.04 kg/h and the standard deviation is 0.09 kg/h for mass flow rate or 27 of the 30 points lie within the ±10 % bounds.

4) The use of correlations and models which describe evaporation delay are of no use in its current form [13], [28]. Although it is reported that they are helpful for refrigerants like R134a, R12 or R22, no improvement in terms of better predictability for R600a could

be observed. This may be due to the fact that these semi-empirical formulae are not tuned to be used with other refrigerants. Additionally, the reported, nearly erratically changing behaviour of the point of onset of evaporation gives rise to the apprehension that the accuracy of capillary tube models can't be increased arbitrarily.

5) Concerning the simplified models, the concluding remark is that they work well for steady state points, dimensionless correlations appear manifoldly in literature. Usually trained with experimental data, they may unknowingly cover also effects which are not thought of in a 1d simulation. If such a formula is needed for an adiabatic case the natural option is to use one of the many and not to perform own experiments. Also Neural Networks don't show bad performance. For non-adiabatic capillaries few dimensionless formulae are known to be in use. These formulations prove to be not sufficient when it comes to two-phase boundary conditions which is always the case for transiently operated refrigeration devices. Additionally, most of the available correlations are generated by the help of experimental data which does not cover a representative range in order to generalize these correlations. This problem can be circumvented by taking simulative training data and applying ANN. Due to the higher number of input parameters and two output parameters, a much higher number of degrees of freedom and hence training data compared to the adiabatic case should be available. From this work's point of view, ANN is the preferred choice despite its drawbacks – are a more complicated setup and training, but also the fact that no convenient formula but a clumsy network of "meaningless" matrices has to be set up.

6) A first trial of the heat exchanger model implemented in a realistic setup under real-world boundary conditions shows satisfying performance. Different models from literature have been compared to ANN and the 1d-code. Only during the Off-periods where superheated vapour is present at the capillary tube inlet, the models fail.

7) Experimentally, a few things have to be mentioned. Firstly, accurate diameter measurements are most important when it comes to validation since a uncertainty of 0.01 mm results under normal conditions approximately in an uncertainty of mass flow rate by as much as 0.05 kg/h. Therefore micrographs of carefully cut cross sections are an adequate procedure of measuring inner diameters. Also flow experiments as mentioned in section 6.3.4 lead to good results, comparable to those of microscopy. In case of doubtable quality of the microscope, flow experiments shall even be preferred over microscopy. Secondly, a well chosen mass flow meter avoids troubles in terms of high pressure drop, high uncertainty of measurement or heating of the refrigerant, therefore Coriolis-type mass flow meter are perfectly suited. Thirdly, the measurement of start-up and shut down processes in real refrigeration devices can't be performed with conventional measuring equipment. The mass flow rate measurements are distorted by two phase flow entering the capillary. Furthermore, the lack of a second thermodynamic property aside from the pressure can't be measured easily without distorting the thermodynamic state of the fluid and gives room for new inventions.

8. Future work

To leave some place for ideas which popped up in the course of this work and which haven't been touched since, this chapter is the perfect place to sum them up, refresh them and bring it into mind again. Also, the next steps which will follow the completion of this capillary tube model will be summarized shortly.

1) Apply model in real case scenarios

The model as a stand-alone tool is quite nice, but after a while the user will certainly lose interest after all parameters are varied and all available datasets are used for means of validation. So, the main goal for the capillary tube model lies in its application, in its ability to serve as a part of a complex cycle simulation. This thought has to be picked up and followed consequently. Test-cases are a nice thing since they cover certain scenarios but only an application in real world scenarios can finally approve or disapprove the suitability of the model.

2) Validate against transient measurement

To keep up with the intended use, transient measurements would be perfect to validate the response of the capillary tube model to real world systems. A good match between simulation and measurement in this case would be a most valuable prove of the flexibility of the model. No reported cases of such transient validation of capillary tube models have been presented up to now.

3) Similar strategy for lateral heat exchanger

Another thing which is not straight forward are lateral heat exchangers. Due to the indefinite heat transfer between capillary and suction line – several designs exist: covered with heat conduction paste, wrapped with aluminium foil, wrapped with heat shrinking tube, or soldered together – all in all these designs are more or less efficient and implemented in real world refrigerators. Therefore, an aim is to be able to model also these types of suction line heat exchangers in a similar manner it has been done here for a coaxial type.

4) Find workflow how to repeat all steps easily

A thing which goes hand in hand with the previous comment is the strategy, how the procedure of implementing a new kind of capillary tube heat exchanger looks like from the software point of view. One of the findings is that a 1d code is not sufficient in terms of speed to be used in cycle simulations. Therefore, the program has been used to tune other software

tools. This process contains a chain of steps which are all in all easily understandable but tedious and nerve-racking. For instance: Firstly, set up an input file with points that can be used as training points for the Neural Network. Chose the points according to their relevance for the intended application (i.e. a reasonable capillary tube length is between 1 and 5 meters and not between 1 and 100 m), chose a refrigerant and start computing. Then, the output data shall be checked for any implausibilities and then the data is ready to be used as training data for other means. A preconfigured Neural Network for instance can be taken to use this output-file and train the capability to predict mass flow rates and transferred heat. This is basically what is meant by "workflow" and should be automatized to avoid errors which often occur if every step is done manually.

5) Documentation of all steps

Documentation for maintenance purposes doesn't seem necessary if one is into the topic day by day but from own experience and personal communication with more sophisticated programmers it will take time if one tries to capture self-written lines of code from previous projects. What will a person do who hadn't been in touch with the code yet and is supposed to apply it? Therefore, detailed comments and manuals shall follow each step and give a summary in such a way that successor in this field will have a fair chance of getting into it with less effort than programming from the scratch.

6) To raise accuracy, studies on the onset of evaporation should be carried out

There is still some room for improvement on the issue concerning the influence of evaporation delay. A few publications base on experiments which don't use R600a and therefore the resulting equations (section 4.4) are obviously not applicable for cases with evaporating isobutane. Reported cases of difficult predictability of the onset of evaporation directly result in an uncertainty in predicting mass flow rates. Of course, other factors like heat transfer correlations, pressure drop models, simplified geometry (straight, not inclined) also contribute to the overall uncertainty of the simulation. Letting this topic unsolved, the industrial method of optimizing capillary tubes still is cutting it shorter and measuring the electric energy consumption of the system until the optimum length (and mass flow rate) is found.

9. Literature

capillary tubes

[1] Ablanque, N.; Rigola, J.; Perez-Segarra, C. D. & Oliva, A. (2010), 'Numerical simulation of capillary tubes. application to domestic refrigeration with isobutane', International Refrigeration and Air Conditioning Conference at Purdue, West Lafayette, USA.

[2] Asano, H.; Murakawa, H.; Takenaka, N.; Takiguchi, K.; Okamoto, M.; Tsuchiya, T.; Kitaide, Y. & Maruyama, N. (2011), 'Visualization and void fraction measurement of decompressed boiling flow in a capillary tube', *Nuclear Instruments and Methods in Physics Research A* **651**, 258-263.

[3] Bansal, P. & Wang, G. (2004), 'Numerical analysis of choked refrigerant flow in adiabatic capillary tubes', *Applied Thermal Engineering* **24**, 851-863.

[4] Bansal, P. & Xu, B. (2003), 'A parametric study of refrigerant flow in non-adiabatic capillary tubes', *Applied Thermal Engineering* **23**, 397-408.

[5] Bansal, P. & Yang, C. (2005), 'Reverse heat transfer and re-condensation phenomena in non-adiabatic capillary tubes', *Applied Thermal Engineering* **25**, 3187-3202.

[6] Bansal, P. K. & Rupasinghe, A. S. (1998), 'An homogeneous model for adiabatic capillary tubes', *Applied Thermal Engineering* **18, No 3**, 207-219.

[7] Bansal, P. K. & Rupasinghe, A. S. (1996), 'An empirical model for sizing capillary tubes', *International Journal of Refrigeration* **19, No. 8**, 497-505.

[8] Bergander, M. J. (2006), 'Refrigeration Cycle With Two-Phase Condensing Ejector', International Refrigeration and Air Conditioning Conference at Purdue, West Lafayette, USA, paper 748.

[9] Björk, E. & Palm, B. (2006), 'Performance of a domestic refrigerator under influence of varied expansion device capacity, refrigerant charge and ambient temperature', *International Journal of Refrigeration* **29**, 789-798.

[10] Chang, S. D. & Ro, S. T. (1996), 'Experimental and Numerical Studies on Adiabatic Flow of HFC Mixtures in Capillary Tubes', International Refrigeration and Air Conditioning Conference at Purdue, West Lafayette, USA, paper 305.

[11] Chang, S.-D. & Ro, S. T. (1996), 'Pressure drop of pure HFC refrigerants and their mixtures flowing in capillary tubes', *International Journal of Multiphase Flow* **22, No. 3**, 551-561.

[12] Chen, D. & Lin, S. (2001), 'Underpressure of vaporization of refrigerant R134a through a diabatic capillary tube', *International Journal of Refrigeration* **24**, 261-271.

[13] Chen, Z. H.; Li, R. Y. & Chen, Z. Y. (1990), 'A correlation for metastable flow of refrigerant R-12 through capillary tubes', ASHRAE Trans. 96, 550-554.

[14] Chingulpitak, S. & Wongwises, S. (2010), 'Two-phase flow model of refrigerants flowing through helically coiled capillary tubes', *Applied Thermal Engineering* **30**, 1927-1936.

[15] Chingulpitak, S. & Wongwises, S. (2010), 'Effects of coil diameter and pitch on the flow characteristics of alternative refrigerants flowing through adiabatic helical capillary tubes', *International Communications in Heat and Mass Transfer*, **37**, No. 9, 1305-1311.

[16] Chingulpitak, S. & Wongwises, S. (2011), 'A comparison of flow characteristics of refrigerants flowing through adiabatic straight and helical capillary tubes', *International Communications in Heat and Mass Transfer* **38**, 398-404.

[17] Choi, J.; Kim, Y. & Kim, H. Y. (2003), 'A generalized correlation for refrigerant mass flow rate through adiabatic capillary tubes', *International Journal of Refrigeration* **26**, 881-888.

[18] Choi, J.; Chung, J. T. & Kim, Y. (2004), 'A generalized correlation for two-phase flow of alternative refrigerants through short tube orifices', *International Journal of Refrigeration* **27**, 393-400.

[19] Choi, J.; Kim, Y. & Chung, J. T. (2004), 'An empirical correlation and rating charts for the performance of adiabatic capillary tubes with alternative refrigerants', *Applied Thermal Engineering* **24**, 29-41.

[20] Coberan, J. M.; Fuentes, D. & Goncalves, J. (2004), 'Numerical calculations of mass flow rate in capillary tubes using 'ART', an advanced simulation software', *Proceedings of the International Refrigeration Conference, Indiana (Estados Unidos)*, 100-105.

[21] Corberan, J. M.; Fuentes, D. & Gonzalvez, J. (2004), 'Numerical Calculation of Mass Flow Rate in Capillary Tubes Using 'ART', an Advanced Simulation Software', International Refrigeration and Air Conditioning Conference at Purdue, West Lafayette, USA, paper 688.

[22] Ding, G. L. (2007), 'Recent developments in simulation techniques for vapour-compression refrigeration systems', *International Journal of Refrigeration* **30**, 1119-

1133.

[23] Elsayed, A. O. (2006), 'Experimental study on the performance of twisted capillary tube', International Refrigeration and Air Conditioning Conference at Purdue, West Lafayette, USA.

[24] Erth, R. A. (1970), 'Two phase flow in refrigeration capillary tubes: analysis and prediction', PhD thesis, Purdue University, USA.

[25] Escanes, F.; Perez-Segarra, C. D. & Oliva, A. (1995), 'Numerical simulation of capillary-tube expansion devices', *International Journal of Refrigeration* **18**, 113-122.

[26] Fang, X. (1999), 'Advances in fixed-area expansion devices', Technical report, Air Conditioning and Refrigeration Center, University of Illinois, USA.

[27] Fatouh, M. (2007), 'Theoretical investigation of adiabatic capillary tubes working with propane/n-butane/iso-butane blends', *Energy Conversion and Management* **48**, 1338-1348.

[28] Feburie, V.; Giot, M.; Granger, S. & Seynhaeve, J. M. (1993), 'A model for choked flow through cracks with inlet subcooling', *International Journal of Multiphase Flow* **19**, No. 4, 541-562.

[29] Fiorelli, F. A. S.; Huerta, A. A. S. & Silvares, O. d. M. (2002), 'Experimental analysis of refrigerant mixtures flow through adiabatic capillary tubes', *Experimental Thermal and Fluid Science* **26**, 499-512.

[30] Fukuta, M.; Yanagisawa, T.; Araib, T. & Ogi, Y. (2003), 'Influences of miscible and immiscible oils on flow characteristics through capillary tube-part I: experimental study', *International Journal of Refrigeration* **26**, 823-829.

[31] Garcia-Valladares, O. (2007), 'Numerical simulation and experimental validation of coiled adiabatic capillary tubes', *Applied Thermal Engineering* **27**, 1062-1071.

[32] Garcia-Valladares, O. (2007), 'Numerical simulation of non-adiabatic capillary tubes considering metastable region. Part I: Mathematical formulation and numerical model', *International Journal of Refrigeration* **30**, 642-653.

[33] Garcia-Valladares, O. (2007), 'Numerical simulation of non-adiabatic capillary tubes considering metastable region. Part II: Experimental validation', *International Journal of Refrigeration* **30**, 654-663.

[34] Garcia-Valladares, O. (2004), 'Review of numerical simulation of capillary tube using refrigerant mixtures', *Applied Thermal Engineering* **24**, 949-966.

[35] Garcia-Valladares, O.; Perez-Segarra, C. & Oliva, A. (2002), 'Numerical simulation of capillary-tube expansion devices behaviour with pure and mixed refrigerants considering metastable region. Part II: experimental validation and parametric studies', *Applied Thermal Engineering* **22**, 379-391.

[36] Garcıa-Valladares, O.; Perez-Segarra, C. & Oliva, A. (2002), 'Numerical simulation of capillary-tube expansion devices behaviour with pure and mixed refrigerants considering metastable region. Part I: mathematical formulation and numerical model', *Applied Thermal Engineering* **22**, 173-182.

[37] Goodson, M. P. & Bullard, C. W. (1994), 'Refrigerator/Freezer System Modeling', Technical report, Air Conditioning and Refrigeration Center.

[38] Gu, B.; Li, Y.; Wang, Z. & Jing, B. (2003), 'Analysis on the adiabatic flow of R407C in capillary tube', *Applied Thermal Engineering* **23**, 1871-1880.

[39] Heimel, M.; Lang, W. & Almbauer, R. (2013), 'Performance predictions using Artificial Neural Network for isobutane flow in non-adiabatic capillary tubes', *International Journal of Refrigeration*, In Press, Accepted Manuscript, Available online 20 August 2013.

[40] Heimel, M.; Lang, W.; Berger, E. & Almbauer, R. (2012), 'A Homogeneous Capillary Tube Model – Comprehensive Parameter Studies Using Isobutane As Refrigerant', International Refrigeration and Air Conditioning Conference at Purdue, West Lafayette, USA.

[41] Hermes, C.; Melo, C.; Negrao, C. & Mezavila, M. (2000), 'Dynamic simulation of HCF-134a flow through adiabatic and non-adiabatic capillary tubes', International Refrigeration and Air Conditioning Conference at Purdue, West Lafayette, USA.

[42] Hermes, C. J.; Melo, C. & Goncalves, J. M. (2008), 'Modeling of non-adiabatic capillary tube flows: A simplified approach and comprehensive experimental validation', *International Journal of Refrigeration* **31**, 1358-1367.

[43] Hermes, C. J.; Melo, C. & Knabben, F. T. (2010), 'Algebraic solution of capillary tube flows. Part II: Capillary tube suction line heat exchangers', *Applied Thermal Engineering* **30**, 770-775.

[44] Hermes, C. J.; Melo, C. & Knabben, F. T. (2010), 'Algebraic solution of capillary tube flows Part I: Adiabatic capillary tubes', *Applied Thermal Engineering* **30**, 449-457.

[45] Huerta, A. A. S.; Fiorelli, F. A. S. & Silvares, O. d. M. (2007), 'Metastable flow in capillary tubes: An experimental evaluation', *Experimental Thermal and Fluid Science*

31, 957-966.

[46] Huerta, A. A. S.; Fiorelli, F. A. S. & de Mattos Silvares, O. (2009), 'Experimental evaluation on the oil influence in capillary tubes', *Applied Thermal Engineering*, **29**, 3066-3072.

[47] Huerta, A. A. S. & Silvares, O. M. (1998), 'Simulation of the Effects of Oil in Capillary Tubes Considering a Separated Flow Model', International Refrigeration and Air Conditioning Conference at Purdue, West Lafayette, USA, paper 451.

[48] Ishii, M. & Mishima, K. (1984), 'Two-Fluid Model and hydrodynamic constitutive relations', *Nuclear Engineering and Design* **82**, 107-126.

[49] Islamoglu, Y.; Kurt, A. & Parmaksizoglu, C. (2005), 'Performance prediction for non-adiabatic capillary tube suction line heat exchanger: an artificial neural network approach', *Energy Conversion and Management* **46**, 223-232.

[50] Jabaraj, D.; Kathirvel, A. V. & Lal, D. M. (2006), 'Flow characteristics of HFC407C/HC600a/HC290 refrigerant mixture in adiabatic capillary tubes', *Applied Thermal Engineering* **26**, 1621-1628.

[51] Jung, D.; Park, C. & Park, B. (1999), 'Capillary tube selection for HCFC22 alternatives', *International Journal of Refrigeration* **22**, 604-614.

[52] Kakac, S. & Bon, B. (2008), 'A Review of two-phase flow dynamic instabilities in tube boiling systems', *International Journal of Heat and Mass Transfer* **51**, 399-433.

[53] Kang, J. & Yamaguchi, H. (2012), 'Internal finishing of capillary tubes by magnetic abrasive finishing using a multiple pole-tip system', *Precision Engineering* **36**, 510-516.

[54] Khan, M. K.; Kumar, R. & Sahoo, P. K. (2009), 'Flow characteristics of refrigerants flowing through capillary tubes – A review', *Applied Thermal Engineering* **29**, 1426-1439.

[55] Kim, S. G.; Kim, M. S. & Ro, S. T. (2002), 'Experimental investigation of the performance of R22, R407C and R410A in several capillary tubes for air-conditioners', *International Journal of Refrigeration* **25**, 521-531.

[56] Kuijpers, L. & Janssen, M. (1983), 'Influence of thermal non-equilibrium on capillary tube mass flow', XVIth International Congress of Refrigeration, Paris, France.

[57] Liang, S. M. & Wong, T. N. (2001), 'Numerical modeling of two-phase refrigerant flow through adiabatic capillary tubes', *Applied Thermal Engineering* **21**, 1035-1048.

[58] Lin, T. Y. (2007), 'Experimental Analysis on Forced Convective Heat Transfer Characteristics in Micro Tubes by the Method of Liquid Crystal Thermography', PhD thesis, Department of Mechanical Engineering, National Taiwan University, Taipei, Taiwan.

[59] Liu, Y. & Bullard, C. (1997), 'An Experimental and Theoretical Analysis of Capillary Tube-Suction Line Heat Exchangers', Technical report, Air Conditioning and Refrigeration Center, University of Illinois, USA.

[60] Madsen, K. B.; Poulsen, C. S. & Wiesenfarth, M. (2005), 'Study of capillary tubes in a transcritical CO2 refrigeration system', *International Journal of Refrigeration* **28**, 1212-1218.

[61] Melo, C.; Ferreira, R.; Boabaid Neto, C. & Goncalves, J. (1995), 'Experimentation and analysis of refrigerant flow through adiabatic capillary tubes', symposium on heat pump and refrigeration systems design / ASME.

[62] Melo, C.; Ferreira, R.; Boabaid Neto, C.; Goncalves, J.; Pereira, R. H. & Thiessen, M. R. (1994), 'Evaluation of HC-600a, HFC-134a and CFC-12 mass flow rates through capillary tubes', New Applications to Reduced Global Warming and Energy Consumption Conference, Hannover, Germany', 621-630.

[63] Melo, C.; Ferreira, R.; Neto, C. B.; Goncalves, J. & Mezavila, M. (1999), 'An experimental analysis of adiabatic capillary tubes', *Applied Thermal Engineering* **19**, 669-684.

[64] Melo, C.; Ferreira, R. T. S. & Pereira, R. H. (1992), 'Modelling Adiabatic Capillary Tubes: A Critical Analysis.

[65] Melo, C.; Vieira, L. A. T. & Pereira, R. H. (2004), 'Experimental Study on Adiabatic Flow of R-22 Alternatives in Capillary Tubes', Refrigeration and Air Conditioning Conference at Purdue, West Lafayette, USA, paper 704.

[66] Melo, C.; Vieira, L. A. T. & Pereira, R. H. (2002), 'Non-adiabatic capillary tube flow with isobutane', *Applied Thermal Engineering* **22**, 1661-1672.

[67] Mittal, M.; Kumar, R. & Gupta, A. (2010), 'An experimental study of the flow of R-407C in an adiabatic helical capillary tube', *International Journal of Refrigeration* **33**, 840-847.

[68] Motta, S. F. Y.; Parise, J. A. & Braga, S. L. (2002), 'A visual study of R-404A/oil flow through adiabatic capillary tubes', *International Journal of Refrigeration* **25**, 586-596.

[69] Negrao, C. O. R. & Melo, C. (1999), 'Shortcomings of the numerical modelling of capillary tube suction line heat exchangers', Technical report, Academic Department of Mechanics, Federal Centre of Technological Education of Parana / Brazil.

[70] Nino, V. G.; Hrnjak, P. S. & Newell, T. A. (2002), 'Analysis Of Void Fraction In Microchannels', International Refrigeration and Air Conditioning Conference at Purdue, West Lafayette, USA, paper 574.

[71] Paiva, M. A.; Silvares, O. d. M.; Vodianitskaia, P.; Neto, A. H. & Fiorelli, F. (1994), 'The Behavior of Lateral and Concentric Capillary Tube-Suction Line Heat Exchangers Using CFC-12 and HFC-134a', International Refrigeration and Air Conditioning Conference at Purdue, West Lafayette, USA, paper 270.

[72] Paliwal, H. K. & Kant, K. (2006), 'A model for helical capillary tubes for refrigeration systems', International Refrigeration and Air Conditioning Conference at Purdue, West Lafayette, USA.

[73] Park, C.; Lee, S.; Kang, H. & Kim, Y. (2007), 'Experimentation and modeling of refrigerant flow through coiled capillary tubes', *International Journal of Refrigeration* **30**, 1168-1175.

[74] Pate, M. B. & Tree, D. R. (1986), 'Two-Phase Flow in a Diabatic Capillary Tube', International Refrigeration and Air Conditioning Conference at Purdue, West Lafayette, USA, paper 5.

[75] Peixoto, R. A. & Bullard, C. W. (1994), 'A Design Model for Capillary Tube-Suction Line Heat Exchangers', Technical report, Air Conditioning and Refrigeration Center, University of Illinois, USA.

[76] Richter, H. J. (1983), 'Separated two-phase flow model: application to critical two-phase flow', *International Journal of Multiphase Flow* **9 No. 5**, 511-530.

[77] Ruspini, L.; Dorao, C. & Fernandino, M. (2010), 'Dynamic simulation of Ledinegg instability', *Journal of Natural Gas Science and Engineering* **2**, 211-216.

[78] Sami, S. M.; Maltais, H. & Desjardins, D. E. (2000), 'Influence of Geometrical Parameters on Capillary Behavior with New Alternative Refrigerants', Technical report, Mechanical Engineering, School of Engineering University of Moncton, Canada.

[79] Sami, S. M. & Tribes, C. (1998), 'Numerical prediction of capillary tube behavior with pure and binary alternative refrigerants', *Applied Thermal Engineering* **18**, 491-502.

[80] Sarker, D. & Jeong, J. (2012), 'Development of empirical correlations for non-

adiabatic capillary tube based on mechanistic model', *International Journal of Refrigeration*, ***in press***.

[81] Schenk, M. & Oellrich, L. R. (2012), 'Experimentelle Untersuchung des Kältemitteldurchflusses von Isobutan (R600a) durch adiabate Kapillaren', DKV-Tagung, Würzburg, Deutschland, AA II.2.

[82] Schenk, M. & Oellrich, L. R. (2013), 'Experimental investigation of the refrigerant flow of isobutane (R600a) through adiabatic capillary tubes', *International Journal of Refrigeration*, **in press**.

[83] Seixlack, A. & Barbazelli, M. (2009), 'Numerical analysis of refrigerant flow along non-adiabatic capillary tubes using a two-fluid model', *Applied Thermal Engineering* **29**, 523-531.

[84] Seixlack, A. L.; Prata, A. T. & Melo, C. (1996), 'Modeling the HFC 134a Flow Through Capillary Tubes Using a Two-Fluid Model', International Refrigeration Conference at Purdue, West Lafayette, USA, July, pp. 89-94.

[85] Shiferaw, D.; Huo, X.; Karayiannis, T. & Kenning, D. (2007), 'Examination of heat transfer correlations and a model for flow boiling of R134a in small diameter tubes', *International Journal of Heat and Mass Transfer* **50**, 5177-5193.

[86] da Silva, D.; Ronzoni, A.; Melo, C. & Hermes, C. (2011), 'A study of transcritical carbon dioxide flow through diabatic capillary tubes', *International Journal of Refrigeration* **34**, 834-843.

[87] Sinpiboon, J. & Wongwises, S. (2002), 'Numerical investigation of refrigerant flow through non-adiabatic capillary tubes', *Applied Thermal Engineering* **22**, 2015-2032.

[88] Son, K.; Park, S.; Jeong, J.; Hong, L. & Kim, L. (2009), 'An Assessment of Friction Factor and Viscosity Models for Predicting the Refrigerant Characteristics in Adiabatic Capillary Tubes', *Korean Journal of Air-Conditioning and Refrigeration Engineering* **21, No. 3**, 140-148.

[89] Son, K.; Park, S.; Jeong, J. & Kim, L. (2008), 'A Simulation for Predicting the Refrigerant Flow Characteristics Including Metastable Region in Non-Adiabatic Capillary Tubes', Refrigeration and Air Conditioning Conference at Purdue, West Lafayette, USA, paper 968.

[90] Tuomas, R. (2006), 'Properties of Oil and Refrigerant Mixtures – Lubrication of ball bearings in refrigeration compressors', PhD thesis, Dept. of Applied Physics and Mechanical Engineering, Luleå University of Technology, Sweden.

[91] Vacek, V. & Vins, V. (2005), 'A Study of the Flow through Capillary Tube Tunned up for the Cooling Circuit with Fluoroinert Refrigerants', Technical report, Department of Applied Physics, Technical University in Prague, Czech Republic.

[92] Vins, V. & Vacek, V. (2009), 'Mass flow rate correlation for two-phase flow of R218 through a capillary tube', *Applied Thermal Engineering* **29**, 2816-2823.

[93] Wein, M. (2002), 'Numerische Simulation von kritischen und nahkritischen Zweiphasenströmungen mit thermischen und fluiddynamischen Nichtgleichgewichtseffekten', Dissertation, Technischen Universität Dresden, Deutschland.

[94] Wijaya, H. (1992), 'Adiabatic Capillary Tube Test Data for HFC-134a', International Refrigeration and Air Conditioning Conference at Purdue, West Lafayette, USA, paper 142.

[95] Wong, T. N. & Ooi, K. T. (1996), 'Adiabatic capillary tube expansion devices: a comparison of the homogeneous flow and the separated flow models', *Applied Thermal Engineering* **16, No. 7**, 625-634.

[96] Wolf, D. A.; Bittle, R. R. & Pate, M. B. (1995), 'Adiabatic Capillary Tube Performance with Alternative Refrigerants: Final Report', ASHRAE Research Project Report 762.

[97] Wolf, D. A. & Pate, M. B. (2002), 'Capillary Tube-Suction Line Heat Exchanger Performance with Alternative Refrigerants', ASHRAE Research Project Report 948.

[98] Wong, T. N. & Ooi, K. T. (1995), 'Refrigerant flow in capillary tube: an assessment of the two-phase viscosity correlations on model prediction', *International Communications in Heat and Mass Transfer* **22, No. 4**, 595-604.

[99] Wong, T. N.; Ooi, K. T. & Khoo, C. T. (1994), 'A Study on Capillary Tube Flow', International Refrigeration and Air Conditioning Conference at Purdue, West Lafayette, USA, paper 275.

[100] Wongwises, S.; Songnetichaovalit, T.; Lokathada, N.; Kritsadathikarn, P.; Suchatawat, M. & Pirompak, W. (2000), 'A comparison of the flow characteristics of refrigerants flowing through adiabatic capillary tubes', *International Communications in Heat and Mass Transfer* **27, No. 5**, 611-621.

[101] Wongwises, S.; Chan, P.; Luesuwanatat, N. & Purattanarak, T. (2000), 'Two-phase separated flow model of refrigerants flowing through capillary tubes', *International Journal of Heat and Mass Transfer* **27**, 343-356.

[102] Xu, B. & Bansal, P. (2002), 'Non-adiabatic capillary tube flow: a homogeneous model and process description', *Applied Thermal Engineering* **22**, 1801-1819.

[103] Yan, G.; Cao, X.; Wu, Y. & Cui, J. Ma, Z. (2002), 'Numerical Simulation Of The Flow Of Natural Refrigerants In a Capillary Tube', International Refrigeration and Air Conditioning Conference at Purdue, West Lafayette, USA, paper 596.

[104] Yang, C. & Bansal, P. (2005), 'Numerical investigation of capillary tube-suction line heat exchanger performance', *Applied thermal Engineering* **25**, 2014-2028.

[105] Yang, L. & Wang, W. (2008), 'A generalized correlation for the characteristics of adiabatic capillary tubes', *International Journal of Refrigeration* **31**, 197-203.

[106] Zhang, C.-L. & Ding, G. L. (2001), 'Modified General Equation for the Design of Capillary Tubes', Technical report, Institute of Refrigeration and Cryogenics, Shanghai Jiaotong University, China.

[107] Zhang, C.-L. & Ding, G. (2004), 'Approximate analytic solutions of adiabatic capillary tube', *International Journal of Refrigeration* **27**, 17-24.

[108] Zhang, C.-L. (2005), 'Generalized correlation of refrigerant mass flow rate through adiabatic capillary tubes using artificial neural network', *International Journal of Refrigeration* **28**, 506-514.

[109] Zhang, C.-L. & Zhao, L.-X. (2007), 'Model-based neural network correlation for refrigerant mass flow rates through adiabatic capillary tubes', *International Journal of Refrigeration* **30**, 690-698.

[110] Zhou, G. & Zhang, Y. (2006), 'Numerical and experimental investigations on the performance of coiled adiabatic capillary tubes', *Applied Thermal Engineering* **26**, 1106-1114.

[111] Zhou, G.; Zhang, Y.; Yang, Y. & Wang, X. (2010), 'Numerical model for matching of coiled adiabatic capillary tubes in a split air conditioner using HCFC22 and HC290', *Applied Thermal Engineering* **30**, 1477-1487.

[112] Zhou, G. & Zhang, Y. (2012), 'Inlet pressure fluctuation characteristics of coiled adiabatic capillary tubes', *Applied Thermal Engineering* **33-34**, 183-189.

variable expansion devices

[113] Elliott, M. S. & Rasmussen, B. P. (2010), 'On reducing evaporator superheat nonlinearity with control architecture', *International Journal of Refrigeration* **33**, 607-614.

[114] Fallahsohi, H.; Changenet, C.; Place´, S.; Ligeret, C. & Lin-Shi, X. (2010), 'Predictive functional control of an expansion valve for minimizing the superheat of an evaporator', *International Journal of Refrigeration* **33**, 409-418.

[115] Langmaack, L. N. & Knudsen, H. J. H. (2006), 'Heat transfer from the Evaporator outlet to the charge of thermostatic expansion valves', International Refrigeration and Air Conditioning Conference at Purdue, West Lafayette, USA.

[116] Maia, A. A. T.; Silva, M. A.; Koury, R. N. N.; Machado, L. & Eduardo, A. C. (2010), 'Control of an Electronic Expansion Valve Using an Adaptive PID Controller', International Refrigeration and Air Conditioning Conference at Purdue, West Lafayette, USA.

[117] Marcinichen, J. B.; Holanda, T. N. & Melo, C. (2008), 'A dual SISO Controller for a Vapor Compression Refrigeration System', International Refrigeration and Air Conditioning Conference at Purdue, West Lafayette, USA.

[118] Marcinichen, J. B. & Melo, C. (2006), 'Comparative analysis between a capillary tube and an electronic expansion valve in a household refrigerator', International Refrigeration and Air Conditioning Conference at Purdue, West Lafayette, USA.

[119] Qi, Q.; Deng, S.; Xu, X. & Chan, M. (2010), 'Improving degree of superheat control in a direct expansion (DX) air conditioning (A/C) system', *International Journal of Refrigeration* **33**, 125-134.

friction

[120] Alciatore, D. (1988), 'Modified Pipe Friction Diagrams That Eliminate Trial And Error Solutions', Technical report, Department of Mechanical Engineering, University of Texas, Austin.

[121] Ali, S. (2001), 'Pressure drop correlations for flow through regular helical coil tubes', *Fluid Dynamics Research* **28**, 295-310.

[122] Ardiansyah, T.; Yoshizawa, Y.; Asaba, M.; Takahashi, M.; Nakagawa, M. & Miura, K. (2010), 'Numerical Simulation of Cavitation for Comparison of Sodium and Water Flows', *Proceedings of the 18th International Conference on Nuclear Engineering* 'Proceedings of the 18th International Conference on Nuclear Engineering, Xian, China.

[123] Dalkilic, A.; Agra, O.; Teke, I. & Wongwises, S. (2010), 'Comparison of frictional pressure drop models during annular flow condensation of R600a in a horizontal tube at low mass flux and of R134a in a vertical tube at high mass flux', *International Journal of Heat and Mass Transfer* **53**, 2052-2064.

[124] Dias, J. P. & Gasche, J. (2008), 'Analysis of mean viscosity correlations on numerical simulation of the oil/refrigerant R134a mixture two-phase flow in a small diameter tube', *5th European Thermal-Sciences Conference, The Netherlands* '5th European Thermal-Sciences Conference, Clemson, USA.

[125] Field, B. & Hrnjak, P. (2007), 'Two-Phase Pressure Drop and Flow Regime of Refrigerants and Refrigerant-Oil Mixtures in Small Channels', Technical report, Air Conditioning and Refrigeration Center.

[126] Friedel, L. (1978), 'Druckabfall bei der Strömung von Gas/Dampf-Flussigkeits-Gemischen in Rohren', *Chemie Ingenieur Technik* **50**, 167-180.

[127] Friedel, L. (1979), 'Improved friction pressure drop correlations for horizontal and vertical two phase pipe flow', European Two Phase Flow Group Meeting, 5-8 June, Ispra, Italy, paper E2.

[128] Gnielinski, V. (2007), 'Berechnung des Druckverlustes in glatten konzentrischen Ringspalten bei ausgebildeter laminarer und turbulenter isothermer Strömung', *Chemie Ingenieur Technik* **79,** (1-2).

[129] Khodabandeh, R. (2005), 'Pressure drop in riser and evaporator in an advanced two-phase thermosyphon loop', *International Journal of Refrigeration* **28**, 725-734.

[130] Müller, H.; Steinhagen & Heck, K. (1986), 'A Simple Friction Pressure Drop

Correlation for Two-Phase Flow in Pipes', *Chemical Engineering and Processing* **20**, 291-308.

[131] Rohonczi, G. (1939), 'Druckabfall und Wärmeübergang bei turbulenter Strömung in glatten Rohren mit Berücksichtigung der nichtisothermen Strömung', Doktorarbeit, ETH Zürich.

[132] Romeo, E.; Royo, C. & Monzon, A. (2002), 'Improved explicit equations for estimation of the friction factor in rough and smooth pipes', *Chemical Engineering Journal* **86**, 369-374.

[133] Souza, A. L.; Chato, J. C.; Jabardo, J. M. S.; Wattelet, J. P.; Panek, J.; Christoffersen, B. & Rhines, N. (1992), 'Pressure Drop During Two-Phase Flow of Refrigerants in Horizontal Smooth Tubes', Technical report, Air Conditioning and Refrigeration Center.

[134] Yildirim, G. (2009), 'Computer-based analysis of explicit approximations to the implicit Colebrook – White equation in turbulent flow friction factor calculation', *Advances in Engineering Software* **40**, 1183-1190.

[135] Zheng, Q.; Kiihler, W. & Kastner, W. und Riedle, K. (1991), 'Druckverlust in glatten und innenberippten Verdampferrohren', *Wärme- und Stoffübertragung* **26**, 323-330.

multiphase flow, heat transfer, oil-mixing

[136] Buchlin, J.-M. (1998), 'Natural and forced convection heat transfer on slender cylinders', *Rev. Gen. Therm.* **37**, 653-660.

[137] Bücker, D. & Wagner, W. (2006), 'Reference equations of state for the thermodynamic properties of fluid phase n-butane and isobutane', *J. Phys. Chem. Ref. Data* **35,** 929-1019.

[138] Churchill, S. W. (1977), 'Comprehensive Correlating Equations For Heat, Mass and Momentum Transfer in Fully Developed Flow in Smooth Tubes', *Industrial and Engineering Chemistry Fundamentals* **16**, 109-116.

[139] Coleman, J. W. & Garimella, S. (2003), 'Two-phase flow regimes in round, square and rectangular tubes during condensation of refrigerant R134a', *International Journal of Refrigeration*, **26**, 117-128.

[140] Daniels, B. J. (2009), 'A Study of Adiabatic and Diabatic Flow Boiling in Parallel Microchannels and Fractal-like Branching Microchannels', PhD thesis, Oregon State University, USA.

[141] El Hajal, J.; Thome, J. R. & Cavallini, A. (2003), 'Condensation in horizontal tubes, part 1: two-phase flow pattern map', *International Journal of Heat and Mass Transfer*, **46**, 3349-3363.

[142] Fujii, T. & Uehara, H. (1970), 'Laminar natural-convective heat transfer from the outer surface of a vertical cylinder', *International Journal of Heat and Mass Transfer* **13**, 607-615.

[143] Gnielinski, V. (1975), 'Neue Gleichungen für den Wärme- und Stoffübergang in turbulent durchströmten Rohren und Kanälen', *Forsch. Ing.-Wes.* **41** (1), 8-16.

[144] Hermes, C. J. L. & Melo, C. (2008), 'A first-principles simulation model for the start-up and cycling transients of household refrigerators', *International Journal of Heat and Mass Transfer*, **31**, 1341-1357.

[145] Janssens-Maenhout, G. (1999), 'Beiträge zur Modellierung und numerischen Simulation von Zweiphasenströmungen mit Wärmeübertragung', Dissertation, Forschungszentrum Karlsruhe, Deutschland.

[146] Lex, T. (2004), 'Fluiddynamik von Gas-Flüssigkeits-Gemischen in Kugelhähnen', Dissertation, Technischen Universität München, Deutschland.

[147] Liles, D. R. & Reed, W. H. (1978), 'A Semi-Implicit Method for Two-Phase Fluid

Dynamics', *Journal of Computational Physics* **26**, 390-407.

[148] Liu, Z. & Winterton, R. H. S. (1991), 'A general correlation for saturated and subcooled flow boiling in tubes and annuli, based on a nucleate pool boiling equation', *International Journal of Heat and Mass Transfer* **34**, No. 11, 2759-2766.

[149] Lottin, O.; Guillemet, P. & Lebreton, J.-M. (2003), 'Effects of synthetic oil in a compression refrigeration system using R410A. Part I: modelling of the whole system and analysis of its response to an increase in the amount of circulating oil', *International Journal of Refrigeration*, **26**, 772-782.

[150] Nagengast, B. (1997), 'History of Sealed Refrigeration Systems', *ASHRAE Journal*, 44-52.

[151] Neuhaus, T. (2005), 'Mathematische Modellierung und vergleichende Untersuchungen zur Beschreibung von transienten Ein- und Mehrphasenströmungen in Rohrleitungen', Dissertation, Universität Dortmund, Deutschland.

[152] Polifke, W. & Carneiro, J. (2009), 'Grundlagen der Mehrphasenströmungen', Technical report, Fakultät für Maschinenwesen, Technische Universität München.

[153] Sami, S. M. & Comeau, J. D. (2002), 'Influence of thermophysical properties on two-phase flow convective boiling of refrigerant mixtures', *Applied Thermal Engineering* **22**, 1535-1548.

[154] Schwellnus, C. F. & Shoukri, M. (1991), 'A Two-Fluid Model for Non-Equilibrium Two-Phase Critical Discharge', *The Canadian Journal of Chemical Engineering* **69**.

[155] Shah, M. M. (1979), 'A general correlation for heat transfer during film condensation inside pipes', *International Journal of Heat and Mass Transfer* **22**, 547-556.

[156] Triplett, K.; Ghiaasiaan, S.; Abdel-Khalik, S.; LeMouel, A. & McCord, B. (1999), 'Gas-liquid two-phase flow in microchannels Part II: void fraction and pressure drop', *International Journal of Multiphase Flow* **25**, 395-410.

[157] Wu, H.; Peng, X.; Ye, P. & Gong, Y. E. (2007), 'Simulation of refrigerant flow boiling in serpentine tubes', *International Journal of Heat and Mass Transfer* **50**, 1186-1195.

[158] Yang, Z.; Peng, X. & Ye, P. (2008), 'Numerical and experimental investigation of two phase flow during boiling in a coiled tube', *International Journal of Heat and Mass Transfer* **51**, 1003-1016.

[159] Yashar, D.; Wilson, M.; Kopke, H.; Graham, D.; Chato, J. & Newell, T. (2001), 'An Investigation of Refrigerant Void Fraction in Horizontal, Microfin Tubes', *HVAC&R*

Research **7, No. 1**, 67-82.

[160] Youbi-Idrissia, M. & Bonjour, J. (2008), 'The effect of oil in refrigeration: Current research issues and critical review of thermodynamic aspects', *International Journal of Refrigeration* **31**, 165-179.

[161] Zhang, X.; Coupland, P.; Fletcher, P. D. & Haswell, S. J. (2009), 'Monitoring of liquid flow through microtubes using a micropressure sensor', *Chemical Engineering Research and Design* **87**, 19-24.

[162] Zhelezny, V. P.; Nichenko, S. V.; Semenyuk, Y. V.; Kosoy, B. V. & Kumar, R. (2009), 'Influence of compressor oil admixtures on theoretical efficiency of a compressor system', *International Journal of Refrigeration*, **32**, 1526 – 1535.

books

[163] Baehr, H. D., Kabelac, S. (2012), 'Thermodynamik', 15. Auflage, Springer-Verlag, Berlin Heidelberg, Germany.

[164] Bar-Meir, G. (2002), 'Fundamentals of Compressible Fluid Mechanics', GNU Free Documentation License 0.1, Free Software Foundation Inc., Boston, USA.

[165] Brennen, C. E. (2005), 'Fundamentals of Multiphase Flow', Cambridge University Press, New York, USA.

[166] Collier, J. & Thome, J. (1996), 'Convective Boiling and Condensation', Oxford University Press, Oxford, England.

[167] Gidaspow, D. (1994), 'Multiphase Flow and Fluidization', Academic Press, Inc., San Diego, California, USA.

[168] Hewitt, G. & Hall Taylor, N. (1970), 'Annular Two Phase Flow', Pergamon Press Ltd., Headington Hill Hall, Oxford, England.

[169] Pischinger, R.; Klell, M.; Sams, T. (2004), 'Thermodynamik der Verbrennungs-kraftmaschine', Zweite überarbeitete Auflage, Springer-Verlag, Vienna, Austria.

[170] Soo, S. (1990), 'Multiphase Fluid Dynamics', Science Press and Gower Technical, Bejing, China.

[171] Wallis, G. B. (1969), 'One-dimensional Two-phase Flow', McGraw-Hill, Inc., New York, USA.

manuals, standards, online sources

[172] JCGM 100:2008 GUM 1995 with minor corrections, 'Evaluation of measurement data – Guide to the expression of uncertainty in measurement'.

[173] JCGM 101:2008 Evaluation of measurement data – Supplement 1 to the "Guide to the expression of uncertainty in measurement" – 'Propagation of distributions using a Monte Carlo method'.

[174] JCGM 104:2009 Evaluation of measurement data – An introduction to the "Guide to the expression of uncertainty in measurement" and related documents.

[175] JCGM 102:2011 Evaluation of measurement data – Supplement 2 to the "Guide to the expression of uncertainty in measurement" – Extension to any number of output quantities.

[176] JCGM 200:2012 International vocabulary of metrology – Basic and general concepts and associated terms (VIM) 3rd edition 2008 version with minor corrections.

[177] Richtlinie 2004/22/EG des Europäischen Parlaments und des Rates vom 31. März 2004 über Messgeräte.

[178] Demuth, H.; Beale, M. & Hagan, M. (2009), 'Neural Network Toolbox 6 – User's Guide', Online only: http://filer.case.edu/pjt9/b378s10/nnet.pdf (accessed 24.04.2012).

[179] Sonin, A. (2001), 'The physical basis of dimensional analysis', 2nd ed., Department of Mechanical Engineering, MIT, Cambridge, MA, USA.

[180] NIST ITS90 Thermovoltage Table
http://srdata.nist.gov/its90/download/all.tab (accessed 15.02.2013).

[181] Dannfoss Filter Drier
http://www.danfoss.com/Products/Categories/Literature/RA/Filter-Driers/c5bc6789-2ed4-410e-a626-ca5749800413.html (accessed 06.03.2013).

[182] Bronkhorst Mini Coriolis Mass Flow Meters
http://www.bronkhorst-cori-tech.com/en/products/coriolis_meters_controllers/mini_cori-flow/mass_flow_meters_mfms/ (accessed 08.03.2013).

[183] Hill, T. P. (2009), 'Conflations of Probability Distributions', Georgia Institute of Technology, Atlanta, USA, http://arxiv.org/abs/0808.1808v4 (accessed 08.03.2013).

[184] NYNAS Base Oil Handbook

http://www.engnetglobal.com/documents/pdfcatalog/NYN001_200412073535_Base%20oil%20handbookENG.pdf (accessed 19.09.2013).

[185] Thome, J. R. (2010), 'Wolverine Engineering Data Book III', Wolverine Tube, Inc..

[186] Franco, J. M. & Partal, P., Rheology, Vol. 1, 'The Newtonian Fluid' http://www.eolss.net/sample-chapters/c06/e6-197-03-00.pdf (accessed: 15.10.2013).

[187] Barenblatt, G. I. (1996), 'Scaling self-similarity, and intermediate asymptotics', Cambridge University Press, Cambridge, UK.

[188] Buckingham, E. (1914), 'On physically similar systems; illustrations of the use of dimensional analysis', *Physical Review*, **4**, 345-376.

[189] KEY Industries Capillary Tubing http://www.kte.com.au/dyn/media/r1/shop/attrib/pdf_brochure/9 (accessed 08.01.2014).

[190] Nau, M. (2004), 'Elektrische Temperaturmessung mit Thermoelementen und Widerstandsthermometern', JUMO, FAS 146, Ausgabe 2007-01. http://www.jumo.net/attachments/JUMO/attachmentdownload?id=5116 (accessed 13.01.2014).

[191] International Energy Agency (IEA), (2009), 'Gadgets and Gigawatts – Policies for Energy Efficient Electronics', Paris, France. http://www.iea.org/publications/freepublications/publication/gigawatts2009.pdf (accessed 15.01.2014).

[192] International Richtlinie 2003/66/EG der Kommission vom 3. Juli 2003 zur Änderung der Richtlinie 94/2/EG zur Durchführung der Richtlinie 92/75/EWG des Rates betreffend die Energieetikettierung für elektrische Haushaltskühl- und Gefriergeräte sowie entsprechende Kombinationsgeräte.

[193] Kältemittel-Report 16, (2010), BITZER Kühlmaschinenbau, Sindelfingen, Germany. www.bitzer.de/ger/content/download/1620/65274/file/a-500-16.pdff (accessed 23.01.2014).

[194] United Nations Environment Programme / Ozone Secretariat. http://montreal-protocol.org/new_site/en/ (accessed 23.01.2014).

[195] United Nations Environment Programme, (2011), 'HFCs: A Critical Link in Protecting Climate and Ozone Layer.' http://www.unep.org/dewa/portals/67/pdf/HFC_report.pdf (accessed 23.01.2014).

[196] Eichelseder, H.; Sturm, P. (2014), 'Thermodynamik Vorlesung', lecture notes, Institut für Verbrennungskraftmaschinen und Thermodynamik, Graz, Austria.

[197] Klell, M.; Almbauer, R. (2013), 'Höhere Thermodynamik', lecture notes, Institut für Verbrennungskraftmaschinen und Thermodynamik, Graz, Austria.

[198] Product Data Sheet HXD30AA Revision 3 http://www.secop.com/fileadmin/user_data/SEPS/datasheets/hxd30aa-d1_16260300_r600a_220v_50hz_01-2014_cdo-00-000058-g.pdf (accessed 27.11.2014).

[199] ANSI/ASHRAE Standard 23-2005, 'Methods of Testing for Rating Positive Displacement Refrigerant Compressors and Condensing Units'.

[200] Schlemmer, S.; Liebherr-Hausgeräte Lienz GmbH; personal communication, 10.01.2014.

[201] Lemmon, E. W., Huber, M.L., McLinden, M.O. (2012), 'NIST Standard Reference Database 23: Reference Fluid Thermodynamic and Transport Properties-REFPROP', Version 9.0, National Institute of Standards and Technology, Gaithersburg, MD, USA.

Appendix

Table A 1 Dataset for steady state adiabatic capillary tube measurements.

p_{in} bar	σ_{pin} bar	p_{out} bar	σ_{pout} bar	$\dot{m}$ kg/h	$\sigma_{\dot{m}}$ kg/h	T_{in} °C	σ_{Tin} °C	D_i mm	L m
7.060	0.011	1.596	0.004	1.4573	0.004	44.67	0.03	0.712	4.000
6.620	0.013	1.013	0.004	1.4019	0.006	41.77	0.02	0.712	4.000
5.007	0.010	0.795	0.004	1.0713	0.009	33.63	0.02	0.712	4.000
5.773	0.009	0.884	0.003	1.2388	0.005	37.56	0.02	0.712	4.000
6.602	0.010	1.006	0.003	1.4296	0.004	41.92	0.02	0.712	4.000
7.515	0.012	1.118	0.003	1.5779	0.003	46.31	0.04	0.712	4.000
7.700	0.010	1.334	0.004	1.5800	0.004	47.30	0.05	0.712	4.000
7.956	0.013	1.661	0.005	1.6030	0.004	48.68	0.05	0.712	4.000
4.991	0.010	0.751	0.008	0.9295	0.004	32.58	0.02	0.712	5.000
5.344	0.009	0.803	0.003	0.9962	0.004	34.65	0.01	0.712	5.000
5.724	0.011	0.862	0.003	1.0711	0.004	36.61	0.02	0.712	5.000
6.123	0.009	0.914	0.003	1.1386	0.003	38.65	0.02	0.712	5.000
6.542	0.015	0.969	0.002	1.2221	0.004	40.78	0.02	0.712	5.000
7.254	0.006	1.055	0.001	1.3052	0.001	44.60	0.02	0.712	5.000
7.391	0.008	1.158	0.002	1.1765	0.002	45.52	0.02	0.712	5.000
7.629	0.012	1.388	0.003	1.2206	0.005	46.70	0.03	0.712	5.000
7.802	0.010	1.473	0.005	1.2343	0.004	47.45	0.02	0.712	5.000
7.456	0.010	1.016	0.002	1.2907	0.004	45.84	0.03	0.712	5.000
4.908	0.011	0.660	0.005	0.9624	0.008	34.47	0.01	0.712	6.000
5.264	0.012	0.708	0.004	1.0272	0.007	36.30	0.01	0.712	6.000
6.465	0.011	0.877	0.002	1.2485	0.006	42.02	0.02	0.712	6.000
6.897	0.010	0.925	0.002	1.3193	0.005	44.19	0.02	0.712	6.000
7.355	0.005	0.976	0.001	1.3976	0.001	46.26	0.02	0.712	6.000
7.841	0.004	1.027	0.001	1.4719	0.001	48.46	0.02	0.712	6.000
8.353	0.005	1.523	0.002	1.5475	0.001	50.63	0.03	0.712	6.000
5.491	0.008	0.877	0.002	1.3162	0.009	33.12	0.01	0.712	6.000
5.583	0.009	0.791	0.002	1.1682	0.009	33.05	0.01	0.712	6.000
6.096	0.008	0.863	0.002	1.2758	0.005	35.60	0.01	0.712	6.000
6.758	0.011	0.968	0.002	1.4203	0.005	38.71	0.02	0.712	6.000
6.616	0.008	0.943	0.002	1.3885	0.004	38.97	0.02	0.712	6.000
5.016	0.007	0.640	0.004	0.9337	0.005	32.39	0.01	0.712	7.000
5.011	0.005	0.641	0.001	0.9346	0.005	32.36	0.02	0.712	7.000
5.009	0.005	0.651	0.001	0.9445	0.005	32.11	0.02	0.712	7.000
5.008	0.006	0.652	0.004	0.9477	0.005	32.05	0.01	0.712	7.000
5.351	0.009	0.731	0.002	1.0746	0.003	34.04	0.02	0.712	7.000
6.103	0.010	0.822	0.002	1.2143	0.003	37.93	0.03	0.712	7.000
6.504	0.009	0.854	0.003	1.2586	0.004	40.29	0.02	0.712	7.000
6.936	0.012	0.912	0.003	1.3251	0.003	42.67	0.02	0.712	7.000
5.001	0.008	0.681	0.003	0.9967	0.008	32.24	0.02	0.712	7.000
5.712	0.011	0.772	0.002	1.1412	0.003	35.94	0.02	0.712	7.000

7.402	0.016	0.969	0.002	1.3935	0.004	44.81	0.03	0.712	7.000
7.851	0.005	1.023	0.002	1.4751	0.001	46.79	0.02	0.712	7.000
6.804	0.011	1.154	0.004	1.8343	0.005	42.68	0.04	0.790	5.000
6.451	0.012	1.087	0.005	1.7205	0.009	40.85	0.03	0.790	5.000
6.106	0.011	1.032	0.005	1.6236	0.007	39.02	0.03	0.790	5.000
5.781	0.009	0.984	0.006	1.5436	0.010	37.36	0.02	0.790	5.000
5.471	0.008	0.928	0.004	1.4458	0.006	35.64	0.02	0.790	5.000
4.897	0.005	0.826	0.002	1.2726	0.010	32.46	0.01	0.790	5.000
5.182	0.009	0.886	0.004	1.3743	0.005	34.05	0.03	0.790	5.000
5.485	0.008	0.943	0.005	1.4725	0.008	35.78	0.02	0.790	5.000
7.928	0.010	1.301	0.004	2.0909	0.005	48.48	0.07	0.790	5.000
7.753	0.016	1.279	0.005	2.0421	0.006	47.66	0.07	0.790	5.000
7.372	0.013	1.228	0.004	1.9551	0.006	45.82	0.06	0.790	5.000
6.998	0.010	1.173	0.004	1.8609	0.006	43.95	0.05	0.790	5.000
6.813	0.012	1.145	0.004	1.8122	0.006	42.95	0.04	0.790	5.000
6.647	0.011	1.121	0.005	1.7762	0.007	42.00	0.04	0.790	5.000
5.077	0.011	0.825	0.004	1.2237	0.004	33.44	0.02	0.790	7.000
5.448	0.010	0.895	0.004	1.3350	0.004	35.58	0.02	0.790	7.000
5.832	0.011	0.956	0.003	1.4348	0.005	37.67	0.02	0.790	7.000
6.239	0.010	1.012	0.003	1.5235	0.004	39.88	0.03	0.790	7.000
6.675	0.014	0.992	0.003	1.6191	0.005	42.10	0.03	0.790	7.000
7.133	0.013	1.062	0.003	1.7445	0.005	44.61	0.05	0.790	7.000
7.590	0.014	1.130	0.003	1.7949	0.005	46.60	0.05	0.790	7.000
6.723	0.014	1.051	0.006	1.6715	0.008	41.90	0.03	0.790	7.000
7.098	0.012	1.118	0.003	1.7841	0.003	43.91	0.04	0.790	7.000
7.480	0.012	1.165	0.003	1.8677	0.003	45.85	0.05	0.790	7.000
7.742	0.016	1.457	0.005	1.8372	0.004	47.08	0.05	0.790	7.000
7.410	0.013	1.246	0.004	1.7704	0.004	45.65	0.05	0.790	7.000
5.269	0.008	0.948	0.003	1.568	0.005	34.69	0.02	0.883	7.000
4.976	0.005	0.885	0.002	1.428	0.005	33.05	0.02	0.883	7.000
6.522	0.015	1.373	0.002	2.305	0.004	35.49	0.03	0.883	7.000
6.246	0.012	1.317	0.002	2.186	0.005	35.43	0.03	0.883	7.000
6.522	0.014	1.359	0.003	2.262	0.006	36.85	0.04	0.883	7.000
6.822	0.013	1.398	0.003	2.329	0.007	38.32	0.04	0.883	7.000
7.082	0.014	1.429	0.003	2.382	0.008	40.01	0.04	0.883	7.000
7.402	0.014	1.471	0.003	2.454	0.007	41.64	0.06	0.883	7.000
7.692	0.014	1.510	0.004	2.515	0.007	43.38	0.07	0.883	7.000
7.610	0.012	1.491	0.003	2.465	0.007	43.92	0.07	0.883	7.000
7.578	0.011	1.481	0.003	2.437	0.006	44.29	0.07	0.883	7.000
7.511	0.011	1.456	0.003	2.372	0.006	45.42	0.07	0.883	7.000
7.879	0.012	1.488	0.004	2.416	0.006	47.06	0.10	0.883	7.000
9.244	0.009	1.638	0.002	2.625	0.002	54.91	0.08	0.883	7.000
5.619	0.009	1.389	0.003	2.435	0.008	34.91	0.04	0.980	7.000
6.054	0.009	1.480	0.004	2.563	0.007	38.23	0.06	0.980	7.000
5.966	0.009	1.409	0.006	2.380	0.008	39.31	0.05	0.980	7.000
6.443	0.012	1.483	0.007	2.521	0.010	42.48	0.07	0.980	7.000
6.961	0.013	1.572	0.007	2.634	0.010	45.67	0.07	0.980	7.000

7.507	0.013	1.673	0.006	2.819	0.009	48.50	0.06	0.980	7.000
8.085	0.013	1.809	0.004	3.050	0.008	51.81	0.06	0.980	7.000

The uncertainties for the length and diameter measurements can be looked up in section 6.3. Also the uncertainties for pressure temperature and mass flow rates have to be taken from section 6.3 since the values from Table A 1 only depict the standard deviation of the measuring signal during the a 30 minute steady state operation point.

Concerning the models for adiabatic capillary tubes, Neural Network parameters for a 7-neuron network are presented. Reference point of enthalpy is at $T_0 = 298.15$ K and $p_0 = 1013.25$ hPa. The mass flow rate is the output parameter. A static two layer network is chosen with seven neurons and a tan-sigmoid function, eq. (149), as transfer function for the first layer (hidden layer). Three variants are possible, the first is for one-phase-, the second for two-phase- and the third one for enthalpy-inlet conditions.

The input-vector looks like:

$$\boldsymbol{n} = [p_{\mathrm{in}}, p_{\mathrm{diff}}, T_{\mathrm{sub}}, D, L\,] \quad \text{or} \quad \bar{\boldsymbol{n}} = [p_{\mathrm{in}}, p_{\mathrm{diff}}, x, D, L] \quad \text{or} \quad \bar{\boldsymbol{n}} = [p_{\mathrm{in}}, p_{\mathrm{diff}}, h, D, L] \tag{162}$$

The range of application is given in Table A 2 and should not be exceeded. Next, the specific vectors and matrices are given (Table A 3). The calculation of the output (mass flow) is described in section 5.2.2.

Table A 2 Min- and max- values for data normalization. Units are according to SI units apart mass flow (kg/h).

	p_{in} Pa	p_{diff} Pa	T_{sub} K	x_{in} -	h_{in} J/kg	D m	L m	$\dot{m}$ kg/h
one phase inlet								
min	$3 \cdot 10^5$	0.0	1.0	-	-	0.0006	3.0	0.0
max	$1 \cdot 10^6$	$8.7128 \cdot 10^5$	15.0	-	-	0.0012	8.0	10.1107
two phase inlet								
min	$3 \cdot 10^5$	0.0	-	0.1	-	0.0006	3.0	0.0
max	$1 \cdot 10^6$	$9.2531 \cdot 10^5$	-	0.5	-	0.0012	8.0	4.8236
enthalpy and pressure as inlet boundary conditions								
min	$3 \cdot 10^5$	0.0	-	-	$-3.90639 \cdot 10^5$	0.0006	3.0	0.0
max	$1 \cdot 10^6$	$3.2115 \cdot 10^6$	-	-	-98302.7	0.0012	8.0	10.1107

Table A 3 Numeric values of weight matrices, scaling parameters and biases. Vectors and matrices are denoted as bold type.

$\boldsymbol{b_1}$	b_2	$\boldsymbol{IW}$					$\boldsymbol{LW}$
one phase inlet							
0.91108	0.31609	-0.15600	-0.13754	-0.37743	-0.07837	0.12084	1.94446
3.07499		-0.07210	2.17102	-0.06332	-0.16810	0.08244	11.00712
-0.01626		-0.00063	-0.31532	-0.00243	-0.35909	0.23932	0.93825
1.08623		-0.09846	-0.02565	-0.14119	-0.18781	0.11866	-10.58951
0.18556		0.39261	-0.56515	0.60245	-0.57635	0.17484	-0.20079
-2.79158		0.07215	-2.68030	0.05724	0.18242	-0.10261	2.77512
-1.75240		-0.15454	0.59969	0.15077	-0.21184	0.19186	2.09297
two phase inlet							
-1.28183	1.74590	0.50938	0.43054	-0.14899	0.19613	-0.14963	-1.42029

-3.14392		0.02897	0.37182	-0.84130	0.49053	-0.18305	2.28961
4.20744		-0.36988	2.94217	0.18165	-0.42616	0.17058	2.28440
-1.35422		0.33042	0.24850	-0.11995	0.41825	0.01864	2.20054
1.60904		-0.51738	0.41012	0.23387	-0.33908	0.24341	-1.03031
0.97963		-0.31438	-0.45216	0.13296	-0.12600	0.76211	0.91618
1.05689		-0.30266	-0.42291	0.11203	-0.19739	0.58784	-1.85264
enthalpy and pressure as inlet boundary conditions							
-1.87019	-1.84914	0.32426	-1.40544	-0.43543	0.64563	-0.15118	-0.34846
2.99304		-0.06813	-0.19812	-0.01436	-0.51957	1.07583	-1.15183
6.29993		-0.88162	-3.27848	6.94690	-0.52923	0.46224	1.61194
-2.22429		0.73223	0.07239	-1.98273	0.57818	-0.19857	2.20643
-0.25924		0.40167	0.01708	-0.47534	0.81740	-0.11187	0.22879
2.46887		1.65699	-1.99079	1.05886	-0.69784	0.21486	0.54789
7.18227		-0.79393	4.83454	2.09745	-0.60502	0.20505	1.94114